Interaction of the Hedgehog and vitamin D receptor signaling pathways in *Patched* associated cancers

Dissertation

for the award of the degree

"Doctor rerum naturalium"

of the Georg-August-Universität Göttingen

within the doctoral program Molecular Biology of Cells

of the Georg-August University School of Science (GAUSS)

submitted by

Benedikt Linder (birth name: Albert), M.Sc.

from Wetzlar

Göttingen 2015

Thesis Committee

Prof. Dr. Heidi Hahn
Dept. of Human Genetics; University Medical Center Göttingen

Prof. Dr. Matthias Dobbelstein
Dept. of Molecular Oncology; Georg-August-University of Göttingen

Prof. Dr. Michael Schön
Dept. of Dermatology, Venereology and Allergology; University Medical Center Göttingen

Members of the Examination Board

Referee: **Prof. Dr. Heidi Hahn**
Dept. of Human Genetics; University Medical Center Göttingen

2nd Referee: **Prof. Dr. Matthias Dobbelstein**
Institute of Molecular Oncology; Georg-August-University of Göttingen

3rd referee: **Prof. Dr. Michael Schön**
Dept. of Dermatology, Venereology and Allergology; University Medical Center Göttingen

Further members of the Examination Board

Prof. Dr. Peter Burfeind
Dept. of Human Genetics; University Medical Center Göttingen

Prof. Dr. Steven Johnsen
Clinic for General, Visceral and Pediatric surgery; University Medical Center Göttingen

Prof. Dr. Ralph Kehlenbach
Dept. of Biochemistry I; University Medical Center Göttingen

Date of oral examination:

7th of May, 2015

Affidavit

I hereby declare that the PhD thesis entitled "Interaction of the Hedgehog and vitamin D receptor signaling pathways in *Patched* associated cancers" has been written independently and with no other sources and aids than quoted.

Benedikt Linder
March, 2015
Göttingen

Parts of this work have been submitted for publication:

Linder, B., Weber, S., Dittmann, K., Adamski J., Hahn, H., Uhmann, A.. „ A functional and putative physiological role of calcitriol in Patched1/Smoothened interaction.“ JBC, submitted

The most exciting phrase to hear in science,
the one that heralds the most discoveries,
is not "Eureka!" (I found it!), but "That's funny..."

- Isaac Asimov -

Contents

List of Figures

List of Tables

1. Summary

Tumor formation can be linked to the misregulation of the developmentally important Hedgehog (Hh) signaling pathway. In general, Hh signaling is initiated by the secretion of Hh ligands. This is followed by the binding of Hh to the 12-pass transmembrane protein Patched (Ptch). Ptch normally represses the activity of the 7-pass transmembrane protein Smoothened (Smo). Binding of Hh to Ptch inhibits Ptch, thereby relieving the inhibition of Smo. Smo translocates into the primary cilium and mediates the activation of the members of the Glioma associated (Gli) family of transcription factors, leading to the transcription of target genes. The Smo protein harbors two domains important for its regulation by small-molecules, the seven-transmembraneous domain (7TM) and the N-terminal, extracellular cysteine-rich-domain (CRD). The mechanism by which Ptch inhibits Smo is not completely understood. A direct interaction of Ptch and Smo has been excluded and the inhibition is rather based on a catalytic mechanism involving small-molecule signal transmitters that are secreted in a Ptch-mediated manner. Indeed, recent data suggested that Ptch may secrete Smo inhibiting sterol-derivatives.

Our recent data demonstrated that the secosteroid and hormonally active form of vitamin D_3 ($vitD_3$), calcitriol, inhibits Hh signaling at the level of Smo and reduces tumor growth in murine models for basal cell carcinoma (BCC) and rhabdomyosarcoma (RMS). In the present study we aimed to enhance the calcitriol-mediated antitumoral effects on BCC with antifungal azoles. Indeed, itraconazole (ITZ) but not the well-known Smo inhibitor cyclopamine (CP) strongly enhances calcitriol-mediated antitumoral response of the murine BCC cell line ASZ001. Furthermore, the combined effects of ITZ and calcitriol were not mediated by an enhanced bio-availability of calcitriol but by a synergistic inhibition of Hh signaling. Despite these promising *in vitro* data, no cooperative antitumoral effects of calcitriol and ITZ were achieved in two mouse models for BCC.

Based on the findings that calcitriol inhibits Hh signaling at the level of Smo we next hypothesized that calcitriol is secreted by Ptch and investigated if calcitriol plays a key role in the physiological regulation of Hh signaling. Media transfer experiments and mass spectrometric analyses show that Ptch is indispensable for calcitriol release from the cells, but not for its synthesis. Second, generation of concentration-response curves, direct-competition assays and analyses of mutant Smo variants revealed that calcitriol does neither bind to the 7TM nor the CRD of Smo. This is in line with the current opinion that Ptch-mediated

inhibition of Smo is unlikely to occur at the 7TM or the CRD. Taken together, our results indicate that calcitriol could be the first physiologically-existing Smo inhibitor to be discovered.

2. Introduction

2.1. Basal cell carcinoma

Cancer is one of the most leading causes of death in humans. In 2012 approximately 14 million people diseased and 8 million patients died due to cancer-related diseases (WHO 2015). Most cancer types are characterized by malignant growth and spreading of metastases, which finally lead to organ failure and the death of the patients.

Throughout all cancers the group of the non-melanoma skin cancers (NMSC) or "white skin cancers" has the highest incidence. The majority of NMSC are basal cell carcinomas (BCC) and squamous cell carcinoma (SCC). BCC is the most commonly diagnosed cancer among Caucasians (reviewed in (Berking *et al.* 2014; Lomas *et al.* 2012)) with a lifetime risk of about 30 %. Yearly incidence rates differ from 70-80 new cases per 100,000 people in Germany, 115 per 100,000 in the UK and up to 2 per 100 in Australia, (Basset-Seguin *et al.* 2015; Roewert-Huber *et al.* 2007) with an estimated 2-3 fold increase throughout the last three decades. BCCs metastasize only in 0.0028 % to 0.55 % of all cases (Berking *et al.* 2014; Walling *et al.* 2004). But the fact that the tumors usually develop at sun-exposed skin like the head and neck region, especially the face, often complicates the surgical removal of those tumors (Roewert-Huber *et al.* 2007). Intermittent UV exposure, fair skin, male gender as well as geographically high UV radiation (e.g. Australia) significantly enhance the risk for BCC development (Roewert-Huber *et al.* 2007; Walling *et al.* 2004).

Apart from epidemiological risk factors, patients who suffer from the rare heritable, autosomal-dominant basal cell nevus syndrome or Gorlin-Goltz-syndrome develop multiple BCCs throughout their lifetime (Epstein 2008; Gorlin and Goltz 1960). Genetically, this syndrome is caused by mutations in the *Patched1* gene (*PTCH*) located on the human chromosome 9q22 (Hahn *et al.* 1996; Johnson *et al.* 1996). Since the PTCH protein negatively regulates the activity of the Hedgehog (HH) signaling pathway, mutations in *PTCH* result in excessive HH pathway activation (Epstein 2008; Goodrich *et al.* 1997). Upon this discovery it was revealed that the majority of sporadic BCCs (90 %) display *PTCH* mutations and frequently show biallelic loss of *PTCH* (reviewed in (Albert and Hahn 2014; Epstein 2008)).

2.2.Hedgehog signaling

The Hh signaling pathway was initially described by the two Nobel laureates Nüsslein-Volhard and Wieschaus (Nusslein-Volhard and Wieschaus 1980). They showed that this pathway is implicated in body patterning, since the loss of the *Hh* gene led to a hedgehog-like appearance of the mutant *Drosophila melanogaster* (*D. melanogaster*) larvae (Nusslein-Volhard and Wieschaus 1980). Additional screens revealed other components of this pathway, like the Hh receptor Ptch, its interacting partner Smo, the kinase Fused (Fu) and the transcription factor cubitus interruptus (Ci) (reviewed in (Albert and Hahn 2014; van den Brink 2007)).

In mammals, Hh signaling also regulates embryonic development and its misregulation leads to congenital malformations like cyclopia or holoprosencephaly (Briscoe and Therond 2013; Hooper and Scott 2005). In the adult organism, the pathway is mainly silenced except for its implication in cell differentiation and proliferation, stem cell maintenance and regenerative responses after injury (Hooper and Scott 2005; Machold *et al.* 2003; Shin *et al.* 2011). Recently, Teperino *et al.* showed that Hh signaling is also involved in the control of metabolism (Teperino *et al.* 2014). Although the Hh pathway is evolutionary conserved (Roberg-Larsen *et al.* 2014), it displays a far more complex picture in mammals. In contrast to *D. melanogaster* three *Hh* genes and proteins are known in vertebrates: *Sonic (Shh), Indian (Ihh) and Dessert hedgehog (Dhh)* (Echelard *et al.* 1993; Varjosalo and Taipale 2008) of which Shh is the best characterized and most broadly expressed (Varjosalo and Taipale 2008). Furthermore, two *Ptch* homologues, *Ptch* and *Patched2* (*Ptch2*), are known in vertebrates. Of those, *Ptch* is better characterized and considered to be the key player in Hh signaling regulation. Finally, the *D. melanogaster* transcription factor *Ci* has three orthologues in mammals: glioma-associated oncogene family members 1, 2 and 3 (*Gli1*, *Gli2* and *Gli3* (see below)).

Although the exact interplay of the pathway components still contains many gaps, it is established that in the absence of Shh, the receptor Ptch inhibits its interacting partner Smo by a hitherto unidentified, indirect mechanism (Fig. 1 A). Upon binding of Shh to Ptch, the Hh pathway is activated by internalization of the Ptch protein (Denef *et al.* 2000) which leads to a loss of Smo inhibition (Fig. 1 B). Subsequently, Smo facilitates the translocation of the Gli transcription factors into the nucleus where they induce the expression of Hh signaling target genes (Fig. 1B) (Hooper and Scott 2005). Known target genes include the proto-oncogene N-Myc (Kenney *et al.* 2003) and the cell-cycle regulators Cyclin D1 and Cyclin D2 (Kenney and

Rowitch 2000). Additionally, activation of Hh signaling leads to the expression of the pathway components *Ptch* (Marigo and Tabin 1996) and *Gli1* (Lee *et al.* 1997). This results in a negative and positive feedback loop, respectively. Constitutively active Hh signaling can lead to or is observed in a variety of cancers. This overactivation can be caused by many different mechanisms like overexpression of the Hh ligands (Oro *et al.* 1997), mutational inactivation of the tumor suppressor *Ptch* (Goodrich *et al.* 1997; Hahn *et al.* 1996), activating mutations of *Smo* (Lam *et al.* 1999) or overexpression of the *Gli* transcription factors (Gli TFs) (Nilsson *et al.* 2000) (Fig. 1C).

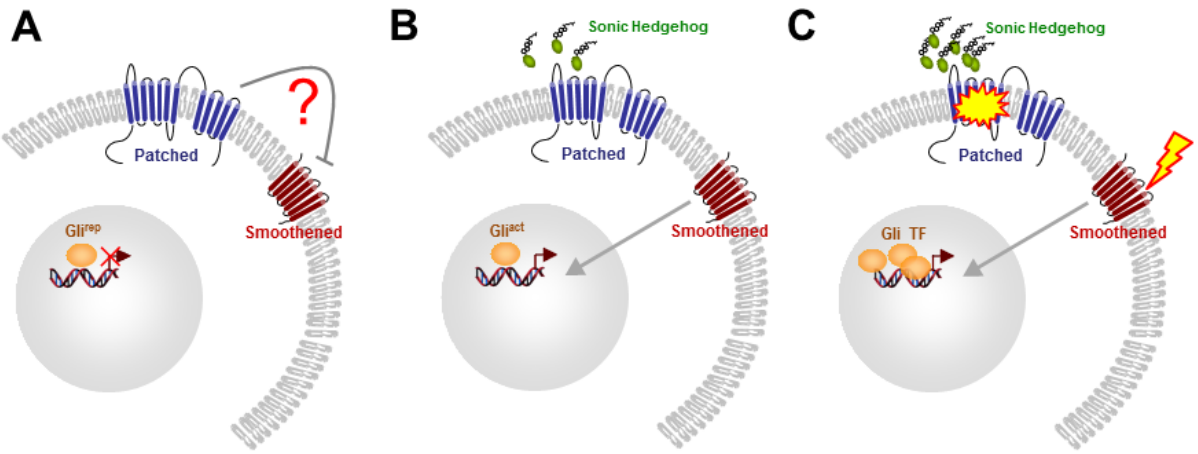

Figure 1: Schematic representation of the Hh signaling pathway. The figure shows a simplified model of the Hh pathway, displaying the four key components Patched (Ptch), Smoothened (Smo), Glioma-associated oncogene (Gli) and Sonic Hedgehog (Shh). **(A)** In the absence of its ligand Shh, the Ptch receptor inhibits its interaction partner Smo by an unknown, catalytic mechanism. This results in the inactivation or proteolytic cleavage of the Gli transcription factors (Gli TF) resulting in the formation of the Gli repressor forms (Gli^{rep}), which repress target gene expression. **(B)** Shh binding inhibits Ptch, which suspends the inhibition of Smo. Smo then activates a signaling cascade finally resulting in the activation or inhibition of the proteolytic cleavage of the Gli TF leading to the stabilization of Gli activator forms (Gli^{act}). This terminally leads to the translocation of the Gli TFs into the nucleus, where they induce target gene expression. **(C)** In cancer, Hh signaling can be misregulated by several mechanisms, including overexpression of Shh, inactivating mutations in Ptch, activating mutations in Smo or overexpression of the Gli TFs. Graphic modified from (Nitzki 2008).

2.2.1. The Ptch/Smo-Axis

A direct interaction of Ptch and Smo during Hh signaling has been excluded because a 1:45 ratio of Ptch to Smo expression constructs resulted in a nearly 80 % reduction of Smo activity, despite a great excess of Smo protein (Taipale *et al.* 2002). Thus, the Ptch/Smo interplay is rather based on a catalytic mechanism (Taipale *et al.* 2002) by which small-molecule signal transmitters are secreted in a Ptch-mediated manner that regulate Smo action (Bijlsma *et al.* 2006; Nachtergaele *et al.* 2012; Taipale *et al.* 2002). This hypothesis is strengthened by the structures of both proteins and the finding that several small molecules can bind to and modulate Smo action (see below).

The 12-transmembrane protein Ptch consists of two intracellular regions at the C- and N-terminus, two extracellular loops for Hh ligand binding (Briscoe *et al.* 2001) as well as a sterol-sensing-domain (SSD) in the transmembraneous region (Strutt *et al.* 2001). Interestingly, SSDs are usually found in proteins that are involved in sterol-level sensing (Kuwabara and Labouesse 2002) such as bacterial transporters of the resistance-nodulation-division (RND) family (Taipale *et al.* 2002) and the Niemann-Pick C1 disease protein (NP-C1) (Carstea *et al.* 1997; Loftus *et al.* 1997). In accordance with other proteins of the RND family Ptch also forms stable trimers (Lu *et al.* 2006). Moreover, Ptch is involved in cholesterol transport (Bidet *et al.* 2011). Thus, a function of Ptch as a small-molecule transporter seems reasonable. Nevertheless a distinct molecule that is released by Ptch and exerts Smo-modulating function has not been discovered so far.

The Ptch-interacting partner Smo (Fig. 2) belongs to the superfamily of G-protein coupled receptors (GPCR) (Wang *et al.* 2013) and contains a 7 transmembrane domain (7TM), an intracellular C-terminal tail (CTD, C-terminal domain) and an extracellular N-terminal region harboring a cysteine-rich-domain (CRD) (Nachtergaele *et al.* 2013; Nedelcu *et al.* 2013).

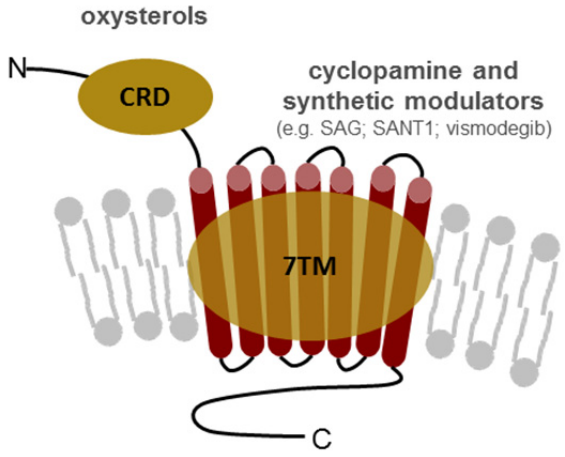

Figure 2: Schematic structure of Smo. The Smo protein consists of a C-terminal tail, a 7-transmembrane domain (7TM) and an N-terminal cysteine-rich domain (CRD). The 7TM contains the binding pocket for the majority of modulators like cyclopamine, the Smo agonist SAG, the Smo antagonist SANT1 or the FDA-approved drug for advanced BCC vismodegib (Chen *et al.* 2002a; Chen *et al.* 2002b; Wang *et al.* 2014). The CRD harbors the binding pocket for oxysterols like 20(S)-hydroxy cholesterol (McCabe and Leahy 2015; Nachtergaele *et al.* 2012; Nachtergaele *et al.* 2013; Nedelcu *et al.* 2013).

Several small-molecule modulators of Smo have been identified in the last years. The first discovered was the plant alkaloid cyclopamine (CP), a teratogen derived from the corn lily that inhibits Smo by binding to its 7TM (Chen *et al.* 2002a). This binding mechanism is employed by the majority of other Smo-modulators, which often are structurally related to sterols (reviewed in (Briscoe and Therond 2013)) such as the antagonists SANT-1 and SANT-2 (Ali *et al.* 2013), the FDA-approved drug for the treatment of advanced BCC vismodegib (Sekulic *et al.* 2012) and the Smo agonist SAG (Ali *et al.* 2013). Interestingly, the recent crystallization of the Smo heptahelical bundle with 5 modulators bound, including the above-mentioned drugs CP, SAG and SANT-1, showed that they all act on the same site (McCabe and Leahy 2015; Wang *et al.* 2014).

Additionally, the antifungal drug itraconazole (ITZ) inhibits Hh signaling at the level of Smo by a mechanism distinct from that of CP (Kim *et al.* 2010). It also has been published that it does not interact with the 7TM (Kim *et al.* 2010) or the CRD of Smo (Nachtergaele *et al.* 2012). In contrast, oxysterols, oxidized derivatives of cholesterol like 25-hydroxy cholesterol or 20(S)-hydroxycholesterol (20S)OHC, exclusively bind to the CRD of Smo and activate Hh signaling (Corcoran and Scott 2006; Dwyer *et al.* 2007; Michoel and Nachtergaele 2012; Nachtergaele *et al.* 2013; Nedelcu *et al.* 2013).

A recent study suggests that Ptch mediates the secretion of Smo-inhibitory 3β-hydroxysteroids, like 7-dehydrocholesterol (7-DHC) and vitamin D_3 ($vitD_3$). Interestingly, 7-DHC is the immediate precursor of $vitD_3$ (Bijlsma *et al.* 2006)(reviewed in (Albert and Hahn 2014; Roberg-Larsen *et al.* 2014)). Furthermore, $vitD_3$ effectively inhibits Hh signaling at the level of Smo, apparently by binding to the 7TM (Bijlsma *et al.* 2006; Tang *et al.* 2011). Recently, we showed that the secosteroid and hormonally active form of $vitD_3$, calcitriol ($1\alpha,25(OH)_2$-vitamin D_3), also inhibits Hh signaling *in vitro* and acts anti-tumorigenic *in vivo* by inhibiting Hh signaling also at level of Smo (Uhmann *et al.* 2011a; Uhmann *et al.* 2012). Importantly, calcitriol is active in the nanomolar range, whereas its progenitor vitD3 is needed at a 100-1,000-fold higher concentration (Bijlsma *et al.* 2006; Tang *et al.* 2011; Uhmann *et al.* 2011a).

2.2.2. The Gli-transcription factors

Structurally, all three mammalian Gli proteins contain a conserved DNA binding domain that recognizes the same *Gli binding site* (*GliBS*) (5'-GACCACCCA-3' (Hallikas *et al.* 2006; Winklmayr *et al.* 2010)), a C-terminal activation domain, and an N-terminal repressor domain in case of Gli2 and Gli3 (Briscoe and Therond 2013). In the inactive state of the Hh pathway Gli2 and Gli3 are proteolytically processed into N-terminal-truncated transcriptional repressors ($Gli2^{rep}$ and $Gli3^{rep}$) (Aberger *et al.* 2012; Roberg-Larsen *et al.* 2014). Upon Hh signaling activation (e.g. Shh binding to Ptch) Smo, probably indirectly, resolves the Gli-inhibitory complex, which results in accumulation of the Gli2 and Gli3 activator forms ($Gli2^{act}$ and $Gli3^{act}$) (Roberg-Larsen *et al.* 2014) and the transcription of target genes, including *Gli1* and *Ptch* (Ruiz i Altaba *et al.* 2007). Although the Gli proteins apparently have overlapping functions it is generally acknowledged that Gli2 mainly acts as a transcriptional activator whereas Gli3 mainly represses target gene expression (Briscoe and Therond 2013). The major target of the Hh pathway Gli1 seems to have only minor influence on the direct regulation of Hh target gene expression. It rather enhances the responses of the other Gli proteins (Briscoe and Therond 2013). Furthermore, it has been reported that Gli1 can regulate its own expression by activating $Gli3^{act}$ that is only a weak transcriptional activator by itself (Roberg-Larsen *et al.* 2014). Nevertheless, the balance of Gli^{act}/Gli^{rep}, referred to as the "Gli code", seems to be highly dependent on the cellular and species-specific context (Aberger and Ruiz 2014; Ruiz i Altaba *et al.* 2007) and can also be controlled independently of Smo by non-canonical regulation (Aberger and Ruiz 2014).

2.3.Vitamin D receptor signaling

$VitD_3$ is a steroidal hormone that is synthesized by keratinocytes in the skin via UV-B-mediated photo conversion of 7-DHC. Alternatively, it can be absorbed from dietary sources (e.g. fatty fish, liver cod oil), although this only accounts for a small amount (DeLuca 2004). Bound to vitamin D binding proteins (DBP) $vitD_3$ circulates through the body and is delivered to the liver where it is hydroxylated by the enzyme 25-hydroxylase (encoded by the gene *CYP27A1*) resulting in the formation of the major circulating form 25-hydroxy vitamin D_3 ($25(OH)D_3$) (Christakos *et al.* 2010). DBP-bound $25(OH)D_3$ is transported to the kidney where it is hydroxylated to calcitriol by the 1α-hydroxylase (encoded by the gene *CYP27B1*) (Chen *et al.* 2012; Christakos *et al.* 2010). Aside from the kidney, the 1α-hydroxylase is also present in a plethora of other tissues, including keratinocytes of the skin (Vantieghem *et al.* 2006). Therefore calcitriol-synthesis from its direct precursor $25(OH)D_3$ is not only possible in the kidney, but throughout most tissues of the body. The degradation of $25(OH)D_3$ and calcitriol is catalyzed by the 24-hydroxylase (encoded by the gene *CYP24A1*). Thus, the amount of calcitriol is limited by both calcitriol catabolism and decreased amounts of $25(OH)D_3$ available for calcitriol synthesis (Christakos *et al.* 2010; Deeb *et al.* 2007)(Fig. 3).

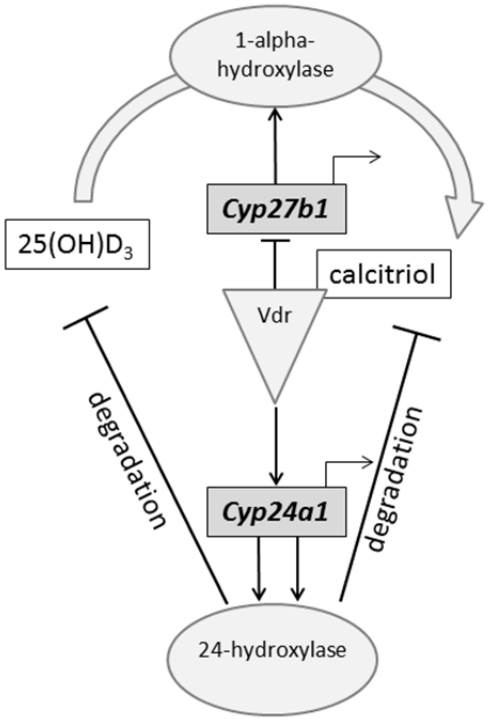

Figure 3: Schematic representation of the metabolism of calcitriol. Calcitriol (1α,25(OH)$_2$ vitamin D$_3$), the hormonally active form of vitamin D$_3$ (vitD$_3$) is synthesized from its progenitor 25-hydroxy vitamin D$_3$ (25(OH)D$_3$) by the enzyme 1α-hydroxylase, which is transcribed from the *Cyp27b1* gene. Upon binding of calcitriol to the vitamin D receptor (Vdr), the Vdr forms heterodimers with the retinoid-X-receptor α (RXRα) and the complex translocates into the nucleus (not depicted) and regulates gene expression. One negatively regulated target is the *Cyp27b1* gene, thus representing a negative feedback loop. One positively regulated target is the *Cyp24a1* gene. This gene encodes for the enzyme 24-hydroxylase, which can add a hydroxyl-group at the C24-position of both 25(OH)D$_3$ and calcitriol. This leads to the degradation of both compounds, thus, offering another negative feedback loop.

Calcitriol acts via the genomic and the non-genomic signaling pathways. The activity of both pathways is mediated by binding of calcitriol to the vitamin D receptor (Vdr). Non-genomic calcitriol signaling is mediated by a membrane-bound Vdr that leads, among others, to the accumulation of Ca^{2+} in the cells (Bikle 2011b). In contrast, genomic calcitriol signaling is mediated by an intracellular Vdr that form heterodimers with the retinoid X receptor α (RXRα) (MacDonald *et al.* 1993). This complex translocates to the nucleus and regulates target gene expression by binding to specific *vitamin D response elements (VDRE*) (Campbell *et al.* 2010; Haussler *et al.* 1998). *VDREs* can activate or inhibit target gene expression. Active genomic Vdr signaling inhibits the expression of genes for calcitriol synthesis (e.g. *CYP27B1*, (Takeyama *et al.* 1997)) and activates *Vdr* expression (Costa and Feldman 1987; Wiese *et al.* 1992) as well as the expression of genes responsible for calcitriol degradation such as *CYP24A1* (Ohyama *et al.* 1994). Thus, *CYP24A1* expression is widely

used as a surrogate marker for active Vdr signaling (Deeb *et al.* 2007; Haussler *et al.* 1998). The activation of genomic Vdr signaling also induces anti-tumorigenic effects, like inhibition of proliferation and stimulation of differentiation processes and apoptosis (Bikle 2011a; Bikle 2011b). Known target genes are cell cycle inhibitors like *CDKN1A* (encoding for cyclin-dependent kinase (CDK) inhibitor p21) or growth inhibitors like transforming growth factor β (*TGF-β*) (Bikle 2012; Deeb *et al.* 2007; Yang *et al.* 2001).

In fact, the anti-tumorigenic effects of vitD_3 are known for several decades. The first evidence came from a study in 1980, showing that increased sunlight exposure reduces the risk of colon cancer (Garland and Garland 1980). Subsequent studies revealed that low 25(OH)D_3 serum levels are associated with increased cancer risk and mortality (Deeb *et al.* 2007) and that calcitriol inhibits proliferation and induces differentiation of keratinocytes by changing the expression levels of Vdr target genes (Trump *et al.* 2010). Moreover *Vdr*$^{-/-}$ mice are prone to chemically induced tumorigenesis (Zinser *et al.* 2005; Zinser *et al.* 2002) indicating a tumor-preventive function of Vdr signaling. Interestingly, human BCCs as well as other human tumors frequently overexpress the *VDR* (Majewski *et al.* 1994; Shabahang *et al.* 1996) or the *CYP24A1* gene (Albertson *et al.* 2000).

Up to date several studies were conducted to analyze the anti-tumoral effects of calcitriol or synthetic derivatives. Indeed, calcitriol or synthetic derivatives can stimulate differentiation of leukemia cell lines (Munker *et al.* 1996; Tanaka *et al.* 1982). Additionally it can inhibit proliferation and induce cell cycle arrest of SCC cell lines *in vitro* and *in vivo* (Akutsu *et al.* 2001; Prudencio *et al.* 2001).

2.4.Crosstalk between Hh and Vdr Signaling

As mentioned above *Vdr*$^{-/-}$mice are prone to chemically induced carcinogenesis (Zinser *et al.* 2005; Zinser *et al.* 2002). Remarkably, the induced tumors overexpress key components of active Hh signaling like *Ptch* and *Gli1* (Teichert *et al.* 2011). Furthermore, human BCCs, which are characterized by constitutively active HH signaling, overexpress the *VDR* and *CYP24A1* genes (Mitschele *et al.* 2004)(reviewed in (Albert and Hahn 2014)). These findings are suggestive for a potential crosstalk between Hh and Vdr signaling. Other hints for a crosstalk of the two pathways came from the hereditary diseases Smith-Lemli-Opitz syndrome (SLOS), and the SLOS-like diseases lathosterolosis and desmosterolosis, which are caused by a defective cholesterol metabolism. SLOS is caused by mutations of the 7-

dehydrocholesterolreductase (*DHCR7*), which catalyzes the synthesis of 7-DHC, the direct precursor of vitD$_3$ (Cunniff *et al.* 1997; Opitz *et al.* 1987; Tint *et al.* 1994; Wassif *et al.* 1998), whereas lathosterolosis and desmosterolosis are caused by mutations in 3β-Hydroxysteroid-δ5-desaturase (*SC5D*) (Brunetti-Pierri *et al.* 2002) and 3β-Hydroxysterol-δ24-reductase (*DHCR24*) (FitzPatrick *et al.* 1998; Waterham *et al.* 2001), respectively. These enzymes are involved in cholesterol metabolism that can also lead to the synthesis of vitD$_3$ (Bijlsma *et al.* 2006; Porter and Herman 2011). Analyses of *Dhcr7*$^{-/-}$ and *Sc5d*$^{-/-}$ mice, SLOS-like disease models , demonstrated low cholesterol levels and/or accumulation of different metabolites in these animals in tissues and structures, which require functional Hh signaling (Bijlsma *et al.* 2006; Cooper *et al.* 2003; Cunniff *et al.* 1997; Opitz *et al.* 1987; Porter and Herman 2011; Tint *et al.* 1994; Wassif *et al.* 1998). Accordingly, mutations in the Hh signaling pathway lead to similar symptoms (Cooper *et al.* 2003; Porter 2006).

However, the exact crosstalk between Hh and Vdr signaling is still a topic with many open questions. Recently it has been demonstrated that Hh signaling is enhanced by cholesterol and that inhibition of Ptch upon Hh binding decreased the cellular cholesterol efflux (Bidet *et al.* 2011). Furthermore, oxysterols can mediate Smo activity by binding to its CRD (Corcoran and Scott 2006; Dwyer *et al.* 2007; Nachtergaele *et al.* 2012; Nachtergaele *et al.* 2013; Nedelcu *et al.* 2013). This led to the hypothesis that the Ptch/Smo interaction might involve oxysterols or sterol-like compounds. Moreover, 7-DHC and vitD$_3$ seem to be released from the cell in a Ptch-dependent manner and, strikingly, these molecules efficiently inhibit Hh signaling (Bijlsma *et al.* 2006). Accordingly, our lab showed that calcitriol also inhibits Hh signaling in murine mouse models for BCC and RMS (Uhmann *et al.* 2011a; Uhmann *et al.* 2012) and that this inhibition occurs independently of the Vdr and supposedly at the level of Smo (Uhmann *et al.* 2011a)(reviewed in(Albert and Hahn 2014)).

Due to the facts that a) Ptch shows similarities to oxysterol transporters (Carstea *et al.* 1997; Loftus *et al.* 1997), b) *Ptch*$^{-/-}$cells are unable to secrete Hh-inhibitory factors (Bijlsma *et al.* 2006; Uhmann *et al.* 2011a), c) Smo activity is controllable by oxysterols (Corcoran and Scott 2006; Dwyer *et al.* 2007; Nachtergaele *et al.* 2012) and that d) the natural occurring cholersterol-derivative calcitriol efficiently inhibits Hh signaling (this work and (Uhmann *et al.* 2011a; Uhmann *et al.* 2012)) we have speculated that calcitriol might be an endogenous mediator of the Ptch/Smo interaction and Smo inhibition.

3. Aim of the study

The main aim of this study was to unravel the interaction of the Hh and Vdr signaling pathways, to validate calcitriol-based therapies for the treatment of *Ptch*-associated BCCs in mouse models and to investigate the molecular basis for calcitriol-mediated Smo inhibition.

Based on the findings that the *VDR* is frequently upregulated in human BCCs the first goal was to investigate if *Vdr* expression is regulated by Hh signaling. Hence, *Gli3* was overexpressed in wt *Ptch* and *Ptch*$^{-/-}$ cells as well as in *Gli1/Gli2* double knockout cells (*Gli1*$^{-/-}$/*Gli2*$^{-/-}$) and the expression of the *Vdr* was quantified by real-time PCR. Additionally, luciferase reporter assays were performed to analyze if the Gli TFs regulate the expression of the *Vdr* promoter.

Previous data from our lab showed that calcitriol exhibits antitumoral potential and inhibits Hh signaling and tumor growth of *Ptch*-associated BCC and RMS. Thus, the second project focused on the enhancement of calcitriol-mediated anti-tumorigenic potential by combining calcitriol with the previously described Smo inhibitor family of azoles. As model systems the BCC cell line ASZ001, murine BCC-bearing skin biopsies and transgenic BCC-bearing mice were used.

Finally, we investigated whether calcitriol might represent a potential endogenous inhibitor of Hh signaling and analyzed the potential role of Ptch in calcitriol release and/or metabolism of calcitriol in wt *Ptch*, *Ptch*$^{-/-}$ and a *Ptch*-deficient BCC cell line from vitD_3 and 25(OH)D_3. Experimental procedures covered medium transfer experiments using reporter assays and mass spectrometry. Furthermore, the mode of action of calcitriol on Smo was investigated by performing functional and direct competition assay using other Smo modulators and mutant Smo variants.

4. Materials

4.1. Technical equipment

Table 1: List of laboratory equipment

Equipment	Supplier
(CO_2-) Incubator (6000, BBD 6220)	Kendro Laboratory Products GmbH, Hanau
1260 HPLC System	Agilent Technologies, Santa Clara, CA, USA
-80 °C Freezer (MDF-U71V)	Sanyo Electric Co., Ltd., Japan
8-well pipette	Costar, Corning Incorporated, Corning, USA
96-Well Tabless Tube Holder	Phenomenex Inc., Aschaffenburg
Accu-jet	Brand GmbH & Co. KG, Wertheim
Agarose gel electrophoresis chamber	Peqlab Biotechnology GmbH, Erlangen
Arium® 611 VF water purification system	Sartorius, Göttingen
Autoclave (sanoclav)	W. Krannich GmbH & Co. KG, Göttingen
Biophotometer (6131)	Eppendorf AG, Hamburg
Bunsen burner (Gasprofi 2 scs)	WLD-TEC GmbH, Göttingen
Centrifuges (Biofuge pico, fresco, primo, Multifuge 3LR)	Kendro Laboratory Products GmbH, Hanau, Germany
Clean bench (Euroflow Class IIA)	Clean Air Techniek bv, Woerden, Netherlands
Cold light source (KL 200)	Schott Glas, Mainz
Cryolys temperature controller	BERTIN Corp, MD, USA
Digital Monochrome Printer P91D	Mitsubishi, Ratingen
Digital Photocamera (PowerShot G2)	Canon Deutschland GmbH, Krefeld
FACScalibur	BD Biosciences GmbH, Heidelberg
Fluorchem Q	Fisher Scientific GmbH, Schwerte
Freezer (-20 °C)	Liebherr GmbH, Ochshausen
Fridge (4 °C)	Robert Bosch GmbH, Stuttgart
Heating block (Thermomixer)	Eppendorf AG, Hamburg
Heating stirrer (MR 3000/3001)	Heidolph Instruments, Schwabach
High-precision scales (Sartorius Basic plus)	Sartorius AG, Göttingen
Homogenizer (Miccra D-1)	ART Prozess- & Labortechnik GmbH & Co. KG, Müllheim
HTC-xt autosampler	CTC Analytics AG, Zwingen, Switzerland
Hybridization oven (HB-1000 Hybridizer)	UVP, Inc., Upland, USA
Inverse microscope with fluorescence filter (Axiovert 25, FilterSet 43, 01, 09)	Carl Zeiss Jena GmbH, Jena
Liquid nitrogen tank	L'air liquid S.A., Paris, France
LSR II	BD Biosciences GmbH, Heidelberg

Equipment	Supplier
Luminometer (Synergy Mx)	BioTek Instruments, Inc., Bad Friedrichshall
Mastercycler ep gradient S	Eppendorf AG, Hamburg
Mercury-short-arc lamp (HBO 50W/AC)	OSRAM AG, Munich
Microtome (HN 40)	New Brunswick Scientific GmbH, Nürtingen, Germany
MilliQ-Devices	Sartorius Stedim Biotech GmbH, Göttingen
Mini centrifuge	Carl Roth GmbH & Co. KG, Karlsruhe
Mr. Frosty™ Freezing Container	Thermo Fisher Scientific GmbH, Schwerte
Multipette	Eppendorf AG, Hamburg
Nitrogen-driven Positive Pressure-96 Processor	Water GmbH, Eschborn
One-channel pipettes	Eppendorf AG, Hamburg
Paraffin dispenser (Dispenser PAG 12)	MEDITE GmbH, Burgdorf
pH-meter (inoLab pH Level 1)	WTW GmbH, Vienna, Austria
PCR machine	Eppendorf, Hamburg
PCR-machine (PrimusHT)	MWG AG Biotech, Ebersberg
PCR-machine (Robocycler Gradient 96 Combo)	Stratagene, Amsterdam Zuidoost, Netherlands
Power supply for electrophoresis	Peqlab Biotechnology GmbH, Erlangen
Precellys 24 tissue homogenizer	BERTIN Corp, MD, USA
Qtrap5500 mass spectrometer	AB SCIEX, Framingham, MA, USA
Sequencer (ABI 3500 XL)	Life Technologies GmbH, Darmstadt
Shaking incubator	New Brunswick Scientific GmbH, Nürtingen
Shaking waterbath (1083)	GFL mbH, Burgwedel
Stereo microscope (Stemi 2000)	Carl Zeiss Jena GmbH, Jena
Sterile bench (Euroflow class IIA)	Clean Air Techniek bv, Woerden, Netherlands
Tank for liquid nitrogen	L'air liquid S.A., Paris Cedax, France
TaqMan (ABI Prism 7900HT)	Life Technologies GmbH, Darmstadt
Thermoprinter (DPU-414)	Eppendorf AG, Hamburg
Tissue embedding and rehydrating machine (TP 1020)	Leica Microsystems GmbH, Bensheim
Trans-Blot SD semi-dry transfer cell	Bio-Rad Laboratories GmbH, Munich
UV transilluminator	Intas Science Imaging Instruments GmbH, Göttingen
Vacuum pump	Schütt Labortechnik, Göttingen, Germany
Vortexer-Genie 2	Scientific Industries, Inc., Woburn, USA
Weighing scale (Sartorius Basic plus)	Sartorius AG, Göttingen
Xcell4 Surelock Midi-Cell	Invitrogen GmbH, Karlsruhe

4.2. Consumables

Table 2: List of consumable materials

Consumer good	Supplier
1.5 ml reaction tubes	Ochs GmbH, Bovenden/Lenglern
1.5 ml Safeseal Microtubes	Sarstedt AG & Co., Nürnberg
13 ml tubes	Sarstedt AG & Co., Nürnberg
15 ml tubes	Greiner Bio-One GmbH, Frickenhausen
2.0 ml reaction tubes	Sarstedt AG & Co., Nürnberg
384-well Optical Reaction Plate	Life Technologies GmbH, Darmstadt
50 ml tubes	Greiner Bio-One GmbH, Frickenhausen
96-Well Assay Plate	Costar, Corning Incorporated, Corning, USA
96-Well Optical Reaction Plate	Life Technologies GmbH, Darmstadt
Balance oeco multi-function paper	inapa tecno, Hamburg
BD Discardit™ II (2, 10, 20 ml)	BD Biosciences GmbH, Heidelberg
BD Microfine + Demi	BD Biosciences GmbH, Heidelberg
BD Plastipak	BD Biosciences GmbH, Heidelberg
BD Plastipak 1 ml Sub-Q	BD Biosciences GmbH, Heidelberg
Blotting paper (GB 33 B003)	Heinemann Labortechnik GmbH, Duderstadt
Cell culture dishes, 35 mm, 50 mm, 100 mm (Nunclon Surface)	Nunc GmbH & Co.KG, Wiesbaden
Cell scraper	Sarstedt AG & Co., Nürnberg
Coverslips	Menzel GmbH & Co.KG, Braunschweig
Cryo Pure	Sarstedt AG & Co., Nürnberg
Cuvettes (UVette)	Carl Roth GmbH & Co. KG, Karlsruhe
Disposable needles (Sterican Ø 0,45 x 12 mm)	B. Braun Medical AG, Emmenbrücke, Germany
Eppendorf Combitips Plus/Advanced (0.2, 0.5, 2.5, 5, 10, 25, 50 ml)	Eppendorf AG, Hamburg
Filter tips (10 µl)	Sarstedt AG & Co., Nürnberg
Filter tips (100 µl, 200 µl, 1000 µl)	Kisker Biotech GmbH & Co. KG, Steinfurt
Flow Cytometry Tube	Sarstedt AG & Co., Nürnberg
Fluted filters	Sartorius AG, Göttingen
Framestar 384	4titude Ltd., Berlin
Glassware	Schott AG, Mainz
Hyperfilm ECL	Amersham Biosciences Europe GmbH, Freiburg
Milliporefilter (Nuclepore Track-Etch Membran)	Whatman GmbH, Dassel
Miscroscope slides (SuperFrost Plus)	Menzel GmbH & Co.KG, Braunschweig
MultiScreenHTS-HV plate	Millipore GmbH, Schwalbach am Taunus
Neubauer counting chamber	Brand GmbH & Co KG, Wertheim
Nitrocellulose membrane(Hybond ECL)	GE Healthcare Europe GmbH, Freiburg

Consumer good	Supplier
NuPAGE Novex 4 – 12 % Bis-Tris Midi Gel	Invitrogen GmbH, Karlsruhe
Pasteur pipettes	Brand GmbH & Co.KG, Wertheim
PCR-Reaction tubes (ThermoFast 96, nonskirted, natural domed cap strips)	Sarstedt AG & Co., Nürnberg
Petri dishes	Ochs GmbH, Bovenden/Lenglern
Pipette tips (10 µl, 200 µl)	Ochs GmbH, Bovenden/Lenglern
Pipette tips (1000 µl)	Sarstedt AG & Co., Nürnberg
Pipette tips (20 µl)	Sarstedt AG & Co., Nürnberg
Precellys ceramic kit 1.4/2.8 mm 2.0 ml tubes	BERTIN Corp, MD, USA
QPCR Adhesive Clear Seal	4titude Ltd., Berlin
Scalpel blade #10, #24	Aesculap AG & Co.KG, Tuttlingen
Serological pipettes (2 ml, 5 ml, 10 ml, 25 ml, 50 ml)	Sarstedt AG & Co., Nürnberg
SOC Medium	Invitrogen GmbH, Karlsruhe
Strata-X 33 µm polymeric reversed phase (30 mg/ml) tubes	Phenomenex, Aschaffenburg
Sterile filter	Omnilab-Krannich, Göttingen
Terumo Syringe 30, 50 ml	Terumo Medical Corp., Elkton, MD, USA
Tissue Culture Plate 24-Well	Sarstedt AG & Co., Nürnberg
Tissue Culture Plate 6-Well	Sarstedt AG & Co., Nürnberg

4.3. Reagents and chemicals

The chemicals not listed below were purchased from AppliChem GmbH, Darmstadt, Carl Roth GmbH & Co. KG, Karlsruhe, or from Sigma-Aldrich Chemistry GmbH, Steinheim.

Table 3: List of used reagents and chemicals

Chemicals and reagnets	Supplier
0.9 % NaCl Solution	B. Braun Melsungen AG, Melsungen
25-hydroxy vitamin D_2 [25,26,27-$^{13}C_3$]	Cambridge Isotope Laboratories, Andover, MA, USA
50 bp, 100 bp plus and 1 kb DNA Ladder	Fermentas GmbH, St. Leon-Rot
Agarose	Bio-Budget Technologies GmbH, Krefeld
Ampuwa	Fresenius Kabi Deutschland GmbH, Bad Homburg,
Boric acid	MP Biomedicals LLC, Illkirch, France
Deoxyribonucleotide triphosphate (dNTP)	Roche Diagnostics GmbH, Mannheim
Dithiotreitol, 100mM (DTT)	Invitrogen GmbH, Karlsruhe
DNase/Rnase-free water	GIBCO Invitrogen GmbH, Karlsruhe
Ethidium bromide (0.07 %)	inna-TRAIN-Diagnostics, Kronberg
EtOH 99 %	J.T. Baker B.V., Deventer, Netherlands
EtOH 99 % denatured	CVH Chemie-Vertrieb GmbH & Co. Hannover KG, Hannover
Formamide	Acros Organics b.v.b.a, Geel, Belgium
Glycergel mounting medium	Dako GmbH, Hamburg
Hematoxiline MAYER	Medite GmbH, Burgdorf
Ketanest S	Pfizer Pharma GmbH, Karlsruhe
Matrigel	BD Biosciences GmbH, Heidelberg
NBT/BCIP	Roche Diagnostics GmbH, Mannheim
NuPAGE MES SDS Running Buffer, 20 x	Invitrogen GmbH, Karlsruhe
PBS-Tablets	GIBCO Invitrogen GmbH, Karlsruhe
Pertex mounting medium	Medite Medizintechnik GmbH, Burgdorf
Ringer Lactate	B. Braun Melsungen AG, Melsungen
RNase-, DNase free destilled water	GIBCO Invitrogen GmbH, Karlsruhe
Rompun (Xylazin 2 %)	Bayer AG, Leverkusen
SeeBlue® Plus2 Pre-Stained Standard	Invitrogen GmbH, Karlsruhe
Sporanox	Sporanox, Eurim-Pharm Arzneimittel GmbH
TRIzol Reagent	Invitrogen GmbH, Karlsruhe
Xylene	J.T. Baker B.V., Deventer, Netherlands

4.4. Kits and ready-to-use reaction Systems

Unless stated otherwise, all kits and ready-to-use reaction systems were used as described in manufacturer's instructions.

Table 4: List of kits and ready-to-use reaction systems

Reaction system	Supplier
Amersham ECL Plus™ Western Blotting Detection Reagents	GE Healthcare Europe GmbH, Freiburg
BigDye Terminator v3.1 Cycle Sequencing kit	Life Technologies GmbH, Darmstadt
Cell Proliferation ELISA, BrdU (chemiluminscent)	Roche Diagnostics GmbH, Mannheim
Dual-Luciferase® Reporter Assay System	Promega GmbH, Mannheim
Pierce BCA Protein Assay kit	Fisher Scientific GmbH, Schwerte
Platinum SYBR Green qPCR SuperMix-UDG with ROX	Invitrogen GmbH, Karlsruhe, Germany
PureLink®HiPure Plasmid Filter Midiprep kit	Invitrogen GmbH, Karlsruhe
PureLink®HiPure Plasmid Midiprep	Invitrogen GmbH, Karlsruhe
QIAEX II Gel Extraction kit	Qiagen GmbH, Hilden
QuantiTect SYBR Green RT-PCR	Qiagen GmbH, Hilden
Quikchange II Site-Directed Mutagenesis kit	Agilent Technologies, Santa Clara, CA, USA
Quikchange II XL Site-Directed Mutagenesis kit	Agilent Technologies, Santa Clara, CA, USA
RNeasy Fibrous Tissue kit	Qiagen GmbH, Hilden
Roti-Fect transfection reagent	Carl Roth GmbH & Co. KG, Karlsruhe
SuperScriptII® Reverse Transcriptase	Invitrogen GmbH, Karlsruhe
MolTaq Taq-Polymerase	Molzym GmbH & Co. KG, Bremen
TRIzol reagent	Life Technologies GmbH, Darmstadt

4.5. Buffers and solutions

Unless mentioned otherwise, all solutions were prepared using double distilled water (ddH_2O).

Table 5: List of buffers and solution and their composition

Buffer	Composition
6 x SDS loading buffer	35 % (v/v) Glycerol
	9 % (w/v) SDS
	8.5 % (w/v) DTT
	0.1 % (w/v) Bromphenolblue
	in Upper gel buffer
Blotting buffer	6 % (w/v) tris
	3 % (w/v) glycin
	0.075 % (w/v) SDS
	20 % (v/v) methanol

Buffer	Composition
Citric Acid buffer, pH6	10 mM sodium citrate pH 6.0
Cresol	0.1 % (w/v) Cresol
	Saturated sucrose solution
Eosin, 1%	1 % (w/v) Eosin y (water soluble)
	80 % (v/v) ethanol
LB-agar	LB-medium
	1.5 % (w/v) agar
Lysis buffer	30 mM tris/HCl, pH 8.8
	150 mM NaCl
	1 % (v/v) triton X-100
	10 % (v/v) glycerol
	Protease and phosphatase inhibitors (1 tablet/50 ml)
	500 µM PMSF (added before use)
	2 mM DTT (added before use)
Lysogeny broth medium (LB-medium)	1 % (w/v) bacto-tryptone
	0.5 % (w/v) yeast extract
	1% (w/v) NaCl (pH7.0)
Paraformaldehyde	4 % (w/v) paraformaldehyde
	1 x PBS
PBS (cell culture)	1 PBS tablet ad 500 ml ddH_2O
Phosphate buffered saline solution, 10x, pH 7,4 (PBS, stock solution)	1.4 M NaCl
	27 mM KCl
	15 mM KH_2PO4
	65 mM Na_2HPO_4
Proteinase K	50 mM tris/HCl pH 8.0
	5 mM EDTA
	40 µg/ml proteinase K
RIPA-buffer (modified)	50 mM tris/HCl, pH7.4
	150 mM NaCl
	1 mM EDTA
	1 % (v/v) Nonidet NP-40
	0.25 % (w/v) Na-deoxycholate
	Protease and phosphatase inhibitors (1 tablet/10 ml)
STE-Buffer	50 mM tris/HCl pH 8.0
	100 mM NaCl
	1 mM EDTA
	1% (w/v) SDS
Tris-boric acid-EDTA solution, 10x (TBE; stock solution)	890 mM tris/HCl pH 8.0
	730 mM boric acid
	12.5 mM EDTA

Buffer	Composition
Tris-buffered saline solution, 10x (TBS; stock solution)	0.5 M tris/HCl pH 7.4
	1.5 M NaCl
Upper gel buffer	6 % (w/v) tris , pH 6.8
	4 % (v/v) SDS

4.6. Media

4.6.1. Media and agar plates for culture of prokaryotic cells

LB medium and LB agar plates were prepared as described in table 5. After autoclaving and cooling to 55°C either 50 µg/ml ampicillin (Carl Roth GmbH, Karlsruhe) or 25 µg/ml kanamycin (Carl Roth GmbH) were added. Both, media and plates, were stored at 4°C.

4.6.2. Media and reagents for culture of eukaryotic cells

Cell culture media and supplements for culture of eukaryotic cell lines are listed in table 6.

Table 6: Cell culture media and supplements for culture of eukaryotic cell lines

Medium or reagent	Supplier
154CF medium	Gibco, Invitrogen GmbH, Karlsruhe
Blasticidin S hydrochloride (3 mg/ml)	Sigma-Aldrich Chemistry GmbH, Steinheim
DMEM phenol-red free	Gibco, Invitrogen GmbH, Karlsruhe
Dulbecco's Modified Eagle Medium (DMEM)	Gibco, Invitrogen GmbH, Karlsruhe
F12 Nutrient Mix(Ham)	Gibco, Invitrogen GmbH, Karlsruhe
Fetal calf serum (FCS)	PAN Biotech GmbH, Aidenbach
G 418 disulfate salt solution (50 mg/ml)	Sigma-Aldrich Chemistry GmbH, Steinheim
Penicillin (10.000 U/ml)/streptomycin (10 mg/ml) (P/S)	PAN Biotech GmbH, Aidenbach
Puromycin dihydrochloride (10 mg/ml)	Sigma-Aldrich Chemistry GmbH, Steinheim
S.O.C. medium	Invitrogen GmbH, Karlsruhe
Sodium butyrate (100 mg/ml)	Invitrogen GmbH, Karlsruhe
Tetracycline (10 mg/ml)	Invitrogen GmbH, Karlsruhe
Trypsin/EDTA and TrypLE Express	Gibco, Invitrogen GmbH, Karlsruhe
Zeocin™ Selection Antibiotic (100 mg/ml)	Life Technologies GmbH, Darmstadt

4.7. Biological material

4.7.1. Bacterial strains and growth

For transformation and amplification of plasmid DNA chemical competent *Escherichia coli* (*E. coli*) strain DH5α (Invitrogen GmbH, Karlsruhe) was used. For transformation after site-directed mutagenesis (see chapter 5.1.3.6) *E. coli* XL-10 gold were used (Agilent technologies, included in the Quikchange II and Quikchange II XL-site directed mutagenesis kits).

4.7.2. Eukaryotic cell lines

The cell lines used in this thesis are listed in table 7.

Table 7: List of the eukaryotic cell lines, media, supplements and references

Name	Description	Culture medium	Supplements	Reference
ASZ001	Murine BCC cell line	154CF	2 % chelexed FCS, 1 % PS, 0.05 mM $CaCl_2$	(So *et al.* 2006)
Gli1$^{-/-}$ *Gli2*$^{-/-}$	MEF	DMEM (+++)	10 % FCS, 1 % PS	(Lipinski *et al.* 2008)
HaCaT	Human keratinocyte cell line	DMEM (+++)	10 % FCS, 1 % PS	(Boukamp *et al.* 1988)
HEK293	Human embryonic kidney cell line	DMEM (+++)	10 % FCS, 1 % PS	ATCC LGC Promochem, Wesel; CRL-1573
HEK293S	Tetracycline-inducible Smo-overexpressing HEK cells	DMEM/F12*	10 % FCS, 1 % PS, 2µg/ml G418, 5 µg/ml Blasticidin	(Dwyer *et al.* 2007)
HEK293Shh	Shh-N secreting HEK cells	DMEM (+++)	10 % FCS, 1 % PS, 0.4 mg/ml G418	(Chen *et al.* 2002b)
NIH/3T3	Adult, murine fibroblast cell line	DMEM (+++)	10 % FCS, 1 % PS	ATCC LGC Promochem, Wesel; CRL-1658
Platinum E	Packaging cell line for viral transduction	DMEM (+++)	10 % FCS, 1 % PS, 10 µg/ml blasticidin, 1 µg/ml puromycin	(Morita *et al.* 2000)
Ptch$^{-/-}$	Ptch-deficient adult, murine fibroblast	DMEM (+++)	10 % FCS, 1 % PS	(Uhmann *et al.* 2011a)
Shh light II	NIH/3T3 stably transfected with Gli-responsive luciferase-reporter	DMEM (+++)	10 % FCS, 1 % PS, 0.4 µg/ml G418, 0.15 mg/ml Zeocin	(Chen *et al.* 2002b)
Shh light II mSmo^{wt} mCherry	mSmo^{wt}-overexpressing Shh light II	DMEM (+++)	10 % FCS, 1 % PS, 0.4 µg/ml G418, 0.15 mg/ml Zeocin, 2 µg/ml puromycin	this work

Name	Description	Culture medium	Supplements	Reference
Shh light II mSmo$^{\Delta CRD}$ mCherry	mSmo$^{\Delta CRD}$-overexpressing Shh light II	DMEM (+++)	10 % FCS, 1 % PS, 0.4 µg/ml G418, 0.15 mg/ml Zeocin, 2 µg/ml puromycin	this work
Smo$^{-/-}$	Smo-deficient MEFs	DMEM (+++)	10 % FCS, 1 % PS	(Ma *et al.* 2002)
Smo$^{-/-}$ mSmo^{wt} mCherry	mSmo^{wt}-overexpressing Smo$^{-/-}$	DMEM (+++)	10 % FCS, 1 % PS, 2 µg/ml puromycin	this work
Smo$^{-/-}$ mSmo$^{\Delta CRD}$ mCherry	mSmo$^{\Delta CRD}$-overexpressing Smo$^{-/-}$	DMEM (+++)	10 % FCS, 1 % PS, 2 µg/ml puromycin	this work
wt *Ptch*	Adult, murine fibroblast; parental cell line of Ptch$^{-/-}$	DMEM (+++)	10 % FCS, 1 % PS	(Nitzki *et al.* 2010)

*: 1:1 mixture of DMEM (+++) and F12 nutrient mixture (Ham), FCS: fetal calf serum, PS: penicillin/streptomycin. (+++): supplemented with 4.5g/l D-Glucose, L-glutamine and Sodium pyruvate; MEF: murine embryonic fibroblasts

4.7.3. Mouse lines

The inbred C57BL/6N mice were bred in-house or purchased from Charles River Laboratories, Sulzfeld. Nude mice (NMRI-*Foxn1*^{nu}) were bred in-house or purchased from the department hematology and oncology, University medical center, Göttingen. *Ptch*$^{flox/flox}$ *CreERT2*$^{+/-}$ mice were bred as described in (Uhmann *et al.* 2007). *Ptch*$^{flox/flox}$ mice have *loxP* sites in *Ptch* introns 8 and 9 that can be recognized by Cre-recombinase (Uhmann *et al.* 2007). *R26RCreERT2* mice express a tamoxifen-inducible Cre-recombinase under the control of the ubiquitous *Rosa26*-promoter (Soriano 1999). Initially, the mice were on mixed C57BL/6N x BALB/c background (Uhmann *et al.* 2007; Uhmann *et al.* 2011a), but backcrossed to a more pure C57BL/6N background (this thesis).

4.8. Synthetic DNA-oligonucleotides

Synthetic DNA-oligonucleotides were purchased from Eurofins MWG Operon, Ebersberg and a 100 µM stock solution in ddH_2O was prepared for long-term storage at -80°C. Unless mentioned otherwise 10 µM working solution were used for PCR methods.

The following oligonucleotides were used for the genotyping of transgenic mice (table 8). The specific PCR-protocols are listed in chapter 5.1.2.2.

Table 8: Gene-specific DNA-oligonucleotides (primers) for mouse genotyping

Genotype	Primer name	Amplification product	Primer sequence (5'-3' orientation)	Reference
Ptch$^{flox/+}$	mPTCwt_R.2	445 bp^{wt}	ACACAACAGGGTGGAGACCACT	(Uhmann *et al.* 2007)
	mPTCNx_f	150 bp^{flox}	TGGTAATTCTGGGCTCCCGT	
	mPTCNx_r		CCGGTAGAATTAGCTTGAAGTTCCT	
Ptch^{del}	Exon 7-F	950 bp^{del}	AGGAAGTATATGCATTGGCAGGAG	(Uhmann *et al.* 2007)
	Neo-R		GCATCAGAGCAGCCGATTGTCTG	
CreERT2	Ella-Cre-F	600 bp	CCAGGCTAAGTGCCTTCTCTACA	(Uhmann *et al.* 2007)
	Ella-Cre-R		AATGCTTCTGTCCGTTTGCCGGT	

flox: floxed *Ptch*-locus, del:*Ptch* locus after after Cre-mediated recombination, wt: wildtype allele.

The following primer pair was used to amplify the *Gapdh* gene as a quality control after cDNA synthesis.

Table 9: List of primers used for semiquantitative RT-PCR

Application	Primer name	Primer sequence (5'-3' orientation)
murine *Gapdh* expression analysis	Gapdh-F	ATCTTCTTGTGCAGTGCCAG
	Gapdh-R	ATGGCATGGACTGTGGTCAT

The following oligonucleotides were used for quantification of gene expression levels by qRT-PCR (quantitative *real-time* PCR).

Table 10: List of primers used for qRT-PCR

cDNA	Primer name	Primer sequence (5'-3' orientation)	Reference
murine *Gli1*	mGli1-tq-f mGli1-tq-r	TACATGCTGGTGGTGCACATG ACCGAAGGTGCGTCTTGAGG	(Ecke *et al.* 2008)
murine *18S*-rRNA	18S-fwd 18S-rev2	CGCAAATTACCCACTCCCG TTCCAATTACAGGGCCTCGAA	(Nitzki *et al.* 2010)
murine *Cyp24a1*	Cyp24a1-F Cyp24a1-R	GTGTGGCAAGCGCACACGCT CCGTGACAGCAGCGTACAGT	(Uhmann *et al.* 2011a)
murine *Gli2*	Gli2-RT-PCR-F Gli2-RT-PCR-R	GGTCATCTACGAGACCAACTGC GTGTCTTCAGGTTCTCCAGGC	(Uhmann *et al.* 2011b)
murine *Gli3*	Gli3F2 Gli3-sybrgree R	GAAGGAACAACCCTAGTCAAGGAGGA CCAGCGGCACACGAACTCCTTCT	(Fritsch 2014)
murine *Vdr*	Vdr-F Vdr-R2	AGAACATGTGCTGCTCATGGC TCATCTTGGCGTAGAGCTGGTTGGCT	(Uhmann *et al.* 2011a)
murine *Involucrin*	Ivl-1-F1 Ivl-1-R1	CCTCCTGTGAGTTTGTTTGGTCT CTGAGGATATGATCTGGAGAAC	this work
murine *K1*	mK1-F mK1-R	TCAACGTTGAGGTTGACCCTC ACCTTCCTTCTGAGGATGCTG	(Nitzki *et al.* 2010)
murine *K10*	mK10-F mK10-R	GGATGCTGAAGAGTGGTTCAA TCTGTTTCTGCCAAGGAGGCT	(Nitzki *et al.* 2010)
murine *Loricrin*	Lor-F1 Lor-R1	CACTCATCTTCCCTGGTGCTTC GTCTTTCCACAACCCACAGGAG	this work
murine *Mdr1a*	Mdr1a-F Mdr1a-R	GAAGAGGACCTTAAGGGAAGAGC CTGTCCAGCCAACCTGCATAACG	this work
murine *Mdr1b*	Mdr1b-F Mdr1b-R	CCCTCTTGATGCTGGTGTTTGG GCAACTATGAGCACACCAGCACC	this work
murine *Mdr2*	Mdr2-F Mdr2-R	GAGGCAGCGAGAAACGGAACAG GAGCTATGGCCATGAGGGTGC	this work
murine *Hprt*	mHPRT-Fw-Q mHPRT-Rev-Q	AGCCCCAAAATGGTTAAGGTTGC TTGCAGATTCAACTTGCGCTCAT	this work
murine *TBP*	mTBP-Q-Fw mTBP-Q-Rev	CACCAATGACTCCTATGACCCCTA CAGTTGTCCGTGGCTCTCTTATTC	this work

The following oligonucleotides were used to generate and verify the plasmids *pMSCVmSmo*^{wt} and *pMSCVmSmo*$^{\Delta CRD}$ via Sanger sequencing. The primer mSmo_D54_F has been described in (Nedelcu *et al.* 2013).

Table 11: Primers used to generate and sequence the *pMSCV* mSmo plasmids

Application	Primer name	Primer Sequence (5'-3' orientation)
amplification of mSmo from pHAGE mSmo mCherry overlap-extension PCR	SmoKlon1AF	CGCCATCCACGCTGTTTTGACCTCCATTC
PCR-based amplification of mSmo from pHAGE mSmo mCherry overlap-extension PCR	SmoKlon 1BF	GTACTGCTGGGCCAAACGAGGTAC
Mutagenesis of pMSCV mSmoW113Y to mSmowt	CRD_mut_F2	CGGCAAGCTCGTGCTCTGGTCCGGCCTC
	CRD_mut_R2	GAGGCCGGACCAGAGCACGAGCTTGCCG
frameshift-repair of pMSCV mSmoDeltaCRD_shift	CRD_Ins_1636_F	GCTGGTACTGCTGGGGCCAAACGAGGTAC
	CRD_Ins_1636_R	GTACCTCGTTTGGCCCCAGCAGTACCAGC
Sanger sequencing	mSmo_D54_F	CTCGAGGAGGGACGTGCCGG
	SmoCRD_R	CACGTCCTCATACCAGCTCTTGGG
	SmoKlon 1BF2	CCAAACGAGGTACAAAACATCAAG
	SmoKlon_Seq_F	CACCTTCAGCTGCCACTTCTATGAC
	SmoKlon_Seq_F3	GCCTCAGCTTTTGCTGAGTTGGC
	SmoKlon_Seq_F5	GATCCATTTCTCCCTGGTGCCTC
	SmoKlon_SeqChe1	CGAGGGCTTCAAGTGGGA
	SmoKlon_SeqChe3	CCTCCCACAACGAGGACTACA

4.9. Plasmids

The following plasmids were either used for transfection of eukaryotic cells or served as basis for new plasmids. For details see respective chapters.

Table 12: Plasmids

Name	Application	Supplier/Reference
pCMV/SV-Flag1-mGli2	Overexpression of *Gli2*	(Hui and Angers 2011)
pCMV-AD-VDR	Part of VDR/RXRα-heterodimerization assay	(Jacobs *et al.* 2013)
pCMV-BD-RXRα	Part of VDR/RXRα-heterodimerization assay	(Jacobs *et al.* 2013)
pCR 3.1-mGli1	Overexpression of *Gli1*	(Fritsch 2014)
pCR 3.1-mGli3	Overexpression of *Gli3*	(Fritsch 2014)
pCR3.1	Control plasmid	Invitrogen GmbH, Karlsruhe
pEGFP-N1	Transfection efficiency	BD Bioscience Clontech, Heidelberg
pFR-Luc	Part of VDR/RXRα-heterodimerization assay	Agilent Technologies, Santa Clara, USA
pGL-TK	Positive control for transient luciferase-assays	Promega GmbH, Mannheim
pHAGEmSmo(W113Y) mCherry	Subcloning of mSmo-cherry	(Nedelcu *et al.* 2013)
pMSCV mSmo^{W113Y}	Basis of mSmo variants	this work
pMSCV mSmo^{wt}	Stable overexpression of *mSmo^{wt}*	this work
pMSCV mSmo$^{\Delta CRD}$	Stable overexpression of *mSmo$^{\Delta CRD}$*	this work
pMSCVpuro	Backbone for *pMSCV mSmo* variants	Clontech Laboratories, Inc., Mountain View, USA
pVdrProm^{wt}	Vdr-promoter analysis	(Jehan and DeLuca 2000)
pRL-CMV	Part of VDR/RXRα-heterodimerization assay	Promega GmbH, Mannheim

4.10. Antibodies

All antibodies were stored as described in the manufacturer's instruction and diluted as described in the following table.

Table 13: List of antibodies, application and appropriate dilutions

Immunohistochemistry		
primary antibody	**dilution (diluent)**	**antigen retrieval**
mAb mouse anti-Ki-67, BD Pharmingen	1:50 (TBS)	citric acid pH 6; heat mediated
secondary antibody	**dilution (diluent)**	
En vision+ anti- rabbit/mouse/HRP*; Dako K5007	undiluted	
Western Blot		
primary antibody	**dilution**	**blocking reagent**
mouse anti-HSC70, Santa Cruz (B-6, sc-7298)	1:10,000	5 % (w/v) milkpowder in TBS-tween
Rabbit anti-c-myc, Santa Cruz (A14)	1:100	5 % (w/v) milkpowder in TBS-tween
secondary anitbody	**dilution**	**diluent**
goat anti-rabbit IgG, HRP-conjugated, Sigma-Aldrich (A0545,)	1:5,000	5 % (w/v) milkpowder in TBS-tween
Sheep anti-mouse/HRP, GE Healthcare (NA931)	1:5,000	5 % (w/v) milkpowder in TBS-tween

4.11. Software

The following softwares were licensed and, if possible, used in the most recent version.

Table 14: List of used software

Name	Developer/Reference
Adobe Photoshop CS5	Adobe Systems Incorporated, San Jose, USA
Analyst 1.6	AB SCIEX, Framingham, USA
BD FACSDiva	Becton Dickinson GmbH, Heidelberg
BioEdit	Ibis Biosciences, Carlsbad, USA
Cell F	Olympus Europa GmbH, Hamburg, Germany
CompuSyn	(Chou 2005)
Endnote X5	Thomson ISI ResearchSoft , California, USA
Fiji	(Schindelin *et al.* 2012)
FlowJo	Tree Star Inc., Oregon, USA
GraphPad Prism 6	GraphPad Software, Inc., La Jolla, CA, USA
Intas GDS	Intas Science Imaging Instruments GmbH, Göttingen
Gen5 1.11	BioTek Instruments, Inc., Bad Friedrichshall
MatInspector	(Quandt *et al.* 1995)
Microsoft Office	Microsoft Co., Redmont, USA
SDS 2.2	Applied Biosystems, Darmstadt
Sequencing Analysis Software v5.4	Applied Biosystems, Darmstadt
SnapGene Viewer	GSL Biotech (snapgene.com)

4.12. Databases

The following databases were used to retrieve data.

Table 15: List of databases

MGI_3.43-mouse genome informatics	http://www.informatics.jax.org/
National Center for Biotechnology Information	http://www.ncbi.nlm.nih.gov/
Ensembl	http://www.ensembl.org/index.html
BasicLocalAlignmentSearchTool_BLAST (NCBI)	http://blast.ncbi.nlm.nih.gov/Blast.cg

5. Methods

5.1. Molecular biology methods

5.1.1. Nucleic acid isolation

5.1.1.1. Small-scale plasmid purification

For small-scale plasmid purification the buffer system of the PureLink®HiPure Plasmid Midiprep or PureLink®HiPure Plasmid Filter Midiprep kits was used. 1.5 ml of a bacterial overnight (O/N) culture was transferred to a 1.5 ml reaction tube and the cells were pelleted by centrifugation for 30'' at 13,000 rpm. The supernatant was discarded, the pellet was resuspended in 200 µl buffer R3 supplemented with RNase (see chapter 5.1.1.3) and vortexed in short pulses until it was visibly homogeneous. After the addition of 200 µl buffer L7 the sample was incubated for 5' at room temperature (RT). Hereafter, 200 µl buffer N3 were added and the sample was inverted until the solution was homogeneous. The cell debris was pelleted by centrifugation at 13,000 rpm for 10' and 500 µl of the supernatant was transferred to a new 1.5 ml reaction tube containing 1 ml 99 % EtOH. The DNA was precipitated at -20°C for 1 h and pelleted by centrifugation for 30' at 13,000 rpm at 4°C. The pellet was washed with 70 % ethanol (EtOH), centrifuged for 10' at 13,000 rpm and dried at 55°C for 10' and finally resuspended in sterile-filtered DNase-free ddH_2O in an appropriate volume (50-100 µl) for 10' at 42°C and 1,400 rpm on a heating block.

5.1.1.2. Medium-Scale Plasmid Purification

Medium-scale plasmid purifications were performed using the PureLink®HiPure Plasmid Midiprep or PureLink®HiPure Plasmid Filter Midiprep kit according to the manufacturer's instructions. The plasmid DNA was solved in sterile-filtered DNase-free ddH_2O. To increase plasmid purity an additional precipitation step was performed. Hence, the plasmid DNA was diluted to a final volume of 500 µl and either 1 volume-unit isopropyl-alcohol or 2.5 volume units 99 % EtOH were added. After thorough mixing by inverting, the DNA was precipitated O/N at -20°C and pelleted by centrifugation at 13,000 rpm for 30'. The pellet was washed, dried and resuspended as described in chapter 5.1.1.1. Plasmid stocks were stored at -20°C.

5.1.1.3. Isolation of genomic DNA

For isolation of genomic DNA (gDNA) mouse tail biopsies (see chapter 5.5.2) were incubated overnight (O/N) in 400 µl STE-buffer supplemented with 25 µl of proteinase K (10 mg/ml). Thereafter, the samples were briefly vortexed and centrifuged for 10' at 13,000 rpm to remove tissue debris. 400 µl of the supernatant were transferred into a fresh reaction tube containing 1 ml cold 99 % EtOH. The samples were briefly vortexed and the DNA was precipitated for 10' at -20°C, pelleted for 25' at 13,000 rpm, washed with 500 µl 70 % EtOH and centrifuged again for 10' at 13,000 rpm. Finally, the DNA was dried for 10' at 55°C and resuspended in 125 µl ddH_2O on a heating block for 10' at 42°C and 1,400 rpm.

5.1.1.4. Isolation of total RNA from cell culture

Total RNA from cells was isolated using TRIzol-reagent according to the manufacturer's instructions. In short, the cells were washed with cold sterile 1 x PBS and 1 ml TRIzol was added to the cells. To ensure the integrity of RNA the following steps were performed on ice unless stated otherwise. The samples were first transferred into 2 ml reaction tubes and vortexed for 2' on the highest setting. Afterwards the samples were kept at RT for 5'. After the addition of 200 µl chloroform the samples were vortexed for 15'' and incubated for another 3' at RT. The solution was centrifuged for 10' at 13,000-14,000 rpm and 4°C. The upper phase was transferred to a fresh 1.5 ml reaction tube containing 1 ml 99 % DNAse/RNAse-free EtOH and inverted several times to ensure proper mixing. Subsequently, the RNA was precipitated O/N at -20°C, pelleted by centrifugation at 13,000 rpm for 30' and 4°C and washed two times with 500 µl 70 % DNase/RNase-free EtOH. Finally, the pellet was dried for 10' at 55°C, resuspended in 20 µl DNase/RNase-free H_2O and solved for 10' at 56°C on a heating block. Until further use the RNA was stored at -80°C.

5.1.1.5. Isolation of total RNA from murine skin samples

The isolation of RNA from mouse skin, skin biopsies and nude mice allografts (see chapters 5.2.11, 5.5.7 and 5.5.8) was performed using the RNeasy Fibrous Tissue kit according to the manufacturer's instructions, with some modifications. In brief, a maximum of 30 mg tissue was minced using sterile scalpels and transferred into a 1.5 ml reaction tube containing 300 µl buffer RLT supplemented with 3 µl of the supplied β-mercapto-EtOH. The tissue was homogenized on ice using a tissue homogenizer for 90''. After each sample the

tissue homogenizer was cleaned and rinsed in sterile, RNase-free ddH_2O two times and once with RLT-buffer. The homogenate was processed as stated in the manufacturer's instructions. After the elution of the RNA a second DNase-treatment was included. For this purpose, the eluate was supplemented with 3.22 µl RDD-buffer and 1.4 µl DNase I and subsequently incubated for 1 h at 37°C. To inactivate the DNase the solution was incubated for 5' at 65°C. Afterwards 500 µl 99 % DNase/RNase-free EtOH was added to the solution and the RNA was precipitated at -20°C O/N. Finally, the RNA was pelleted and solved (see chapter 5.1.1.4). Until further use the RNA was stored at -80°C.

5.1.1.6. Reverse transcription of RNA (cDNA-synthesis)

For cDNA synthesis 2 µg RNA in a final reaction volume of 20 µl were reversely transcribed using the SuperScript II Reverse Transcriptase System. 250 ng hexamers were incubated with the RNA for 10' at 70°C. Afterwards 1 x 1st Strand Buffer, 10 mM dithiothreitol (DTT) and 0.5 mM deoxynucleotides (dNTPs) were added and the mixture was incubated for 10' at RT. After pre-warming to 42°C for 2', 1 µl of SuperScript II (200 U/µl) was added and the mixture was incubated for 1 h at 42°C. Finally, the reaction was stopped at 70°C for 10'. Assuming the reverse transcription reaction is 50 % efficient the final concentration of cDNA was 50 ng/µl.

5.1.1.7. Photometric quantification of nucleic acids

To quantify the concentration of DNA or RNA, 1 µl of the sample solution was diluted with 200 µl DNase/RNase-free ddH_2O. The concentration was measured on a photometer by determination of the optical density (OD) at A_{260}. The final concentration was calculated according to the formula:

$$c = OD260 \times 50\ (DNA)\ or\ 40\ (RNA)$$

with c being the concentration (ng/µl). Additionally, the OD at A_{280} was measured to determine the amount of protein. With these values the purity was calculated as the ratio of OD_{260} and OD_{280}. A ratio between 1.8 and 2.0 was considered sufficiently pure.

5.1.2. Polymerase-Chain-Reaction (PCR)

5.1.2.1. PCR-based genotyping of mouse tail gDNA and semiquantification of cDNA

For PCR-based amplification of gDNA or cDNA the following reactions were carried out in a 10 or 20 µl reaction volume. For the primer combinations mPTCNx_f/mPTCNx_R/mPTCwt_R.2, EIIa-Cre-F/EIIa-Cre-R and Exon7-F/Neo-R the following conditions were applied:

1x	10 x reaction buffer
10-100 ng	template DNA
0.5 µM	forward primer
0.5 µM	reverse primer
0.2 mM	dNTP Mix
1 µl	Cresol solution (10x)
0.1 U	Taq polymerase (Moltaq)

5‘	95°C	
1‘	95°C	35 cycles
1‘	62°C	
3‘	68°C	
5‘	68°C	
∞	8°C	

Amplification of *Gapdh* transcripts was conducted using the following settings, but the same reaction mixture:

Denaturation	5’	95°C	
Denaturation	30	95°C	30-40 cycles
Annealing	1’	58°C	
Elongation	1‘	72°C	
Elongation	5‘	72 °C	
	∞	8°C	

The resulting amplification products were separated and visualized by agarose gel electrophoresis.

5.1.2.2. Quantitative Real-Time PCR (qRT-PCR)

Differential gene expression was analyzed by SYBR-green based quantitative *real-time* PCR (qRT-PCR). Primer combinations are listed in table 10. The following reagents were used in a total reaction volume of 10 µl.

2.5 ng	template cDNA
1 x	SYBR-green
0.4 µM	forward primer
0.4 µM	reverse primer

Gene expression values were calculated using the standard curve method. For this purpose, 5-fold serial dilutions from tissue or cells known to express the target gene, starting with 20 ng cDNA, were prepared and amplified by qRT-PCR. The experimental Ct values

were interpolated from the standard curve by nonlinear-regression using the semilog-line model of the GraphPad Prism 6. Afterwards, the expression values of each sample were normalized to the respective expression of the housekeeper genes *18S* rRNA or *TBP*. For housekeeper quantification 0.8 pg or 0.25 ng cDNA, respectively, were used as template in the qRT-PCR reaction. The first dilution standard-series of the standard-curve contained 20 ng cDNA obtained from a tissue that was known to express the gene of interest. The first dilution for *18S* rRNA expression measurement contained 80 pg cDNA. The samples were measured in triplicates and the data was analyzed using SDS 2.2 (and higher) and GraphPad Prism 6.

5.1.2.3. Agarose gel electrophoresis

To separate DNA by its size, agarose gel electrophoreses were performed. For this, agarose gels containing 0.5 to 2 % (w/v) agarose in 1 x TBE buffer were prepared by boiling for 2-3 min at 1,000 W in a microwave. After cooling down, the still liquid gels were supplemented with 5-7 drops of a 0.07 % ethidiumbromide solution. The electrophoresis chamber was filled with 1 x TBE buffer. To ease the gel-loading, the samples were either diluted with 10 x cresol solution or 6 x loading dye to obtain a final concentration of 1 x. In parallel to the samples an appropriate DNA ladder was loaded. The gels were run at a constant voltage of 80 to 150 V. For documentation a UV transilluminator was used.

5.1.3. Cloning techniques

5.1.3.1. Transformation of E.coli with plasmid DNA

Competent *E. coli* DH5α were thawed on ice and 50-100 µl of the cells were mixed with 50-100 ng of plasmid DNA. The remaining cells were immediately frozen and stored at -80°C. After two freeze-thaw-cycles the bacteria were discarded. The plasmid/bacteria mixture was incubated on ice for 20’ and subsequently subjected to a heat shock at 42°C for 45’’. Afterwards, the cells were incubated again on ice for 2’. After the addition of 500 µl super optimal broth with catabolite repression (SOC) medium the cells were incubated for 1 h at 37°C and 900 rpm. Finally, an appropriate volume of the cell suspension (usually 20 to 200 µl) was plated onto lysogeny broth (LB) agar plates containing the adequate antibiotic as a selection marker. The plates were incubated in an incubator O/N at 37°C. The next day single colonies were chosen for further applications.

5.1.3.2. Restriction hydrolysis

Restriction endonucleases cut DNA on specific sites according to their sequence. The recognition site usually consists of 4-8 palindromic nucleotides. In this work test-restriction hydrolysis and preparative restriction hydrolysis were performed. For the test restriction the following mixture was prepared, in which the buffer was chosen according to the manufacturer's instructions:

100-250 ng	plasmid DNA
0.1 U	restriction enzyme
1 x	buffer
ad 10 µl	ddH_2O

If necessary and possible, a double restriction was performed. If not, a sequential restriction was performed by increasing the total volume to adjust for different salt concentrations of the different buffer systems of up to 50 µl. If the buffers were not compatible the DNA was precipitated after the first restriction reaction and, once solved again, subjected to the second restriction reaction. The restriction reaction was usually carried out for one hour at the optimal temperature for each enzyme. If possible, enzymes were heat-inactivated afterwards. Finally, the complete sample was separated by agarose gel electrophoresis.

In case of preparative restrictions the amount of DNA was increased as needed and the amount of enzymes used was increased accordingly, following the manufacturer's instructions. Also, the restriction reaction duration was increased to ensure maximal restriction to a maximum time of 16 h. All used enzymes were purchased from NEB (Ipswich, USA) or Invitrogen (Karlsruhe).

5.1.3.3. Isolation of DNA fragments from agarose Gels

DNA-fragments were excised from agarose gels with a sterile scalpel under 70 % UV-light to reduce the risk of UV-induced mutations (e.g. thymidin dimers). The DNA was cleaned-up using the QIAEX II Gel extraction kit according to the manufacturer's instructions including all optional washing steps.

5.1.3.4. Ligation

During a ligation reaction two pieces of DNA with compatible restriction ends are being connected. The ligation reactions were performed by employing the T4 DNA Ligase system. The molar ratio of the respective insert to vector was 3:1. The molar ratio was calculated according the following formula:

$$Insert\ [ng] = \frac{Insert\ [bp] \times vector\ [ng]}{Vector\ [bp] \times molar\ ratio\ (insert{:}\ vector)}$$

A reaction with a total amount of 100 ng DNA was set up according to the ligation protocol below.

X ng	vector DNA
Y ng	insert DNA
4 U	T4 DNA Ligase
1x	T4 Ligase buffer
ad 10 µl	ddH_2O

The ligation reaction was conducted at 4°C for at least 48 h, stopped by heat-inactivation for 10' at 65°C and transformed into *E.coli* (see 5.1.3.1).

5.1.3.5. DNA sequencing

The nucleotide sequence of plasmids was determined by the Sanger sequencing method using the BigDye® reagent and an ABI3500XL sequencing device. For sequencing the following reagent mixture and conditions were used.

1x	BigDye buffer	1'	95°C	
1x	BigDye 3.1	30''	95°C	30 cycles
20-200 ng	plasmid DNA	2.5'	60°C	
100 pmol	sequencing primer	5'	60°C	
ad 10 µl	ddH2O	∞	8°C	

The primers used for sequencing are listed in table 11. The obtained electropherograms were evaluated and the obtained sequences were analyzed using the freely available software BioEdit.

5.1.3.6. Site-directed mutagenesis

The QuikChange II site-directed mutagenesis kit or the QuikChange II XL site-directed mutagenesis kit were used to induce point mutations in plasmid DNA as described in

the manufacturer's instructions. The specific PCR reagent mixtures and conditions are described in the respective chapters. *DpnI* restriction was performed immediately after the respective PCR. For transformation of the *E.coli* strain XL-10 gold SOC-medium was used.

5.1.3.7. Generation of Smo expression plasmids

The plasmid *pHAGE mSmo^{W113Y} mCherry* carrying a point mutation in the Smo CRD (W113Y) was a kind gift from Dr. Adrian Salic, Harvard Medical School, USA (Nedelcu *et al.* 2013). To generate the *pMSCV mSmo^{W113Y} mCherry* plasmid (see Appendix) the *mCherry*-tagged *mSmo*-sequence from *pHAGE mSmo^{W113Y} mCherry* plasmid was amplified using the primer pair SmoKlon1AF/SmoKlon1BR and Phusion High-fidelity polymerase in a 20 µl reaction volume according to the following protocol:

50 ng	template plasmidDNA	Hotstart	98°C	
0.5 µM	SmoKlon1AF (forward Primer)	10‘‘	98°C	35 cycles
0.5 µM	SmoKlon1BR (reverse Primer)	30‘‘	60°C	
0.2 mM	dNTP mix	2‘	72°C	
1x	HF buffer	10‘	72°C	
2.5 mM	$MgCl_2$	∞	8°C	
0.05 U	Phusion High-fidelity polymerase			

The amplified 3,635 bp fragment was purified by agarose gel extraction (see chapter 5.1.3.3) and eluted in 30 µl ddH_2O. Next, the DNA was restricted by *Bcl*I at 50°C O/N and *Not*I at 37°C for 2 h. The DNA was separated on a 0.7 % agarose gel and the 3,559 bp fragment was excised, purified and subcloned into the *pMSCVpuro* vector after *Bgl*II/*Not*I digestion (kindly provided by Dr. Michael Engelke). The insertion of the respective fragments was verified by Sanger sequencing using the primers given in table 11.

To generate the *pMSCV mSmo^{wt} mCherry* (see Appendix) plasmid the W113Y mutation of the *pMSCV mSmo^{W113Y} mCherry* plasmid was reversed to the wildtype (wt) sequence using the primers CRD_mut_F2/CRD_mut_R2 and the QuikchangeII-XL site-directed mutagenesis kit in accordance to the manufacturer's instructions. The following PCR settings were used:

1x	10 x reaction buffer	1‘	95°C	
10 ng	*pMSCV mSmo^{W113Y} mCherry*	50‘‘	95°C	18 cycles
125 ng	CRD_mut_F2 (forward primer)	50‘‘	60°C	
125 ng	CRD_mut_R2 (reverse primer)	9‘ 50‘‘	68°C	
1 µl	dNTP mix (proprietary solution)	7‘	68°C	
3 µl	Quiksolution	2‘	37°C	
2.5 U	PfuUltra HF DNA polymerase			

After the PCR reaction the amplification product was restricted by *Dpn*I and transformed to *E. coli* XL-10 Gold bacteria, clones were picked as described above and small-scale plasmid preparations were performed. The site-directed mutagenesis was verified by Sanger sequencing using the primers mSmo_D54F and CRD_R. After medium-scale plasmid preparation of one positive clone, the integrity of the Smo sequence was verified by Sanger sequencing and the primers given in table 11.

The plasmid *pMSCVpuro mSmo$^{\Delta CRD}$ mCherry* (see Appendix) was generated according to the sequence described by Nedelcu *et al.* (Nedelcu *et al.* 2013). The CRD-deletion was achieved by performing a two-step overlap-extension PCR. First, two fragments were generated using the primer-combination 1A2F/1AR (206 bp) and 1BF/1BR (2,899 bp) using the following conditions in a 20 µl reaction volume for each PCR reaction:

overlap extension small fragment				
50 ng	*pMSCV mSmo^{W113Y} mCherry*	Hotstart	98°C	
0.5 µM	SmoKlon 1A2F (forward primer)	30"	98°C	
0.5 µM	SmoKlon 1AR (reverse primer)	8"	98°C	
0.2 mM	dNTP mix	20"	60°C	35 cycles
1x	HF buffer	15"	72°C	
0.05 U	Phusion High-fidelity polymerase	10'	72°C	
		∞	8°C	

overlap extension large fragment				
50 ng	*pMSCV mSmo^{W113Y} mCherry*	Hotstart	98°C	
0.5 µM	SmoKlon 1BF (forward primer)	30"	98°C	
0.5 µM	SmoKlon 1BR (reverse primer)	8"	98°C	
0.2 mM	dNTP mix	20"	65°C	35 cycles
1x	HF buffer	50"	72°C	
0.05 U	Phusion High-fidelity polymerase	10'	72°C	
		∞	8°C	

The amplification products were validated on a 1 % agarose gel and the overlap-extension-PCR was performed using the 1A2F/1AR (206 bp) and 1BF/1BR (2,899 bp) amplification products as template for the following protocol:

overlap extension PCR	
2 µl	small fragment PCR
2 µl	large fragment PCR
0.5 µM	SmoKlon 1BF (forward primer)
0.5 µM	SmoKlon 1BR (reverse primer)
0.2 mM	dNTP mix
1x	HF buffer
2.5 mM	$MgCl_2$
0.05 U	Phusion High-fidelity polymerase

Hotstart	98°C	
30"	98°C	
8"	98°C	35 cycles
20"	65°C	
1'	72°C	
10'	72°C	
∞	8°C	

The amplification products were separated on a 0.5 % agarose gel and the 3,077 bp fragment was excised and purified as described in chapter 5.1.3.3. Afterwards, the fragment were digested with *Bcl*I and *Not*I and cloned into *pMSCVpuro* vector linearized with *Bcl*I and *Not*I. The CRD deletion was confirmed by Sanger sequencing using the primer CRD_R. A deletion at position 1,636 was repaired using the QuikChangeII XL site-directed mutagenesis kit and the primers CRD_Ins_1636_F/CRD_Ins_1636_R.

5.2. Cell biology methods

5.2.1. Culture of eukaryotic cells

All eukaryotic cell lines were cultured in an incubator with constant 37 °C, 5 % CO_2 and 95 % humidity. The media were refreshed every 3-4 days and the cells were splitted when reaching 80 to 90 % confluence. Splitting of the cells was conducted by detaching the cells with 1-3 ml of TrypLE express or for ASZ001 cells with 2-3 ml of trypsin/EDTA. After the cells started to detach, the reaction was stopped by the addition of FCS-containing medium and an appropriate volume was transferred to a new culture plate containing fresh medium. The culture media and supplements are listed in table 7.

5.2.2. Cryopreservation of eukaryotic cells

For long-term storage of eukaryotic cell lines the cells were stored in liquid nitrogen. For this purpose, 1-3 10 cm culture plates with 90 % cell confluency were rinsed with 1 x PBS and detached as described above. The detached cells were transferred into a 15 ml reaction tube und pelleted by centrifugation at 300 x g for 5’ and 4°C. Afterwards the cells were resuspended in 10 ml culture medium supplemented with 10 % DMSO and appropriate

antibiotics. 1 ml aliquots were frozen in Cryovials at -80°C in the freezing device Mr. Frosty™ for 16 h. Afterwards, the cells were stored in liquid nitrogen.

To thaw the cells they were rapidly warmed and transferred to 10 ml 1 x PBS, pelleted as described above and resuspended in fresh culture medium. Cells were transferred to a 5 or 10 cm culture dish and stored in an incubator. The next day the medium was replaced with fresh medium to ensure the complete removal of DMSO.

5.2.3. Transfection of eukaryotic cells

For the transfection of plasmid DNA, the cells were seeded as described in the respective experiments at a density of approximately 70 %. The cells were transfected using RotiFect® according to the supplier's instructions. For each cell line a specific ratio of DNA to RotiFect® and a specific transfection time was used. In brief, one day after seeding, the transfection mixture was prepared by pipetting the appropriate volumes of DNA and RotiFect to culture medium without any supplements. This mixture was thoroughly vortexed to allow for forming complexes for 40' at RT. Afterwards an appropriate volume of culture medium supplemented with 10 % FCS was added and mixed by gentle pipetting. This solution was added to cells, which were rinsed before with 1 x PBS. After the transfection time the solution was aspirated, the cells were rinsed with 1 x PBS and normal culture medium was added. If the transfection solution was not removed, the same volume of normal culture medium (including 1 % Penicillin/Streptomycin) was added to the cells after 6 h to prevent microbial contamination.

Table 16: Transfection conditions

cell line	well type	plasmids [µg]	Ratio Rotifect®:DNA	transfection time [h]
wt *Ptch*	24-well plate	0.5	2:1	3 h
Ptch$^{-/-}$	24-well plate	0.5	2:1	3 h
Gli1$^{-/-}$/*Gli2*$^{-/-}$	24-well plate	0.5	4:1	6 h
NIH/3T3	6-well plate	2	3:1	6 h
	96-well plate	0.1 – 0.12	3:1	6 h
Smo$^{-/-}$	24-well plate	0.5	3:1	/

5.2.4. Retroviral transduction of eukaryotic cells

For retroviral transduction of murine cells Platinum-E cells were used as packaging cell line. The latter cells were seeded at a confluency of 50-60 % in 5 cm culture dishes one day before transfection with the retroviral vectors. For the transfection the following reagents were mixed in the given order:

400 µl	medium of the target cell line without supplements
5 µl	RotiFect®
2.5 µg	retroviral expression vector

The reagents were mixed by tapping and were incubated at RT for 30'. Hereafter, the Platinum-E cells were washed and the medium was replaced with 4 ml fresh medium used for the target cell line. The transfection mixture was added drop wise onto the plates and mixed by swirling. After 48 h the cell supernatant (Platinum-E conditioned medium; Platinum-E-CM) containing the viruses was sterile-filtered using a 0.45 µm pore sterile filter. 3 ml Platinum-E-CM was supplemented with 1.5 ml fresh medium and 3 µg/ml polybrene and applied to a 50 % confluent cell culture dish (5 cm) of the target cell line. The sterile-filtered polybrene stock solution (3 mg/ml) was freshly prepared prior to the infection in 1 x PBS. The target cells were washed after 24 h and supplied with fresh medium. After additional 24 h the culture media were supplemented with the respective selection antibiotics (see table 7).

5.2.5. Dual-Luciferase assay

Dual-luciferase assays of transiently or stably transfected cells were performed using the Dual-Luciferase® reporter assay system according to the manufacturer's instruction. In brief, the washed cells were lysed by addition of 20 µl or 100 µl per well of 1 x passive lysis buffer (PLB) for 96- or 24-well-plates, respectively. The plates were incubated on an orbital shaker at 250 to 300 rpm for 15'. Afterwards, the plates were frozen at -80°C for at least 15' and measurement was conducted once the lysates were thawed again. LAR II and Stop'n'Glo solutions were prepared and stored as described in the manufacturer's instruction. Prior to the measurements the LAR II and Stop'n'Glo solutions were allowed to equilibrate to RT for at least 15'. The measurement was conducted on a Synergy MX luminometer. The firefly-luciferase values were normalized to the respective renilla-luciferase values.

5.2.6. Generation of Shh-N conditioned medium

For generation of Shh-N-conditioned medium (Shh-N-CM) and respective control medium (CoM) HEK293Shh and HEK293 at a density of 70 % were incubated with DMEM supplemented with 2 % FCS and 1 % PS for 24 h. Afterwards, the media were sterile-filtered (0.2 µm pore size) and stored at 4°C for a maximum of 3 months until prior use. If necessary, the media were diluted with DMEM supplemented with 2 % FCS and 1 % PS.

5.2.7. Proliferation assay

Cellular proliferation was assessed using the BrdU Cell proliferation kit according to the manufacturer's instructions. In brief, 8,000 cells were seeded per well of a 96-well plate and treatment was conducted as described in the respective experiments. 22 h prior to the measurement 10 µM BrdU reagent was added. The cells were fixed for 30' and peroxidase-coupled BrdU-antibody (anti-BrdU-POD) was added for 1 h. After thorough washing, BrdU-incorporation was determined by the addition of peroxidase substrate. The measurement was conducted on a Synergy MX luminometer.

5.2.8. BODIPY-replacement assay

For analyses of a direct competition of Smo modulators with BODIPY-labeled cyclopamine (BD-CP) for Smo-binding a replacement assay was performed. The displacement of BD-CP from its binding to Smo was measured by decreased fluorescence intensity of cells.

For the experiments 250,000 HEK293S cells per well of a 6-well-plate were seeded in the respective culture medium. The next day, Smo overexpression was induced by changing the medium to DMEM/F12 supplemented with 10 % FCS, 1 % PS, 1 µg/ml tetracycline and 5 mM sodium butyrate for 48 h. Afterwards the medium was changed to DMEM/F12 supplemented with 10 % FCS / 1 % PS and the compounds described in the respective experiments. After 4 h incubation the cells were washed, detached using 1 ml TrypLE express and transferred to 15 ml reaction tubes containing 2 ml 1 x PBS. The wells were rinsed with 1 ml 1 x PBS and the solution was transferred to the same reaction tube to increase the total cell number. The cells were pelleted by centrifugation for 5-8' by 300 to 400 x *g* and washed again with 2 ml 1 x PBS and centrifuged again. Finally, the pellet was resuspended in 350 to 600 µl phenol-red free DMEM supplemented with 0.5 % FCS by brief vortexing and

pipetting. The cells were analyzed on a BD LSR II within 2 h. 50,000 cells per sample were counted.

For statistical analysis and generation of bar graphs the mean fluorescence intensity values of the respective histograms were exported using FlowJo software. The data are represented as the cumulative distribution function (CDF), which denotes the percentage of cells with a given fluorescence intensity. For each experiment the fluorescence intensity of BD-CP-single treated cells was set to 100 %.

5.2.9. Generation of concentration response curves and determination of half maximal effective or inhibitory drug doses

Concentration response curves (CRC) were generated to determine the half maximal effective concentration (ED_{50}) or the half maximal inhibitory concentration (IC_{50}) of Smo modulators in Hh signaling inhibition. For this purpose, the Hh signaling activity of Shh light II cells was measured after treatment with increasing amounts of one Smo modulator in combination with constant concentrations of a second Smo modulator.

For this assay 5,000 to 6,000 Shh light II were seeded per well of 96-well plates in the respective culture medium. The next day, the medium was replaced with Shh-N-CM, if two inhibitors were used, or DMEM supplemented with 0.5 % FCS, if an inhibitor and an agonist were used. After 24 h the cells were treated with the Smo modulators diluted in the respective media as described in the respective experiments for additional 48 h. Afterwards the cells were lysed for Dual-luciferase assay as described (see chapter 5.2.5).

The renilla-normalized firefly values were first normalized to the respective solvent value, which was set to 100 % using MS Excel. Employing GraphPad Prism6, the values were normalized again to range from 0 % to 100 % and the used concentration was transformed to its logarithm. Finally, the curves were fitted by non-linear regression using the function “log(inhibitor) vs. response – Variable slope (four parameters)” or the respective log (agonist) function. Curve fitting was calculated using 1,000 iterations. For EC_{50}-shift experiments the respective solvent-treated control was set to 100 %.

5.2.10. Medium transfer experiments

For medium-transfer experiments 2 to 4 10 cm cell culture dishes of 70-80 % confluent wt *Ptch* or *Ptch*$^{-/-}$ cells were washed, trypsinized and pelleted by centrifugation at 300 x *g* for 5' at 4°C. The cells were resuspended in culture medium and 2,000,000 cells were transferred to a 50 ml reaction tube in a total volume of 10 ml pre-warmed culture medium supplemented with 100 nM calcitriol or solvent. The suspensions were incubated rotating in a hybridization oven at 37°C for 1 h. Hereafter, the cells were washed two times with 20 ml cold 1 x PBS. Each time, the reaction tube was inverted several times to ensure complete removal of the calcitriol-supplemented medium. The cells were pelleted by centrifugation and resuspended in 9 ml pre-warmed medium. 1 ml of the obtained cell suspension was seeded into each well of 6-well plates for conditioning. After 4, 6 and 8 h the medium was sterile-filtered (0.2 µm pore size). The same procedure was performed using medium in reaction tubes und 6-well-plates without cells in order to verify background levels of calcitriol. The conditioned media were stored in 2 ml reaction tubes at 4°C for no longer than 1 week. A schematic representation of the workflow is presented in Fig. 4.

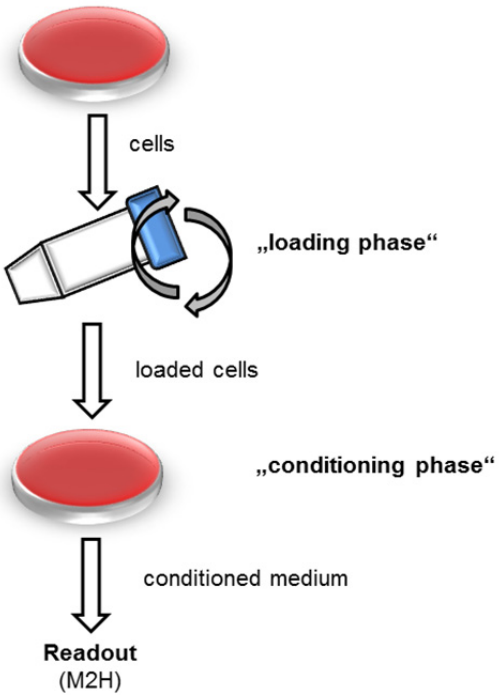

Figure 4: Workflow of the medium transfer experiment. Trypsinized wt *Ptch* and *Ptch*$^{-/-}$ cells were loaded with calcitriol in a rotating 50 ml falcon ("loading phase"). After extensive washing, the cells were seeded in 6-well plates. After for 4, 6 and 8 h ("conditioning phase") the medium was collected, sterile-filtered and transferred to NIH/3T3 cells transfected with the plasmids *pFR-Luc*, *pCMV-BD-RXRα*, *pCMV-AD-VDR* and *pRL-TK* or Shh light II stimulated with Shh-N-CM. After 16 h or 48 h dual-luciferase assays were performed, respectively.

To analyze the rate of VDR/RXRα-heterodimerization after incubation with conditioned medium 200,000 NIH/3T3 cells per well of 6-well plates were seeded in the normal culture medium. The following day, the cells were transfected with the plasmids *pFR-Luc*, *pCMV-BD-RXRα*, *pCMV-AD-VDR* and *pRL-TK* in a ratio of 50:5:5:1. 6 h after the transfection, the cells were washed, trypsinized and transferred to 96-well plates at a density of approximately 70 %. The next day, the transfected cells were incubated with 100 µl/well of the respective conditioned media for 16 h and finally, dual-luciferase assays were performed.

To analyze the effect on Hh signaling inhibition 5,000 Shh light II cells per well of 96-well plates were seeded in the respective culture medium. The following day the medium was replaced with Shh-N-CM for 48 h. Then, the cells were incubated with 100 µl/well of the respective conditioned media for 48 h. Finally, dual-luciferase assays were performed.

5.2.11. Isolation and culture of mouse skin biopsies

For culture of mouse skin biopsies, 8-10 week old *Ptch*$^{flox/flox}$ *CreERT2*$^{+/-}$ mice were intramuscularly injected with 10 µl tamoxifen-solution (10 µg/µl, see chapter 5.5.4). After 60 days the tail skin of the mice was depilated using customary depilatory cream as stated in the manufacturer's instructions and treated with 70 µl nystatin (1.2 mg/ml in EtOH). The nystatin treatment was repeated the next day. After one additional day the mice were sacrificed, the tail skin was disinfected with 70 % EtOH and removed using a sterile scalpel. Afterwards the skin was shortly rinsed in a petri dish containing sterile 1 x PBS and transferred into fresh 1 x PBS in a petri dish. All following steps were performed under a sterile bench. First, the skin was excised into 1 mm^2 large pieces. Then, 4 skin biopsies (with the dermis down) were transferred to one micropore filter, which was floating in a 24-well plate well filled with 1 ml DMEM supplemented with 10 % FCS and 1 % PS. The next day the medium was changed to DMEM supplemented with 1.5 % BSA and 1 % PS. After one additional day the medium was changed with DMEM supplemented with 1.5 % BSA, 1 % PS and the compounds described in the respective experiments. After 72 h the medium containing the compounds was refreshed and after additional 72 h three skin biopsies were stored at -80°C for RNA isolation and one biopsy was used for histological analyses.

5.3. Protein chemistry and immunohistochemistry

5.3.1. Protein isolation from cell culture

To isolate proteins of cultured cells, the cells were washed and scraped in 1 ml 1 x PBS using a cell scraper, and pelleted by centrifugation for 5' at 2,000 rpm. The supernatant was discarded and the pellet was resuspended in 700 µl 1 x PBS and transferred into a 1.5 ml safelock-tube. After a second washing step the cell pellet was frozen in liquid nitrogen and afterwards thawed on ice. The thawed pellet was incubated with 50 - 100 µl lysis buffer for 30' on ice. Afterwards, the mixture was centrifuged for 30' at 13,000 rpm and the supernatant, containing the soluble proteins, was transferred to a new 1.5 ml reaction tube. The protein concentration was determined using the Pierce BCA Protein Assay kit according to the manufacturer's instruction. The proteins were stored at -80°C.

5.3.2. Western blot

For Western blot analyses protein samples were prepared by adding 6 x loading buffer to obtain a 1 x concentration. Prior to loading, the proteins were denatured by boiling for 5', 450 rpm at 96°C on a shacking heating block. Proteins and 4 µl SeeBlue Plus2 Prestained Standard were loaded on NuPAGE® Novex® 4-12 % Bis-Tris Protein Gels in 1 x NuPAGE® MES SDS running buffer and separated at 160 mA, 160 V and 100 W for 1.5 to 2 h. Afterwards the proteins were transferred from the gel to a nitrocellulose membrane by semi-dry blotting for 1 h 20' at 120 mA, 20 V and 100 W. Next, the membrane was washed three times for 10' with 1 x PBS containing 0.1 % Tween (PBS-Tween) and blocked in 5 % (w/v) milk powder/PBS-Tween for 1 h at RT. The membrane was washed again and incubated with the primary antibody O/N at 4°C on an orbital shaker. The next day, the membrane was washed again and incubated with the secondary antibody for 1 h at RT (see table 13). After an additional washing step ECL Plus Western Blotting Detection System was used according to the manufacturer's instruction. The detection was accomplished with a Fluorchem Q Detection System.

5.3.3. Haematoxylin/Eosin staining

For Haematoxylin/Eosin (HE) staining tissue was fixed in 4 % PFA for 2 weeks and embedded in paraffin. Paraffin sections were prepared on a microtome and mounted on glass slides. The sections were deparaffinized in xylene for 2 x 10'. Next, the sections were hydrated by descending EtOH solutions (99 % to 70 %). After thoroughly washing with ddH_2O, the hydrated sections were transferred to a hemalaun solution for 20'. Color development was achieved by a constant flow of lukewarm tap water for as long as there was no more coloring of the water. Subsequently, the slides were transferred to a 1 % eosin solution for no longer than 20'' and extensively washed with ddH_2O until the water stayed clear. To prepare the mounting with cover slides, the sections were dehydrated with ascending EtOH solution (70 % to 99 %) and were left in xylene prior to mounting in Pertex. For hardening the mounting medium, the slides were placed in a 55°C warm oven for at least 20'.

To analyze the tumor area, pictures were taken on an Olympus BX60-microscope operated by Cell F software at 100-fold magnification. Next, the tumor area was depicted using the "polygon ROI tool" of three pictures per mouse. The mean of these values was used for further calculations.

5.3.4. Ki67-staining

For immunohistochemical visualization of Ki67-positive cells, microtome sections of paraffin-embedded tissue were prepared and mounted on Superfrost slides. The sections were first rehydrated for two times 10' in xylene, followed by descending EtOH solution (99 % to 70 %). After washing in ddH_2O antigen-retrieval was conducted by boiling the slides in citric acid buffer (pH 6.0) once for 4' and 4 times for 3' at 600 W in a microwave. Afterwards the sections were allowed to cool down to RT and washed 2 times for 2' with 1 x TBS. Endogenous peroxidases were blocked by incubating the sections for 20' in 3 % H_2O_2 on an orbital shaker. Afterwards the sections were washed for 5' in ddH_2O and rinsed with 1 x TBS. Subsequently, the sections were blocked for 20' with 5 % FCS / 10 % BSA in 1 x PBS at RT in a moist chamber. Prior to the primary antibody incubation the sections were shortly dipped in 1 x TBS and antibody incubation was conducted at 4°C O/N in moist chambers. After washing with 1 x TBS two times for 2' the sections were incubated with the secondary antibody for 30' at RT in moist chamber. Subsequently, the sections were washed again and the DAB chromogen was added for 10' in moist chambers at RT. The sections were dipped in TBS and washed with ddH_2O for 5'. Counterstaining was conducted for 20'' in hemalaun

followed by a 5' constant flow of lukewarm tap water. Finally, the sections were mounted with Glycergel.

For the counting of Ki67-positive cells at least three images per section were taken at a 200 x magnification on an Olympus BX 60 microscope operated by Cell F software. The pictures were further analyzed using the freely available software Fiji (Fiji.sc; (Schindelin *et al.* 2012)). To do so, the "smooth"-function was applied; the contrast was enhanced (0.4 %) and after channel-splitting the pictures were converted to binary. $Ki67^+$ cells as well as all nuclei per picture were automatically counted by adjusting the threshold values. The ratio of $Ki67^+$ cells/all nuclei per picture was determined and used for further calculations.

5.4. Mass spectrometry

The methods for the measurements of $vitD_3$ metabolites and itraconazole have been developed by Susanne Weber (Helmholtz-Centre Munich, Institute for Experimental Genetics, Prof. Dr. Jerzy Adamski).

5.4.1. Measurement of intracellular $vitD_3$ metabolites

Cellular uptake and generation of the different $vitD_3$ metabolites calcitriol (1α,25-dihydroxy vitamin D_3), 24,25-dihydroxy vitamin D_3 ($24,25(OH)_2D_3$), $25(OH)D_3$ and $vitD_3$ were analyzed by liquid chromatography coupled to tandem mass spectrometry (LC-MS/MS). ASZ001 cells were seeded at a density of 200,000 cells/well, whereas all other cells were seeded at densities of 150,000 cells/well in 6-well plates in the respective culture medium. After 24 h the medium was removed and culture medium without FCS and 1 % PS was added. Next, the cells were treated with the compounds described in the respective experiments. Cells were washed with 1 x PBS and harvested by scraping using 750 µl of 60 % methanol (MetOH) in water supplemented with 40 ng/ml of internal standard 25-hydroxy vitamin D_2 [25,26,27-$^{13}C_3$]. After the transfer of the scraped cells into 1.5 ml safelock reaction tubes, the dishes were rinsed again with 500 µl of 40 % MetOH in water. Both cell fractions were combined, immediately put on dry ice and stored at -80 °C until analysis.

Prior to LC-MS/MS analysis, $vitD_3$ metabolites were extracted via offline solid phase extraction (SPE) using a nitrogen-driven Positive Pressure-96 Processor coupled with a 96-Well Tabless Tube Holder. To do so, the harvested samples were thawed at RT and loaded onto an SPE cartridge. After three washing steps the metabolites were eluted twice with 2 %

formic acid in MetOH. Eluates were evaporated to dryness under constant nitrogen flow and reconstituted with an appropriate solvent mixture.

LC-MS/MS analysis was performed on a system composed of an HTC-xt autosampler, a 1260 HPLC System, and a QTrap5500 mass spectrometer which was controlled by Analyst 1.6 software. The vitD_3 metabolites were separated on a reversed phase column using a solvent gradient and detected by multiple reaction monitoring (MRM) after electrospray ionization (ESI) in positive mode. In case of calcitriol, 24,25$(OH)_2D_3$, and 25$(OH)D_3$ three MRMs were monitored, whereas only one MRM was monitored for vitamin D_3. The peaks of the respective vitD_3 metabolites (sum of respective MRMs) were integrated by the Analyst 1.6 software and the areas were normalized by the peak area of the internal standard 25-hydroxy vitamin D_2 [25,26,27-$^{13}C_3$] which was added within the harvesting process.

5.4.2. Detection of intracellular ITZ by LC/MS-MS-based assay

LC-MS/MS was also used for the analysis of intracellular ITZ concentrations. Seeding and treatment of the cells, as well as sample preparation was conducted as described above. For ITZ two MRMs were monitored. The analysis and downstream calculations were performed similar to the vitD_3 metabolites.

5.4.3. Detection of vitD_3 metabolites and ITZ in ASZ001-allografts

For the detection of vitD_3 metabolites and ITZ from transplanted ASZ001 cells (5.5.7) by mass spectrometry, approximately 100 mg of tumor tissue was shredded using a sterile scalpel. The homogenate was transferred to Precellys ceramic kit 1.4/2.8 mm 2.0 ml tubes and 500 µl 100 % MetOH was added. Furthermore, 1 µl per 10 mg tumor of internal standard solution (1α,25-$(OH)_2$-D_2, 1 µg/ml) was added and the tumors were homogenized using a Precellys 24 tissue homogenizer by three cycles of 20'' homogenization at 5,500 rpm and 30'' pausing in between. The temperature was kept at 4°C with a Cryolys temperature controller. The homogenate was shortly centrifuged and the supernatant was transferred to Sephadex columns containing 400 µl ddH_2O. The remaining tissue debris was rinsed with 500 µl MetOH, vortexed and centrifuged again to ensure maximal yield. The supernatant was again transferred to sephadex columns containing 400 µl ddH_2O. All following steps were performed as described in chapter 0. To analyze the data, the values obtained were first normalized to the IS and then normalized again to the analyzed tumor amount (weight).

5.5. Animal experiments

All experiments using animals were performed in compliance with all relevant legal and ethical requirements.

5.5.1. Breeding of mice

All mouse strains were housed and bred in the animal facility of the Institute of Human Genetics, University of Göttingen, Germany. The animals were housed in Makrolon cages type II and III, with a twelve-hour light-dark cycle, 20 +/- 2 °C and a relative humidity of 50 +/- 10 %. Food pellets (complete diets for mice breeding) and tap water were given *ad libitum*. Immune deficient nude mice were kept under specified pathogen free (SPF) conditions and fed with sterilized food pellets and water. For experiments using calcitriol the animals received vitD_3-free, Ca^{2+} and phosphate-reduced food 1 week prior to the experiments and throughout the whole experiment (Ssniff Spezialdiäten: E15312-1).

5.5.2. Tail biopsy and genotyping of mice

Ear marking and tail clipping were done at 4 weeks of age to mark and identify the genotype of the respective mouse (see chapter 5.1.2.1). Genotyping was conducted on gDNA isolated from tail clipping using the primers and conditions given in table 8.

5.5.3. Anesthesia of mice

For the anesthesia of mice the animals were injected intraperitoneally (i.p.) with 64 µg Ketanest S and 12 µg Rompun per 1 g of body weight. To prevent a drying of the eyes they were covered in 0.9 % NaCl for the time of anesthesia.

5.5.4. Intramuscular injection of tamoxifen

For the induction of Cre-recombinase activity in *Ptch*$^{flox/flox}$ *CreERT2*$^{+/-}$ mice, a 100 mg/ml tamoxifen-solution (in EtOH) was prepared. This solution was diluted 1:10 with sterile sunflower seed oil to obtain a final concentration of 10 mg/ml. To induce BCC-development in *Ptch*$^{flox/flox}$ *CreERT2*$^{+/-}$ mice 6-9 week old animals were fixed and 10 µl of the

tamoxifen-solution (equating to 100 µg tamoxifen) were injected into the right *musculus soleus*. Macroscopically visible BCC developed from day 30 post-induction on.

5.5.5. Intraperitoneal injection of calcitriol

Mice were injected daily with 100 ng calcitriol per 1 kg of body weight i.p.. For this purpose, a 10 or 20 µM stock solution of calcitriol was diluted in 20 µl EtOH. This solution was further diluted in 1.2 ml sterile sun flower seed oil to obtain the final solution. The mice were injected with 50 µl (equating 100 ng/kg) of the final solution. The solution was stored frozen for no longer than 1 week. As controls, mice were injected with solvent only.

5.5.6. Oral treatment with azoles

KTZ tablets were pulverized and ITZ capsules were opened and both compounds were dissolved at a concentration of 40 mg/ml in 0.25 % xanthan gum by thorough shaking and vortexing. Xanthan gum was prepared in sterile 0.9 % NaCl and stored at -20°C. Azole stock solutions were also stored at -20°C. For animal treatment the stock solutions were diluted with xanthan gum to reach a final concentration of 100 mg/per kg body weight. Oral treatment by gavage was conducted by fixing the animals on their neck and tail and injection of 200 µl azole solution into the stomach. Control animals received 200 µl xanthan gum orally. The mice were weighed twice a week and the treatment was conducted thrice a week.

5.5.7. ASZ001 allografts

ASZ001 cells were grown until they reached a confluency of 70 – 80 %. The cells were trypsinized, pelleted by centrifugation at 300 x *g* for 5’ and washed for two times with 154-CF medium supplemented with 1 % PS. Afterwards the cells were resuspended in culture medium in an appropriate volume and the number of viable cells was determined by counting trypan blue stained cells in a Neubauer counting chamber. Using pre-chilled syringes 1 x 10^6 ASZ001 cells in a total volume of 250 µl 20 % matrigel in culture medium were subcutaneously transplanted into the right and left flank of 8 to 10 week old anesthetized nude mice. Tumor development was monitored thrice a week using a digital caliper. The volume of the tumors was calculated using the formula (Tomayko and Reynolds 1989):

$$V = \frac{1}{2} \times L \times W \times H$$

At the end of the experiments the animals were sacrificed, the tumors were removed and fixed in 4 % paraformaldehyde or stored at -80°C for further analysis.

5.5.8. Perfusion of mice

In preparation for the perfusion the mice were injected with a lethal dose of a mixture of 4 mg Ketanest S and 0.9 mg Rompun. Next, the animals' chest was opened and the heart was exposed. The right atrium was opened for bleeding. Afterwards, the animal's left ventricle was punctured and the animal was infused with Ringer lactate for 10'. Simultaneously, the tail was removed and the skin was carefully stripped from the bone. A small part of the tail skin was frozen on dry ice for molecular analyses; another part was transferred to a biopsy cassette and incubated in 4 % paraformaldehyde for 2 weeks in preparation for embedding in paraffin. Subsequently, the animal was infused with 4 % paraformaldehyde for 10' or until the animal was completely fixed. The animals, as well as the remaining tail, were stored for 2 weeks at 4°C in 4 % paraformaldehyde. Afterwards the animals were stored in 1 x PBS at 4°C.

5.6. Statistics

All statistical and graphical analyses were conducted with GraphPad Prism6, unless mentioned elsewise. For *Gli3* overexpression experiments (see 6.1**Fehler! Verweisquelle konnte nicht gefunden werden.**), *Vdr*-promoter dual-luciferase assays (see 6.1), the calcitriol-combination treatment of ASZ001 cells (see 6.2.1.1), BCC-skin biopsies (see 6.2.1.2), and *in vivo* experiments (see 0) unpaired, nonparametric one-way ANOVA (Kruskal-Wallis-Test), followed by Dunn's multiple comparison tests were performed. For medium-transfer experiment (see 6.3.1.1) the data were tested for Gaussian distribution using D'Agostino-Pearson omnibus reality test followed by an ordinary one-way ANOVA with Sidak's multiple comparisons test. For comparison of reporter system sensitivity (see 6.3.1.1; Fig. 34) unpaired t-tests were performed.

To test for statistically increased concentration compared to solvent-treated cells for the 25(OH)D_3 and vitD_3 timecourse experiments (see 6.3.1.2; Fig. 35 and 36) unpaired t-tests

were performed using the function "Multiple t-tests – one per row" of GraphPad Prism 6, without assuming consistent standard deviation (SD) and without correcting for multiple comparisons. To test for statistically significant concentrations over time, unpaired, nonparametric one-way ANOVA (Kruskal-Wallis-Test), followed by Dunn's multiple comparison test was performed against the first (0.5 h) time point.

Concentration-response-curves (CRC, see 6.3.2.1) were calculated using GraphPad Prism 6 by normalizing the renilla-normalized firefly-values to solvent-treated cells (100 %) using MS Excel. Afterwards the concentration was transformed to the logarithm and the range of the data was normalized by setting the highest and lowest value to 0 and 100 %, respectively. The curve was fitted by non-linear regression using the function "log(inhibitor) vs. response – variable slope (four parameters)" or the respective log(agonist) function. Curve fitting was calculated using 1,000 iterations.

For generation of Fa-CI-plots (see 6.3.2.1, Fig. 38) the fractional inhibition (Fa) was calculated by normalizing to the data from 0 (lowest inhibition, i.e. solvent) to 1 (highest inhibition) and the combination index (CI) was calculated by the freely available software CompuSyn using the "non-constant ratio" setting (combosyn.com). The values were plotted using GraphPad Prism 6 using the linear regression tool. The obtained lines were tested for statistically significant different slopes using the built-in compare function in GraphPad Prism 6.

For the BD-CP replacement assays (see 6.3.2.2) unpaired, non-parametric t tests (Mann-Whitney) against BD-CP single-treated cells were performed. For Smo overexpression experiment (see 6.3.2.3) the data were tested for Gaussian distribution using D'Agostino-Pearson omnibus reality test. For Shh light II ordinary one-way ANOVA and a Sidak's multiple comparisons test were performed. The results from *Smo*$^{-/-}$ experiments failed the test for Gaussian distribution, thus unpaired, non-parametric t tests (Mann-Whitney) against solvent-treated cells were performed.

6. Results

6.1. Regulation of *Vdr* expression by Gli TFs

BCCs, which are characterized by active Hh signaling, overexpress the VDR (Mitschele *et al.* 2004). This indicates that Hh signaling may regulate VDR expression. Using the software MatInspector (Quandt *et al.* 1995), we recently discovered a consensus motif for binding of Gli transcription factors (Lee *et al.* 2010; Winklmayr *et al.* 2010) 312 bp upstream of the first exon in the murine *Vdr* promoter region (unpublished data, see below). Moreover, our initial experiments indicated a Gli3-mediated regulation of *Vdr* expression, since overexpression of *Gli3* in wt *Ptch* cells resulted in upregulation of *Vdr* (Fritsch 2014). Here, we assessed if the Gli binding motifs of the *Vdr* promoter are functional regulatory elements by analyzing the activity of *Vdr* promoter reporter constructs in the presence of Gli3.

To determine the effect of Gli3 on *Vdr* expression we overexpressed Gli3 in three different cell lines. As a control cell line wt *Ptch* fibroblasts were chosen since these cells display an intact and Shh-inducible Hh signaling pathway (Uhmann *et al.* 2011a). We also used *Ptch*$^{-/-}$ fibroblasts, because these cells display constitutive activation of the Hh pathway due to a biallelic *Ptch* mutation (Uhmann *et al.* 2011a) to analyze the effect of Gli3 independently of Gli1 and Gli2. Finally we employed a *Gli1/Gli2* double knockout cell line (*Gli1*$^{-/-}$*/Gli2*$^{-/-}$) (Lipinski *et al.* 2008). Since Hh signaling activation by Shh promotes the processing of the full-length Gli3 repressor form (Gli3^{rep}) to its activator form (Gli3^{act}) (Wang *et al.* 2007a), *Gli3*-transfected wt *Ptch* and *Gli1*$^{-/-}$*/Gli2*$^{-/-}$cells were additionally stimulated with Shh-N-CM. Afterwards the *Vdr* expression levels were determined. The Hh signaling activation status and the transfection efficiency were controlled by quantification of the expression of *Gli* transcription factors.

In Hh-responsive wt *Ptch* cells Shh-N-CM stimulation led to a significant increase of *Gli1* expression with and without *Gli3* transfection (Fig. 5 A). *Gli2* expression was significantly increased after *Gli3* transfection and additional stimulation with Shh-N-CM (Fig. 5 B). Significantly elevated *Gli3* expression levels were detected only after *Gli3* transfection (Fig. 5 C) which confirmed an efficient transfection procedure. However, *Vdr* expression was not regulated (Fig. 5 D).

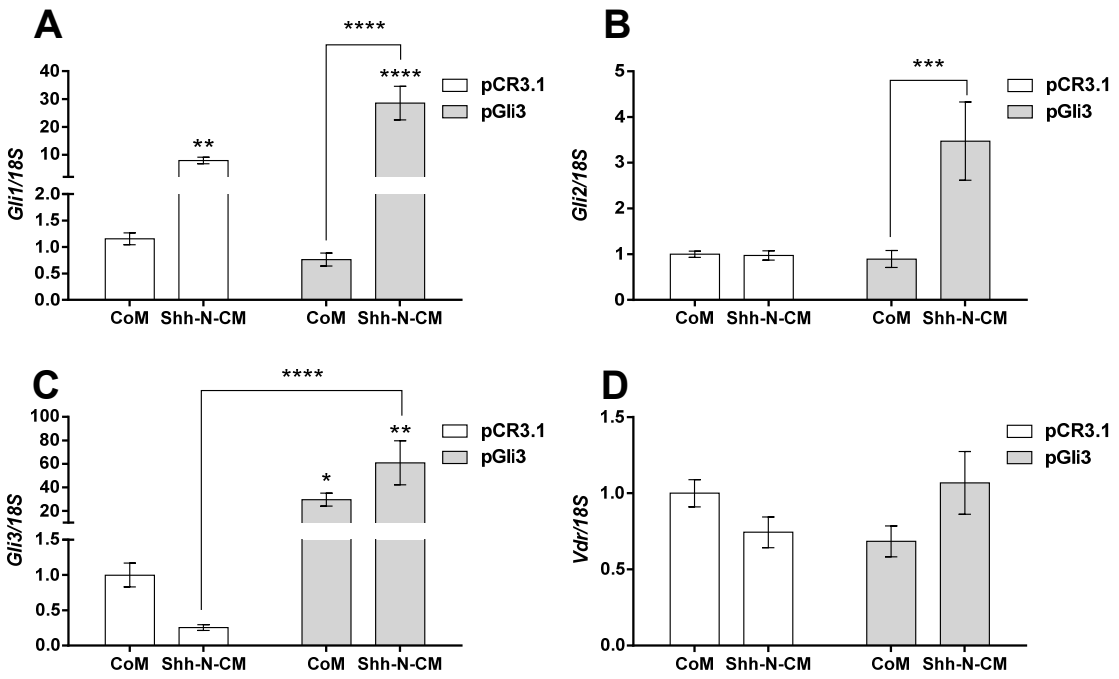

Figure 5: *Vdr* expression is not regulated by Gli3 in wt *Ptch* cells. Relative quantification of **(A)** *Gli1*, **(B)** *Gli2*, **(C)** *Gli3* and **(D)** *Vdr* expression levels of wt *Ptch* fibroblasts after *Gli3* overexpression and Shh-N-CM treatment. Gene expression levels were normalized to *18S* rRNA expression. Expression levels of control vector-transfected cells (*pCR3.1*) treated with control medium (CoM) were set to 1. All data are represented as mean +/- SEM of at least three experiments. * $p<0.05$, ** $p<0.01$, *** $p<0.001$, **** $p<0.0001$.

Next, *Ptch*$^{-/-}$ cells were transfected with *Gli3* (Fig. 6). In contrast to the assumption that in *Ptch*$^{-/-}$ cells Hh signaling activity cannot be further enhanced, *Gli3* transfection resulted in significant induction of *Gli1* and *Gli2* expression (Fig. 6 A, B). This indicates that Hh signaling activity can be further increased by Gli3 in *Ptch*$^{-/-}$ cells. Efficient *Gli3* transfection was revealed by significantly elevated *Gli3* levels (Fig. 6 C). Nevertheless, overexpression of Gli3 did not significantly increase *Vdr* expression in these cells (Fig. 6 D).

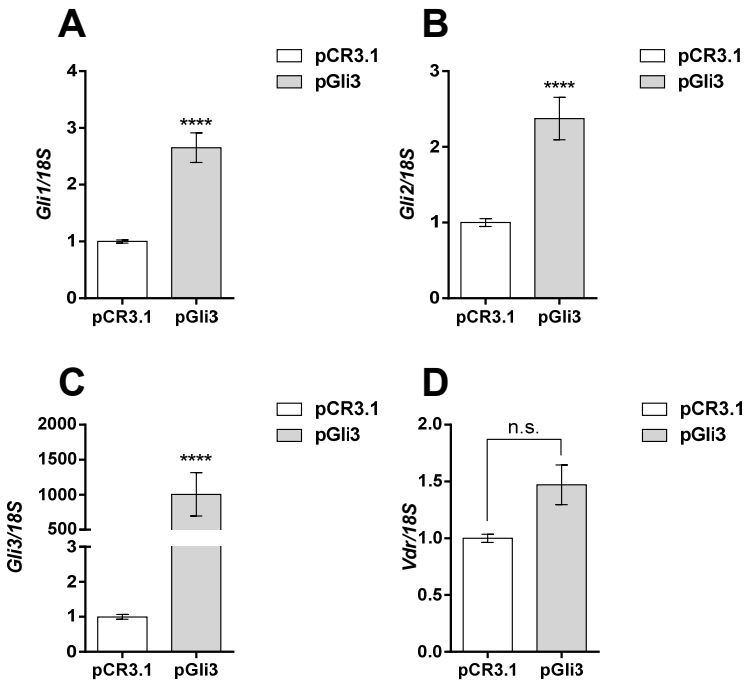

Figure 6: *Vdr* expression is not regulated by Gli3 in *Ptch*$^{-/-}$ cells. Relative quantification of **(A)** *Gli1*, **(B)** *Gli2*, **(C)** *Gli3* and **(D)** *Vdr* expression levels of *Ptch*$^{-/-}$ fibroblasts after *Gli3* overexpression. Gene expression levels were normalized to *18S* rRNA expression. Expression levels of control vector-transfected cells (*pCR3.1*) were set to 1. All data are represented as mean +/- SEM of at least three experiments. **** $p<0.0001$.

Finally, *Gli3*-transfected and/or Shh-N-CM-stimulated *Gli1*$^{-/-}$/*Gli2*$^{-/-}$cells were analyzed (Fig. 7). These cells are devoid of any endogenous *Gli1* and *Gli2* expression (Lipinski *et al.* 2008). Thus any Gli1- or Gli2-mediated effect including activation of Hh signaling can be excluded in these cells. *Gli3* transfection led to significant elevated *Gli3* expression levels which confirmed the efficient transfection procedure (Fig. 7 A). However, Gli3 did not induce *Vdr* expression (Fig. 6 B). Interestingly, irrespective of *Gli3* transfection Shh-N-CM significantly increased *Vdr* mRNA levels.

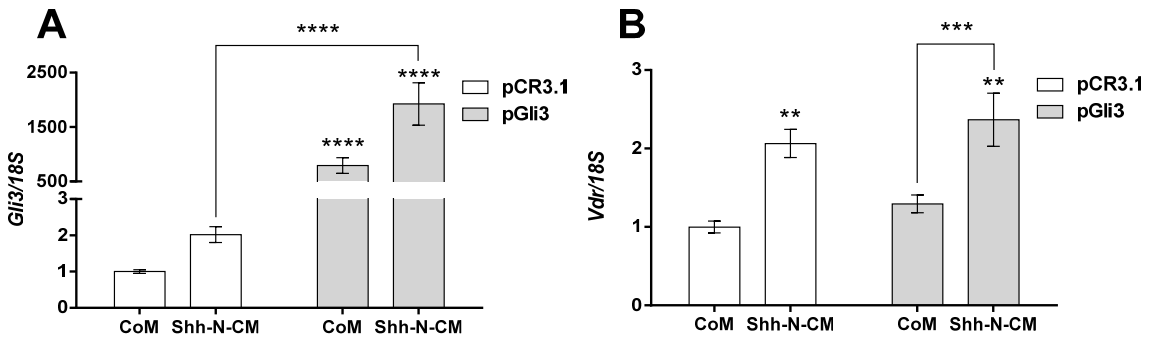

Figure 7: Regulation of *Vdr* expression by Shh in *Gli1*$^{-/-}$/*Gli2*$^{-/-}$ cells. Relative quantification of **(A)** *Gli3* and **(B)** *Vdr* expression levels of *Gli1*$^{-/-}$/*Gli2*$^{-/-}$cells after *Gli3* overexpression and/or Shh-N-CM treatment. Gene expression levels were normalized to *18S* rRNA expression. Expression levels of control vector-transfected cells (pCR3.1) treated with control medium (CoM) were set to 1. All data are represented as mean +/- SEM of at least three experiments, * $p<0.05$, ** $p<0.01$, *** $p<0.001$, **** $p<0.0001$.

Taken together the experiments suggested that the expression of the *Vdr* gene is not regulated by Gli3, but may be regulated by Shh in dependency of the cellular context.

Using the software Matinspector (Quandt *et al.* 1995) one putative Gli binding site (*GliBS*) was identified in the vicinity of the *Vdr* gene. This putative *GliBS* is located 312 bp upstream of the first exon of the *Vdr* gene in a reverse complement orientation (Fig. 8 and Tab. 17). To assess the activation status of the *Vdr* promoter (*pVdrProm*^{wt}) in the presence of Gli transcription factors, NIH/3T3 cells, which have an intact Hh signaling pathway (Myers *et al.* 2013), were co-transfected with *Gli1*, *Gli2* or *Gli3* expression plasmids and a murine *Vdr* promoter reporter plasmid (*pVdrProm*^{wt}). The *pVdrProm*^{wt} plasmid consists of a firefly-luciferase gene under the control of a 481 bp long *Vdr* promoter fragment that includes the *GliBS* (Jehan and DeLuca 2000) (Fig. 8).

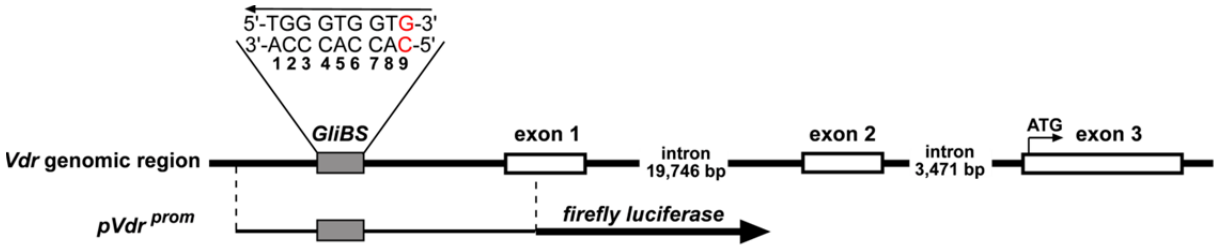

Figure 8: Schematic representation of the *Vdr* promoter region. The Gli binding site (*GliBS*) is located 312 bp upstream of the first exon (exon 1) of the *Vdr* gene. The *pVdrProm*^{wt} reporter plasmid contains 481 bp of the *Vdr* promoter region, including 46 bp of exon 1. The 9th nucleotide (red) of the *GliBS* of the *Vdr* promoter is different than the consensus sequence described (Winklmayr *et al.* 2010)(compare table 17).

Table 17: *GliBS* of the *Vdr* promoter

		1	2	3	4	5	6	7	8	9	
active *GliBS**	5‘-	G	A	C	C	A	C	C	C	A	-3‘
	3‘-	C	T	G	G	T	G	G	G	T	-5‘
inactive *GliBS**	5‘-	G	A	C	C	A	**G**	**G**	C	A	-3‘
	3‘-	C	T	G	G	T	**C**	**C**	G	T	-5‘
		1	2	3	4	5	6	7	8	9	
***GliBS Vdr* promoter** (reverse complement consensus sequence)	5‘-	T	G	G	G	T	G	G	T	**G**	-3‘
	3‘-	A	C	C	C	A	C	C	A	**C**	-5‘

* indicates *GliBS* according to (Winklmayr *et al.* 2010). Arrows indicate the genomic orientation of the *GliBS*. Differences to the optimal binding site (active *GliBS*) are indicated in red (according to (Winklmayr *et al.* 2010)). The *GliBS* of the Vdr promoter has a reverse complement orientation.

Dual-luciferase assays revealed that the *pVdrProm*^{wt} reporter (Fig. 9) was not stimulated by any of the co-transfected Gli TFs. (Fig. 9). These results strongly suggest that the analyzed *Vdr* promoter fragment is not regulated by Gli TFs and support the findings that transfection of *Gli3* did not result in upregulation of *Vdr* gene transcription.

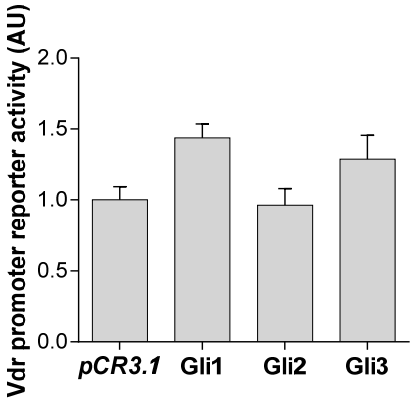

Figure 9: Analysis of *Vdr* promoter reporters in presence of Gli transcription factors. Dual-luciferase based analysis of NIH/3T3 co-transfected with *pVdrProm*^{wt} (endogenous Gli binding motif; wt *GliBS*) and *Gli1*, *Gli2* or *Gli3* expression plasmids. Transfection of empty vector (*pCR3.1*) served as a control. Firefly luciferase activities were normalized to the respective renilla luciferase activities. All data are represented as mean +/- SEM of at least three experiments in triplicates. Values obtained from *pCR3.1/pVdrProm*^{wt} co-transfected cells were set to 1. * $p<0.05$, ** $p<0.01$, *** $p<0.001$, AU: arbitrary units.

6.2. Role of calcitriol as an anticancer agent

Recently our group showed that calcitriol, the hormonally active form of vitD_3, effectively inhibits Hh signaling *in vitro* and *in vivo* (Uhmann *et al.* 2011a; Uhmann *et al.* 2012). Moreover other labs demonstrated *in vitro* inhibition of Hh signaling by the calcitriol precursor vitD_3 (Bijlsma *et al.* 2006; Tang *et al.* 2011). Here, the mechanism resulting in calcitriol-mediated Hh signaling inhibition was investigated. In addition, calcitriol was combined with other drugs to enhance the Hh-inhibitory effect and to potentially increase its anti-tumoral properties.

6.2.1. Enhancement of potential antitumoral effects of calcitriol *in vitro*

Recently it has been described that the antifungal drugs azoles ITZ and KTZ efficiently inhibit Hh signaling and show anti-tumoral potential (Kim *et al.* 2014; Kim *et al.* 2013; Kim *et al.* 2010). Moreover, azoles have been described as inhibitors of cytochrome P450 enzymes, that are, among others, involved in calcitriol metabolism (see chapter 2.3 and below). For the azole ITZ has been demonstrated that it acts on the level of Smo via a mechanism distinct from that of CP (Kim *et al.* 2010). Since the efficiencies of anti-cancer therapies often are enhanced by combination of drugs that intensify the effects of each other (Chou 2010) we hypothesized that azoles might enhance the anti-tumoral potential of calcitriol due to the following two mechanism: 1) Azoles may increase the intracellular concentrations or increase the stability of calcitriol due to the inhibition of the calcitriol degrading 24-hydroxylase (*Cyp24a1*) (Hansdottir *et al.* 2008; Muindi *et al.* 2010; Vanden Bossche *et al.* 2004) and 2) Calcitriol and azoles might inhibit Smo by binding to different sites that may result in an enhancement of Hh signaling inhibition superior to that of single drug treatments. Moreover, since most BCCs show loss-of-function mutations of the tumorsuppressor Ptch and treatment-resistance usually occurs at the levels of Smo (reviewed in (Epstein 2008)) we assumed that combination of two distinct Smo inhibitors could be a beneficial therapy strategy. Since the effects of calcitriol are best studied in BCCs (Uhmann *et al.* 2011a) we used the murine BCC cell line ASZ001 as an *in vitro* model.

6.2.1.1. Hh-inhibitory effects of calcitriol are specifically enhanced by azoles

ASZ001 cells were treated with calcitriol in combination with ITZ or KTZ using normal culture medium containing 2 % FCS. As expected from our recent studies, single calcitriol treatment significantly inhibited *Gli1* expression (Fig. 10 A and D), induced *Cyp24a1* expression (Fig. 10 B and E) and reduced proliferation of ASZ001 cells (Fig. 10 C and F). Single KTZ or ITZ treatments had no effects on *Gli1* or *Cyp24a1* expression or proliferation, but the combinations calcitriol/KTZ and calcitriol/ITZ also significantly inhibited *Gli1* and induced *Cyp24a1* expression and reduced proliferation. Only the combination calcitriol/KTZ resulted in significantly reduced *Gli1* expression compared to both single treatments. Only *Cyp24a1* expression was significantly lower after calcitriol/ITZ treatment compared to calcitriol alone (Fig. 10 E).

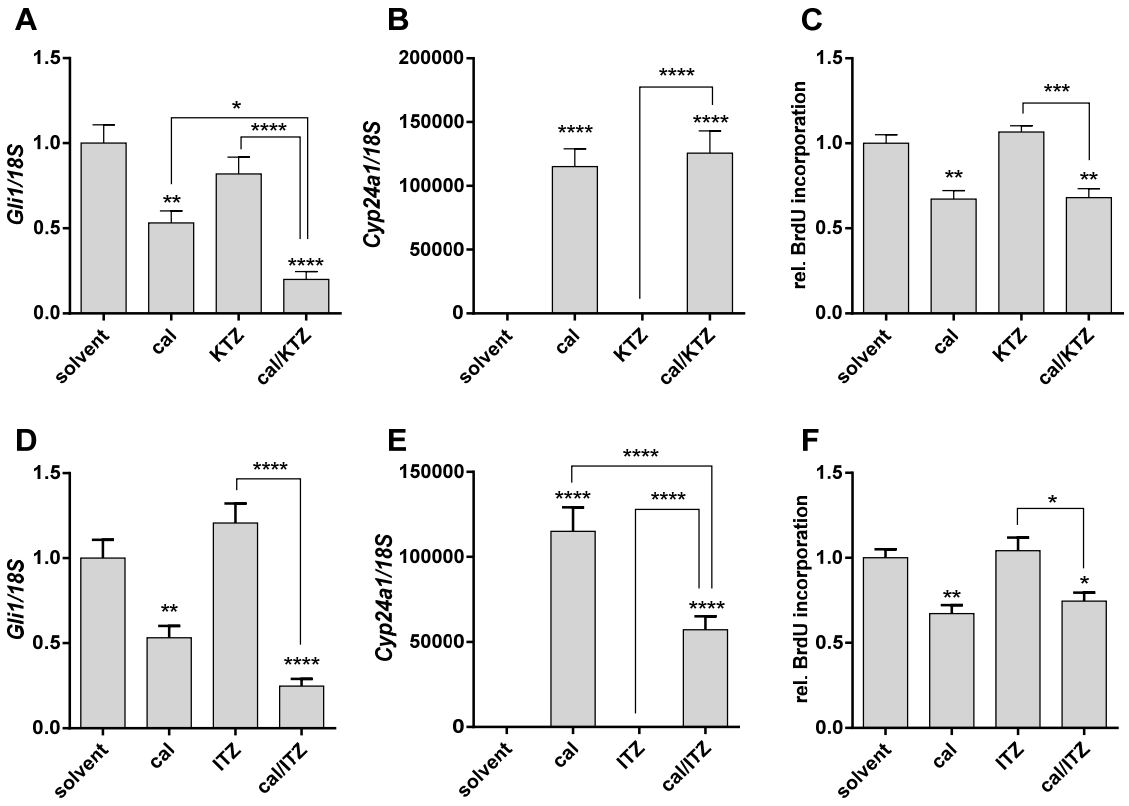

Figure 10: Combined calcitriol/azole treatment of ASZ001 cells using FCS-containing medium. Relative quantification of **(A and D)** *Gli1* or **(B and E)** *Cyp24a1* expression levels and **(C and F)** BrdU-incorporation assays of ASZ001 cells after treatment with 10 nM calcitriol (cal), (**A to C**) 1 µM ketoconazole (KTZ), (**D to F**) 1 µM itraconazole (ITZ) or a combination of both. Gene expression levels were normalized to *18S* rRNA expression. The respective solvent-treated controls (solvent) for each experiment were set to 1. All experiments were performed in 154-CF supplemented with 2 % heat-inactivated, chelexed FCS, 0.05 mM $CaCl_2$ and 1 % PS as described in the material and method section. The treatments for gene expression were conducted for 24 h, BrdU-incorporation-assays for 48 h. All data represent at least 3 independent experiments measured in triplicates, represented as mean +/-SEM; *, $p<0.05$; **, $p<0.01$; ***, $p<0.001$; ****, $p<0.0001$.

Together these results show that ITZ and KTZ do not have an impact on Hh signaling activity or cellular proliferation. They also do not enhance the calcitriol-mediated anti-tumoral effects if used in FCS-containing medium.

Because the effectiveness of ITZ-mediated Hh signaling inhibition can be quenched by FCS concentration higher than 2 % in the culture medium (Kim *et al.* 2010), we next performed a similar experiment using FCS-free medium. To decrease the colloid-osmotic pressure on the cells 1.5 % (w/v) BSA was added to the medium. Using these settings we found that single treatments with the azoles significantly inhibited Hh signaling activity as measured by reduced *Gli1* expression (Fig. 11 A and D). Moreover, the combination of the

azoles with calcitriol significantly intensified Hh signaling inhibition compared to either of the single treatments. Again *Cyp24a1* expression was strongly induced by single calcitriol and calcitriol/azole treatments (Fig. 11 B and E). In addition, calcitriol/ITZ, but not calcitriol/KTZ-treatment, significantly induced *Cyp24a1* expression compared to the respective single calcitriol treatments (Fig. 11 E). The combination of calcitriol with the azoles also significantly reduced cellular proliferation compared to solvent (ITZ, Fig. 11 F) or single-treatments (KTZ, Fig. 11 C).

Taken together, these experiments reveal that under serum-starved conditions azoles significantly intensify the Hh-inhibitory potential of calcitriol. Moreover the data suggest that azoles also cooperate with calcitriol in inhibition of cellular proliferation.

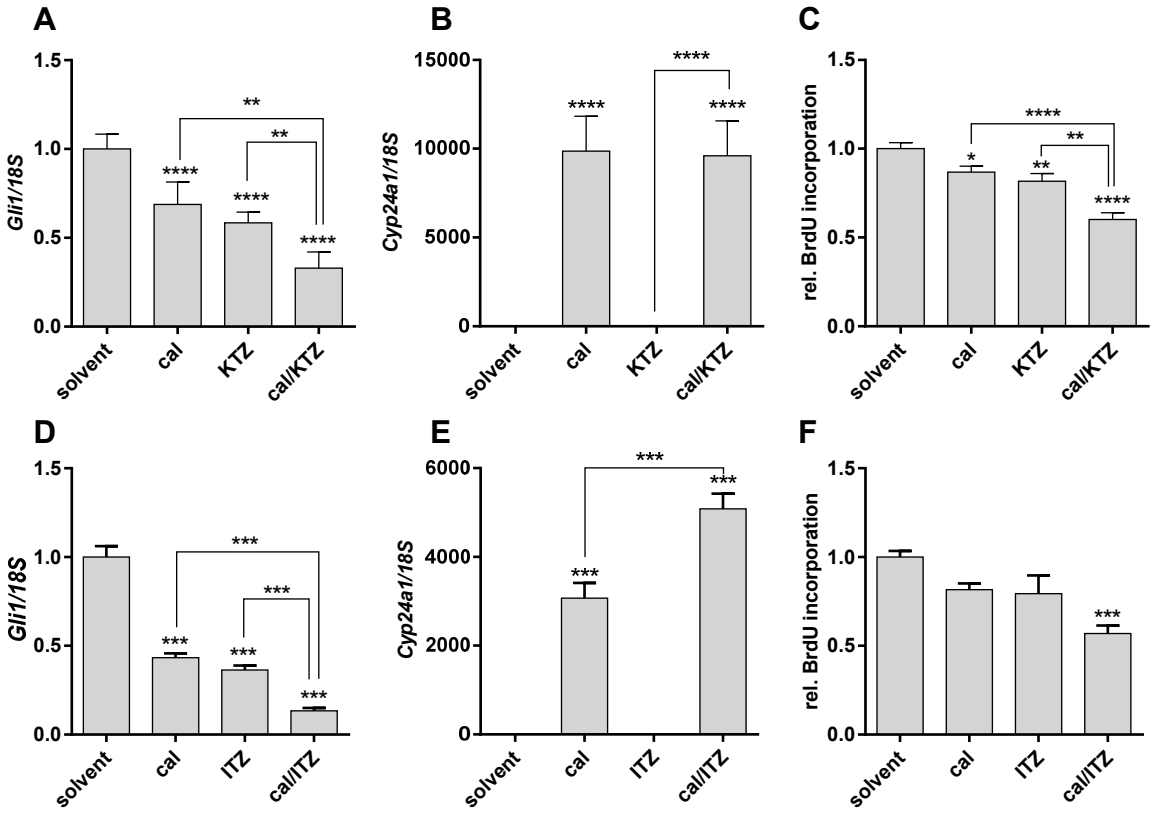

Figure 11: Combined calcitriol/azole treatment of ASZ001 cells using FCS-free medium. Relative quantification of **(A and D)** *Gli1* or **(B and E)** *Cyp24a1* expression levels and **(C and G)** BrdU-incorporation assays of ASZ001 cells after treatment with 10 nM calcitriol (cal), **(A to C)** 1 µM ketoconazole (KTZ), **(D to F)** 1 µM itraconazole (ITZ) or a combination of both. Gene expression levels were normalized to *18S* rRNA expression. The respective solvent-controls for each experiment were set to 1. All experiments were performed in 154-CF supplemented with 1.5 % BSA, 0.05 mM $CaCl_2$ and 1 % PS as described in the material and method section. Prior to the treatment a 24 h starvation step was included. For gene expression analyses the cells were treated with the substances for 24 h, for BrdU-incorporation assays 48 h. All data represent at least 3 independent experiments measured in triplicates, represented as mean +/-SEM. *, $p<0.05$; **, $p<0.01$; ***, $p<0.001$; ****, $p<0.0001$.

To analyze if the enhancement of calcitriol-mediated inhibition of Hh signaling and proliferation is specific for KTZ and ITZ, we next replaced the azoles with the well-known Hh inhibitor CP. Since the effectiveness of CP is not altered by FCS (Uhmann *et al.* 2011a) these experiments were conducted in FCS-containing growth medium. As expected single treatments with calcitriol and CP significantly reduced *Gli1* expression levels compared to solvent-treated controls (Fig. 12 A). However, the combination did not intensify this inhibition when compared to the single treatments. *Cyp24a1* expression was strongly induced by calcitriol, both alone or in combination with CP (Fig. 12 B). Furthermore, the cellular proliferation was significantly reduced by calcitriol and the combination calcitriol/CP, but not

by CP alone (Fig. 12 C). Again, the anti-proliferative effect of the combined treatment was not enhanced compared to the single calcitriol treatment. These results suggest that the combination of calcitriol and CP, in contrast to azoles, does not enhance Hh inhibition or anti-proliferative effects in ASZ001 cells.

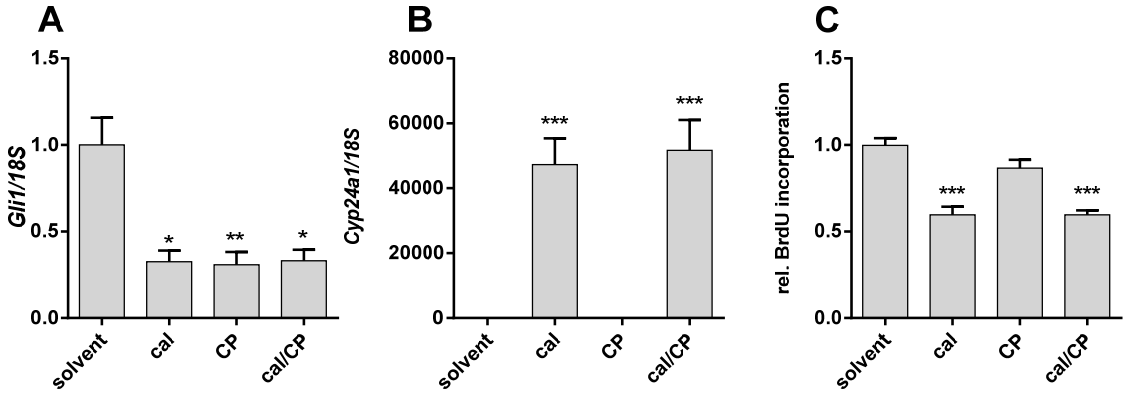

Figure 12: Combined calcitriol/CP treatment of ASZ001 cells does not result in combined antitumoral effects. Relative quantification of **(A)** *Gli1* or **(B)** *Cyp24a1* expression levels and **(C)** BrdU-incorporation assays of ASZ001 cells after treatment with 10 nM calcitriol (cal) and 5 µM cyclopamine (CP) alone or in combination. Gene expression levels were normalized to *18S* rRNA expression levels. The respective solvent-treated controls for each experiment were set to 1. Experiments were performed in 154-CF supplemented with 2 % chelexed FCS, 0.05 mM $CaCl_2$ and 1 % PS. The treatments for gene expression were conducted for 24 h, the BrdU-incorporation assays for 48 h. All data represent at least 3 independent experiments measured in triplicates represented as mean +/-SEM. *, $p<0.05$; **, $p<0.01$; ***, $p<0.001$.

Finally, ASZ001 cells were treated with ITZ and CP. These experiments were conducted in FCS-free medium supplemented with 1.5 % BSA. Both compounds significantly reduced *Gli1* expression (Fig. 13 A). However, no cooperative effect was observed. As expected none of the treatments altered *Cyp24a1* expression (Fig. 13 B). Significant anti-proliferative effects were observed by the single ITZ and combined CP/ITZ treatment (Fig. 13 C).

Taken together these experiments reveal that azoles can significantly intensify the Hh-inhibitory potential of calcitriol. Moreover these data suggest a cooperative antiproliferative effect of the substances. In contrast, neither the combination of calcitriol and CP nor of CP and an azole are sufficient to enhance the anti-tumoral effects of the respective other drug. Therefore, the observed cooperative effects must be a specific phenomenon for calcitriol and azoles.

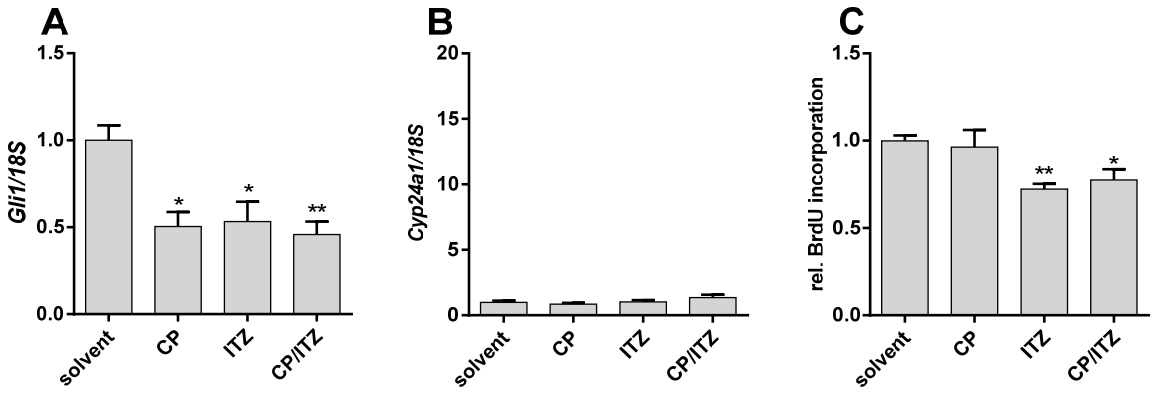

Figure 13: Combined treatment of ASZ001 with CP and ITZ does not result in combined antitumoral effects. Relative quantification of **(A)** *Gli1* or **(B)** *Cyp24a1* expression levels and **(C)** BrdU-incorporation-assays of ASZ001 cells after treatment with 5 µM cyclopamine (CP) and 1 µM itraconazole (ITZ) alone or in combination. Gene expression levels were normalized to *18S* rRNA expression levels. The respective solvent-controls for each experiment were set to 1. Experiments were performed in 154-CF supplemented with 1.5 % BSA, 0.05 mM $CaCl_2$ and 1 % PS. The treatments for gene expression were conducted for 24 h, the BrdU-incorporation-assays for 48 h. All data represent at least 3 independent experiments measured in triplicates represented as mean +/-SEM; *, $p<0.05$; **, $p<0.01$.

6.2.1.2. Combined calcitriol/azole treatment of murine BCC biopsies

To evaluate the effect of a combined calcitriol/azole treatment in a more sophisticated cell culture experiment, murine BCC biopsies were isolated from BCC-bearing skin of 3 *Ptch*$^{flox/flox}$ *CreERT2*$^{+/-}$ mice 60 days after tumor induction (see chapter 5.5.4). Since our previous analyses on ASZ001 cells showed that FCS quenched the azole-mediated Hh signaling inhibition the short-term culture and calcitriol/azole treatment was conducted in medium supplemented with 1.5 % BSA for 7 days (for details see chapter 5.2.11).

Unfortunately, most biopsies showed signs of necrosis (e.g. destructed dermis; fragmented nuclei), a fact that was never observed for skin biopsies cultured in FCS-supplemented medium. Nevertheless, gene expression analyses were still possible. This was demonstrated by *Cyp24a1* expression that was significantly induced by single calcitriol and combined calcitriol/azole treatment (Fig. 14 B and D). Single calcitriol as well as single ITZ treatment reduced *Gli1* expression (Fig. 14 A and C), whereas single KTZ treatment did not (Fig 14 A). However, in contrast to the cell culture experiment using ASZ001 cells, the combined calcitriol/azole treatments did not further reduce *Gli1* expression, but rather increased it in *in vitro* cultured BCC-bearing skin (Fig 14 A and C).

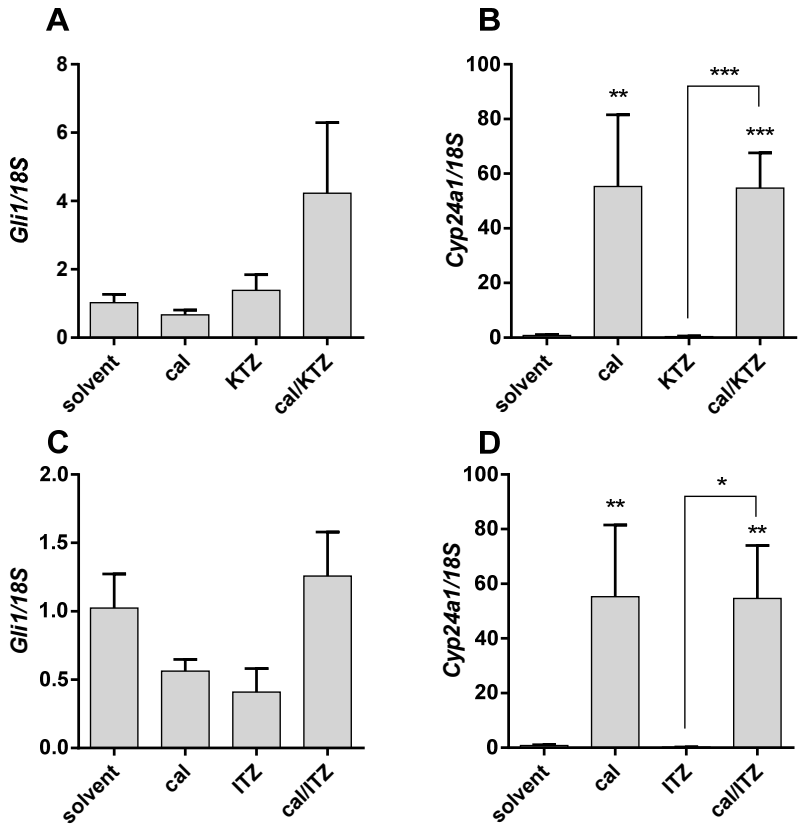

Figure 14: Combined treatment of *Ptch*$^{flox/flox}$ *CreERT2*$^{+/-}$ skin biopsies with calcitriol and azoles. Relative quantification of **(A and C)** *Gli1* or **(B and D)** *Cyp24a1* expression levels of cultured BCC-biopsies after treatment with 10 nM calcitriol (cal) and **(A and B)** 1 µM ketoconazole (KTZ) or **(C and D)** 1 µM itraconazole (ITZ) alone or in combination. Gene expression levels were normalized to *18S* rRNA expression levels. The respective solvent-treated controls for each experiment were set to 1. Experiments were performed in 154-CF supplemented with 1.5 % BSA, 0.05 mM $CaCl_2$ and 1 % PS. All data were measured in triplicates represented as mean +/-SEM; *, p<0.05; **, p<0.01; ***, p<0.001; ****, p>0.0001.

6.2.2. Evaluation of combined calcitriol/azole treatments *in vivo*

Our *in vitro* analyses showed that azoles intensify calcitriol-mediated Hh signaling inhibition and anti-proliferative effects in ASZ001 cells, but not in BCC-biopsies. In a final approach we therefore tested the anti-tumoral effects of the calcitriol/azole combination *in vivo*.

6.2.2.1. Combined calcitriol/azole treatment of BCC-bearing Ptch$^{flox/flox}$ CreERT2$^{+/-}$ mice

Recently our group treated BCC-bearing *Ptch$^{flox/flox}$ CreERT2$^{+/-}$* mice with 100 ng/kg/d calcitriol. When the drug was applied for 90 days immediately after tumor induction, tumor growth was significantly inhibited (Uhmann *et al.* 2011a). In order to combine calcitriol with azoles, we first tested the tolerance of the mice towards azoles in a pilot experiment. The amount of azoles was based on literature data (MacCallum and Odds 2002; McCabe *et al.* 1987; Rodriguez-Cuesta *et al.* 2010; Toledo *et al.* 2003). 12 8 week-old C57BL/6N mice were randomized into two cohorts. One group received 100 ng/kg calcitriol i.p. daily (this dose was adopted from our previous studies (Uhmann *et al.* 2011a)) and 100 mg/kg KTZ orally thrice a week (n=6), the second group received 100 ng/kg calcitriol i.p. daily and 100 mg/kg ITZ orally thrice a week (n=6)(Fig. 15). After 90 days 3 mice of each treatment group were sacrificed. The remaining animals were observed for additional 30 days to observe therapy-induced long-term effects. During the whole experiment and the observation period the animals were weighed twice a week as a marker for the animal's health (Fig. 16).

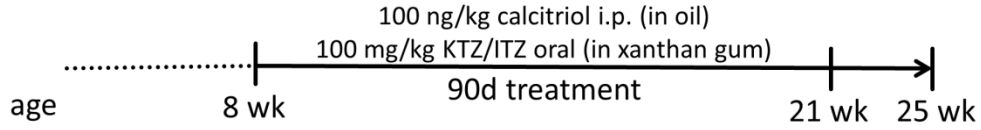

Figure 15: Schematic representation of the treatment schedule for determination of the tolerated dose of the combined calcitriol/azole therapy. 8 week-old C67BL/6N mice were treated with 100 ng/kg calcitriol in combination with 50 or 100 mg/kg ketoconazole (KTZ) or itraconazole (ITZ). Calcitriol treatment was conducted daily by i.p. injection; azole treatment was conducted thrice a week by oral gavage. After 90 days of treatment 3 mice of each treatment cohort were sacrificed and the remaining mice were observed for additional 30 days.

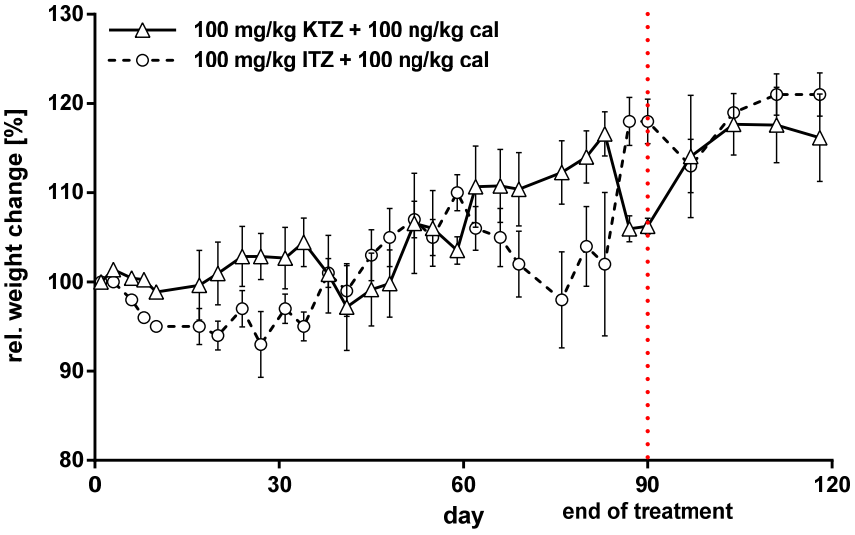

Figure 16: The combined calcitriol/azoles treatment did not impact the general health conditions of C57BL/6N mice. Relative weight changes of C75BL/6N mice treated with 100 ng/kg calcitriol (cal) in combination with 100 mg/kg ketoconazole (KTZ, n=6) or itraconazole (ITZ, n=6). The weight of each animal at the beginning of the treatment was set to 100 % and used to normalize the weight of the respective mouse of the following days. The treatment was conducted for 90 days. At the end of the treatment (day 90, red, dashed line) 3 animals of each treatment group were sacrificed and the remaining mice were observed for additional 30 days.

Irrespective of the received treatment all animals gained weight within the observation period (Fig. 16). No adverse effects or general health problems were determined, indicating that a combined treatment of 100 ng/kg/d calcitriol and 100 mg/kg azole thrice a week should be tolerated by BCC-bearing *Ptch*$^{flox/flox}$ *CreERT2*$^{+/-}$ mice.

BCC were induced in 42 8 week-old *Ptch*$^{flox/flox}$ *CreERT2*$^{+/-}$ mice by i.m. injection of 100 µg tamoxifen (see chapter 5.5.4) (Zibat *et al.* 2009). Directly after the tamoxifen injection the animals were randomized into 6 groups and treated with calcitriol (n=7), KTZ (n=7) or ITZ (n=7) or with the combination calcitriol/KTZ (n=7) or calcitriol/ITZ (n=7). Solvent-treated tamoxifen-injected *Ptch*$^{flox/flox}$ *CreERT2*$^{+/-}$ mice served as controls (n=7). The treatment was continued for 90 days (Fig. 17) as described in the material and method section (5.5.5 and 5.5.6). During the treatment period the animals were weighed twice a week. 5 mice were sacrificed within the treatment period: one solvent-treated control mouse developed a medulloblastoma, two mice from the calcitriol/KTZ treatment group showed extensive weight loss, one mouse from the ITZ treatment cohort developed a hydrocephalus and 1 mouse from the calcitriol/ITZ treatment group developed an ulcerous abscess on the right flank. These mice were excluded from further analyses.

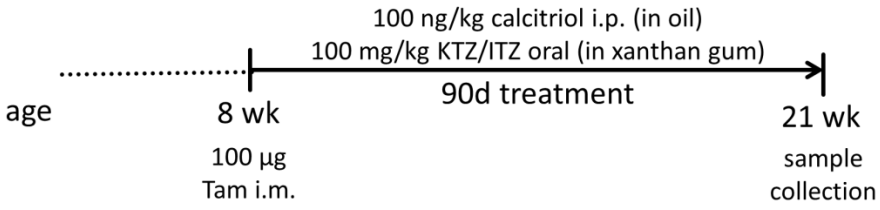

Figure 17: Schematic representation of the schedule of the combined calcitriol/azole treatment of *Ptch*$^{flox/flox}$ *CreERT2*$^{+/-}$ mice. 42 8 week-old *Ptch*$^{flox/flox}$ *CreERT2*$^{+/-}$ were i.m. injected with 100 µg tamoxifen. Directly thereafter the treatment was started and continued for 90 days. 6 mice received 100 ng/kg calcitriol daily by i.p. injection and 100 mg/kg ketoconazol (KTZ, n= 7) or itraconazole (ITZ, n=7) thrice a week by oral gavage or the respective combinations with calcitriol/KTZ (n=7) or calcitriol/ITZ (n=7). 7 mice received the respective solvents.

All remaining mice treated for 90 days gained weight until an age of 12 week (i.e. 45 days after onset of therapy) irrespective of the received treatment (Fig. 18). Thirty days after tamoxifen injection all mice developed macroscopically visible BCC at the tail and ear skin.

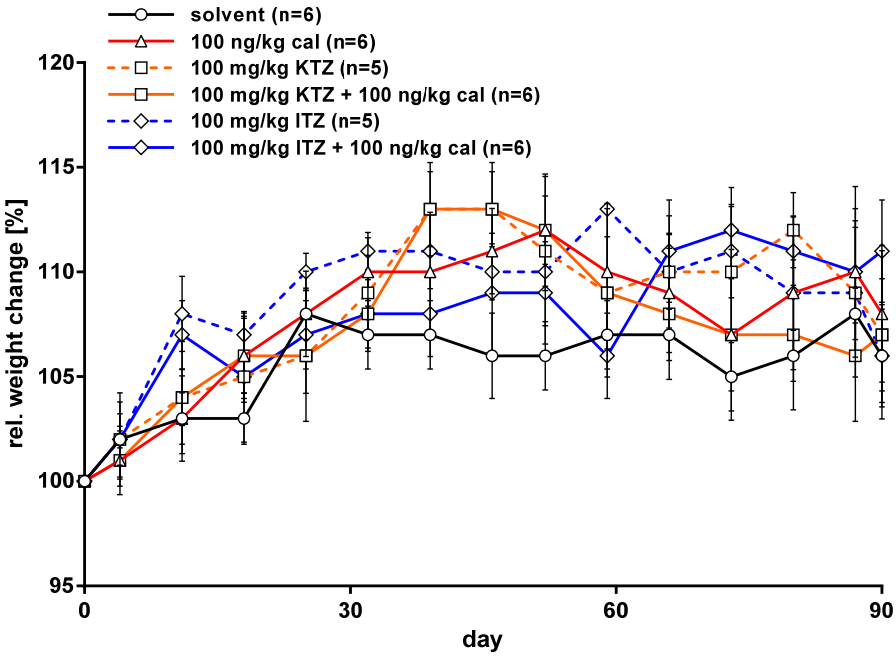

Figure 18: The combined calcitriol/azoles treatment did not impact the general health conditions of *Ptch*$^{flox/flox}$ *CreERT2*$^{+/-}$ mice. Relative weight change of tamoxifen-injected *Ptch*$^{flox/flox}$ *CreERT2*$^{+/-}$ mice under calcitriol/azole therapy as indicated in Fig 17. The weight of each animal at the beginning of the treatment was set to 100 % and used to normalize the weight of the respective mouse of the following days.

Ninety days after therapy start all animals were narcotized and preserved by perfusion as described (Chapter 5.5.3 and 5.5.8). Prior fixation, BCC tissue from the tail skin was sampled for gene expression analyses.

As shown by representative images of HE-stained paraffin section the tumors show typical histological features of nodular BCC (Zibat *et al.* 2009), irrespective of the treatment (Fig. 19).

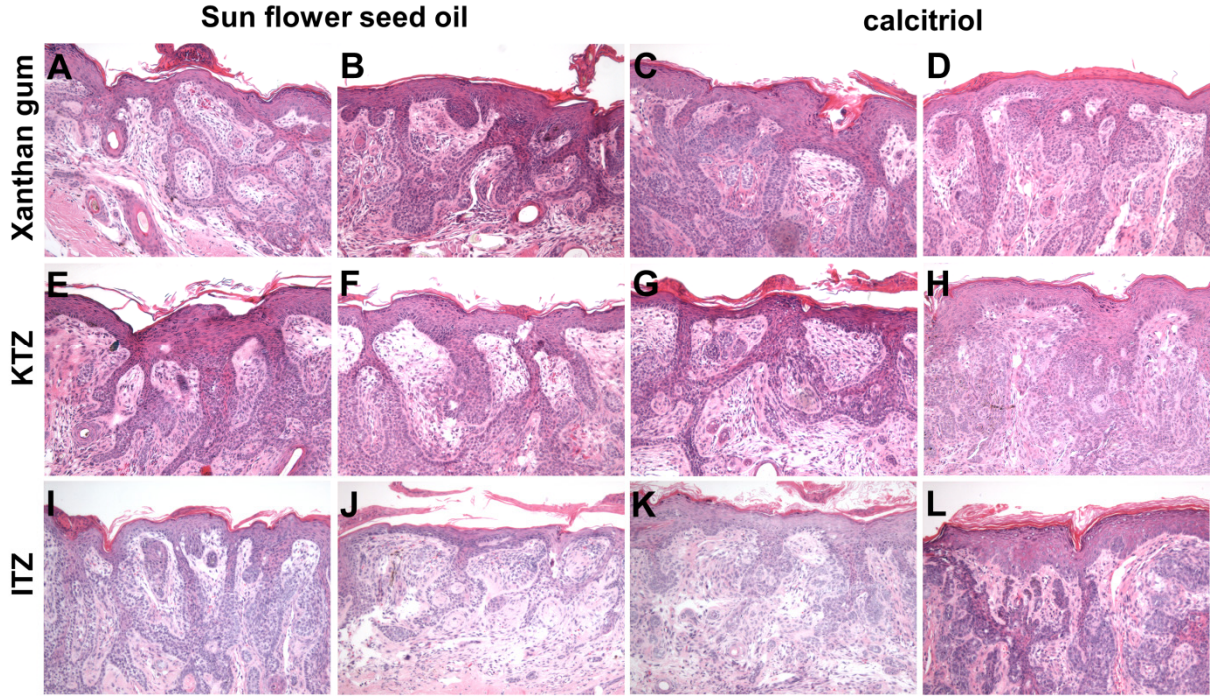

Figure 19: Histological appearance of BCC from calcitriol/azole-treated *Ptch*$^{flox/flox}$*ERT2*$^{+/-}$ mice. Representative HE-stained paraffin sections of BCC-bearing skin from *Ptch*$^{flox/flox}$ *CreERT2*$^{+/-}$ mice 90 days after tumor induction. The mice were treated for 90 days with **(A and B)** solvent (xanthan gum/sun flower seed oil), **(C and D)** 100 ng/kg calcitriol daily (cal), **(E and F)** 100 mg/kg ketoconazole thrice a week (KTZ), **(G and H)** calcitriol/KTZ, **(I and J)** 100 mg/kg itraconazole thrice a week (ITZ) or **(K and L)** calitriol/ITZ. 100 x magnification.

Gene expression analyses of *Cyp24a1* expression in the BCC-bearing skin confirmed that calcitriol alone or in combination with azoles has reached the tumor tissue (Fig. 20 and 21, C). Measurement of *Gli1* revealed that single calcitriol and single azole treatments only slightly inhibited the *Gli1* expression (Fig. 20 and 21, A). Surprisingly, and as seen in BCC biopsies (see chapter 6.2.1.2) the combination of calcitriol with an azole increased *Gli1* expression levels.

Similar results were observed for *Gli2* expression (Fig. 20 and 21 B). Thus, all single treatments slightly decreased *Gli2* expression, whereas the combined calcitriol/KTZ treatment

did not change, and the calcitriol/ITZ treatment increased *Gli2* expression compared to the solvent-treated controls.

Next, the expression levels of several epidermal differentiation markers were analyzed. The intermediate differentiation markers Keratin 1 (K1) and 10 (K10) (Bikle 2004; Blanpain and Fuchs 2006) are not only regulated by Vdr signaling (Bikle 2004), but also by active Hh signaling (Jetten 1990; Regl *et al.* 2004). Late epidermal differentiation is characterized by the expression of Loricirin (Lor) and Involucrin (Ivl) (Sandilands *et al.* 2009) and Transglutaminase (Tgm1) (Bikle 2004; Blanpain and Fuchs 2006). The latter marker is also known to be regulated by Vdr signaling (Bikle 2004).

In contrast to the single calcitriol, ITZ and KTZ treatments, which had no impact *K10* expression levels (Fig. 20 and 21 D), the combined calcitriol/ITZ treatment significantly enhanced *K10* expression (Fig. 21 D) compared to single calcitriol. The *Tgm1* expression level was slightly reduced by single calcitriol and combined calcitriol/KTZ treatments (Fig. 20 and 21, E), whereas application of single azoles did not influence the expression of *Tgm1*. Remarkably, the expression of this differentiation marker was induced in the calcitriol/ITZ treated cohort when compared to the calcitriol- and ITZ-treated animals (Fig. 21 E).

Analyses of the tumor area of HE-stained BCC sections (see chapter 5.3.3) revealed that none of the treatments significantly inhibited BCC growth (Fig 20 and 21 F) although a tendency was seen in animals that have been treated with ITZ or calcitriol/ITZ

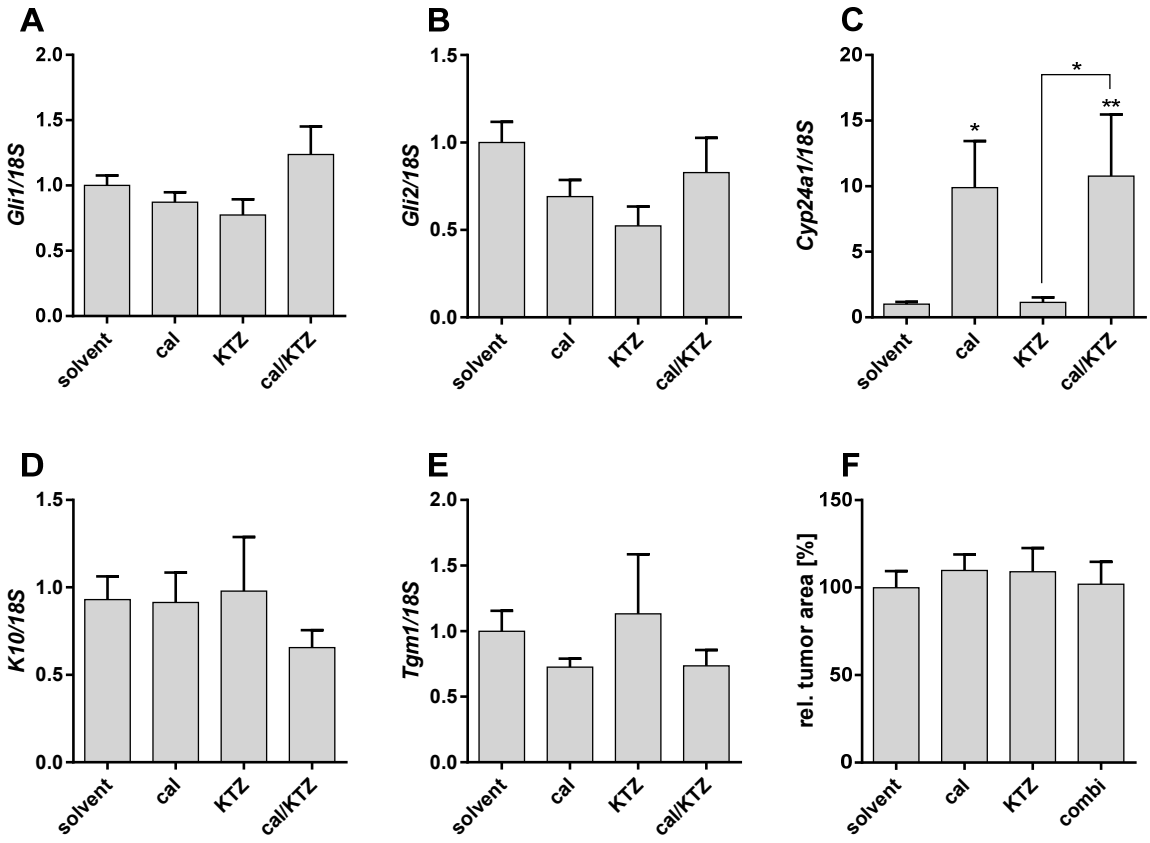

Figure 20: Combined calcitriol/KTZ treatment of BCC-bearing *Ptch*$^{flox/flox}$ *CreERT2*$^{+/-}$ mice. Relative quantification of **(A)** *Gli1*, **(B)** *Gli2*, **(C)** *Cyp24a1*, **(D)** *K10* and **(E)** *Tgm1* expression levels and **(F)** relative tumor area after 90 days of treatment of tamoxifen-injected *Ptch*$^{flox/flox}$ *CreERT2*$^{+/-}$ mice with 100 ng/kg calcitriol (cal) or 100 mg/kg ketoconazole (KTZ) or a combined therapy in comparison to solvent-treated controls. **(A-E)** Gene expression levels were normalized to *18S* rRNA expression and the solvent-treated controls of each experiment were set to 1. **(F)** Tumor areas were assessed from at least three vision fields of HE-stained BCC sections and the solvent-treated controls were set to 100 %. The data are represented as mean +/-SEM. *, $p<0.05$.

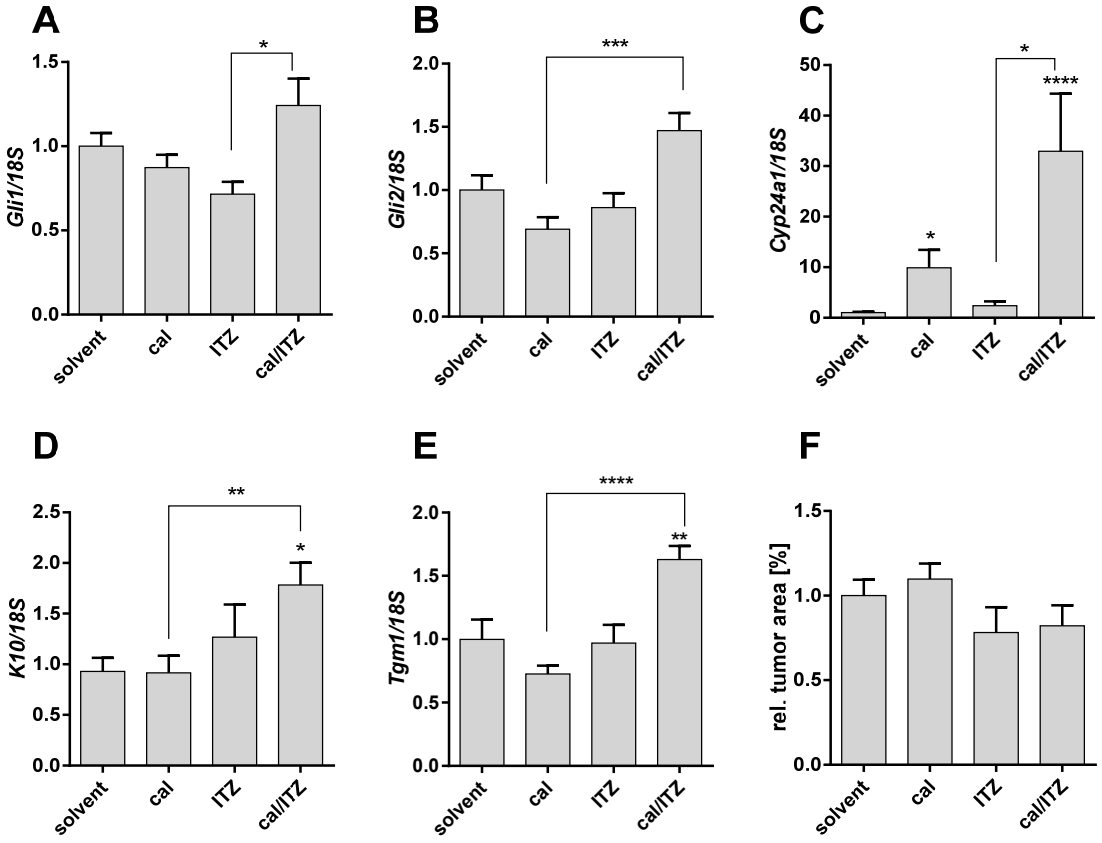

Figure 21: Combined calcitriol/ITZ treatment of BCC-bearing *Ptch$^{flox/flox}$ CreERT2$^{+/-}$* mice. Relative quantification of **(A)** *Gli1*, **(B)** *Gli2*, **(C)** *Cyp24a1*, **(D)** *K10* and **(E)** *Tgm1*, and **(F)** relative tumor area after 90 days of treatment of tamoxifen-injected *Ptch$^{flox/flox}$ CreERT2$^{+/-}$* mice with 100 ng/kg calcitriol (cal) or 100 mg/kg itraconazole (ITZ) or a combined therapy in comparison to solvent-treated controls. **(A-E)** Gene expression levels were normalized to *18S* rRNA expression and the solvent-treated controls of each experiment were set to 1. **(G)** Tumor areas were assessed from at least three vision fields of HE-stained BCC sections and the solvent-treated controls were set to 100 %. The data are represented as mean +/-SEM. *, $p<0.05$; **, $p<0.01$; ***, $p<0.001$.

In summary these data show that the *in vivo* application of calcitriol in combination with an azole neither inhibits Hh signaling nor reduces BCC size of *Ptch$^{flox/flox}$ CreERT2$^{+/-}$* mice, despite the fact that calcitriol has reached the tumor. Paradoxically, the combinations rather enhance *Gli1* and *Gli2* expression levels indicating activation of Hh signaling pathway in the tumors.

6.2.2.2. Combined calcitriol/ITZ treatment of ASZ001-transplanted nude mice

In parallel, we investigated the combined treatment of calcitriol/ITZ on ASZ001-allografted nude mice. To test if ASZ001 can form tumors 1 x 10^6 ASZ001 cells transplanted into the right and the left flank of 3 8 week-old nude mice (see chapter 5.5.7) gave rise to slow-growing tumors which were macroscopically visible and palpable after one week (Fig. 22). The growth of the grafted tumors was determined by measuring height, width and length of the tumors thrice weekly until one of the parameters exceeded 20 mm (Fig. 22). Since 6 to 7 weeks after the transplantation the tumors grew larger than 20 mm in one dimension the experiment was stopped and the mice were sacrificed. Histological examination of the tumors revealed that they displayed BCC-like features (Fig. 23).

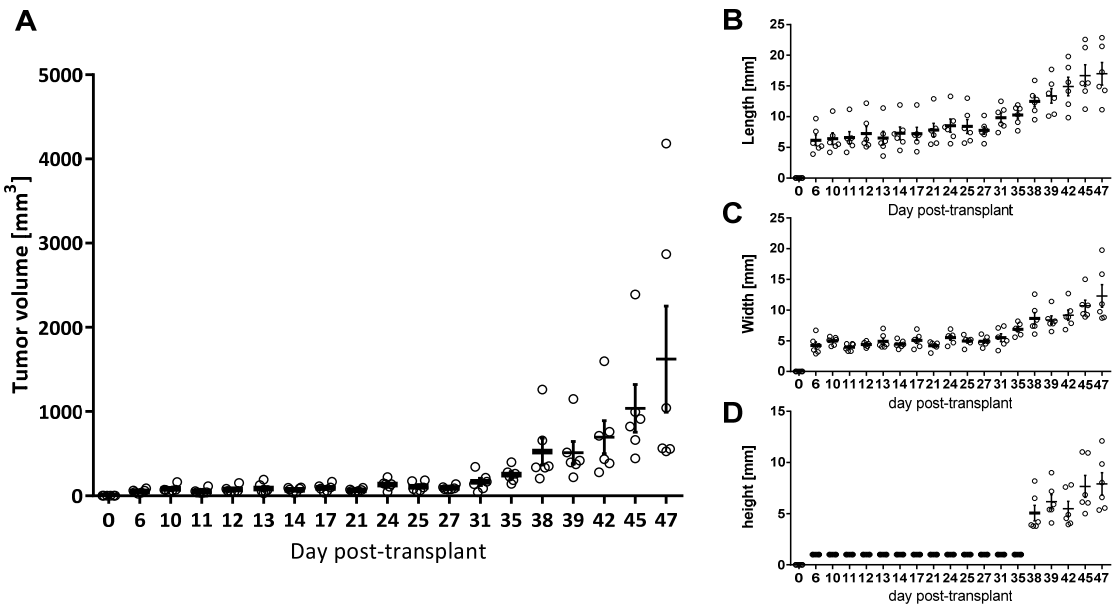

Figure 22: Tumor growth of subcutaneously transplanted ASZ001 cells in nude mice. (A) Tumor volume, **(B)** length, **(C)** width and **(D)** height of tumors from subcutaneously transplanted ASZ001 cells in nude mice. The tumor volumes were calculated by measuring the length, width and the height using a digital caliper (see chapter 5.5.7).

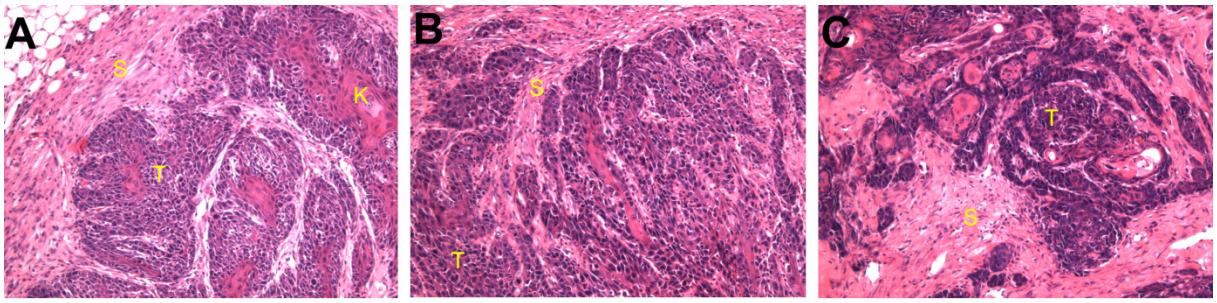

Figure 23: Representative images of ASZ001-allografts of nude mice. (A to C) HE-stained paraffin sections of ASZ001-allografts of nude mice 37 days after transplantation. Some tumors show areas of high keratinization (K in A) in the center of each nodule. T: tumor, S: stroma. 100 x magnification.

In the treatment cohort the mice were randomly grouped into 4 cohorts of 6 mice one week after the transplantation. The animals were treated with 100 ng/kg calcitriol, 100 mg/kg ITZ or a combination of both drugs for 30 days according to the treatment scheme shown in figure 24. Solvent-treated animals served as controls. One mouse from the solvent-treated control cohort was removed from the study due to an injury.

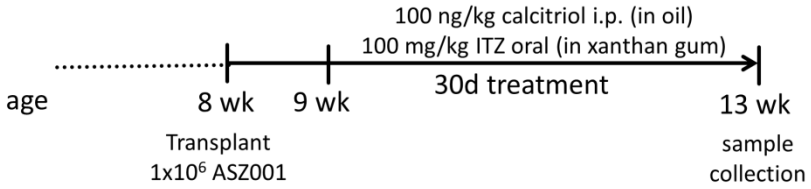

Figure 24: Schematic representation of the treatment schedule of the combined calcitriol/azole therapy of ASZ001-allografted nude mice. 8 week-old nude mice were transplanted with 1 x 10^6 ASZ001 in each flank (see chapter 5.5.7). 1 week after the transplantation the treatment was started and continued for 30 days. 6 mice received 100 ng/kg calcitriol daily by i.p. injection and 100 mg/kg itraconazole (ITZ) thrice a week by oral gavage or a combination of both (n=6) or respective solvent (n=5).

Throughout the experiment the tumor growth was determined thrice per week by measuring the length, width and height of the tumors and the volume was calculated (for details see chapter 5.5.7). Thereafter the mice were sacrificed; the tumors were weighed and preserved for histological and molecular analyses. Irrespectively of the treatment all grafted tumors grew similar to an approximate volume of 400 mm^3 until therapy end (Fig. 25 A). Only at day 16 after transplantation the solvent-treated tumors were significantly larger than those treated with calcitriol/ITZ. The tumor weight at the end of the study was not significantly altered after any treatment (Fig. 25 B).

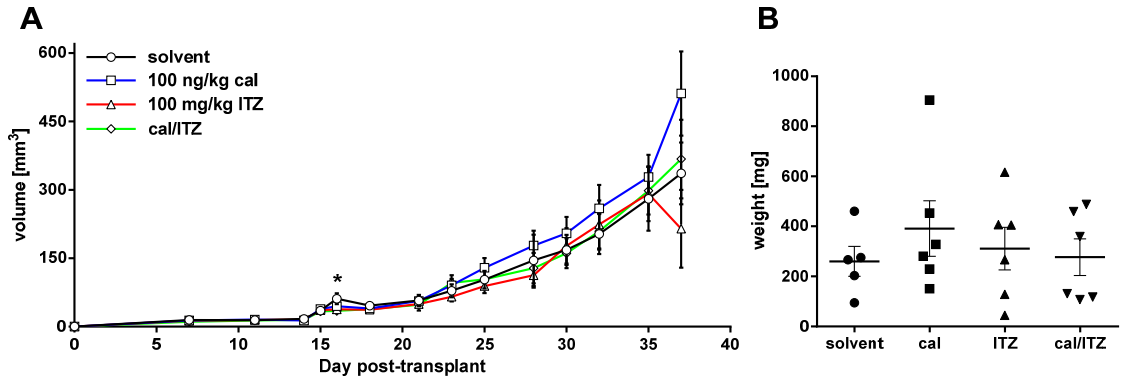

Figure 25: Growth and weight of subcutaneously transplanted ASZ001 tumors during a combined calcitriol/ITZ treatment. (A) Tumor volume and **(B)** weight of subcutaneously transplanted ASZ001 cells in nude mice **(A)** during and **(B)** after 30 day treatment with 100 ng/kg calcitriol (cal) and 100 mg/kg itraconazole (ITZ) or a combination of both. Solvent-treated ASZ001 transplanted mice served as controls. The tumor volumes were calculated by measuring the length, width and the height using a digital caliper (see chapter 5.5.9). At the end of the experiments the excised tumors were weighed. * $p<0.05$

In contrast to the BCC of *Ptch*$^{flox/flox}$ *CreERT2*$^{+/-}$ mice, the single calcitriol and ITZ, as well as the combined calcitriol/ITZ treatment, led to significant changes at the molecular levels (Fig. 26). Significantly reduced *Gli1* expression was observed after single calcitriol and ITZ treatment, with calcitriol being slightly more potent than ITZ (Fig. 26 A). The combined calcitriol/ITZ treatment only slightly decreased *Gli1* expression, which was not statistically significant. *Cyp24a1* expression analyses revealed that single calcitriol as well as combined calcitriol/ITZ therapy led to significantly increased Vdr signaling activity (Fig. 26 B) indicating the successful delivery and accumulation of calcitriol to the tumor. Nevertheless, the Vdr signaling induction after combined calcitriol/ITZ therapy was significantly lower than after single calcitriol treatment. When the proliferative activity of the tumors was analyzed by immunohistochemical stainings of Ki67, the amount of Ki67$^+$ cells was significantly increased in calcitriol- and calcitriol/ITZ-treated tumors (Fig. 26 C). Moreover, the

combination of calcitriol and ITZ significantly elevated the proliferative activity compared to single calcitriol-treated tumors. The single ITZ therapy did not change the proliferative activity of the tumors compared to solvent-treated tumors.

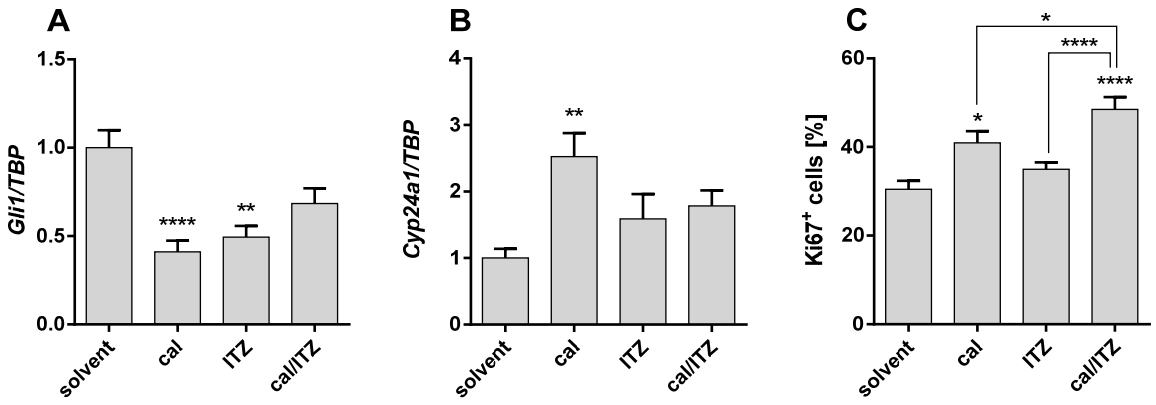

Figure 26: Molecular analyses of subcutaneously transplanted ASZ001 tumors after a combined calcitriol/ITZ treatment. Relative quantification of **(A)** *Gli1* or **(B)** *Cyp24a1* expression levels and **(C)** relative Ki67-positive ($Ki67^+$) cells of subcutaneously transplanted ASZ001 cells in nude mice after 30 day therapy with 100 ng/kg calcitriol (cal) and 100 mg/kg itraconazole (ITZ) or the drugs alone. Solvent-treated ASZ001-transplanted mice served as controls. Gene expression levels were normalized to *TBP* expression. *Gli1* and *Cyp24a1* expression levels of the solvent-treated controls were set to 1. Anti-Ki67 stainings and analyses were performed as described in the material and method section. The data are represented as mean +/-SEM. *, $p<0.05$; **, $p<0.01$; ***, $p<0.001$; ****, $p<0.0001$.

The analyses of the intermediate epidermal differentiation marker *K1* and *K10*, as well as late epidermal differentiation marker *Lor*, *Ivl* and *Tgm1* revealed that none of the treatments significantly altered the expression levels of these genes (Fig. 27).

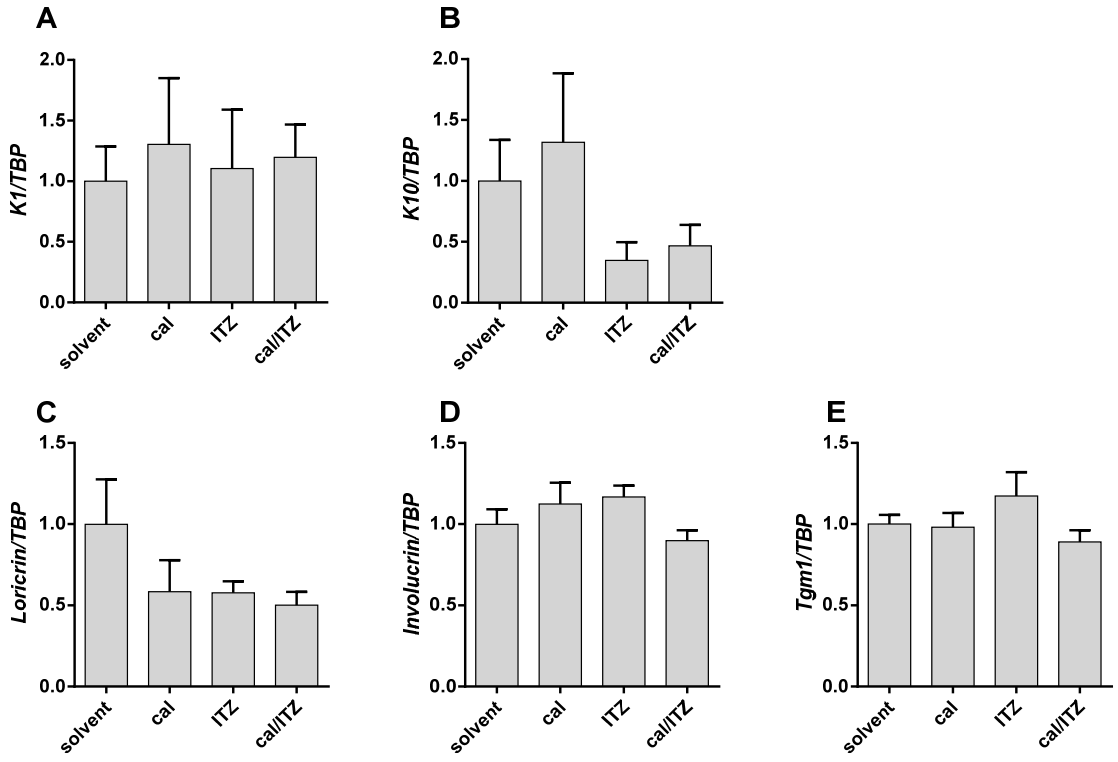

Figure 27: Expression analyses of epidermal differentiation markers of subcutaneously transplanted ASZ001 tumors after a combined calcitriol/ITZ treatment. Relative quantification of **(A)** *K1* or **(B)** *K10* **(C)** *Loricrin* **(D)** *Involucrin* and **(E)** *Tgm1* expression levels of subcutaneously transplanted ASZ001 cells in nude mice after 30 day therapy with 100 ng/kg calcitriol (cal) and 100 mg/kg itraconazole (ITZ) or the drugs alone. Solvent-treated ASZ001 transplanted mice served as controls. Gene expression levels were normalized to *TBP* expression. The respective solvent-treated controls were set to 1. The data are represented as mean +/-SEM. *, $p<0.05$; **, $p<0.01$.

Together these data show that in contrast to their anti-tumoral effects in cell culture (see chapter 6.2.1.1) calcitriol, ITZ as well as a combination of both drugs were not sufficient to inhibit proliferation or to induce differentiation of ASZ001 cells *in vivo*, despite their potential for simultaneous inhibition of Hh signaling and activation of Vdr signaling.

An ineffective anti-tumoral response can be explained by the absence of drug accumulation in the tumor. However, activation of Vdr signaling (Fig. 26 B) showed that calcitriol accumulated in the tumors. In order to determine intra-tumoral accumulation of ITZ we measured the ITZ levels directly in tumor tissue by mass spectrometry (see chapter 5.4.3). As shown in figure 28, ITZ was detected in transplanted ASZ001 tumors both after single ITZ and combined calcitriol/ITZ treatment. These data suggest that calcitriol as well as ITZ have entered the tumor cells.

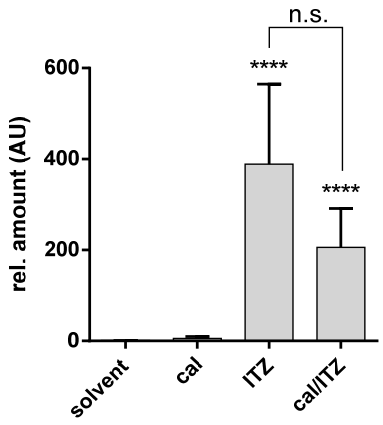

Figure 28: LC-MS/MS-based determination of intra-tumoral ITZ in transplanted ASZ001 tumors. LC-MS/MS-based determination of intraconazole (ITZ) of subcutaneously transplanted ASZ001 cells in nude mice after 30 day treatment with 100 ng/kg calcitriol (cal) and 100 mg/kg ITZ or the combination of both. Solvent-treated ASZ001 transplanted mice served as controls. **** $p<0.0001$; n.s.: not significant; AU: arbitrary units.

Finally we analyzed if the *in vivo* treatment with these drugs might have induced the expression of multidrug resistance proteins (*Mdr*). Mdrs are P-glycoproteins (P-gp) of the cell membrane, which belong to the superfamily of ATP-binding cassette transporters and are known transporters of xenobiotic compounds like anti-cancer drugs (Breier *et al.* 2013; Zhou 2008). However, irrespective of the therapy none of the analyzed *Mdr* transcripts (*Mdr1a*, *Mdr1b* and *Mdr2*) significantly differed in their expression level compared to the solvent-treated tumors (Fig. 29).

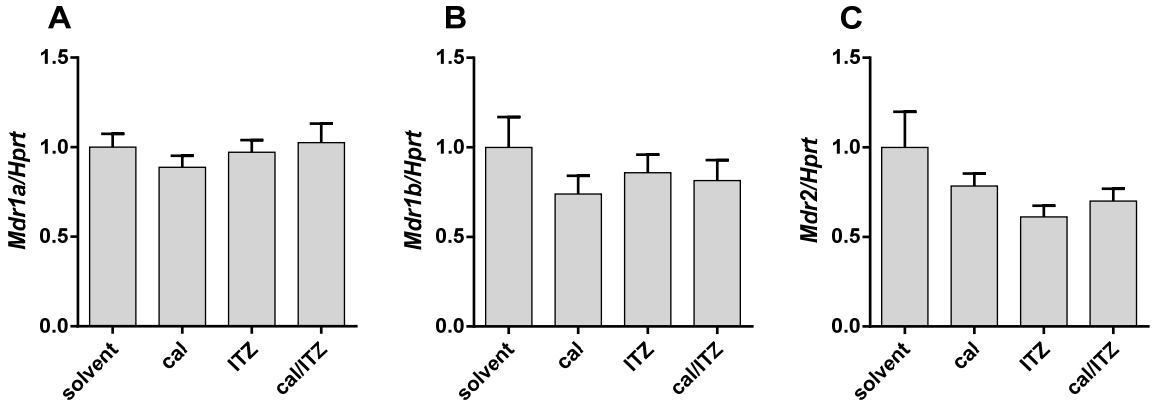

Figure 29: *Mdr* expression of subcutaneously transplanted ASZ001 tumors after a combined calcitriol/ITZ therapy. Relative quantification of **(A)** *Mdr1a* or **(B)** *Mdr1b* and **(C)** *Mdr2* expression levels of subcutaneously transplanted ASZ001 cells in nude mice after 30 day therapy with 100 ng/kg calcitriol (cal) and 100 mg/kg itraconazole (ITZ) or the drugs alone. Solvent-treated ASZ001 transplanted mice served as controls. Gene expression levels were normalized to *Hprt* expression. The respective solvent-treated controls were set to 1. The data are represented as mean +/-SEM.

Taken together these data suggest that the ineffective anti-tumoral response of transplanted ASZ001 cells can be explained neither by the absence of drug accumulation in the tumor cells nor by intra-tumoral activation of *Mdr* genes.

6.2.3. Analysis of the influence of ITZ on calcitriol-metabolism

The *in vitro* studies showed that ITZ significantly cooperates with calcitriol in Hh signaling inhibition and Vdr pathway activation (compare Figs 10 and 11, chapter 6.2.1.1). Moreover, comparison of the effects of combined calcitriol/ITZ and calcitriol/KTZ treatments revealed that KTZ is less effective than ITZ. Based on these findings and the fact that azoles have been described as general inhibitor of cytochrome P450 enzymes (Kota *et al.*

2011Muindi, 2010 #4234) we investigated if ITZ might prevent calcitriol synthesis or degradation by inhibition of 25-hydroxylase or 24-hydroxylase, respectively (Chen *et al.* 2012; Christakos *et al.* 2010).

In order to measure a potential alteration of calcitriol metabolism, we incubated ASZ001 cells for 6 h with 2 µM ITZ in combination with 2 µM 25(OH)D_3. Afterwards, the intracellular amounts of 25(OH)D_3, the 25(OH)D_3 degradation product 24,25$(OH)_2D_3$, and calcitriol (compare Fig. 3) were quantified by LC/MS-MS-based assays (see 0). The detection of the calcitriol degradation product 1α,24,25$(OH)_3D_3$ was not possible in our hands. But since the degradation of 25(OH)D_3 is catalyzed by 24-hydroxylase that also catalyzes the degradation of calcitriol (compare Fig. 3, (Chen *et al.* 2012; Christakos *et al.* 2010)) 24,25$(OH)_2D_3$ was used as a surrogate marker for 24-hydroxylase-activity and a marker for calcitriol degradation. HaCaT cells were simultaneously analyzed as a control, because this cell line has been described to convert 25(OH)D_3 to calcitriol (Lehmann 1997).

In both, ASZ001 and HaCaT cells, the intracellular amount of 25(OH)D_3 was significantly elevated after single 25(OH)D_3 or 25(OH)D_3/ITZ treatment compared to the solvent-treated controls (Fig. 30 A and D). However, the difference between the 25(OH)D_3 and the 25(OH)D_3/ITZ-treated cells was not significant. Similarly, the levels of 24,25(OH)2D3 were significantly elevated in single 25(OH)D_3 and 25(OH)D_3/ITZ-treated cells compared to the control, but did not significantly differ from each other (Fig. 30B and E). An enhanced synthesis of calcitriol upon any treatment was not measurable in ASZ001 cells (Fig. 30 C) whereas in HaCaT cells significantly elevated calcitriol levels were observed after 25(OH)D_3 and 25(OH)D_3/ITZ treatment (Fig. 30 F), that again did not significantly differ from each other (Fig. 30 F).

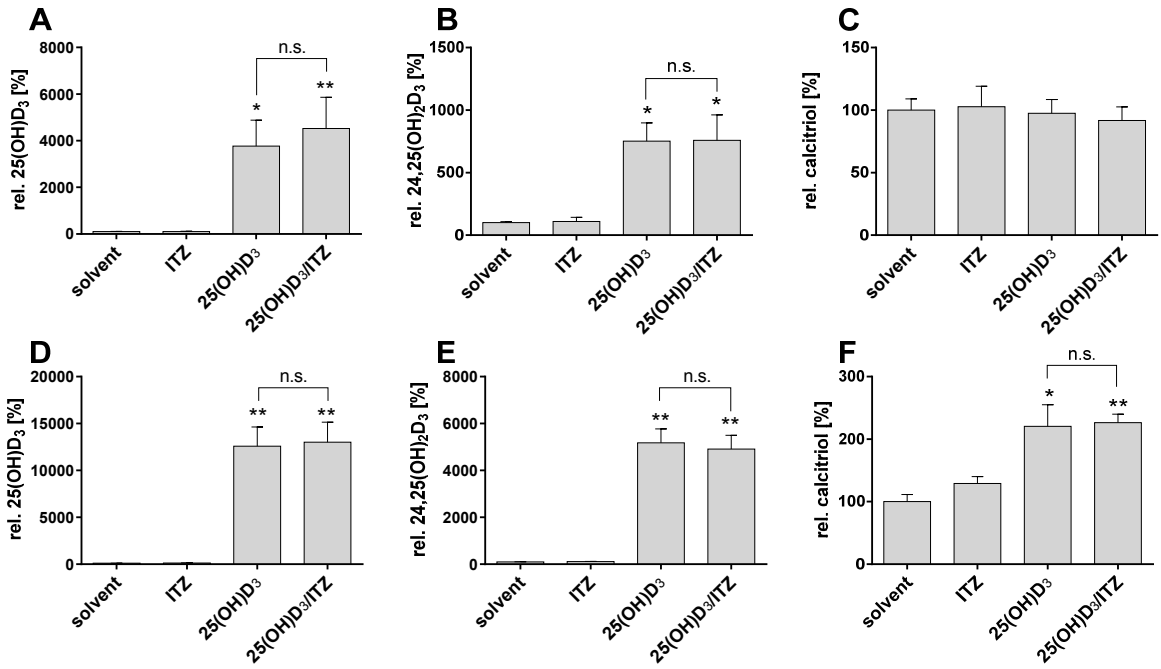

Figure 30: ITZ did not inhibit the enzymatic activity of the 1α-hydroxylase and 24-hydroxylase in ASZ001 and HaCaT cells. LC/MS-MS-based intracellular quantification of the vitD_3 metabolites **(A and D)** 25(OH)D_3, **(B and E)** 24,25$(OH)_2D_3$ and **(C and F)** calcitriol in **(A to C)** ASZ001 or **(D to F)** HaCaT cells after 6 h incubation with 2 µM 25(OH)D_3 or 2 µM itraconazole (ITZ) alone or in combination of both drugs. Solvent-treated cells served as controls. The data were normalized to the respective solvent-treated controls (100 %). The experiments were performed at least three times in triplicates. Each point represents the mean +/- SEM of all experiments. * $p<0.05$, ** $p<0.01$ compared to solvent control, n.s.: not significant.

Based on these data we conclude that ITZ does not influence the enzymatic activity of the 25-hydroxylase or the 24-hydroxylase and thus calcitriol synthesis from 25(OH)D_3 or on calcitriol degradation. Since the degradation of calcitriol was only measured indirectly by hydroxylation of 25(OH)D_3 to 24,25$(OH)_2D_3$ we next investigated if ITZ directly influences the intracellular amount of calcitriol. For this purpose ASZ001 and HaCaT cells were treated with 100 nM calcitriol and 2 µM ITZ and the intracellular amounts of calcitriol and ITZ were measured.

In both cell lines single calcitriol and combined calcitriol/ITZ treatment significantly elevated the intracellular levels of calcitriol (Fig. 31 A and B). However, no significant differences between the calcitriol or calcitriol/ITZ-treated cells were found (Fig. 31 A and C). Analyses of the intracellular ITZ levels revealed that both cell lines have accumulated ITZ after ITZ and calcitriol/ITZ treatment (Fig. 31 C and D). Significantly different ITZ amounts between single ITZ and combined calcitriol/ITZ-treated cells were not observed.

Taken together these experiments suggest that ITZ neither affects the synthesis of calcitriol from its precursor 25(OH)D_3 nor the calcitriol degradation in the analyzed cell lines.

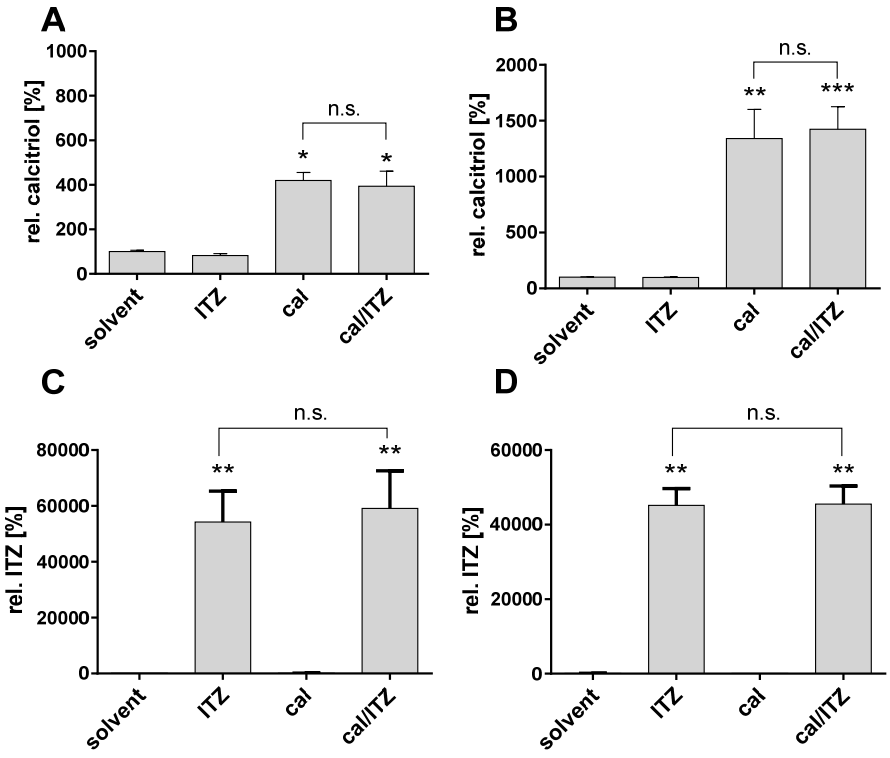

Figure 31: ITZ did not inhibit the enzymatic activity of the 24-hydroxylase in ASZ001 or HaCaT cells. LC/MS-MS-based intracellular quantification of **(A and B)** calcitriol (cal) or **(C and D)** itraconazole (ITZ) in **(A and C)** ASZ001 and **(B and D)** HaCaT cells after 6 h incubation with 100 nM cal or 2 µM ITZ alone or in combination of both drugs. Solvent-treated cells served as controls. The data were normalized to the respective solvent-treated control (100 %). The experiments were performed at least three times in triplicates. Each point represents the mean +/- SEM of all experiments. * $p<0.05$, ** $p<0.01$, *** $p<0.001$ compared to solvent control, n.s.: not significant.

6.3.Role of calcitriol in Hh signaling

6.3.1. Analyses of the synthesis and secretion of calcitriol in *Ptch*-deficient cells

One possible scenario of the Ptch/Smo interaction in Hh signaling regulation is the Ptch-mediated secretion of Smo-inhibitory molecules (see introduction and (Bidet *et al.* 2011; Bijlsma *et al.* 2006; Corcoran and Scott 2006; Myers *et al.* 2013)). To validate the hypothesis that calcitriol is released by Ptch to inhibit Smo, we analyzed if Ptch is sufficient for the calcitriol secretion and if loss of Ptch impairs calcitriol synthesis.

6.3.1.1. Ptch is essential for calcitriol secretion from the cell

As mentioned in the introduction (chapter 2.4), calcitriol is an excellent inhibitor of Hh signaling. Since Ptch shows similarities to RND transporters (Taipale *et al.* 2002) and harbors an essential SSD (Strutt *et al.* 2001) we asked if Ptch is required for calcitriol secretion. This would strengthen our model in which calcitriol acts as the endogenous inhibitor released by Ptch to inhibit Smo. An elegant way to answer this question would have been the quantification of calcitriol in cell culture medium derived from wt *Ptch* and *Ptch*$^{-/-}$ cells. Unfortunately, the detection of calcitriol in the medium was not possible by non-derivatized MS methods in our hands.

We first asked whether media obtained from wt *Ptch* or *Ptch*$^{-/-}$ cells are capable to inhibit Hh signaling. To answer this question the cell line Shh light II that is stably tranfected with a Gli-responsive firefly luciferase reporter gene and a constitutively active renilla-luciferase gene (Chen *et al.* 2002b) was used. Hh signaling activity in Shh light II cells was induced by Shh-N-CM treatment for 48 h.

The conditioned medium (CM) was generated by loading wt *Ptch* and *Ptch*$^{-/-}$ cells with calcitriol or the respective solvent for 1 h. Thereafter the cells were plated in calcitriol-free culture medium. After 4, 6 or 8 h the CM was transferred to Shh-N-CM pre-treated Shh light II (for details see chapter 5.2.10 and Fig. 4). As a background control the same procedure was performed without cells (no cell control). After additional 48 h, dual-luciferase assays were performed.

Irrespectively of the incubation time of 4 (Fig. 32 A), 6 (Fig. 32 B) or 8 h (Fig. 32 C) neither conditioned medium from wt *Ptch* nor from *Ptch*$^{-/-}$ cells significantly inhibited Hh signaling activity. 10 nM calcitriol or 5 µM CP (Fig. 32 D) served as positive controls.

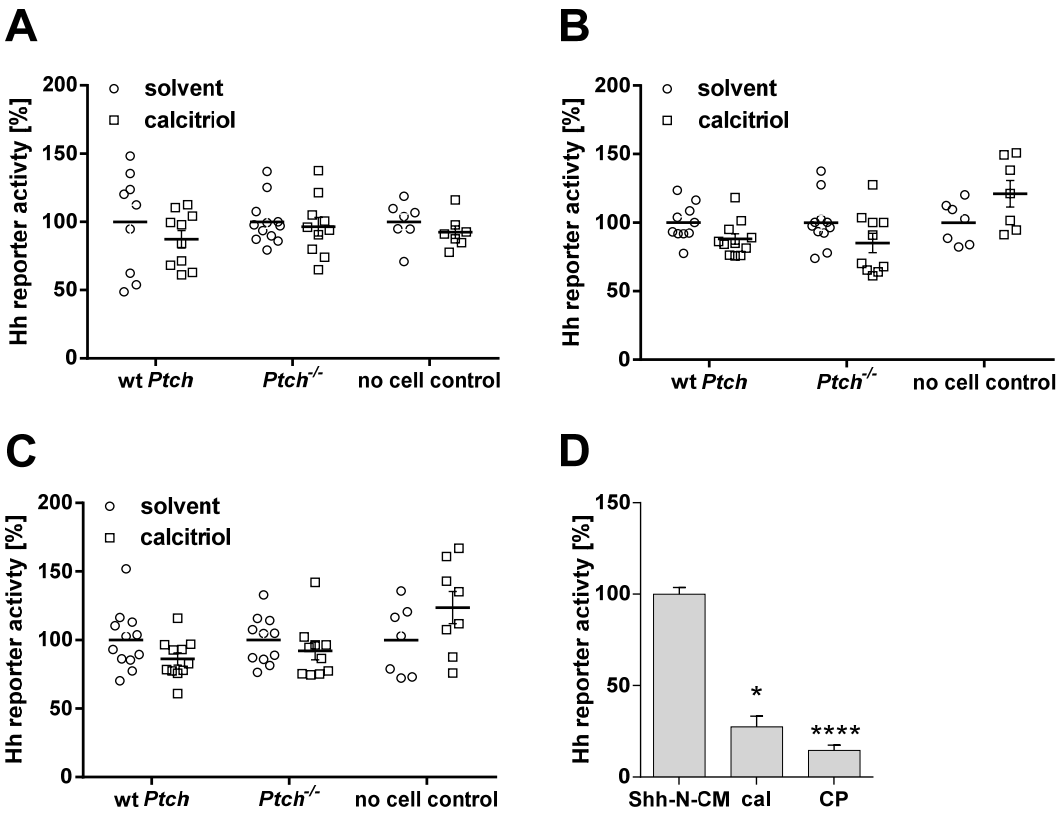

Figure 32: Conditioned medium from wt *Ptch* and *Ptch*$^{-/-}$ cells does not inhibit Hh signaling in Shh light II cells. Dual-luciferase based determination of Hh pathway activity using Shh light II after incubation with medium conditioned from wt *Ptch*, *Ptch*$^{-/-}$ or empty wells (no cell control) for **(A)** 4, **(B)** 6, **(C)** 8 h or **(D)**. The conditioned medium (CM) and the treatment with 10 nM calcitriol (cal) or 5 µM cyclopamine (CP) as positive controls was conducted for 48 h. As a background-control calcitriol-loading was carried out using culture media without cells (no cell control). The conditioned medium was prepared in triplicates, the medium from empty wells in duplicates. The treatment of the transfected cells was conducted in duplicates for each medium. Data represent normalized firefly/renilla luciferase activity. The solvent-loaded control for each cell line and time-point was set to 100 %; * $p<0.05$; ** $p<0.01$; *** $p<0.001$; **** $p<0.0001$.

Since the possibility remained that Shh light II cells were not sensitive enough to detect small amounts of calcitriol in the media, a calcitriol-mediated VDR/RXRα heterodimerization assay was established using a mammalian-two-hybrid system (M2H-assay). For this purpose, NIH/3T3 cells were transfected with a firefly luciferase reporter vector (*pFR-Luc*) and plasmids for the expression of RXRα coupled to a GAL4 binding domain (BD-RXRα; bait) as well as a GAL4 activation domain fused to a VDR (AD-VDR;

prey). The activation of VDR/RXRα heterodimerization by calcitriol then leads to the expression of the *luciferase* gene of the *pFR-Luc* plasmid under the control of the *GAL4* promoter ((Jacobs *et al.* 2013); calcitriol-sensitive M2H reporter system).

As shown in figure 33, the calcitriol treatment induced high luciferase activity in *pFR-Luc,* bait and prey transfected cells. In the absence of calcitriol only a low background induction was detectable. Also *pFR-Luc* alone or in combination with the bait did not induce background luciferase activity (Fig. 33 A). Treatment with a concentration series showed that the assay was highly sensitive towards calcitriol, but not 25(OH)D_3. Thus, 0.01 nM calcitriol was sufficient to induce luciferase activity and maximal pathway activation was achieved using 10 nM calcitriol (Fig. 33 B, orange curve). In contrast, the highest amount used for 25(OH)D_3 (1 µM) was needed for an induction level similar to the half-maximal activation of calcitriol (Fig. 33 B, blue curve).

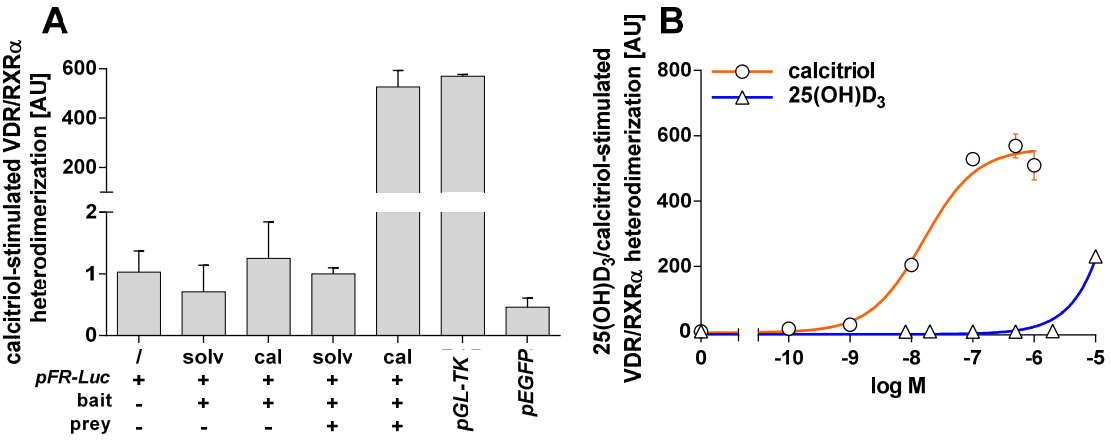

Figure 33: Establishment of the calcitriol-sensitive M2H reporter system. Determination of the **(A)** specificity and **(B)** sensitivity of calcitriol-sensitive M2H reporter system. **(A)** Normalized firefly luciferase activity of 10 nM calcitriol (cal) or solvent-treated (solv) NIH/3T3 cells transfected with the plasmids *pFR-Luc* (reporter), *pCMV-BD-RXRα* (bait) and/or *pCMV-AD-VDR* (prey) as indicated. The transfection with the constitutively active *pGL-TK* plasmid or *pEGFP* served as positive or negative control, respectively. Solvent-treated reporter, bait and prey transfected were set to 1. **(B)** Normalized firefly luciferase activity of NIH/3T3 transfected with the same as in (A) and treated with increasing amounts of calcitriol (orange) or 25(OH)D_3 (blue). The data were normalized to solvent (set to 1) for each drug and curve fitting was achieved using the "log(agonist) vs response (three parameter)"-function of GraphPad Prism 6. The experiments were performed once for establishment purposes. Each point represents the mean +/- SEM of biological triplicates. * $p<0.05$, ** $p<0.01$, *** $p<0.001$ compared to solvent control; AU: arbitrary units.

After establishment of the highly calcitriol-sensitive M2H reporter system we analyzed whether Ptch is essential for the release of calcitriol into the extracellular space (i.e. cell culture medium). The experiments revealed that after 4 (Fig. 34 A), 6 (Fig. 34 B) and 8 h (Fig. 34 C) the medium from calcitriol-loaded wt *Ptch* cells significantly activated VDR/RXRα heterodimerization, whereas the medium from *Ptch*$^{-/-}$ cells only weakly induced the reporter.

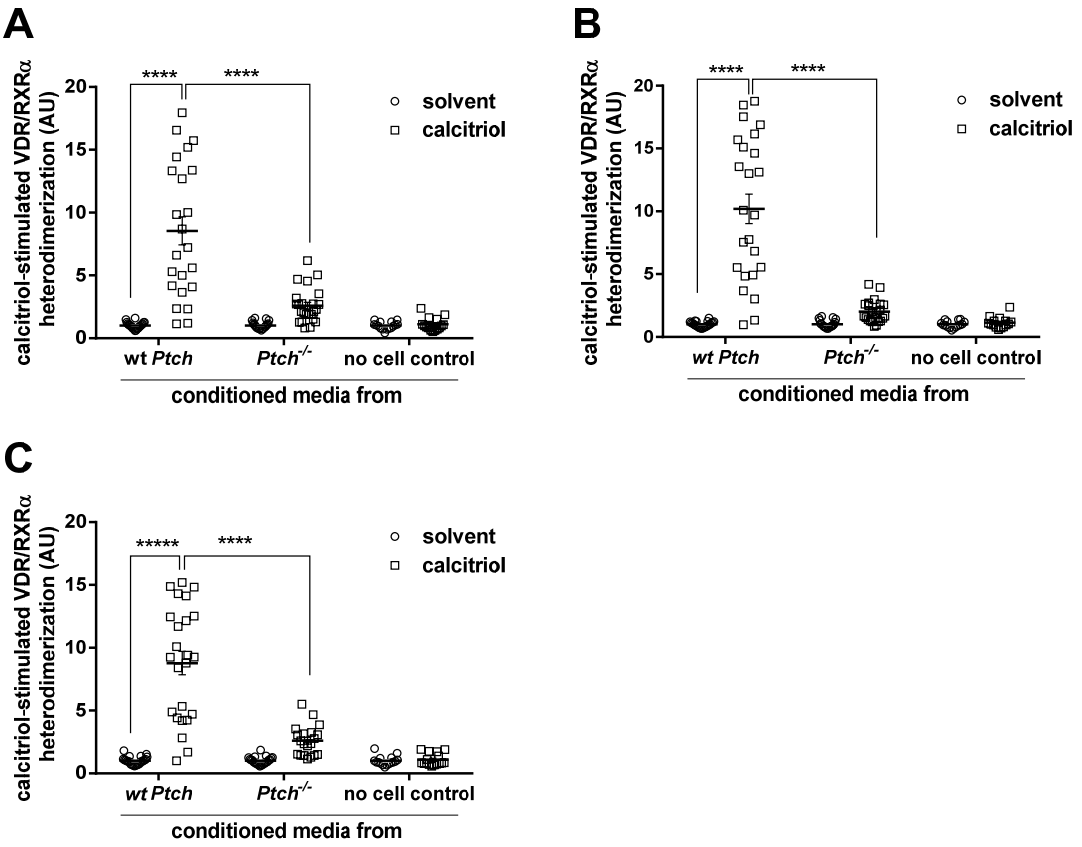

Figure 34: Ptch is necessary for the release of calcitriol. Calcitriol-sensitive M2H reporter assay of NIH/3T3 transfected with the plasmids *pFR-Luc*, *pCMV-BD-RXRα* (bait) and *pCMV-AD-VDR* (prey) after incubation with conditioned media from calcitriol or solvent-loaded wt *Ptch* and *Ptch*$^{-/-}$ fibroblasts . The media were conditioned for **(A)** 4, **(B)** 6 and **(C)** 8 h. The cells were loaded as described in chapter 5.2.11. As a background control calcitriol-loading was carried out using culture media without cells (no cell control). The conditioned medium was prepared in triplicates, the medium from empty wells in duplicates. The treatment of the transfected cells was conducted in duplicates for each medium. Data represent normalized firefly/renilla luciferase activity. The solvent-loaded control for each cell line and time-point was set to 1. All data represent at least 3 independent experiments represented as mean +/-SEM. * $p<0.05$, ** $p<0.01$, *** $p<0.001$, **** $p<0.0001$ compared to solvent-treated control; AU: arbitrary units.

Together, these experiments show that loss of Ptch perturbs the release of calcitriol into the medium. The minimal activation of the reporter by media from *Ptch*$^{-/-}$ fibroblasts (for comparison see empty-well control) can be explained by unspecific membrane shuttling of calcitriol rather than active transport through the cell membrane of *Ptch*$^{-/-}$ cells.

We reasoned that Shh light II cells are probably not as sensitive to calcitriol treatment as the assay for measuring the activation of the VDR/RXRα heterodimerization (calcitriol-sensitive M2H reporter system). To validate this assumption we directly compared the sensitivities of the two assays by treating Shh-N-CoM-induced Shh light II cells and *pFR-Luc*, *pCMV-BD-RXRα*, *pCMV-AD-VDR* transfected NIH/3T3 cells with increasing amounts of calcitriol. As shown in figure 35, inhibition of Hh signaling activity in Shh light II cells was first detectable after treatment with 1 nM calcitriol (Fig. 35 grey bars). In contrast, a significant activation of VDR/RXRα heterodimerization was already observed after treatment with 0.1 nM calcitriol (Fig. 34 white bars; 21-fold induction of baseline). Moreover in the latter assay increasing amounts of calcitriol induced an exponential increase in luciferase activity.

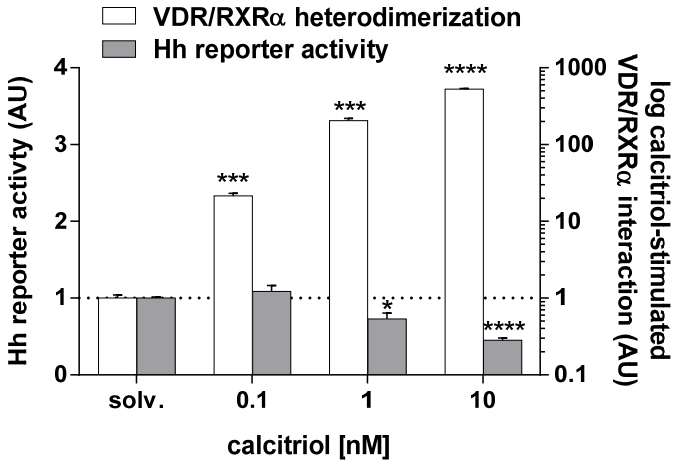

Figure 35: Sensitivity of luciferase-based reporter systems to assay the effects of calcitriol on Hh signaling and VDR/RXRα heterodimerization. Sensitivity of the reporter systems used to assess calcitriol-mediated Hh pathway inhibition (gray bars, left y-axis) and calcitriol-stimulated VDR/RXRα interaction (white bars, right y-axis). Data is representative for one individual experiment conducted in triplicates. For each reporter system values of solvent-treated cells were set to 1 (dashed line). Data are represented as mean +/- SEM. * $p<0.05$, ***$p<0.001$, ****$p>0.0001$, AU: arbitrary units.

Taken together the medium transfer experiments using the VDR/RXRα heterodimerization assay demonstrates that *Ptch*$^{-/-}$, in contrast to wt *Ptch*, cells lost their ability to release calcitriol to the extracellular space. Thus, we conclude that Ptch is essential for the release of calcitriol. Moreover these data strengthen our hypothesis that calcitriol is the endogenous transmitter of the Ptch/Smo-axis.

6.3.1.2. Ptch is dispensable for the synthesis of calcitriol from its precursor 25(OH)D$_3$

Because the lack of calcitriol in the medium of *Ptch*$^{-/-}$ cells may have resulted from a defective synthesis of calcitriol we analyzed if wt *Ptch*, *Ptch*$^{-/-}$ and *Ptch*-deficient ASZ001 cells (So *et al.* 2006) were able to synthetize calcitriol from its direct precursor 25(OH)D$_3$. Hence, the cells were incubated with 2 μM 25(OH)D$_3$ and the intracellular amounts of 25(OH)D$_3$, its degradation product 24,25(OH)$_2$D$_3$ and calcitriol were measured by LC-MS/MS-based assays. The occurrence of a specific metabolite was tested either by comparing to solvent-treated cells (marked by asterisks) or by comparing the values at time points 2, 4 and 6 hour with that obtained after the 0.5 h incubation period (marked by plus-signs). For details see chapter 5.6.

These analyses revealed that the intracellular levels of 25(OH)D$_3$ in all analyzed cell lines increased rapidly (Fig. 36, solid lines) and compared to solvent-treated cells, high amounts of 25(OH)D$_3$ were detected after 0.5 h in all cell lines. In wt *Ptch* and *Ptch*$^{-/-}$ cells the 25(OH)D$_3$ levels slightly declined thereafter (1 h) but increased again in both cell lines after 2 h. In ASZ001 cells a 25(OH)D$_3$ peak was reached after 1 h which decreased thereafter (Fig. 36 C, solid line). In contrast to wt *Ptch* cells, in which the 25(OH)D$_3$ levels reached a plateau after 4 h (Fig. 36 A, solid line) in *Ptch*$^{-/-}$ cells the 25(OH)D$_3$ levels decreased after 4 and 6 h similarly to ASZ001 cells (Fig. 36 B, solid line).

Furthermore, the amount of the degradation product of 25(OH)D$_3$, 24,25(OH)$_2$D$_3$, also significantly increased in all cell lines 0.5 h after 25(OH)D$_3$ supplementation (Fig. 36, dashed lines). In wt *Ptch* and ASZ001 cells the 24,25(OH)$_2$D$_3$ levels decreased after 1 h to baseline but increased again thereafter (Fig. 36 A and C, dashed lines). In contrast to wt *Ptch* and *Ptch*$^{-/-}$ cells in which the amounts of 24,25(OH)$_2$D$_3$ did not change significantly over time (Fig. 36 B, dashed lines), the levels of 24,25(OH)$_2$D$_3$ significantly increased after 4 and 6 h in ASZ001 cells when compared to the 0.5 h value (Fig. 36 C, dashed line).

Calcitriol was first detectable after 4 h in wt *Ptch* cells (Fig. 36 A, dotted line) and after 0.5 h in *Ptch*$^{-/-}$ (Fig. 36 B, dotted line) and ASZ001 cells (Fig. 36 C, dotted line). Calcitriol levels of wt *Ptch* cells significantly increased after 4 or 6 h (Fig. 36 A, dotted line). Compared to the 0.5 h time point, significantly increased amounts of calcitriol were measured in *Ptch*$^{-/-}$ (Fig. 36 B, dotted line) after 4 and 6 h and in ASZ001 cells (Fig. 36 C, dotted line) after 6 h.

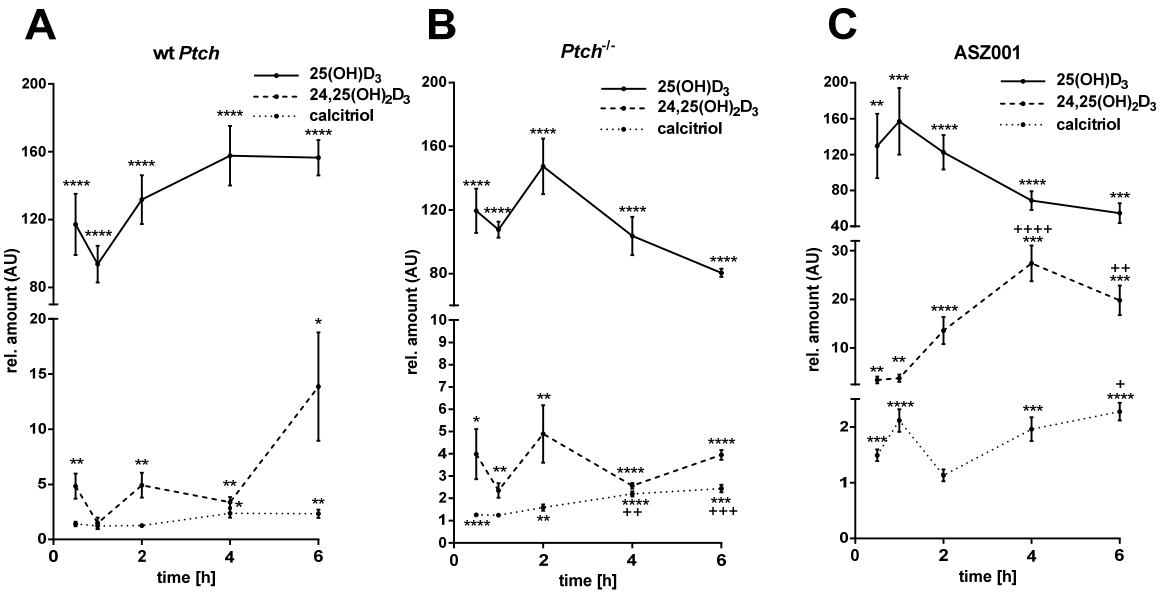

Figure 36: Ptch is dispensable for calcitriol synthesis from 25(OH)D_3. LC-MS/MS based intracellular quantification of 25(OH)D_3 (solid line), 24,25$(OH)_2D_3$ (dashed line) and calcitriol (dotted line) levels in **(A)** wt *Ptch* , **(B)** *Ptch*$^{-/-}$ and **(C)** in AZ001 cells 0.5, 1, 2, 4 and 6 h after incubation with 2 µM 25(OH)D_3. The data were normalized to the respective solvent-treated controls for each time point. The solvent-treated control for each cell line and time-point was set to 1. All data represent at least 3 independent experiments performed in triplicates represented as mean +/-SEM. * $p<0.05$, ** $p<0.01$, *** $p<0.001$, **** $p<0.0001$ compared to solvent control; ++ $p<0.01$, +++ $p<0.001$, ++++ $p<0.0001$ compared to the value 0.5 h after onset of treatment; AU: arbitrary units.

These data show that independently of their *Ptch*-status all cell lines are able to degrade excess intracellular 25(OH)D_3 to 24,25$(OH)_2D_3$ and to synthesize calcitriol from exogenously supplied 25(OH)D_3. Therefore, the data suggest that the last hydroxylation step from 25(OH)D_3 to calcitriol is not disturbed in *Ptch*-deficient cells.

We next investigated if the *Ptch* mutation disturbs the conversion of $vitD_3$ to $25(OH)D_3$. For this purpose, wt *Ptch*, *Ptch*$^{-/-}$ and ASZ001 cells were treated with 10 µM $vitD_3$ and the intracellular amounts of $vitD_3$, $25(OH)D_3$, $24,25(OH)_2D_3$ and calcitriol were measured by LC-MS/MS based assays. In all cell lines highly increased $vitD_3$ levels were already observed 0.5 h after $vitD_3$ treatment compared to solvent-treated cells (Fig. 37 A to C, solid lines, significances compared to the solvent are marked by * in the figures). It peaked after 1 h and slightly declined thereafter in all cell lines, without reaching statistical significance compared to the 0.5 h time point.

$25(OH)D_3$ was significantly elevated 1 h after $vitD_3$ supplementation in wt *Ptch* cells (Fig. 37 A, dashed line) and after 0.5 h in *Ptch*$^{-/-}$ (Fig. 37 B, dashed line) and ASZ001 cells (Fig. 37 C, dashed line). Thereafter, a further increase in $25(OH)D_3$ was detected, which was was significant after 2 or 4 h in wt *Ptch* and ASZ001 or *Ptch*$^{-/-}$ cells, respectively, compared to the 0.5 h value (Fig. 37 A to C, dashed lines, marked by +).

The $25(OH)D_3$ degradation product $24,25(OH)_2D_3$ was first detectable 1 h after $vitD_3$ supplementation in wt *Ptch* (Fig. 37 A, dotted line) and after 2 h in *Ptch*$^{-/-}$ (Fig. 37 B, dotted line) and ASZ001 cells (Fig. 37 C, dotted line). Thereafter it increased continuously and, compared to the 0.5 h value, was significantly elevated after 6 h in wt *Ptch* (Fig. 37 A, dotted line) and after 4 and 6 h in ASZ001 cells (Fig. 37, C dotted line). A slight increase was also detectable in *Ptch*$^{-/-}$ cells which, however, did not reach statistical significance (Fig. 37 B, dotted line).

Similar to the $25(OH)D_3$ treatment, $vitD_3$ supplementation induced calcitriol synthesis with continuously increasing calcitriol amounts over time in all cell lines (Fig. 37 D to F, dotted lines). In wt *Ptch* cells the increase was significant 4 and 6 h after $vitD_3$ treatment. At the latter time point the increase was also significant compared to the 0.5 h value (Fig. 37 D, dotted line). In *Ptch*$^{-/-}$ (Fig. 37 E, dotted line) and ASZ001 cells (Fig. 37 F, dotted line) significantly increased calcitriol levels were detectable 2 h after $vitD_3$ supplementation that further increased after 4 h and 6 h.

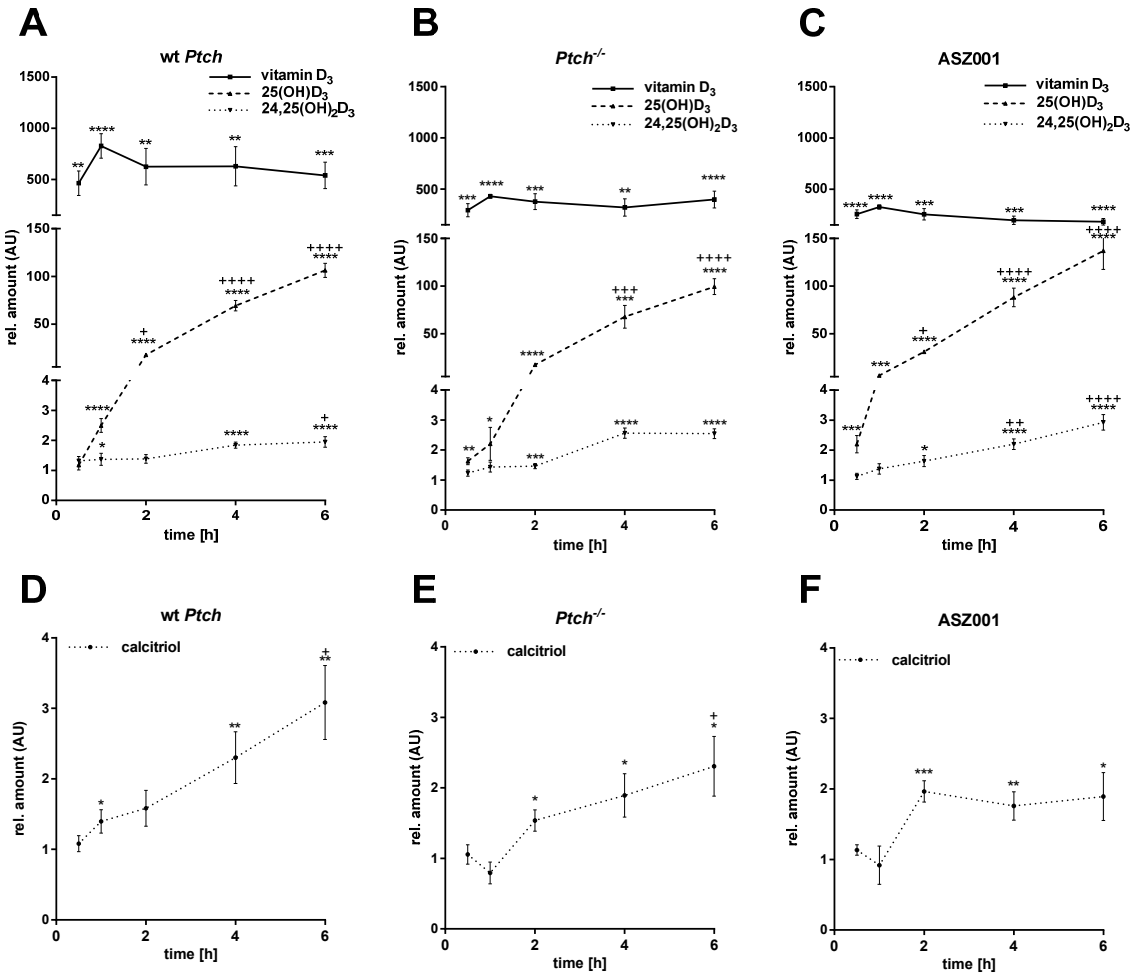

Figure 37: Ptch is dispensable for calcitriol synthesis from vitamin D_3. LC-MS/MS-based intracellular quantification of **(A to C)** vitamin D_3 (solid line), 25(OH)D_3 (dashed line) and 24,25$(OH)_2D_3$ (dotted line) or **(D to F)** calcitriol (dotted line) levels in **(A and D)** wt *Ptch*, **(B and E)** *Ptch*$^{-/-}$ and **(C and F)** ASZ001 cells 0.5, 1, 2, 4 and 6 h after incubation with 10 µM vitamin D_3. The data were normalized to the respective solvent-treated controls for each time point. The solvent-treated control for each cell line and time-point was set to 1. All data represent at least 3 independent experiments represented as mean +/-SEM. * $p<0.05$, ** $p<0.01$, *** $p<0.001$, **** $p<0.0001$ compared to solvent control; + $p<0.05$, ++ $p<0.01$, +++ $p<0.001$, ++++ $p<0.0001$ compared to the 0.5 h value; AU: arbitrary units.

Taken together, these analyses show that wt *Ptch*, *Ptch*$^{-/-}$ and ASZ001 cells synthetize 25(OH)D_3 and also calcitriol from exogenously supplied vitD_3. Moreover, since all three cell lines degraded 25(OH)D_3 to 24,25$(OH)_2D_3$ in comparable amounts, it is likely that calcitriol was degraded as well, because degradation of 25(OH)D_3 and calcitriol is catalyzed by the same enzyme (24-hydroxylase, *Cyp24a1*) (Chen *et al.* 2012; Christakos *et al.* 2010). Therefore the data suggest that Ptch is dispensable for calcitriol synthesis from vitD_3 and for calcitriol degradation.

6.3.2. Functional analyses of calcitriol-mediated Hh signaling inhibition

Previously, our group demonstrated that calcitriol-mediated inhibition of Hh signaling occurs downstream of Ptch at the level of Smo (Uhmann *et al.* 2011a). Our novel data now revealed that calcitriol is released from cells in a Ptch-dependent manner (compare chapter 6.3.1.1) and cooperates with the Smo-binder ITZ in Hh signaling inhibition (chapter 6.2.2.1) *in vitro*. It has been reported that Smo contains at least two distinct binding sites for small molecules (7TM and CRD). In addition, Smo probably possesses a distinct ITZ binding pocket (Myers *et al.* 2013; Nachtergaele *et al.* 2012; Nachtergaele *et al.* 2013; Nedelcu *et al.* 2013). In order to see whether calcitriol equally suppresses Smo activity by direct binding to these binding domains we generated and analyzed concentration-response-curves (CRCs). For this purpose, calcitriol was combined with ITZ and other known Smo modulators. Subsequently, competition assays for Smo binding were performed and we made use of a CRD-deleted Smo variant or the SMO-M2 oncogene and analyzed the effects of calcitriol on suppression of Hh signaling activity and cellular proliferation.

6.3.2.1. Synergistic interaction of calcitriol and ITZ in Smo inhibition

In order to generate concentration-response-curves (CRC) Shh light II cells were stimulated with Shh-N-CoM and simultaneously incubated with increasing amounts of calcitriol and a constant concentration of ITZ or another Smo modulator. The same experiments were also conducted by keeping the doses of ITZ or other Smo modulators constant and increasing those of calcitriol. Afterwards dual-luciferase assays were performed and the half-maximal effective (EC_{50}) or inhibitory (IC_{50}) concentration for activating or inhibitory Smo modulators, respectively, were calculated in the presence of a stable concentration of a second Smo modulator. Significant changes were calculated using an extra sum-of-squares F test by comparing the CRC for a single substance with the CRC in the presence of a second substance.

First, we generated CRCs for calcitriol in the presence of the Smo inhibitors CP, ITZ and vismodegib as well as CRCs for CP, ITZ and vismodegib in the presence of calcitriol. The binding sites of CP and vismodegib have been mapped previously to the 7TM (Chen *et al.* 2002a; Nachtergaele *et al.* 2013) and, in case of CP, also with low affinity to the CRD

(Nachtergaele *et al.* 2013). The binding site of ITZ is not known, but it does not map to any known binding site (Kim *et al.* 2010; Nachtergaele *et al.* 2012).

The data show that all Smo inhibitors efficiently inhibit Hh signaling in a concentration-dependent manner (black lines in Fig. 38). The combination of calcitriol with CP (Fig. 38 A and B) or vismodegib (Fig. 38 E and F) resulted in downward-shifts of the respective CRC without changing its IC_{50} (table 20 and 21). This shows that neither CP nor vismodegib cooperated with calcitriol in Hh signaling inhibition. In contrast, increasing concentrations of ITZ shifted the CRC of calcitriol to lower calcitriol concentration (left-shift) (Fig. 38 C and D) which demonstrates that in the presence of ITZ lower amounts of calcitriol are necessary to inhibit Hh signaling. This finding was validated by significantly decreased IC_{50} of calcitriol from ~1.02 nM without ITZ (table 20, Fig. 38 A, black line) to ~0.13 nM with 2 µM ITZ (table 20, Fig. 38, blue line). *Vice versa*, increasing concentrations of calcitriol caused a significantly decreased IC_{50} of ITZ from ~0.81 µM without calcitriol (table 21, Fig. 38 B, black line) to ~0.32 µM with 1 nM calcitriol (table 21, Fig. 38 B, green line) and ~0.6 µM with 10 nM calcitriol (Table 21, Fig. 38 D, blue line). These data confirm that ITZ and calcitriol cooperate in Hh signaling inhibition and thus confirm the results using ASZ001 cells (see chapter 6.2.1.1).

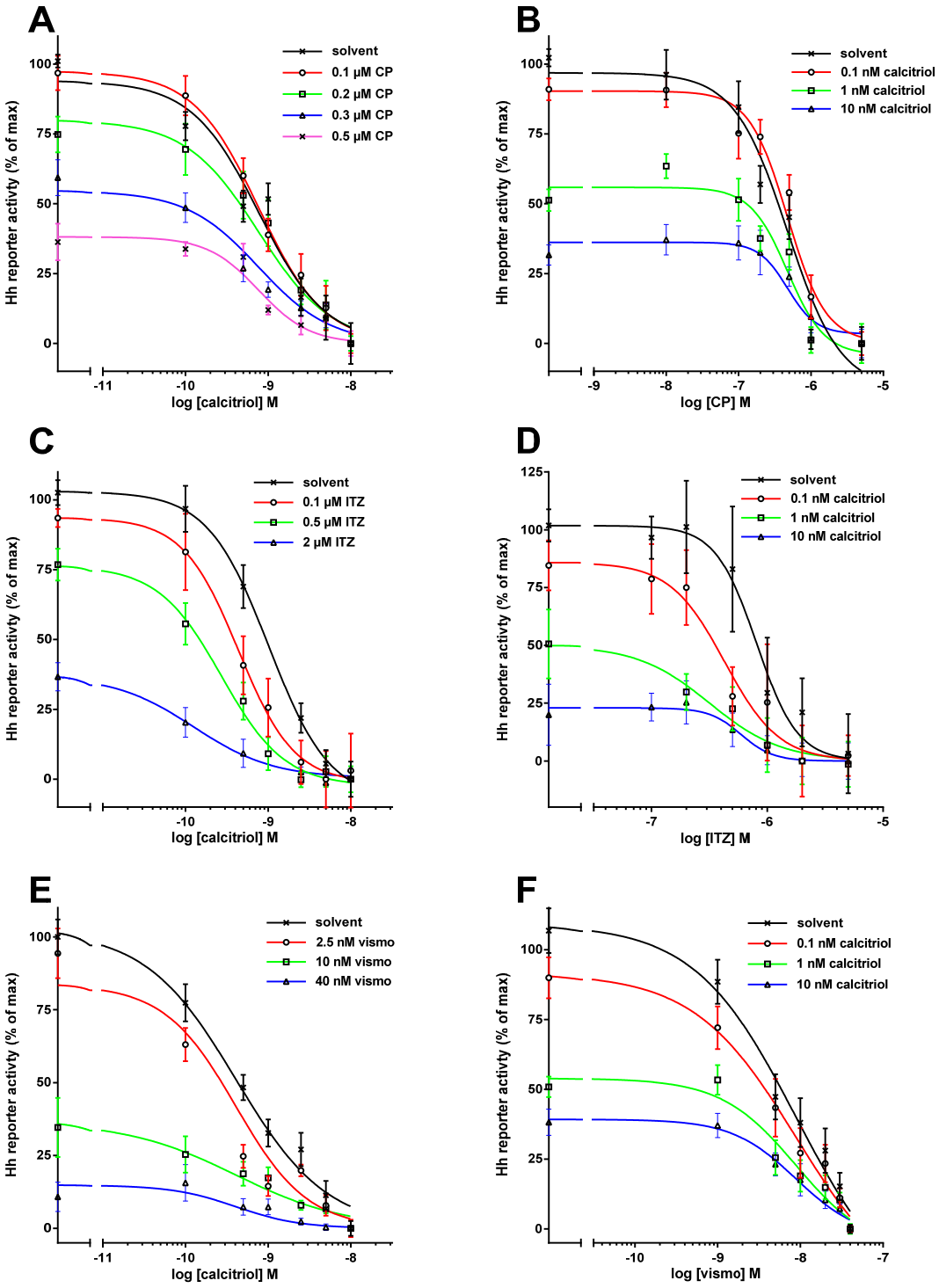

Figure 38: Concentration-response-curves (CRC) of calcitriol and Smo-inhibitors. Concentration-response curves of calcitriol in the presence of the Hh-inhibitor **(A)** cyclopamine (CP), **(C)** itraconazole (ITZ) or **(E)** vismodegib (vismo) or **(B)** CP, **(D)** ITZ or **(F)** vismo in the presence of calcitriol. To activate Hh signaling Shh light II cells were pre-induced with Shh-N-CM for 24 h. Afterwards, the cells were incubated with the respective compounds for additional 48 h in Shh-N-CM. The data were transformed, normalized and fitted using GraphPad Prism 6 (see material and method section). Data represents normalized firefly/renilla luciferase activity. All data represents at least 3 independent experiments measured in triplicates represented as mean +/-SEM.

Using the software CompuSyn (Chou 1976; Chou 2006; Chou 2010; Chou and Talalay 1984; Chou 2005) (combosyn.com, see chapter 5.6 for details) we next determined whether calcitriol and ITZ synergize in Hh signaling inhibition by a computational analyses of the data according to the median-effect principle of the mass-action law and its combination index theorem (Chou 1976; Chou 2010; Chou and Talalay 1984; Chou 2005). Thus, we generated a Fa-Ci-Plot by plotting the combination index (CI) over the range of the fractional inhibition (Fa) of the experimental data shown in figure 38 (C). In accordance to Chou *et al.* CI>1 indicates antagonism, CI=1 additivity, CI<0.7 synergism and CI<0.3 strong synergism (Chou 2005). The respective slopes of each calcitriol concentration were furthermore tested for statistically significant differences. As shown in figure 39 low dosages of calcitriol (0.1, 0.5, 1 and 2.5 nM, Fig. 38, light and dark green, blue and violet line) combined with different amounts of ITZ synergistically inhibited Hh signaling activity. Moreover, the lower the calcitriol concentration the higher was the degree of synergism of calcitriol and ITZ (Fig. 39, e.g., 0.5 nM vs. 2.5 nM; compare table 18). In contrast, increasing concentrations of calcitriol led to increased antagonistic effects when combined with intermediate or low ITZ concentrations. This antagonism disappeared when high ITZ concentrations (5 nM calcitriol Fig 39, orange line) were used. However, high calcitriol and high ITZ concentrations again resulted in antagonism (10 nM, Fig. 39 red line). In fact, the CI slope of 2.5 nM calcitriol (Fig. 39 violet line) was significantly lower than that of 10 nM calcitriol (Fig. 39 red line, table 18). These data show that low to intermediate calcitriol amounts combined with ITZ act synergistically on Hh signaling inhibition whereas high calcitriol concentrations combined with ITZ result in antagonistic effects.

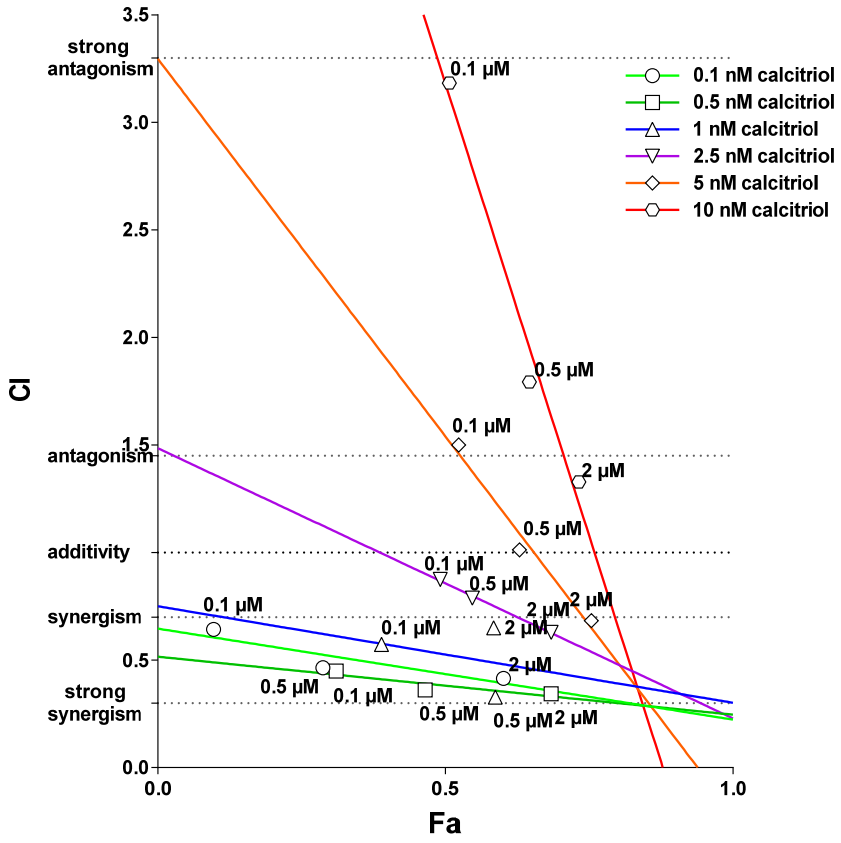

Figure 39: Dual mode of action of calcitriol and ITZ on Hh signaling inhibition. Fa-CI plot of the combination of calcitriol and ITZ. The Fa-CI-Plot was generated by calculating the combination index (CI) over the range of fractional inhibition (Fa) of the experimental data shown in Fig. 38 C. Shown are the CI-values and linear regression of Hh signaling inhibition triggered by 0.1, 0.5, 1, 2.5, 5 and 10 nM calcitriol (circles, squares, upward triangles, downward triangles, rhombs and hexagons, respectively) combined with 0.1, 0.5 or 2 µM ITZ plotted against the respective Fa. Slopes of 0.5 nM and 2.5 nM (p=0.044) as well as 0.5 nM and 5.0 nM calcitriol (p=0.023) are significantly different (compare table 18). CI>1, antagonism; C=1, additivity CI<0.7, synergism; CI<0.3, strong synergism (Chou 2005).

Table 18: Statistical determination of the Fa-CI-Plot

comparison	significant	p-value
0.1 nM cal vs 0.5 nM cal	n.s.	0.63
0.5 nM cal vs 1 nM cal	n.s.	0.893
0.5 nM cal vs 2.5 nM cal	*	0.044
0.5 nM cal vs 5 nM cal	*	0.023
1 nM cal vs. 2.5 nM cal	n.s.	0.648
2.5 nM cal vs 5 nM cal	n.s.	0.067
2.5 nM cal vs 10 nM cal	*	0.033
5 nM cal vs. 10 nM cal	n.s.	0.068

n.s.: not significant; * p<0.05

Kim *et al.* have shown that CP and ITZ cooperate in Hh signaling inhibition (Kim *et al.* 2010). However, we did not see such a cooperation in our *in vitro* experiments using ASZ001 cells (compare chapter 6.2.1.1). We therefore also generated CRCs for CP and ITZ. As already observed in ASZ001 cells (see chapter 6.2.1.1) both CP (Fig. 40 B) and ITZ (Fig. 40 A) efficiently inhibited Hh signaling activity in Shh light II cells. However, the presence of CP (Fig. 40 A) did not change the IC_{50} of ITZ or *vice versa* (Fig. 40 B; table 19) supporting our observation that CP and ITZ do not cooperate in Hh signaling inhibition.

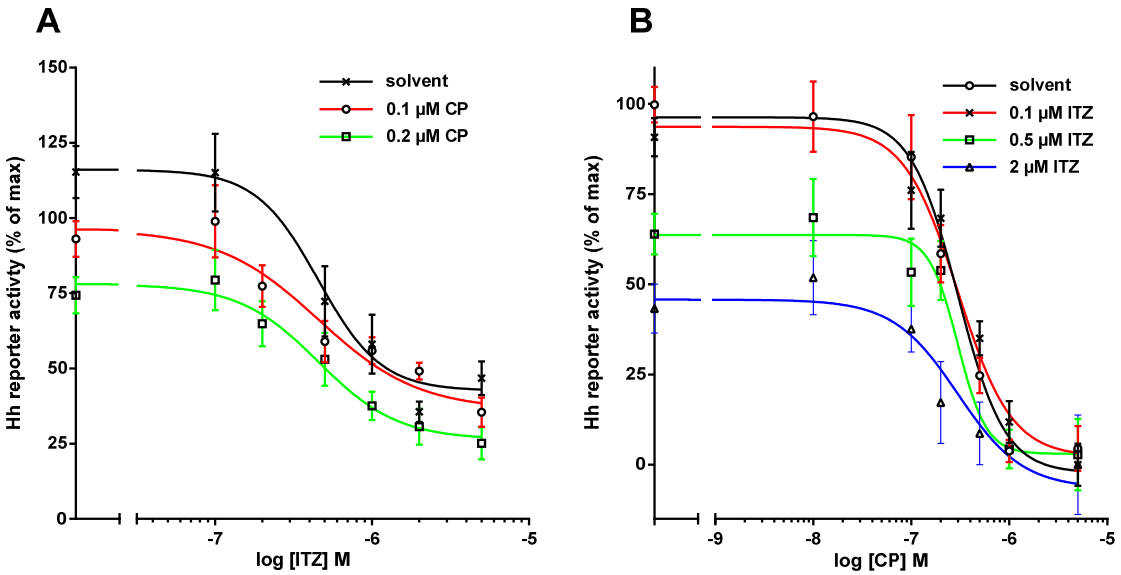

Figure 40: Concentration-response-curves (CRC) of CP and ITZ. CRC of **(A)** itraconazole (ITZ) in the presence cyclopamine (CP) or **(B)** CP in the presence of ITZ. Shh light II cells were pre-induced with Shh-N-CM for 24 h. Afterwards, the cells were incubated with the respective compounds for additional 48 h in Shh-N-CM. The data were transformed, normalized and fitted using GraphPad Prism 6 (see material and method section). Data represents normalized firefly/renilla luciferase activity. All data represents at least 3 independent experiments measured in triplicates represented as mean +/-SEM.

Table 19: IC_{50} of CP or ITZ in the presence of ITZ or CP

CP with	IC_{50} [µM] CP	p-value
solvent	0.2478	0.2889
ITZ 0.1 µM	0.3904	
ITZ 0.5 µM	0.3525	
ITZ 2 µM	0.1617	
ITZ with	**IC_{50} [µM] ITZ**	**p-value**
solvent	0.8083	0.8492
CP 0.1 µM	0.4276	
CP 0.2 µM	0.3177	

The half maximal inhibitory concentration (IC_{50}) of cyclopamine (CP) and itraconazole (ITZ) in combination with each other on Hh signaling activity were calculated from the experiments shown in Fig. 40 as described in the material and method section. To detect significant differences of the IC_{50} of single and combined treatments extra sum-of-squares F tests were conducted.

We also generated CRCs for calcitriol and the Smo agonists (activators) SAG or 20(S)OHC using Shh light II cells. Since Smo agonists induce Hh signaling activity by themselves, incubation with Shh-N-CM was not necessary. Moreover the Smo binding sites for SAG and 20(S)OHC have already been mapped to the 7TM and the CRD, respectively (Chen *et al.* 2002b; Nachtergaele *et al.* 2013). Thus, if calcitriol indeed occupies the 7TM or CRD a competitive inhibitory effect on Hh signaling activity would be expected.

In the absence of calcitriol both Smo agonists led to concentration-dependent activation of Hh signaling (Fig. 41) although 20(S)OHC-induced Hh signaling activation was much lower (Fig. 41 C and D) compared to SAG treatment (Fig. 41 A and B). Additionally, both SAG as well as 20(S)OHC-induced activation of Hh signaling was inhibited by increasing amounts of calcitriol (Fig. 41). However, the ED_{50} of calcitriol was not significantly changed by increasing amounts of SAG or 20(S)OHC or *vice versa* (tables 20 and 21). Additionally, the maximal activation of Hh signaling induced by SAG- (Fig. 41 B) or 20(S)OHC (Fig. 41 D) was clearly reduced by increasing amounts of calcitriol. These data suggest that calcitriol acts as a non-competetive inhibitor of SAG (7TM-binder) and 20(S)OHC (CRD-binder)-induced Hh signaling by binding to a distinct, so far unidentified, Smo binding site.

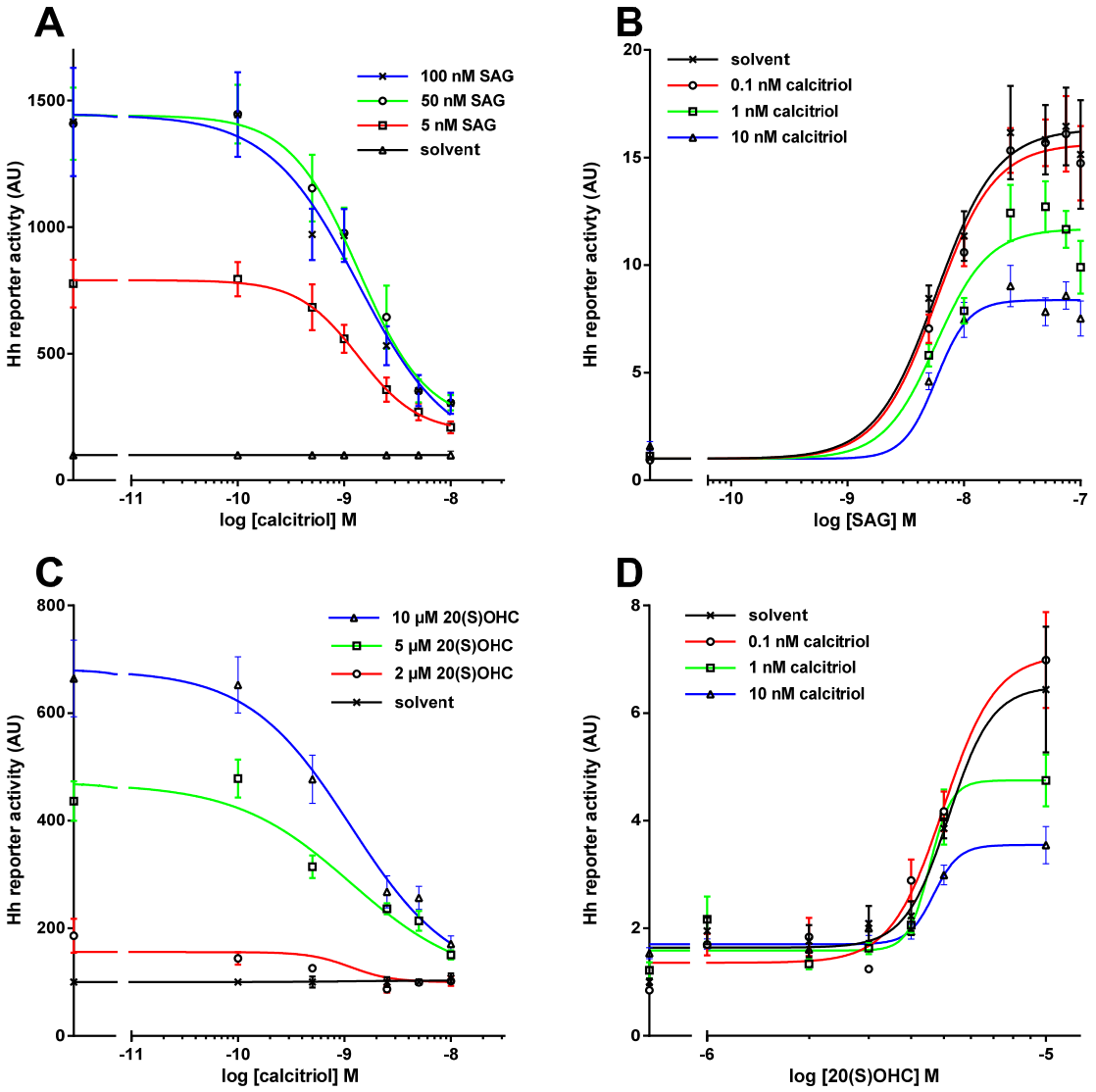

Figure 41: Concentration response curves (CRC) of calcitriol and Smo-agonists. CRC of calcitriol in the presence of the Hh-agonists **(A)** SAG or **(C)** 20(S)-hydroxycholesterol (20(S)OHC) and CRC of **(B)** SAG or **(D)** 20(S)OHC in the presence of calcitriol. Shh light II cells were starved with DMEM supplemented with 0.5 % FCS and 1 % PS for 24 h. Afterwards, the cells were incubated with the respective compounds for additional 48 h in DMEM supplemented with 0.5 % FCS and 1 % PS. The data were transformed, normalized and fitted using GraphPad Prism 6 (see material and method section). Data represents normalized firefly/renilla luciferase activity. All data represents at least 3 independent experiments measured in triplicates represented as mean +/- SEM; AU: arbitrary units.

Table 20: IC_{50} of calcitriol in the presence of various Smo-modulators

calcitriol with	IC_{50} [nM] calcitriol	p-value
solvent	0.555	0.2014
CP 0.1 µM	0.771	
CP 0.2 µM	1.183	
CP 0.3 µM	0.449	
CP 0.5 µM	1.008	
solvent	1.017	0.0004
ITZ 0.1 µM	0.438	
ITZ 0.5 µM	0.273	
ITZ 2 µM	0.126	
solvent	0.460	0.0739
vismo 2.5 nM	0.185	
vismo 10 nM	0.673	
vismo 40 nM	0.917	
solvent	n.d.	0.7716
SAG 5 nM	1.375	
SAG 50 nM	1.495	
SAG 100 nM	1.139	
solvent	n.d.	0.3725
20(S)OHC 2 µM	0.129	
20(S)OHC 5 µM	1.355	
20(S)OHC 10 µM	1.113	

The half maximal inhibitory concentration (IC_{50}) of calcitriol in the combination with cyclopamine (CP), itraconazole (ITZ), vismodegib (vismo), Smo-agonist (SAG) or 20(S)-hydroxycholesterol (20(S)OHC) on Hh signaling activity were calculated from the experiments shown in Fig. 38 and 41 as described in the material and method section. To detect significant differences of the IC_{50} or EC_{50} of single and combined treatments extra sum-of-squares F tests were conducted.

Table 21: EC_{50} and IC_{50} of various Smo-modulators in the presence of calcitriol

	IC_{50} [µM] CP	IC_{50} [µM] ITZ	IC_{50} [nM] vismo	EC_{50} [nM] SAG	EC_{50} [µM] 20(S)OHC
solvent	0.3322	0.8083	6.395	5.424	5.158
calcitriol 0.1 nM	0.5875	0.4276	3.565	6.459	4.978
calcitriol 1 nM	0.4587	0.3177	4.133	6.071	4.546
calcitriol 10 nM	0.687	0.5924	4.204	5.028	4.663
p-value	0.1043	0.0075	0.1788	0.6268	0.3725

The half maximal inhibitory concentration (IC_{50}) of cyclopamine (CP), itraconazole (ITZ) vismodegib (vismo) and half maximal effective concentration (EC_{50}) of Smo-agonist (SAG) or 20(S)-hydroxycholesterol (20(S)OHC) in combination with calcitriol on Hh signaling activity were calculated from the experiments shown in Fig. 38 and 41 as described in the material and method section. To detect significant differences of the IC_{50} or EC_{50} of single and combined treatments extra sum-of-squares F tests were conducted.

Taken together these results show that calcitriol acts synergistically with ITZ but not with CP or vismodegib, to inhibit Hh signaling. Additionally, calcitriol inhibits SAG or 20(S)OHC-induced Smo activation by a non-competitive mechanism. Since we did not find any functional competition of calcitriol with 7TM- (CP, vismodegib or SAG) or CRD-binders (20(S)OHC and CP) (Chen *et al.* 2002b; Kim *et al.* 2010; Myers *et al.* 2013; Nachtergaele *et al.* 2013; Nedelcu *et al.* 2013), we propose that calcitriol potentially acts on a so far unidentified Smo site.

6.3.2.2. Calcitriol does not bind to the 7TM or the CRD of Smo

In order to validate that calcitriol does neither bind to the 7TM nor the CRD of Smo we next performed a BODIPY-CP replacement assay (for details see chapter 5.2.8). For this purpose, Smo was overexpressed in HEK293S cells by treating the cells with tetracycline ((Dwyer *et al.* 2007), see Fig. 42). Next the cells were treated with fluorescently-labeled CP (BODIPY-labeled CP, BD-CP) in combination with calcitriol or other Smo modulators. The replacement of BD-CP from Smo was detected by decreased fluorescence intensity of single cells determined by flow cytometry (Fig. 43). The data are presented as cumulative distribution function (CDF) which reflects the percentage of fluorescence intensity of cells and as bar graphs of the mean fluorescence intensity of each sample.

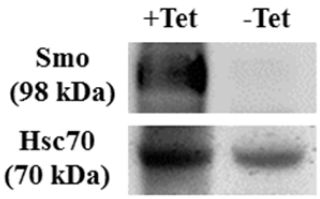

Figure 42: Smo overexpression by tetracycline treatment of HEK293S cells. Western Blot analyses of cell lysates from tetracycline-induced (+Tet) HEK293S cells using a primary anti-Myc antibody for detection of 6x-His, myc-tagged Smo protein. As a negative control uninduced HEK293 cells (-Tet) were used. Detection of Hsc70 served as loading control.

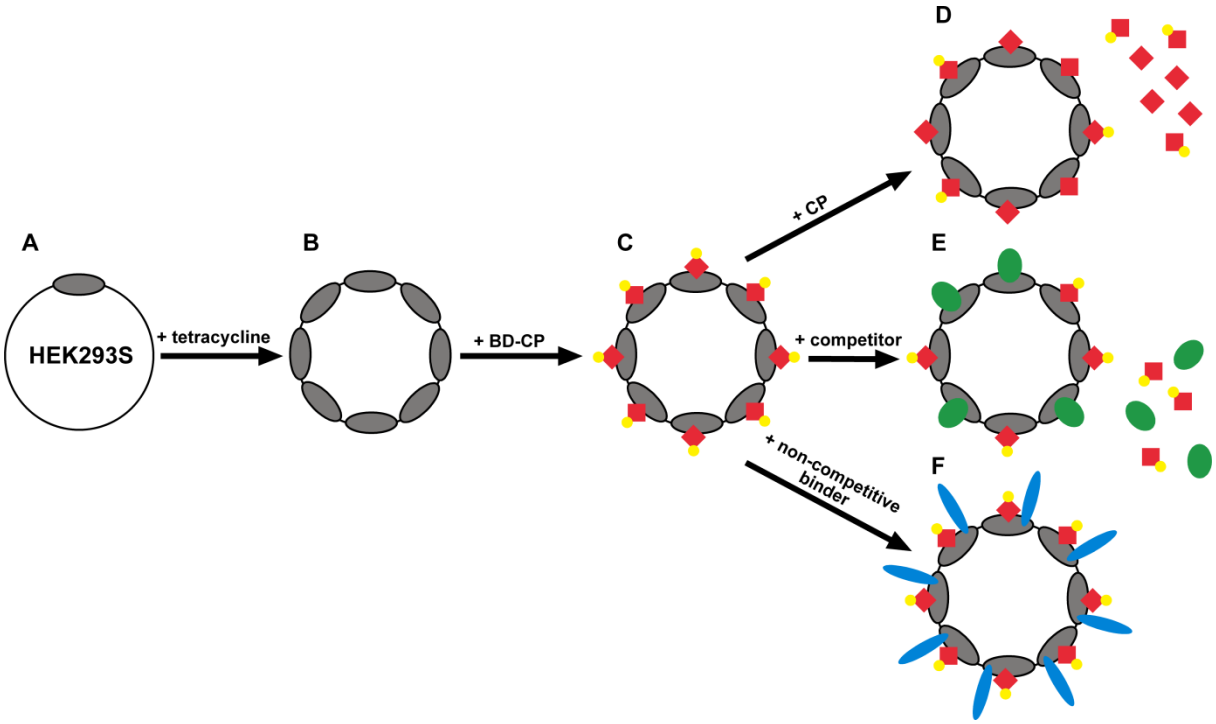

Figure 43: Schematic representation of the BD-CP-replacement assay. (A) HEK293S cells endogenously express small amount of wt Smo. **(B)** Upon tetracycline-induction 6 x His, myc-tagged Smo is overexpressed (grey circles) and **(C)** binds BD-CP (red square with yellow circle)**.** This increases the fluorescence intensity of the cell. **(D)** Simultaneous CP treatment (red square) leads to competitive replacement of BD-CP causing decreased fluorescence intensity. **(E and F)** The addition of a putative competitor (green circle or blue circle) either leads to **(E)** competition with BD-CP or **(F)** simultaneous binding on Smo.

We first tested the efficiency of BD-CP replacement by CP. As expected without BD-CP nearly no flourescence signals were detectable (Fig. 44 A and B). BD-CP treatment of uninduced HEK293S cells led to a slight increase in fluorescence intensity of the cells (Fig. 44 A and grey line in B). In contrast, BD-CP treatment of HEK293S cells overexpressing Smo resulted in a very strong fluorescence intensity of the cells (Fig. 44 and black line in B) which was significantly decreased by combination with CP (Fig. 44 A and red line in B).

These results showed that the BD-CP replacement worked in our hands. This setup was included as a control experiment in all following experiments.

We next re-analyzed the already described replacement of BD-CP by ITZ (Kim *et al.* 2010) and the exclusive 7TM-binders vismodegib (Nachtergaele *et al.* 2013) and SAG (Chen *et al.* 2002b; Wang *et al.* 2014). Accordingly, 0.1 and 1 µM vismodegib and 25 and 100 nM SAG significantly reduced BD-CP binding from Smo-overexpressing cells (Fig. 44 C to F) (Chen *et al.* 2002b; Nachtergaele *et al.* 2013; Wang *et al.* 2014). However, in contrast to Kim *et al.* who reported no effective competition with BD-CP (Kim *et al.* 2010) we found a strong and significant replacement of BD-CP by ITZ (Fig. 44 G and H) that appeared not to be concentration-dependent (Fig. 44 E).

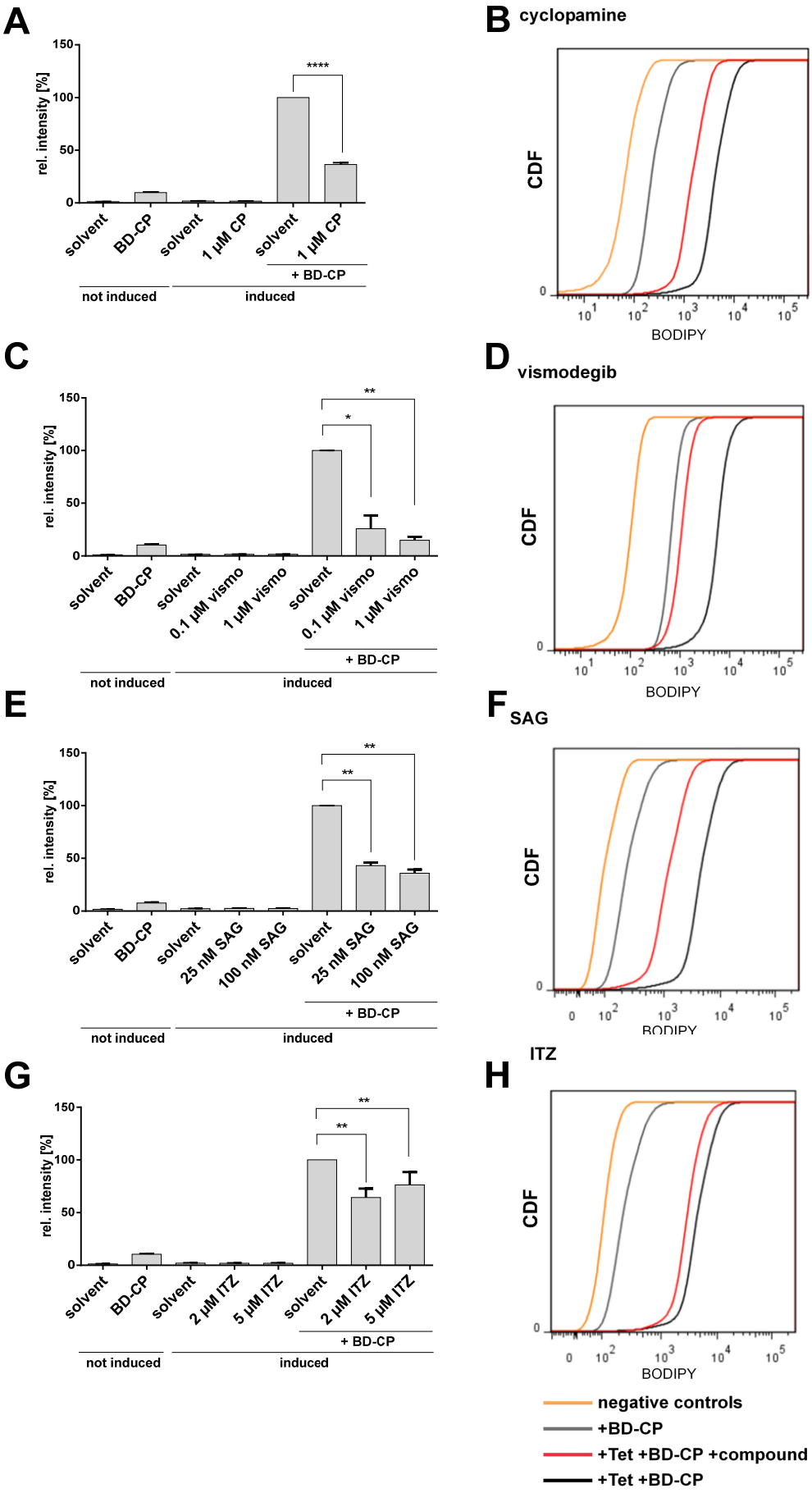
A
rel. intensity [%]
150
100
50
0
****
solvent
BD-CP
solvent
1 µM CP
solvent
1 µM CP
+ BD-CP
not induced
induced
B
cyclopamine
CDF
0
BODIPY
C
rel. intensity [%]
**
*
solvent
BD-CP
solvent
0.1 µM vismo
1 µM vismo
solvent
0.1 µM vismo
1 µM vismo
+ BD-CP
not induced
induced
D
vismodegib
CDF
BODIPY
E
rel. intensity [%]
**
**
solvent
BD-CP
solvent
25 nM SAG
100 nM SAG
solvent
25 nM SAG
100 nM SAG
+ BD-CP
not induced
induced
F
SAG
CDF
BODIPY
G
rel. intensity [%]
**
**
solvent
BD-CP
solvent
2 µM ITZ
5 µM ITZ
solvent
2 µM ITZ
5 µM ITZ
+ BD-CP
not induced
induced
H
ITZ
CDF
BODIPY
negative controls
+BD-CP
+Tet +BD-CP +compound
+Tet +BD-CP

Figure 44: Cyclopamine, vismodegib, SAG and ITZ compete with BD-CP for Smo-binding. (A, C, E and G) Bar graphs and **(B, D, F and H)** representative CDF-plots (cumulative distribution function) of direct competition-assays of 10 nM BODIPY-labeled cyclopamine (BD-CP) and **(A and B)** 1 µM unlabeled cyclopamine (CP), **(C and D)** 0.1 and 1 µM vismodegib (vismo) or **(E and F)** 2 and 5 µM itraconazole (ITZ) **(G and H)** 25 and 100 nM Smo agonist (SAG) of tetracycline-induced conditional Smo-overexpressing HEK293S cells (induced) as described (Dwyer *et al.* 2007). Solvent-, single competitor-, and BD-CP-treated uninduced HEK293S cells (not induced) served as negative controls in all experiments. BD-CP-treatment of induced cells was set to 100 % and for convenience only the single competitor treatment is shown for the CDF-curves (orange curve) representative for all negative controls. Representative CDF-curves are shown for **(D)** 1 µM vismo, **(F)** 2 µM ITZ and **(H)** 100 nM SAG. Data acquisition was conducted as described in the material and method section. All data represent at least 3 independent experiments measured in duplicates represented as mean +/- SEM. * p<0.05; ** p<0.01; *** p<0.001; **** p<0.0001.

Since it has been reported that CP binds to some extent to the CRD, we next used 20(S)OHC that exclusively binds to the CRD (Nachtergaele *et al.* 2013; Nedelcu *et al.* 2013). Indeed, 20(S)OHC significantly reduced the fluorescence intensity of BD-CP-labeled cells (Fig. 45) indicating that CP also binds to some extend to the CRD.

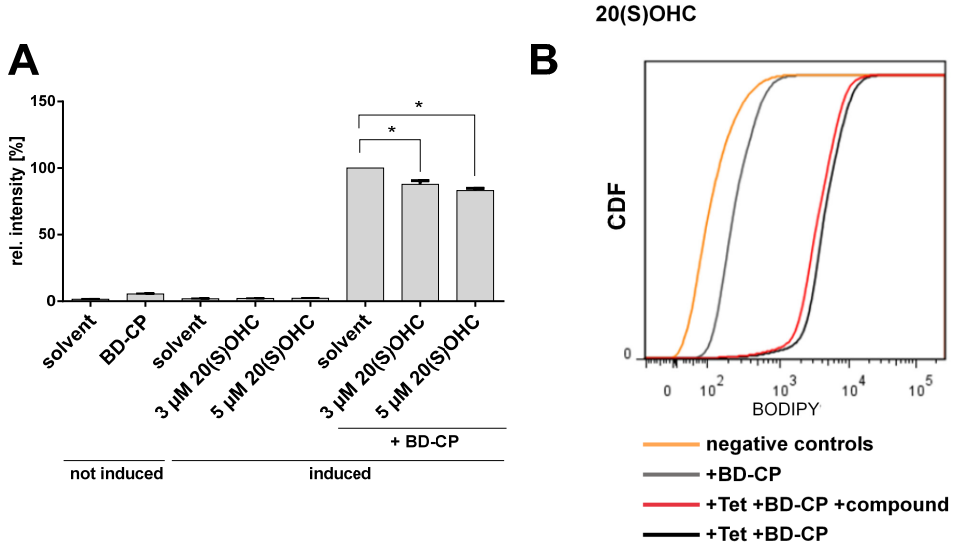

Figure 45: 20(S)OHC competes with BD-CP for Smo-binding. (A) Bar graph and **(B)** representative CDF-plot (cumulative distribution function) of direct competition-assays of 10 nM BODIPY-labeled cyclopamine (BD-CP) and 3 or 5 µM 20(S)-hydroxycholesterol (20(S)OHC) of tetracycline-induced conditional Smo-overexpressing HEK293S cells (induced) as described (Dwyer *et al.* 2007). Negative controls were the same as in Figure 44. Representative CDF-curves are shown for **(B)** 5 µM 20(S)OHC. Data acquisition was conducted as described in the material and method section. All data represent at least 3 independent experiments measured in duplicates represented as mean +/-SEM. * p<0.05.

Finally, we analyzed whether calcitriol, which synergizes with ITZ in Hh signaling inhibition, also replaces BD-CP from Smo overexpressing cells. Hence, HEK293S cells were treated with BD-CP and 2, 5 and 20 nM calcitriol that equate the 2, 10 and 20-fold concentration of the IC_{50}, respectively (compare table 20). We also used the calcitriol precursors $vitD_3$ or $25(OH)D_3$ at concentrations up to 10 µM and 2 µM, respectively. However, neither calcitriol nor its precursors reduced the fluorescence intensity of the BD-CP-labeled cells (Fig. 46). This shows that calcitriol and its precursors do not bind to the same binding pocket/s as CP.

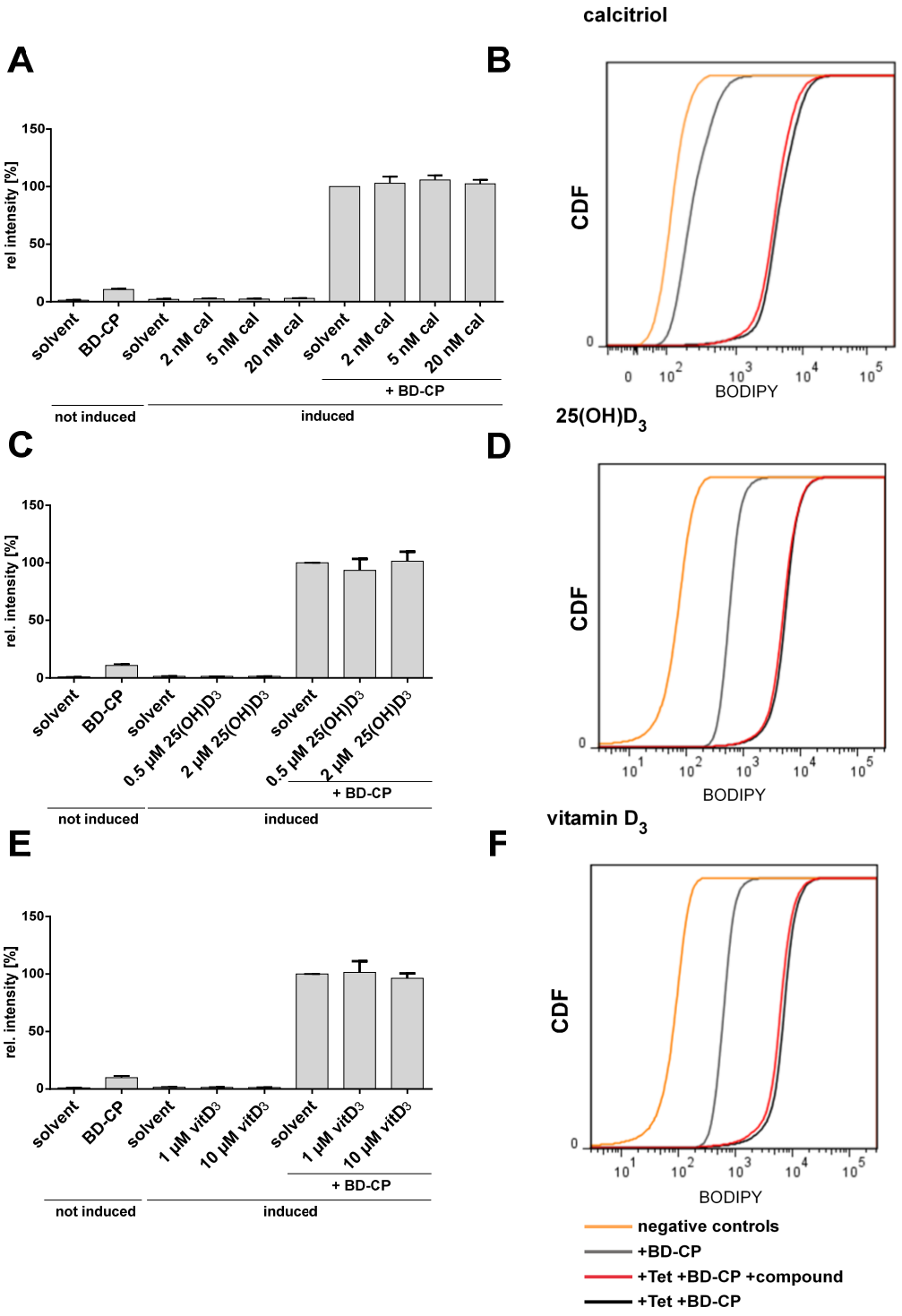
A
B
calcitriol
rel intensity [%]
150
100
50
0
solvent
BD-CP
solvent
2 nM cal
5 nM cal
20 nM cal
solvent
2 nM cal
5 nM cal
20 nM cal
+ BD-CP
not induced
induced
CDF
BODIPY
C
D
25(OH)D3
rel. intensity [%]
solvent
BD-CP
solvent
0.5 µM 25(OH)D3
2 µM 25(OH)D3
solvent
0.5 µM 25(OH)D3
2 µM 25(OH)D3
+ BD-CP
not induced
induced
E
F
vitamin D3
rel. intensity [%]
solvent
BD-CP
solvent
1 µM vitD3
10 µM vitD3
solvent
1 µM vitD3
10 µM vitD3
+ BD-CP
not induced
induced
negative controls
+BD-CP
+Tet +BD-CP +compound
+Tet +BD-CP

Figure 46: Calcitriol and its precursors do not compete with BD-CP for Smo-binding. (A, C and E) Bar graphs and **(B, D and F)** representative CDF-plots (cumulative distribution function) of direct competition-assays of 10 nM BODIPY-labeled cyclopamine (BD-CP) and **(A and B)** 2, 5 or 20 nM calcitriol (cal), **(C and D)** 0.5 and 2 µM 25(OH)D_3 or **(E and F)** 1 and 10 µM vitamin D_3 (vitD_3) of tetracycline-induced conditional Smo-overexpressing HEK293S cells (induced) as described (Dwyer *et al.* 2007). Negative controls were the same as in Figure 44. Representative CDF-curve are shown with **(B)** 20 nM cal, **(D)** 2 µM 25(OH)D_3 and **(F)** 10 µM vitD_3. Data acquisition was conducted as described in the material and method section. All data represent at least 3 independent experiments measured in duplicates represented as mean +/-SEM.

In summary we were able to reproduce already published data showing the replacement of BD-CP from Smo by vismodegib and SAG. In addition, we show that the exclusive CRD-binder 20(S)OHC competes with BD-CP in Smo binding. Finally, the data demonstrates that calcitriol and its precursors vitD_3 and 25(OH)D_3 do not compete with BD-CP in Smo-binding, even at very high concentrations. This indicates that calcitriol binds to a Smo site distinct from the binding pocket/s of CP.

6.3.2.3. Calcitriol inhibits Hh signaling in cells expressing CRD-deleted or constitutive active Smo Variants

6.3.2.3.1. Overexpression of Smo^{wt} and $Smo^{\Delta CRD}$ in Shh light II and $Smo^{-/-}$ cells

To confirm our conclusion that calcitriol does not bind to the CRD of Smo, plasmids for the expression of *mCherry*-tagged wt *Smo* (*Smo^{wt}*) or a CRD-deleted Smo variant (*$Smo^{\Delta CRD}$*) were generated (see chapter 5.1.3.7). These plasmids were transduced in Shh light II cells (see chapter 5.2.4). Since Shh light II cells express endogenous wt Smo that may have interfered with $Smo^{\Delta CRD}$ in calcitriol binding, we furthermore transduced the *Smo^{wt}* or *$Smo^{\Delta CRD}$*-expression plasmids into *$Smo^{-/-}$* cells (see chapter 5.2.4) that do not express endogenous *Smo*. Fluorescence microscopy revealed a high *mCherry* expression in Shh light II (Fig. 47) and *$Smo^{-/-}$* cells (Fig. 48) demonstrating successful transduction of the cells with the plasmids. The images were taken in collaboration with Dr. Nickels Jessen and Maria Kamper (Max-Planck-Institute for biophysical chemistry, Department for NanoBioPhotonics, Prof. Dr. Stefan Hell, Göttingen)

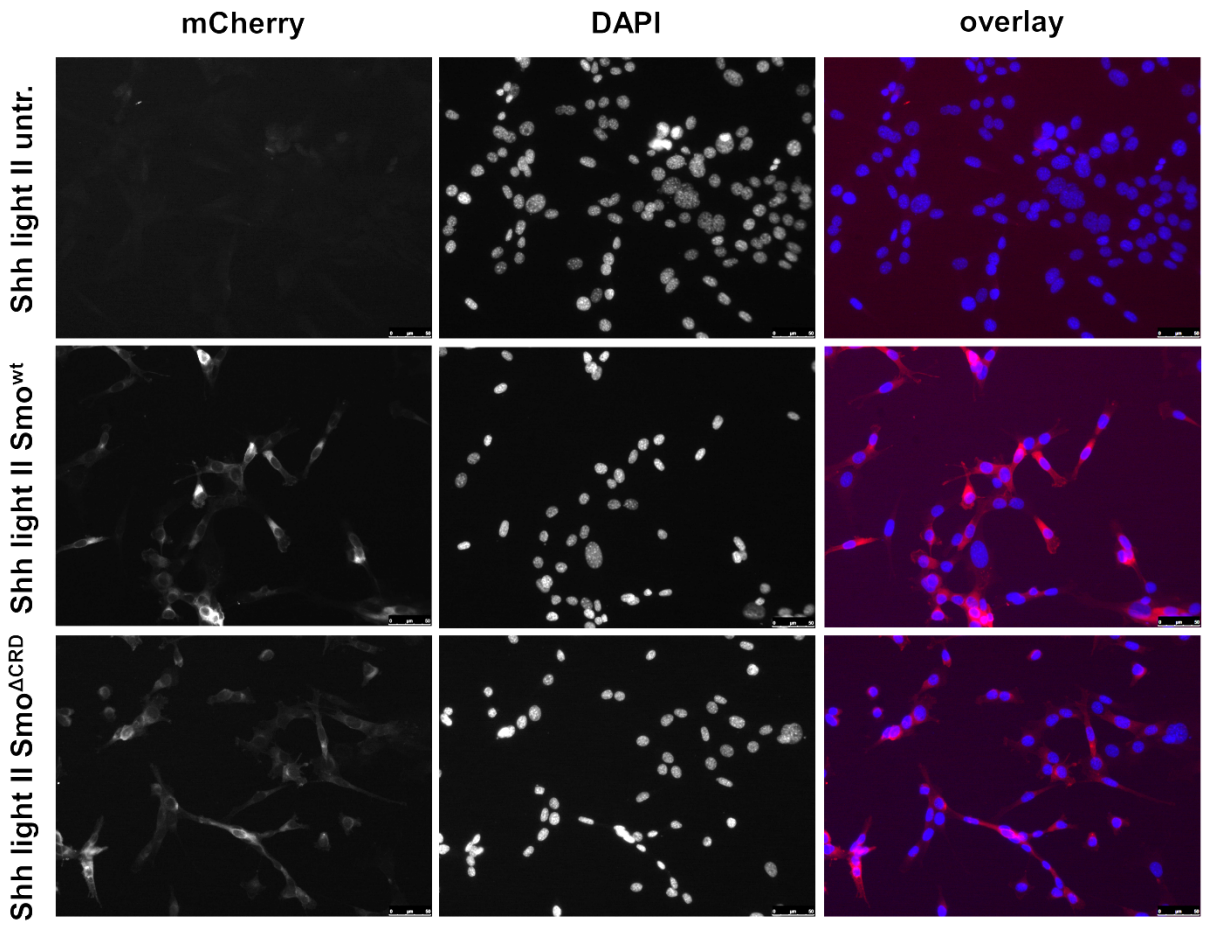

Figure 47: Validation of Smo^{wt} and Smo$^{\Delta CRD}$ expression in transduced Shh light II cells. Visualization of the mCherry expression of untransduced (upper panel), *Smo^{wt}* (middle panel) or *Smo$^{\Delta CRD}$*-transduced (lower panel) Shh light II cells by fluorescence microscopy. DAPI staining was conducted for visualization of the nuclei. DAPI staining and mCherry are shown in grayscale. Magnification: 200x.

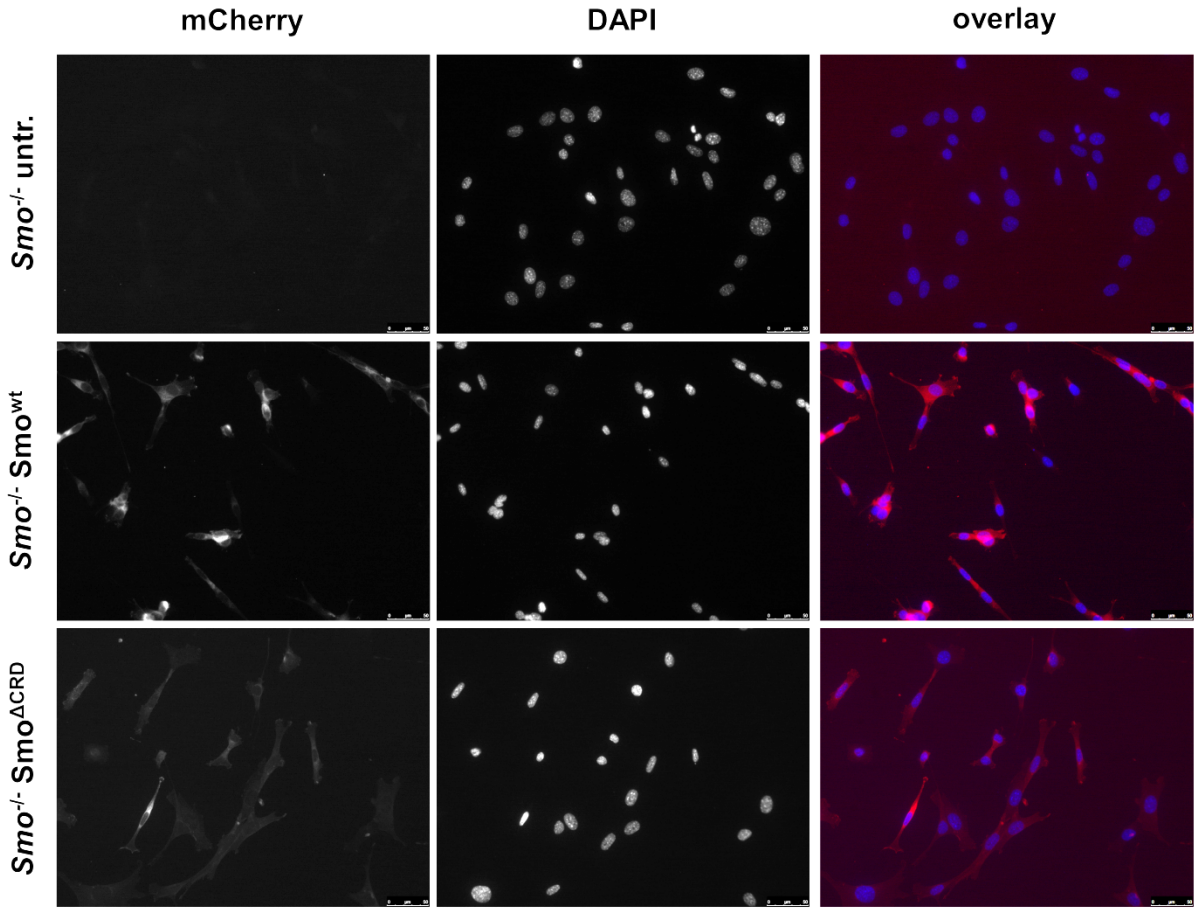

Figure 48: Validation of Smo^{wt} and Smo$^{\Delta CRD}$ expression in transduced *Smo*$^{-/-}$ cells. Visualization of the mCherry expression of untransduced (upper panel), *Smo*^{wt} (middle panel) or *Smo*$^{\Delta CRD}$-transduced (lower panel) *Smo*$^{-/-}$ cells by fluorescence microscopy. DAPI staining was conducted for visualization of the nuclei. DAPI staining and mCherry are shown in grayscale. Magnification: 200x.

6.3.2.3.2. Analyses of the Hh signaling activity of Smo^{wt} or Smo$^{\Delta CRD}$ overexpressing cells

To assess the effect of the CRD-deletion on the Hh signaling regulation by Smo modulators we determined the Hh signaling activity of *Smo*^{wt} or *Smo*$^{\Delta CRD}$-expressing Shh light II and *Smo*$^{-/-}$ cells by dual-luciferase assays or by *Gli1* expression analyses, respectively. First, we tested if overexpressed *Smo*^{wt} or *Smo*$^{\Delta CRD}$ are functionally active. Next, we tested if *Smo*^{wt} or *Smo*$^{\Delta CRD}$-overexpressing cells are still susceptible to induction of Hh signaling by SAG or Shh-N-CM.

As shown in figure 49 and 50, *Smo*^{wt} or *Smo*$^{\Delta CRD}$ overexpression led to significantly higher baseline activity of Hh signaling in both cell lines compared to untransduced cells (Fig. 49 A and B, white bars; Figure 50 A). In contrast to untransduced cells (Fig. 49 A and B, left

column pair) the stimulation with SAG or Shh-N-CM of *Smo*^{wt} or *Smo*$^{\Delta CRD}$-overexpressing Shh light II cells did not further increase Hh signaling activity (Fig. 49 A and B, middle and right column pair). Similar results were observed in SAG-treated *Smo*^{wt} or *Smo*$^{\Delta CRD}$-overexpressing *Smo*$^{-/-}$ cells (Fig. 50 B). These data suggest that Smo overexpression in Shh light II and *Smo*$^{-/-}$ cells induces the maximum of Hh signaling activity and show that the deletion of the CRD merely influences Smo function.

Next, we tested if calcitriol inhibits Hh signaling activity of *Smo*^{wt} or *Smo*$^{\Delta CRD}$-overexpressing cells. As a control we used CP that mainly acts with high affinity at the 7TM (Chen *et al.* 2002a; Nachtergaele *et al.* 2013). As control experiments we additionally analyzed Hh signaling activity in SAG or Shh-N-CM-treated untransduced Shh light II after calcitriol or CP treatment. Figure 49 shows that calcitriol and CP significantly reduced the Hh signaling activity of SAG or Shh-N-CM-treated Shh light II cells (Fig. 49 C). Interestingly, calcitriol and CP also significantly inhibited Hh signaling activity in *Smo*^{wt} or *Smo*$^{\Delta CRD}$-overexpressing Shh light II (Fig. 49 D) and *Smo*$^{-/-}$ cells (Fig. 50 C). However, SAG treatment of *Smo*^{wt} and *Smo*$^{\Delta CRD}$-overexpressing cells rendered the cells irresponsive to CP (Fig. 49 E and Fig. 50 D) whereas all cell lines, except *Smo*^{wt}-expressing Shh light II cells, stayed responsive towards calcitriol (Fig. 49 E and Fig. 50 D). Both, calcitriol and CP can inhibit Hh signaling after treatment with Shh-N-CM (Fig. 49 F).

Taken together these results show that calcitriol efficiently inhibits the activity of Smo$^{\Delta CRD}$ indicating that calcitriol does not bind Smo's CRD. Moreover SAG treatment led to CP-unresponsiveness, possibly by the occupancy of the 7TM by SAG, whereas calcitriol efficiently inhibited the Hh signaling activity in these settings. This again fosters our hypothesis that calcitriol does not bind to the 7TM.

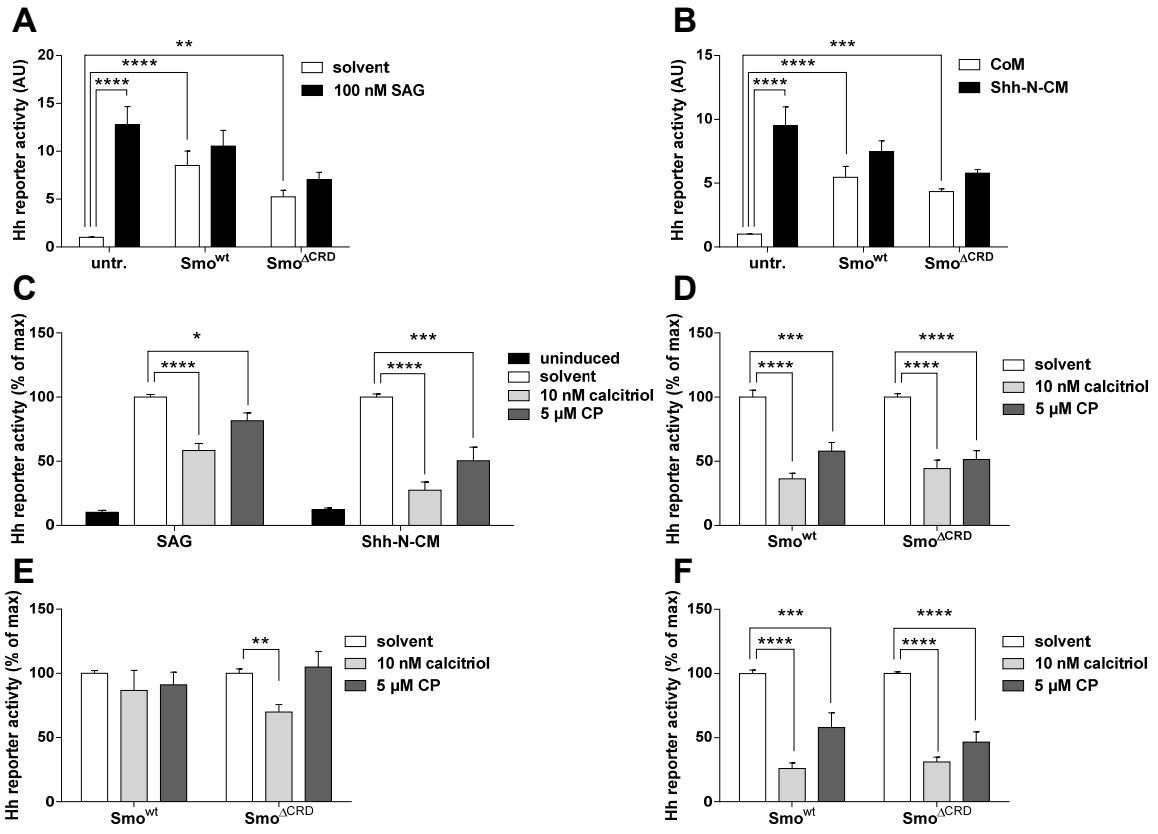

Figure 49: Calcitriol inhibits the Hh signaling activity of *Smo$^{\Delta CRD}$*-expressing Shh light II cells. Dual-luciferase-based analyses to determine the Hh signaling activation of **(A)** SAG or **(B)** Shh-N-CM-treated untransduced and *Smo^{wt}* or *Smo$^{\Delta CRD}$*-overexpressing Shh light II cells. **(C)** SAG- or Shh-N-CM-induced untransduced Shh light II cells, **(D)** uninduced, **(E)** SAG- and **(F)** Shh-N-CM-treated *Smo^{wt}* or *Smo$^{\Delta CRD}$*-expressing Shh light II cells after treatment with 10 nM calcitriol or 5 µM CP. Values of SAG or Shh-N-CM-induced cells in **(C)** and solvent-treated controls in **(D-F)** were set to 100 %. Data represent normalized firefly/renilla luciferase activity. All data represent at least 3 independent experiments measured in triplicates represented as mean +/-SEM. * $p<0.05$, ** $p<0.01$, *** $p<0.001$, **** $p<0.0001$.

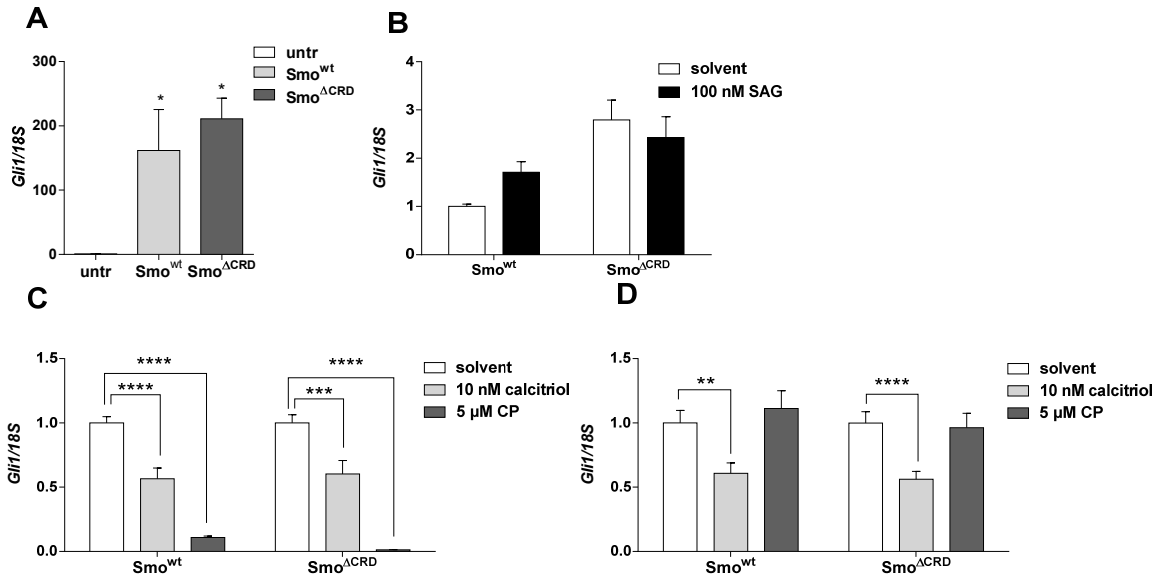

Figure 50: Calcitriol inhibits the Hh signaling activity of *Smo$^{\Delta CRD}$*-expressing *Smo$^{-/-}$* cells Relative quantification of *Gli1* expression levels of **(A)** untransduced, *Smo^{wt}* or *Smo$^{\Delta CRD}$*-overexpressing *Smo$^{-/-}$* cells, **(B)** SAG-treated *Smo^{wt}* or *Smo$^{\Delta CRD}$*-overexpressing *Smo$^{-/-}$* cells, **(C)** uninduced and **(D)** SAG-treated *Smo^{wt}* or *Smo$^{\Delta CRD}$*-expressing *Smo$^{-/-}$* cells after treatment with 10 nM calcitriol or 5 µM CP. *Gli1* expression levels were normalized to *18S* rRNA expression. Values of untranduced cells in **(A)**, solvent-treated Smo^{wt}-expressing cells in **(B)**, solvent-treated controls in **(C)** and SAG-induced cells in **(D)** were set to 1. All data represent at least 3 independent experiments measured in triplicates represented as mean +/-SEM. * $p<0.05$, ** $p<0.01$, *** $p<0.001$, **** $p<0.0001$.

Finally, we analyzed whether calcitriol was able to inhibit the activity of the SMO-M2 oncoprotein that harbors a Trp535 to Leu mutation located at the 7TM (Xie *et al.* 1998). Using the mouse analog SmoA1 it has been shown, that this mutant is partially resistant to CP. It is also resistant to physiological concentrations of Ptch, whereas increased amounts of Ptch retain the ability to inhibit it (Taipale *et al.* 2000). Thus, we assumed that our experimental concentrations of calcitriol (i.e. higher than physiological) should also be capable to inhibit constitutively active SMO-M2. To validate this hypothesis, we transiently transfected *Smo$^{-/-}$* cells with wt *SMO* or *SMO-M2* expression plasmids. Subsequently, the cells were treated with calcitriol or CP and Hh signaling activity was determined by *Gli1* expression analyses. Although SMO-M2 has been reported to be less sensitive to CP-mediated inhibition, CP treatment led to significantly reduced *Gli1* expression levels in wt SMO or SMO-M2-expressing cells compared to solvent-treated cells (Fig. 51, blue bars). More importantly, this experiment revealed that calcitriol efficiently inhibited Hh signaling in wt SMO or SMO-M2 expressing *Smo$^{-/-}$* cells (Fig. 51, green bars). This shows that neither the

SMO-M2 mutation site nor the 7TM of Smo are essential for calcitriol-mediated Hh signaling inhibition.

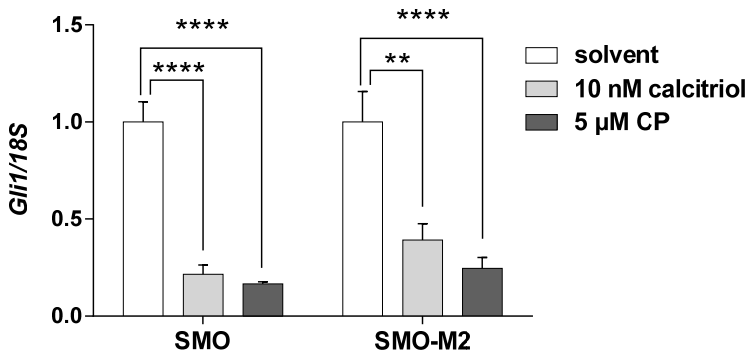

Figure 51: SMO-M2-mediated Hh signaling activation is inhibited by calcitriol. Relative quantification of *Gli1* expression levels of SMO or SMO-M2-expressing *Smo*$^{-/-}$ cells treated with 10 nM calcitriol or 5 µM CP. *Gli1* expression levels were normalized to *18S* rRNA expression levels. Solvent treated controls were set to 1. All data represent at least 3 independent experiments measured in triplicates represented as mean +/-SEM. ** $p<0.01$, **** $p<0.0001$.

7. Discussion

7.1. Regulation of the *Vdr* expression by Gli TFs

Previous work of our group indicated that *Vdr* gene expression is regulated in a Gli3-dependent manner. This was based on the findings that overexpression of Gli3 in wt *Ptch* fibroblasts led to a significantly increased *Vdr* expression (Fritsch 2014). Moreover similar results were obtained in *Gli2*$^{-/-}$/*Gli3*$^{-/-}$ fibroblasts, which do not show functional expression of any Gli TF, since *Gli1* is regulated by Gli2 (Ikram *et al.* 2004; Regl *et al.* 2002). Gli3 is usually proteolitically cleaved and mainly acts as a transcriptional repressor and only as a weak activator (Aberger *et al.* 2012; Roberg-Larsen *et al.* 2014; Wang *et al.* 2007b). However, Gli3 can be shifted towards its full-length activator form Gli3^{act} by activation of Hh signaling. In order to investigate whether Gli3 can activate *Vdr* expression we overexpressed Gli3 in wt *Ptch* or *Ptch*$^{-/-}$ cells that show constitutive activation of this pathway (Uhmann *et al.* 2011a) and wt *Ptch* cells were additionally incubated with Shh-N-CM. We also used *Gli1*$^{-/-}$*/Gli2*$^{-/-}$ fibroblasts in which the effects of Gli3 can be determined without any crosstalk with Gli1 and Gli2. Since the proteolytical processing of Gli3 occurs upstream of the Gli TFs, via phosphorylation of protein kinase A, glycogen synthase kinase 3-beta and casein kinase I (Aberger *et al.* 2012), we also stimulated the cells with Shh-N-CM to cause a shift towards Gli3^{act}.

Whereas no significant regulation of *Vdr* expression was seen in wt *Ptch* or *Ptch*$^{-/-}$ cells after Gli3 transfection or Shh-N-CM treatment, the incubation of *Gli1*$^{-/-}$/*Gli2*$^{-/-}$ cells with Shh-N-CM resulted in an upregulation of Vdr expression (compare Figs. 5 to 7). Thus, the data suggest that the expression of the *Vdr* gene is not regulated by Gli3 but may be regulated by Shh in dependency of the cellular context. These results are contradictory to initial experiments by A. Fritsch that showed increased *Vdr* expression in wt *Ptch* cells after Gli3 transfection (Fritsch 2014). However, the respective experiments were performed in medium supplemented with 10 % FCS (Fritsch 2014) whereas the experiments presented here were performed with CM that was generated from medium supplemented with 2% FCS. It is known that FCS starvation causes cell cycle arrest (Kronemann *et al.* 1999) or inhibition of proliferation (Oya *et al.* 2003). Therefore the differential gene expression pattern might be more likely the result from differential FCS supply than of the presence of Gli3. Moreover, media which are conditioned by cells (e.g. Shh-N-CoM and CM) certainly contain, aside from Shh-N, other factors which are not necessarily present in normal (10% FCS containing)

media. These factors (e.g. growth factors or soluble ligands) also might affect gene expression levels complicating the comparison between the settings even more.

In *Gli1*$^{-/-}$/*Gli2*$^{-/-}$ cells Gli3 is most likely processed to Gli3^{rep} ((Wang *et al.* 2007b), reviewed in (Briscoe and Therond 2013)) since *Gli1* and *Gli2* are completely absent, basal Hh activity is reduced (Lipinski *et al.* 2008) and Gli3^{act} is dependent on the Gli1-mediated feedback induction (Bai *et al.* 2004; Roberg-Larsen *et al.* 2014). However, *Vdr* expression was activated after Shh-stimulation in *Gli1*$^{-/-}$/*Gli2*$^{-/-}$ cells, which was likewise independent of Gli3 transfection. Whereas Gli3 and its activator form Gli3^{act} (that should occur after Shh-N-CoM treatment) probably do not play a role in *Vdr* expression, Shh seems to be able to induce *Vdr* expression in this cell line. Therefore it is possible that Shh induced a non-canonical pathway, resulting in *Vdr* gene expression. Such non-canonical effects of Shh have been reported previously for the expression of the Rho GTPases RacI and RhoA, which are regulated in a Shh-dependent, but Gli-independent manner (Polizio *et al.* 2011). However, because Shh did not enhance Vdr expression in wt *Ptch* and *Ptch*$^{-/-}$ cells, this effect must be specific for *Gli1*$^{-/-}$/*Gli2*$^{-/-}$ cells.

Our data furthermore showed that the expression of *Gli2* is strongly induced by simultaneous *Gli3* overexpression and Shh-N-CM treatment in wt *Ptch* cells and in *Ptch*$^{-/-}$ cells after Gli3 transfection. These results suggest that *Gli2* expression is induced by Gli3^{act}. Although Gli3 is widely known as a transcriptional repressor (Marigo and Tabin 1996), others also found that Gli3 can act as an activator of gene expression (e.g. in the development of the sclerotome (Buttitta *et al.* 2003), the spinal cord (Bai *et al.* 2004) or the limbs (Bowers *et al.* 2012). It is known that Gli3 regulates Gli1 by binding to *GliBS* in the promoter of *Gli1* (Dai *et al.* 1999), whereas no induction of *Gli2* expression by Gli3 has been described yet, probaply because Gli2 does not contain a GliBS in its promoter (Regl *et al.* 2002). Additionally, we analyzed if the putative *GliBS* located 312 bp upstream of the first exon of the Vdr gene is functionally active. Although this *GliBS* is the reverse complement of the consensus sequence (Hallikas *et al.* 2006; Winklmayr *et al.* 2010), TF binding to a reverse consencus sequence has been described previously (Scholz *et al.* 2010). Our analyses of the *pmVdrProm*^{wt} reporter constructs showed that overexpression of any Gli TF does not change luciferase activitiy of the *pmVdrProm*^{wt} reporter. This supports the findings that the *Vdr* gene is not directly regulated by Gli TF binding to the *Vdr* promoter.

Together, these experiments strongly suggest that *Vdr* expression is not regulated by Gli TFs. Nevertheless, since the Gli code is strongly dependent on the cellular context and

developmental stage (Aberger *et al.* 2012; Aberger and Ruiz 2014), it is possible that Gli TFs may regulate *Vdr* expression in other cells lines. Thus, it has been shown that Cyclin D2 is regulated independently of Hh signaling in embryonic kidney development (Hu *et al.* 2006) but is regulated by Hh signaling during hair follicle development (Mill *et al.* 2003). Strikingly, studies of the development of medulloblastoma in mice showed that the mere presence of a *GliBS* is not sufficient for the expression of the respective gene (Lee *et al.* 2010). However, whether this also applies for *Vdr* expression remains to be analyzed in the future. Additionally, a larger proportion of the *Vdr* promoter and thus more regulatory sequences should be employed in the *Vdr* promotor plasmids. Since it is an established fact that gene expression is not only regulated by TF binding at the direct vicinity of a promoter (e.g. the Vdr) but also several kb upstream (Hallikas *et al.* 2006) it is possible that the *Vdr* gene is rather regulated by such distant enhancers.

7.2. The potential of calcitriol as an anticancer agent

The general antitumoral effects of calcitriol are known for several decades (Bikle 2004; Bikle 2011a; Campbell *et al.* 2010; Deeb *et al.* 2007; Garland and Garland 1980; Trump *et al.* 2010). Moreover and as shown by our group, calcitriol has potential as an anticancer agent by modulating two distinct pathways simultaneously: First, it inhibits Hh signaling due to a inhibition of Smo activity and second, it induces Vdr signaling via its cognate receptor (Uhmann *et al.* 2011a; Uhmann *et al.* 2012). In this study we therefore tested if the combination of calcitriol with azoles enhances the calcitriol-mediated Hh signaling inhibition (and maybe Vdr signaling activation) and thus its anti-tumoral effects. This approach was chosen since azoles have been described as 1) efficient inhibitors of Hh signaling acting on Smo (Kim *et al.* 2010) and 2) to inhibit P450 enzymes, like the 24-hydroxylase, (Hansdottir *et al.* 2008; Vanden Bossche *et al.* 2004) which are among others implicated in calcitriol catabolism. Based on these data we hypothesized that the combination of azoles and calcitriol might enhance the inhibition of Hh signaling and activation of Vdr signaling due to calcitriol-stabilization and simultaneous inhibition of Smo.

7.2.1. Enhanced antitumorigenic capacity of a combined calcitriol/azole treatment *in vitro* but not *in vivo*

The simultaneous treatment of the murine BCC cell line ASZ001 with calcitriol and azoles significantly decreased *Gli1* expression levels when compared to single drug treatments (Fig. 11). Since *Cyp24a1* expression was significantly enhanced after combined calcitriol/ITZ treatment compared to calcitriol single treatment, ITZ supposedly stabilized calcitriol. The inhibition of Hh and activation of Vdr signaling, respectivily by single calcitriol is in line with previous findings by us and were also observed by others using the precursor of calcitriol, vitD_3 (Tang *et al.* 2011; Uhmann *et al.* 2011a; Uhmann *et al.* 2012). The combined treatment also resulted in a significant inhibition of proliferation reflecting an enhanced antiproliferative capacity of the agents when used simultaneously. However, these antitumoral effects were only detectable under serum-starved conditions (i.e. by using BSA-containing media) but not with FCS-containing media. Similar effects have been previously described by Kim *et al.* who showed that FCS-containing medium suppresses the Smo inhibitory properties of ITZ (Kim *et al.* 2010). Hence it was shown that this suppression is possibly mediated by low-density lipoproteins (LDL) that sequester ITZ (Kim *et al.* 2010). If so, this LDL-mediated suppression of ITZ must be specific for some cultured cells, since

similar results were not observed *in vivo* (Kim *et al.* 2014; Kim *et al.* 2013; Kim *et al.* 2010) or in other cell culture systems (e.g. human tracheobronchial epithelial cells, A549 cells (Hansdottir *et al.* 2008) or human hepatoma cell lines (Vanden Bossche *et al.* 2004)). The fact, that the antiproliferative effect of the (single) calcitriol treatment was weaker in FCS-free than in FCS-containing medium (compare Figs. 10 and 11), can be explained by a generally decreased proliferation rate of FCS-starved cells ((Oya *et al.* 2003) see also (Uhmann *et al.* 2011a)). Our results are further strengthened by the current literature which describes the potential antitumoral cooperation of calcitriol and azoles, albeit those studies did not focus on Hh signaling inhibition but Vdr signaling activation. Thus, it has been shown that calcitriol and KTZ displayed combined antitumoral effects in prostate cancer cell lines (Kota *et al.* 2011) and respective xenografts (Muindi *et al.* 2010). Moreover, the combination of calcitriol and the azole liarozole significantly decreased the proliferation of the calcitriol-resistant prostate cancer cell line DU145. This is due to enhanced calcitriol levels, probably by the inhibition of 24-hydroxylase activity (Ly *et al.* 1999). Besides 24-hydroxylase activity, 1α-hydroxlase is also inhibited by ITZ (Hansdottir *et al.* 2008; Vanden Bossche *et al.* 2004). Although the reports mentioned above did not focus on the role of calcitriol in Hh signaling inhibition, it is likely that the antitumoral effects of combined calcitriol/azole treatments are not only mediated by active Vdr signaling but also by inhibition of Hh signaling, especially since Hh signaling is implicated in several tumor types (e.g. prostate, lung or breast cancer (Gupta *et al.* 2010; Wilkinson *et al.* 2013)).

This conclusion is furthermore strengthened by our findings that no combined inhibition or activation of Hh or Vdr signaling, respectively were observed when calcitriol was combined with CP or when CP was combined with ITZ. At the first glance the latter result seem to contrast those described by Kim *et al.* who showed combinatory effects in Hh signaling inhibition upon combination of ITZ and KAAD-CP (3-Keto-N-(aminoethyl-N'-aminocaproyldihydrocinnamoyl)-cyclopamine) (Kim *et al.* 2010). However, this observation can be explained by the fact that KAAD-CP shows a higher affinity to Smo compared to CP (Chen *et al.* 2002b).

As already stated above, the azole-suppressing effects of FCS have not been observed *in vivo* and seem to be cell type specific (Hansdottir *et al.* 2008; Kim *et al.* 2014; Kim *et al.* 2013; Kim *et al.* 2010; Vanden Bossche *et al.* 2004). Unfortunately and in contrast to observations made by us using 2 % FCS supplemented culture medium (Nitzki *et al.* 2010; Uhmann *et al.* 2011a), the culture of murine skin biopsies in 1.5 % BSA-supplemented

medium led to necrosis (see 6.2.1.2). Nevertheless gene expression analyses of the samples were possible. Although the interpretation needs precaution, the analyses revealed that the Vdr target gene *Cyp24a1* is induced robustly by calcitriol or by the combination of calcitriol and an azole. Furthermore, although not reaching significance, *Gli1* expression was reduced by single treatments with either calcitriol or ITZ. The fact that calcitriol treatment did not significantly decrease *Gli1* expression levels can be due to necrosis and the associated changes in gene expression (Raza *et al.* 2004; Sato *et al.* 2008). Those might have altered *Gli1* baseline levels or indirectly affected *Gli1* expression. Curiously, the combination calcitriol/KTZ led to an (not statistically significant) increase in *Gli1* expression whereas the combination calcitriol/ITZ did not result in any change compared to solvent. This hints towards a functional contradiction, which was also observed *in vivo* (see below). Thus, the lack of response due to (calcitriol) single treatment might be due to the mouse background that might have caused a diminished response, whereas the contradiction of the combination might result from too high concentration of the drugs, leading to functional antagonism as revealed by the Fa-CI Plot (compare Fig. 39 and see below).

The calcitriol/azole combination was also employed *in vivo* in BCC-bearing $Ptch^{flox/flox}$ $CreERT2^{+/-}$ mice. The dose of 100 ng/kg calcitriol and 100 mg/kg azole was well-accepted by the mice, since no major adverse effects and no weight loss was observed. Unexpectedly, neither of the single treatments led to a significant inhibition of Hh signaling (compare Figs. 20 and 21); although a tendency for either single treatment was apparent. Surprisingly, Hh signaling was activated when calcitriol was combined with either ITZ or KTZ as judged by an increase in *Gli1* and *Gli2* expression. This increase reached statistical significance for calcitriol/ITZ compared to single ITZ treatment but not to solvent-treated animals. These findings indicate that the two drugs negatively influence each other *in vivo* with respect to Hh pathway inhibition.

The weak inhibition of Hh signaling by calcitriol in the mouse model for BCC was unexpected and strongly contradicted our previous findings (Uhmann *et al.* 2011a; Uhmann *et al.* 2012), especially because the same calcitriol treatment scheme was applied. However, the differences might have been caused by the background of the animals. Whereas the mice used by Uhmann *et al.,* were on a mixed C57BL/6N x BALB/c background (Uhmann *et al.* 2007; Uhmann *et al.* 2011a), the mice used in this study were C57BL/6N. This might have introduced some regulatory sequences or modifier regions that may have caused the tumors to be more aggressive or less susceptible towards the treatment. Accordingly, using a mixed

C57BL/6N x BALB/c background it takes 45 days for the tumors to be macroscopically visible (Nitzki *et al.* 2010), whereas in this study the tumors were already visible starting from day 30 post-induction, indicative for enhanced growth rates. Hence, the effect of modifier regions affecting tumor aggressiveness or therapeutic outcome has been described in many murine disease models including those of rhabdomyosarcoma (Hahn *et al.* 2004), kidney diseases (Salzler *et al.* 2007), lung cancer (Manenti *et al.* 1997), colon carcinoma (Dietrich *et al.* 1993) or mammary tumor metastasis (Hunter *et al.* 2001). Therefore it is possible that the two mouse backgrounds (i.e. C57BL/6N x BALB/c and C57BL/6N) are suitable to map genomic regions involved in treatment-susceptibility or aggressiveness of BCCs.

In contrast to Hh signaling, *Cyp24a1* was strongly induced upon calcitriol and calcitriol/azole treatment (Figs. 20 and 21). This is in line with our previous findings that calcitriol treatment of mice led to increased *Cyp24a1* expression levels (Uhmann *et al.* 2011a; Uhmann *et al.* 2012). Importantly, a tendency for an increased *Cyp24a1* expression after calcitriol/ITZ treatment compared to single calcitriol (Fig. 21) was detected. This is similar to our data obtained *in vitro* (compare Fig. 11) and strengthened the suggestion that ITZ stabilizes calcitriol levels *in vivo,* especially since similar observations were also made by others using *in vitro* approaches (Hansdottir *et al.* 2008; Vanden Bossche *et al.* 2004). Furthermore the increased *Cyp24a1* expression can be used as a surrogate marker for successful tumor penetration of calcitriol, thus excluding an inappropriate treatment procedure.

We furthermore assessed the expression levels of tissue-specific differentiation markers. The analyses revealed that *K10* and *Tgm1* expression levels significantly increased upon calcitriol/ITZ treatment, but not by any single treatment or calcitriol/KTZ treatment. Since a) ITZ probably stabilizes intracellular calcitriol levels (see above), b) calcitriol/ITZ activated Vdr signaling (as seen by increased *Cyp24a1* expression) and c) *K10* and *Tgm1* are known to be regulated by active Vdr signaling (Bikle 2004; Blanpain and Fuchs 2006) the increased expression of these differentiation markers most likely resulted from increased and/or stabilized calcitriol levels after calcitriol/ITZ treatment. Again, the data of the single calcitriol treatment contradicted previous findings which showed that *K10* and *Tgm1* expression levels were increased upon *in vivo* application of calcitriol (Uhmann *et al.* 2011a), although neither the amount of calcitriol (100 ng/kg/d) nor the treatment length (90 days) was changed. Additionally, the analyses of the tumor area demonstrated that neither calcitriol, nor any other treatment, significantly reduced the tumor size. Given the fact that reduction of

tumor size is seen upon calcitriol-treatment in the C57BL/6N x BALB/c BCC mouse model (Uhmann *et al.* 2011a) and has been described for ITZ-treated allografts of BCCs from *K-14CreER;Ptch*$^{+/-}$*;p53*$^{fl/fl}$ (Kim *et al.* 2013; Kim *et al.* 2010) and human BCCs (Kim *et al.* 2014), these contradictory data again may reflect differences in the genetic mouse backgrounds. Thus, the knowledge about the respective genetic modifiers that may be responsible for the decreased treatment susceptibility of BCC from *Ptch*$^{flox/flox}$ *CreERT2*$^{+/-}$ on a C57BL/6N x BALB/c background may contribute to the establishment of targeted and personalized therapy of this kind of tumor.

We finally tested the efficacy of the calcitriol/ITZ treatment in ASZ001-transplanted nude mice. As shown in Fig. 11, cultured ASZ001 cells were sensitive towards the combined treatment. After successful establishment of the ASZ001 allograft mouse model (Fig. 22) the calcitriol/ITZ combination treatment was evaluated. This approach (Fig. 26) revealed that both, calcitriol and ITZ alone, efficiently inhibit Hh signaling This was in line with the *in vitro* data (see Fig. 11) and publications by ours and other labs (Kim *et al.* 2010; Kota *et al.* 2011; Tang *et al.* 2011; Uhmann *et al.* 2011a; Uhmann *et al.* 2012). However, the combination of both drugs again negatively influenced each other with respect to Hh pathway inhibition, although not as strong as in *Ptch*$^{flox/flox}$ *CreERT2*$^{+/-}$ mice. Thus, *Gli1* expression was higher after the combined treatment in comparison to the single treatments, but lower than solvent-treated mice. Besides, calcitriol treatment led to significantly enhanced *Cyp24a1* expression, whereas ITZ alone and the calcitriol/ITZ combination only slightly induced *Cyp24a1* expression. The latter data again suggest that calcitriol and ITZ counteract their respective effects *in vivo*. However, calcitriol is known to induce the expression of the drug-transporters *Cyp3a23* (Xu *et al.* 2006) and *CYP3A4* which potentiate the activity and interact with the other multi-drug transporter (P-gps) in rats and humans, respectively leading to increased drug clearance (Chan *et al.* 2004). Furthermore, ITZ is a known potent inhibitor of P-gps (Heiskanen *et al.* 2008) and other transporter of xenobiotica but is also a target of those transporters itself (Miyama *et al.* 1998). Due to these facts, we hypothesized that calcitriol, ITZ or both drugs might have led to the induction of drug transporters in BCC, which finally may have decreased the intracellular concentrations of the two drugs. This could explain the diminished antitumoral effects *in vivo*. Indeed, compared to calcitriol-treated tumors, calcitriol/ITZ treated tumors showed somewhat diminished intratumoral ITZ concentrations by LC-MS/MS. Similarly, *Cyp24a1* induction in calcitriol/ITZ treated tumors was not as high as after single calcitriol treatment. Those observations indicate a decreased tumor penetration of the drugs. Due to these data we analyzed the expression levels of different *Mdr* transcripts

(*Mdr1a, Mdr1b and Mdr2*) but we did not detect any differential expression in the treatment cohorts. However, it is possible that other drug transporters are involved in export of intracellular ITZ. In addition, we cannot exclude an upregulation of drug transporters in other tissues by ITZ for example in the liver (Miyama *et al.* 1998).

Like in BCC-bearing *Ptch*$^{flox/flox}$ *CreERT2*$^{+/-}$ mice we also analyzed the differentiation status of the allografted BCC. However, no significant changes of the *K1*, *K10*, *Tgm1*, *Lor* or *Ivl* expression were observed by neither single nor the combination treatment. Given the fact that 90 day-calcitriol treatment led to enhanced *K10* and *Tgm1* expression in BCC of *Ptch*$^{flox/flox}$ *CreERT2*$^{+/-}$ mice on a C57BL/6 x BALB/c background (Uhmann *et al.* 2011a), it is possible that the treatment scheme of 30 days (that has been applied in the allografted animals) might have been too short to achieve significant induction of keratinocyte differentiation. Since these markers were also not induced in BCC of *Ptch*$^{flox/flox}$ *CreERT2*$^{+/-}$ mice on the C57BL/6 background (see above), the lack again rather argues for genetic background reasons. Moreover, the treatment might have been more effective (concerning induction of differentiation and inhibition of tumor growth) by starting drug application directly after the transplantation like described by others (Kim *et al.* 2010), although it is common practice to allow the tumors to start growing (Ng and Curran 2011).

In summary, we showed that our promising findings concerning the combination of calcitriol and ITZ obtained *in vitro* could not be recapitulated in two different animal models for BCCs. These observations demonstrate the importance and application of preclinical *in vivo* systems to test new drugs or drug combination before applying them to the clinics. Furthermore these findings should be taken into consideration by clinicians, since both, calcitriol and ITZ, are already approved drugs for the treatment of non-cancerous diseases like psoriasis (calcitriol) (Kircik 2009) as well as fungal infections (ITZ) (Doring *et al.* 2015) and are currently being tested as single drugs in clinical trial for the topical treatment of BCCs (NCT02120677; NCT01358045).

Thus, future research should address the search for the genetic modifier region which is responsible for calcitriol insensitivity of *Ptch*$^{flox/flox}$ *CreERT2*$^{+/-}$ mice on a C57BL6/N background. It also would be of great interest to determine the reason for the counteraction of calcitriol and ITZ *in vivo* and to evaluate the combined calcitriol/ITZ therapy in other Hh-driven cancers *in vitro* and *in vivo*.

7.2.2. Analysis of the influence of ITZ on calcitriol-metabolism

Our *in vitro* approaches revealed an enhanced antitumorigenic effect of combined calcitriol/azole treatment. Azoles are known as general inhibitors of P450 enzyme like 1α-hydroxylase and 24-hydroxylase, which are involved in calcitriol metabolism (Kota *et al.* 2011; Muindi *et al.* 2010). Hence, we hypothesized that ITZ might mediate, aside from Smo inhibition, an additional antitumoral effect by preventing the degradation of calcitriol und thus potentiate the calcitriol-mediated effects. In fact, we observed a significant increase of *Cyp24a1* expression after calcitriol/ITZ treatment compared to calcitriol alone in serum-starved ASZ001 cells (Fig. 11) and in BCC from calcitriol/ITZ-treated $Ptch^{flox/flox}$ $CreERT2^{+/-}$ mice (Fig. 14). However, by LC-MS/MS-based quantification we showed that ITZ did not change calcitriol-synthesis or its degradation neither in ASZ001 nor HaCaT cells (Figs. 30 and 31). These data suggests that ITZ does not have an impact on calcitriol bio-availability. However, the treatment with 25(OH)D_3 and calcitriol of the MS-based experiments were conducted for 6 h and relatively high concentration of 25(OH)D_3 (2 µM) and calcitriol (100 nM) were used. It is possible that the time of treatment period of 6 h was too short to induce efficient inhibition of the hydroxylases, leading to the different amounts of the vitD_3-derivatives or that the high intracellular amounts of 25(OH)D_3 or calcitriol (due to the treatment) masked measurable differences. This incubation time was chosen because our timecourse experiment of 25(OH)D_3 and vitD_3 supplementation (compare chapter 6.3.1.2) showed that calcitriol synthesis is well-measurable within 6 h. Also, we wanted to observe ITZ-mediated inhibition of the enzymes 1α- and/or 24-hydroxylase rather than transcriptional responses. Beyond that, different cell types are also known to display different susceptibilities to inhibition of cytochrome P450 enzymes by azoles. Thus, it has been shown that vitD_3 supplementation in the presence of KTZ leads to the synthesis of significantly higher calcitriol levels in dendritic cells but not in monocyte-derived macrophages (Kundu *et al.* 2014). Thus, the proof whether ITZ influences calcitriol-synthesis or its degradation will require more experiments with longer vitD_3 incubation times and a more sensitive method to detect subtle variations in calcitriol levels.

7.3.Role of calcitriol in Hh signaling

7.3.1. Ptch is dispensable for calcitriol synthesis, but essential for its release

Our own research and those of others suggested that Ptch 1) exports vitD$_3$-like and/or Hh-inhibitory molecules (Bijlsma *et al.* 2006; Uhmann *et al.* 2011a), 2) is involved in sterol-transport (Bidet *et al.* 2011) and 3) is a homologue to RND-transporters that transport lipophilic molecules across membranes using a proton gradient (Taipale *et al.* 2002). Due to the fact that calcitriol is the only physiological Hh inhibitor that works in low doses (Uhmann *et al.* 2011a; Uhmann *et al.* 2012), we hypothesized that calcitriol might present an endogenous inhibitor of Smo that is released by Ptch in the absence of Hh ligands. Since the detection of calcitriol in the cell culture medium by means of underivatized LC-MS/MS analyses was not possible in our hands, we established a highly sensitive assay to measure calcitriol by induction of luciferase-expression. Using this assay we showed that wt *Ptch*, but not *Ptch*$^{-/-}$ fibroblast are able to release significant amounts of calcitriol into the cell culture medium (Fig. 34). The calcitriol concentration in the medium was likely less than 0.1 nM (compare fold-change induction of Figs. 35 and 34) and was not able to inhibit Hh signaling in Shh light II cells (Fig. 32). Similar effects were observed by CRC analyses in which 0.1 nM calcitriol had only little potential to inhibit Hh signaling (Fig. 38). Although calcitriol release is difficult to assess, some reported the release of calcitriol in dendritic cells and macrophages (Kundu *et al.* 2014). However, the issue of how this release is mediated has not been addressed. It is known that the uptake of DBP-bound 25(OH)D$_3$ is mediated by the multi-ligand receptor Megalin (Kaseda *et al.* 2011), but no reports for the release of vitD$_3$-like molecules are available. Interestingly, it has also been described that Megalin mediates the Shh response in the nervous system (Ortega *et al.* 2012). A recent study showed the Ptch-mediated release of 3β-hydroxysteroids including the calcitriol-precursors 7-DHC and vitD$_3$ and that those molecules are inhibitors of Hh signaling (Bijlsma *et al.* 2006). Accordingly, we provide evidence that the release of calcitriol is mediated by Ptch.

Furthermore, we show that the Ptch status of cells does not influence the synthesis of calcitriol from its progenitors 25(OH)D$_3$ and vitD$_3$. Both wt *Ptch* and *Ptch*$^{-/-}$adult fibroblasts and the *Ptch*-deficient BCC cell line ASZ001 were able to synthetize calcitriol from its precursors (Fig. 36 and 37). These findings are in line with the plethora of different cell systems capable of the extra-renal synthesis of calcitriol like the skin (Vantieghem *et al.* 2006; Zehnder *et al.* 2001), the lung (Hansdottir *et al.* 2008) or cells of the immune system (Kundu

et al. 2014). Taken together our data demonstrate effective calcitriol synthesis and show that Ptch is dispensable for calcitriol synthesis.

7.3.2. Calcitriol does neither bind to the CRD nor the 7TM of Smo

We previously provided evidence that calcitriol inhibits Hh signaling independently of the Vdr presumably at the level of Smo because it cannot inhibit Hh signaling in *Smo*$^{-/-}$ cells but regains this ability upon Smo-overexpression (Uhmann *et al.* 2011a). This indicates that calcitriol might directly bind to and regulate Smo. As already mentioned, the Smo protein contains two known binding sites for small molecules, which are the 7TM and the CRD. The 7TM resembles the main binding site for (synthetic) modulators (see introduction) and the CRD is the exclusive binding site for oxysterols (Nachtergaele *et al.* 2012; Nachtergaele *et al.* 2013; Nedelcu *et al.* 2013). ITZ, which also inhibits Hh signaling at the level of Smo, is thought to bind a site distinct from the 7TM or the CRD (Kim *et al.* 2010; Nachtergaele *et al.* 2012). The fact that the CRD is the binding site for oxysterols led us to the initial assumption that calcitriol, as an oxidized distant, derivative of cholesterol, might bind to the CRD as well. Thus, we first performed CRCs to detect potential functional competitions of calcitriol with other Smo-modulators. We found that none of the 7TM-binders CP (Chen *et al.* 2002a), vismodegib (Nachtergaele *et al.* 2013) or SAG (Chen *et al.* 2002b), influenced the IC_{50} of calcitriol or *vice versa*. These findings indicate that calcitriol does not bind to the 7TM. Accordingly, the maximal pathway activation of SAG was reduced by increasing amounts of calcitriol. This is suggestive for non-competitive binding of both drugs (Litman *et al.* 1997). Interestingly, we observed a significant decrease of the IC_{50} of ITZ in the presence of calcitriol and *vice versa*. This potential synergistical modulation of Smo, indicates non-competitive binding of the two drugs to Smo. In fact, these results are in line with the *in vitro* data obtained in ASZ001 (compare Fig. 11). Moreover, the analyses of the CRC data using a Fa-CI-Plot, showing that low to intermediate concentrations of calcitriol and ITZ synergize in Hh signaling inhibition, supported our interpretation of the results (Chou 2006; Chou 2010) (Fig. 39). Interestingly, the Fa-CI-Plot also revealed that high concentrations of both drugs led to antagonism. These findings might explain our results from the *in vivo* treatment studies, in which relatively high amounts of calcitriol and ITZ (100 ng/kg calcitriol and 100 mg/kg ITZ, respectively) were applied to the mice. Therefore, it is possible that the drug concentrations used *in vivo* were high enough to cause an antagonistic interplay of calcitriol and ITZ. This may have caused the lack or a diminished Hh signaling inhibition, which was seen in BCC

from *Ptch*$^{flox/flox}$ *CreERT2*$^{+/-}$ and ASZ001-allografted nude mice, respectively. Hence, the future *in vivo* experiments should also be conducted with lower concentrations of both drugs to ensure that they are applied in a synergistical concentration.

Since Kim *et al.* reported a functional, non-competitive synergism of ITZ and KAAD-CP (Kim *et al.* 2010), we also assessed the potential interaction of CP and ITZ. In contrast to Kim *et al.*, our data obtained from the CRC analyses (Fig. 40) and the *in vitro* treatment of ASZ001 (Fig. 13) suggests that CP and ITZ do not functionally synergize. However, KAAD-CP binds Smo with a higher affinity than CP (Chen *et al.* 2002a; Kim *et al.* 2010). Therefore, it probably interacts differently with ITZ and Smo, which might explain these contrasting results. Finally, we showed that calcitriol is a non-competitive inhibitor of 20(S)OHC, which binds to the CRD (Nachtergaele *et al.* 2012; Nachtergaele *et al.* 2013; Nedelcu *et al.* 2013). This is based on the observation that, similar to SAG, calcitriol does not change the ED_{50} of 20(S)OHC but reduces the maximal pathway activation. Together these data suggest that calcitriol binds to a site distinct from the CRD or the 7TM.

In order to verify our interpretation that calcitriol does not directly bind to the 7TM we furthermore performed BD-CP replacement assays (Dwyer *et al.* 2007; Kim *et al.* 2010) (Nachtergaele *et al.* 2013). CP, vismodegib and SAG significantly competed with BD-CP for binding on Smo, indicating that these drugs bind to the 7TM as described previously (Chen *et al.* 2002a; Chen *et al.* 2002b; Nachtergaele *et al.* 2013). In accordance to Nachtergaele *et al.* we also observed a competition of 20(S)OHC with BD-CP for Smo binding (Nachtergaele *et al.* 2013). Beyond that, we also observed a competition of ITZ with BD-CP. This observation is opposed to results described by Kim *et al.* (Kim *et al.* 2010). However, the fact that Kim *et al.* did not perform a statistical evaluation of their data questions their conclusion. Finally and in accordance with our hypothesis, we showed that neither calcitriol nor its precursors $25(OH)D_3$ and $vitD_3$ compete with BD-CP for Smo-binding. Due to the fact that BD-CP was significantly replaced by 7TM binders (i.e. CP, SAG, vismo) and also by the CRD binder 20(S)OHC we conclude that calcitriol, $25(OH)D_3$ or $vitD_3$ neither bind to the 7TM nor (at least calcitriol) the CRD of Smo. Notably, our observation that $vitD_3$ does not bind to the same site as CP, is in contrast to previously published data by Bijlsma *et al.,* who showed that Smo binding of $vitD_3$ can be competed with CP (Bijlsma *et al.* 2006). However, they were employing a yeast-expression system and measured residual radioactivity of [^{3}H]-labeled $vitD_3$ (Bijlsma *et al.* 2006), whereas we measured direct changes in fluorescence intensity, using an assay that is widely used and also might be the more physiological assay to analyze

Smo-binding (Chen *et al.* 2002b; Dwyer *et al.* 2007; Kim *et al.* 2010; Nachtergaele *et al.* 2013; Nedelcu *et al.* 2013). Hence, the observed differences rather relate to the different methods applied.

To verify the assumption that calcitriol does not bind to the CRD of Smo, Shh light II overexpressing wt *Smo* (*Smo*^{wt}) or CRD-deleted *Smo* (*Smo*$^{\Delta CRD}$) were incubated with calcitriol and Hh signaling activity was analyzed. To ensure that endogenous Smo does not interfere with our interpretation we also transduced *Smo*$^{-/-}$ cells with the plasmids (Figs. 49 and 50). The overexpression of both Smo variants resulted in strongly enhanced basal pathway activity which was in line with data of other labs (Myers *et al.* 2013; Taipale *et al.* 2000; Taipale *et al.* 2002). This enhanced pathway activity is most likely caused by excessive amounts of Smo, that can no longer be inhibited by the endogenous amounts of Ptch (Taipale *et al.* 2002). Accordingly, Myers *et al.* showed that pathway activation caused by overexpression of Smo can be inhibited by cotransfection of Ptch (Myers *et al.* 2013).

The pathway inhibition by CP and calcitriol showed that, similar to CP which acts mainly at the 7TM (Chen *et al.* 2002a; Nachtergaele *et al.* 2013), the calcitriol treatment resulted in efficient Hh pathway inhibition in Smo^{wt} and Smo$^{\Delta CRD}$ overexpressing cells, too. This demonstrates that calcitriol inhibits Smo in a CRD-independent manner. Since we excluded a binding of calcitriol to the 7TM using the BD-CP competition assay these data indicate that calcitriol acts independently of the two binding sites.

Besides, we tested the sensitivity of the Smo^{wt} and Smo$^{\Delta CRD}$ overexpressing cells for further pathway activation due to Shh-N-CM or SAG treatment. Others also reported that a further enhancement of Hh signaling activity of Smo$^{\Delta CRD}$ overexpressing cells by Shh-N-CM is not possible but that SAG treatment was still possible, whereas Smo^{wt} overexpressing cells still can be activated by Shh-N-CM and SAG treatment (Myers *et al.* 2013; Nachtergaele *et al.* 2013; Nedelcu *et al.* 2013). This lack of response might be caused by the strong overexpression of Smo facilitated by our *pMSCV*-expression system which leads to strong gene expression (Andersen *et al.* 2011) and likely resembles maximal pathway activity upon Smo overexpression (Rohatgi and Scott 2007; Taipale *et al.* 2000). Nevertheless, control experiments using untransduced Shh light II cells revealed that SAG and Shh-N-CM treatment indeed led to high activation of Hh signaling and that this induction can be effectively inhibited by calcitriol or CP. Thus, we conclude that the maximal induced pathway activity is reached in Smo^{wt} and Smo$^{\Delta CRD}$ overexpressing cells which enables us to analyze pathway inhibition without the presence of any inducer of Smo activity (e.g. SAG) that might

interfere with Smo-binding. The fact that calcitriol was able to inhibit Hh signaling in Smo^{wt} and $Smo^{\Delta CRD}$ overexpressing Shh light II and *Smo*$^{-/-}$ cells shows that calcitriol can act independently of the CRD. Our additional findings that calcitriol does not compete with BD-CP, that mainly acts at the 7TM, further strengthens our hypothesis that calcitriol acts at a yet unidentified site on Smo.

Nonetheless, beyond this conclusion we found that SAG-treated Smo^{wt} and $Smo^{\Delta CRD}$ overexpressing cells were not susceptible for CP-mediated Hh signaling inhibition. This observation might be explained by the fact that the occupancy of the 7TM by SAG (Dockendorff *et al.* 2012; McCabe and Leahy 2015; Wang *et al.* 2014) prevents the binding of CP, that can to a lesser extent also be observed in untransduced SAG-treated Shh light II (compare Fig. 49 C). A reduced susceptibility of CP due to SAG-treatment has also been described for C3H10T1/2 cells (Dockendorff *et al.* 2012), another *in vitro* model for the Hh pathway. Intriguingly, SAG-bound Smo^{wt} and $Smo^{\Delta CRD}$ were sensitive towards calcitriol-mediated Hh signaling inhibition in *Smo*$^{-/-}$ cells (Fig. 50 D). This supports our hypothesis that calcitriol does not bind to the 7TM and exemplifies that calcitriol is a very potent inhibitor of Smo. In Smo^{wt} overexpressing Shh light II cells calcitriol does not mediate an inhibition of Hh signaling inhibition (Fig. 49 E) indicating that SAG-treatment results in an active state of Smo that is less prone to inhibition (Dockendorff *et al.* 2012; Wilson *et al.* 2009). Whether this observation is cell-type specific or due to the endogenous Smo present in Shh light II needs to be addressed in future studies.

In contrast to SAG-treated cells, calcitriol as well as CP efficiently inhibited Shh-N-CM-treated Smo^{wt} and $Smo^{\Delta CRD}$ overexpressing cells (Fig. 49 F). This, more physiological, process of Shh-induced Smo activation, caused by the removal of Shh-bound Ptch from the membrane (Rohatgi and Scott 2007), likely removes any Smo-inhibiting endogeneous molecules that were previously released by Ptch, thus relieving the binding pockets for calcitriol or CP.

Finally, we made use of the SMO-M2 variant that is less sensitive but not resistant to Ptch-mediated inhibition and CP treatment (Taipale *et al.* 2000; Taipale *et al.* 2002). Remarkably, calcitriol as well as CP inhibit SMO-M2 activity but less efficient than wt SMO. But since we used relatively high concentrations of calcitriol and CP the inhibition of SMO-M2 seems plausible. Especially since both drugs are more efficient in cells expressing wt SMO and since KAAD-CP has been previously reported to inhibit the murine equivalent of SMO-M2 as well (Taipale *et al.* 2000). The fact that overexpression of Ptch restores the

inhibition of SMO-M2 (Taipale *et al.* 2002) and assuming that calcitriol might resemble an endogeneous inhibitor of Smo, opens the possibility that increased amounts of Ptch result in increased amounts of calcitriol to be released. This would resemble our findings that higher than physiological concentrations (i.e. 10 nM) of calcitriol can inhibit SMO-M2. Furthermore, since the M2-mutation is located at the 7th transmembrane domain (Taipale *et al.* 2002), these observations foster our assumption that calcitriol acts independently of the 7TM.

Nonetheless, we admit that our experiments do not show a direct binding of calcitriol to Smo. Thus, we cannot exclude the unlikely event that a yet unidentified protein/peptide facilitates the inhibitory effects on Smo. Our approaches in developing an ELISA to measure Smo-binding failed due to the lack of specificity and appropriate positive controls. However, radioactively or fluorescently labeled calcitriol would be beneficial to perform an assay similar to the BD-CP replacement assay to target this question.

7.4.Calcitriol as a candidate molecule for the Ptch/Smo interaction

The currently accepted model for the Ptch/Smo interaction is that Ptch releases a small molecule that inhibits or activates Smo and thereby limits the presence or absence of this putative molecule (Albert and Hahn 2014; Briscoe and Therond 2013; McCabe and Leahy 2015; Myers *et al.* 2013; Nachtergaele *et al.* 2013; Nedelcu *et al.* 2013; Roberg-Larsen *et al.* 2014; Wang *et al.* 2014). Our data provides evidence that this putative molecule is calcitriol.

First, this putative molecule needs to be available locally. Indeed, our data show that calcitriol can be synthesized in non-renal cells including fibroblasts and a BCC cell line. Similar observations were made by other groups who showed calcitriol synthesis in the skin (Vantieghem *et al.* 2006) or the lung (Hansdottir *et al.* 2008).

Second, the putative inhibitor needs to be released by Ptch. Accordingly, we show that wt *Ptch,* but not *Ptch*$^{-/-}$ cells can release calcitriol into the cell culture medium (Fig. 34). This indicates that Ptch is indispensable for calcitriol secretion. The released amount of calcitriol is extraordinarily low (0.1 nM) which correlates with the low calcitriol concentration in human blood serum (38 to 134 pM) (Hollis 2010).

Third, the putative molecule needs to be able to modulate Smo activity. Here and previously (Uhmann *et al.* 2011a; Uhmann *et al.* 2012) we show that calcitriol inhibits Smo activity by a new, uncharted binding site. Furthermore, this is the first report of a physiologically occurring sterol-based molecule with Smo-inhibitory capacity, whereas all other reports have identified oxysterols with Smo-activating activity.

A recent study suggests that neither the CRD nor the 7TM are the major site of Smo regulation (Myers *et al.* 2013). In addition, the CRD is thought to rather function as a site for fine-tuning Smo's activity (Myers *et al.* 2013; Nedelcu *et al.* 2013). This is in line with our analyses showing that calcitriol does not bind to the 7TM because it does not compete with known 7TM-binders (compare Figs. 38, 41 and 46) and also can inhibit mutant SMO-M2 (compare Fig. 51) that carry a mutation in the 7TM (Taipale *et al.* 2000). Calcitriol also does not bind to the CRD as it inhibits Hh signaling activity in Smo$^{\Delta CRD}$-overexpressing Shh light II and *Smo*$^{-/-}$ cells (Figs. 49 and 50) and acts as a non-competetive inhibitor of 20(S)OHC (Fig. 41). Recent publications also describe potential candidates for the Ptch/Smo interaction. As stated above are oxysterols capable to induce Hh signaling via binding to the Smo CRD (Corcoran and Scott 2006; Nachtergaele *et al.* 2012; Nachtergaele *et al.* 2013; Nedelcu *et al.* 2013), although these have been ruled out as the key effectors of Hh signaling (Myers *et al.*

2013). Other candidates are lipids or other sterols that have been shown to traffic through Ptch and to inhibit Smo in *D. melanogaster* (Khaliullina *et al.* 2009), as well as endocannabinoids that are present in lipoproteins (Khaliullina *et al.* 2015). Another group proposed that Ptch inhibits the generation of phospholipid phosphatidylinositol-4 phosphate (PI4P) that is able to activate Smo (Yavari *et al.* 2010).

In order to validate our data it would be helpful to use labeled calcitriol and track its sub-cellular fate in the presence or absence of Ptch, as described in a recent study using the Smo-activating oxysterol 20(S)OHC (Peyrot *et al.* 2014). In addition, mice defective in calcitriol synthesis or degradation could help to analyze if the lack or excess of calcitriol mimics phenotypes associated with high or low Hh signaling activity, like the murine model systems for SLOS-like diseases (Cooper *et al.* 2003; Cunniff *et al.* 1997; Opitz *et al.* 1987; Porter 2006; Tint *et al.* 1994; Wassif *et al.* 1998).

Furthermore it is of importance to unravel the Smo-binding site of calcitriol. This could be achieved by competition assays using immobilized calcitriol (e.g. by beads or using biotin-tags) and mutant Smo proteins that lack different domains. Similar experiments have been performed by Nachtergaele *et al.* and Necelcu *et al.* to identify the Smo-binding site of 20(S)-OHC (Nachtergaele *et al.* 2013; Nedelcu *et al.* 2013). The generation of various Smo mutants lacking different domains, like the extracellular linker domain connecting the CRD and the heptahelical bundle or the intracellular c-terminal tail, will allow for the identification of the calcitriol binding pocket of Smo.

Moreover, it would be interesting to generate the 3D-structure of calcitriol-bound Smo. This has already been done for several 7TM-binders such as SANT-1, CP and SAG (McCabe and Leahy 2015; Wang *et al.* 2014; Wang *et al.* 2013). The results clearly demonstrate that they all are bound to the same cavity, with however different orientation and penetration depth. This caused either agonistic or antagonistic properties of the compounds and also explained the fact that some compounds still can inhibit treatment resistant variants of Smo (Wang *et al.* 2014).

Finally, it would be interesting to see whether calcitriol is the only endogenous inhibitor of Smo or if other endogenous molecules exist that act on Smo and are released from Ptch and if this is a conserved mechanism across mammals and during development.

8. References

Aberger, F., Kern, D., Greil, R. and Hartmann, T. N. (2012). "Canonical and noncanonical Hedgehog/GLI signaling in hematological malignancies." Vitam Horm **88**: 25-54.

Aberger, F. and Ruiz, I. A. A. (2014). "Context-dependent signal integration by the GLI code: the oncogenic load, pathways, modifiers and implications for cancer therapy." Semin Cell Dev Biol **33**: 93-104.

Akutsu, N., Lin, R., Bastien, Y., Bestawros, A., Enepekides, D. J., Black, M. J. and White, J. H. (2001). "Regulation of gene Expression by 1alpha,25-dihydroxyvitamin D3 and Its analog EB1089 under growth-inhibitory conditions in squamous carcinoma Cells." Mol Endocrinol **15**(7): 1127-1139.

Albert, B. and Hahn, H. (2014). "Interaction of hedgehog and vitamin D signaling pathways in basal cell carcinomas." Adv Exp Med Biol **810**: 329-341.

Albertson, D. G., Ylstra, B., Segraves, R., Collins, C., Dairkee, S. H., Kowbel, D., Kuo, W. L., Gray, J. W. and Pinkel, D. (2000). "Quantitative mapping of amplicon structure by array CGH identifies CYP24 as a candidate oncogene." Nat Genet **25**(2): 144-146.

Ali, A., Wang, Z., Fu, J., Ji, L., Liu, J., Li, L., Wang, H., Chen, J., Caulin, C., Myers, J. N., Zhang, P., Xiao, J., Zhang, B. and Li, X. (2013). "Differential regulation of the REGgamma-proteasome pathway by p53/TGF-beta signalling and mutant p53 in cancer cells." Nat Commun **4**: 2667.

Andersen, C. R., Nielsen, L. S., Baer, A., Tolstrup, A. B. and Weilguny, D. (2011). "Efficient expression from one CMV enhancer controlling two core promoters." Mol Biotechnol **48**(2): 128-137.

Bai, C. B., Stephen, D. and Joyner, A. L. (2004). "All mouse ventral spinal cord patterning by hedgehog is Gli dependent and involves an activator function of Gli3." Dev Cell **6**(1): 103-115.

Basset-Seguin, N., Sharpe, H. J. and de Sauvage, F. J. (2015). "Efficacy of Hedgehog pathway inhibitors in basal cell carcinoma." Mol Cancer Ther.

Berking, C., Hauschild, A., Kolbl, O., Mast, G. and Gutzmer, R. (2014). "Basal cell carcinoma-treatments for the commonest skin cancer." Dtsch Arztebl Int **111**(22): 389-395.

Bidet, M., Joubert, O., Lacombe, B., Ciantar, M., Nehme, R., Mollat, P., Bretillon, L., Faure, H., Bittman, R., Ruat, M. and Mus-Veteau, I. (2011). "The hedgehog receptor patched is involved in cholesterol transport." PLoS One **6**(9): e23834.

Bijlsma, M. F., Spek, C. A., Zivkovic, D., van de Water, S., Rezaee, F. and Peppelenbosch, M. P. (2006). "Repression of smoothened by patched-dependent (pro-)vitamin D3 secretion." PLoS Biol **4**(8): e232.

Bikle, D. D. (2004). "Vitamin D and skin cancer." J Nutr **134**(12 Suppl): 3472S-3478S.

Bikle, D. D. (2011a). "The vitamin D receptor: a tumor suppressor in skin." Discov Med **11**(56): 7-17.

Bikle, D. D. (2011b). "Vitamin D: an ancient hormone." Exp Dermatol **20**(1): 7-13.

Bikle, D. D. (2012). "Protective actions of vitamin D in UVB induced skin cancer." Photochem Photobiol Sci **11**(12): 1808-1816.

Blanpain, C. and Fuchs, E. (2006). "Epidermal stem cells of the skin." Annu Rev Cell Dev Biol **22**: 339-373.

Boukamp, P., Petrussevska, R. T., Breitkreutz, D., Hornung, J., Markham, A. and Fusenig, N. E. (1988). "Normal keratinization in a spontaneously immortalized aneuploid human keratinocyte cell line." J Cell Biol **106**(3): 761-771.

Bowers, M., Eng, L., Lao, Z., Turnbull, R. K., Bao, X., Riedel, E., Mackem, S. and Joyner, A. L. (2012). "Limb anterior-posterior polarity integrates activator and repressor functions of GLI2 as well as GLI3." Dev Biol **370**(1): 110-124.

Breier, A., Gibalova, L., Seres, M., Barancik, M. and Sulova, Z. (2013). "New insight into p-glycoprotein as a drug target." Anticancer Agents Med Chem **13**(1): 159-170.

Briscoe, J., Chen, Y., Jessell, T. M. and Struhl, G. (2001). "A hedgehog-insensitive form of patched provides evidence for direct long-range morphogen activity of sonic hedgehog in the neural tube." Mol Cell **7**(6): 1279-1291.

Briscoe, J. and Therond, P. P. (2013). "The mechanisms of Hedgehog signalling and its roles in development and disease." Nat Rev Mol Cell Biol **14**(7): 416-429.

Brunetti-Pierri, N., Corso, G., Rossi, M., Ferrari, P., Balli, F., Rivasi, F., Annunziata, I., Ballabio, A., Russo, A. D., Andria, G. and Parenti, G. (2002). "Lathosterolosis, a novel multiple-malformation/mental retardation syndrome due to deficiency of 3beta-hydroxysteroid-delta5-desaturase." Am J Hum Genet **71**(4): 952-958.

Buttitta, L., Mo, R., Hui, C. C. and Fan, C. M. (2003). "Interplays of Gli2 and Gli3 and their requirement in mediating Shh-dependent sclerotome induction." Development **130**(25): 6233-6243.

Campbell, F. C., Xu, H., El-Tanani, M., Crowe, P. and Bingham, V. (2010). "The yin and yang of vitamin D receptor (VDR) signaling in neoplastic progression: operational networks and tissue-specific growth control." Biochem Pharmacol **79**(1): 1-9.

Carstea, E. D., Morris, J. A., Coleman, K. G., Loftus, S. K., Zhang, D., Cummings, C., Gu, J., Rosenfeld, M. A., Pavan, W. J., Krizman, D. B., Nagle, J., Polymeropoulos, M. H., Sturley, S. L., Ioannou, Y. A., Higgins, M. E., Comly, M., Cooney, A., Brown, A., Kaneski, C. R., Blanchette-Mackie, E. J., Dwyer, N. K., Neufeld, E. B., Chang, T. Y., Liscum, L., Strauss, J. F., 3rd, Ohno, K., Zeigler, M., Carmi, R., Sokol, J., Markie, D., O'Neill, R. R., van Diggelen, O. P., Elleder, M., Patterson, M. C., Brady, R. O., Vanier, M. T., Pentchev, P. G. and Tagle, D. A. (1997). "Niemann-Pick C1 disease gene: homology to mediators of cholesterol homeostasis." Science **277**(5323): 228-231.

Chan, L. M., Cooper, A. E., Dudley, A. L., Ford, D. and Hirst, B. H. (2004). "P-glycoprotein potentiates CYP3A4-mediated drug disappearance during Caco-2 intestinal secretory detoxification." J Drug Target **12**(7): 405-413.

Chen, J. K., Taipale, J., Cooper, M. K. and Beachy, P. A. (2002a). "Inhibition of Hedgehog signaling by direct binding of cyclopamine to Smoothened." Genes Dev **16**(21): 2743-2748.

Chen, J. K., Taipale, J., Young, K. E., Maiti, T. and Beachy, P. A. (2002b). "Small molecule modulation of Smoothened activity." Proc Natl Acad Sci U S A **99**(22): 14071-14076.

Chen, T. C., Sakaki, T., Yamamoto, K. and Kittaka, A. (2012). "The roles of cytochrome P450 enzymes in prostate cancer development and treatment." Anticancer Res **32**(1): 291-298.

Chou, T. C. (1976). "Derivation and properties of Michaelis-Menten type and Hill type equations for reference ligands." J Theor Biol **59**(2): 253-276.

Chou, T. C. (2006). "Theoretical basis, experimental design, and computerized simulation of synergism and antagonism in drug combination studies." Pharmacol Rev **58**(3): 621-681.

Chou, T. C. (2010). "Drug combination studies and their synergy quantification using the Chou-Talalay method." Cancer Res **70**(2): 440-446.

Chou, T. C. and Talalay, P. (1984). "Quantitative analysis of dose-effect relationships: the combined effects of multiple drugs or enzyme inhibitors." Adv Enzyme Regul **22**: 27-55.

Chou, T. C. M., N. (2005). CompuSyn for Drug Combinations: PC Software and User's Guide. http://www.combosyn.com/, ComboSyn Inc, Paramus, (NJ), .

Christakos, S., Ajibade, D. V., Dhawan, P., Fechner, A. J. and Mady, L. J. (2010). "Vitamin D: metabolism." Endocrinol Metab Clin North Am **39**(2): 243-253, table of contents.

Cooper, M. K., Wassif, C. A., Krakowiak, P. A., Taipale, J., Gong, R., Kelley, R. I., Porter, F. D. and Beachy, P. A. (2003). "A defective response to Hedgehog signaling in disorders of cholesterol biosynthesis." Nat Genet **33**(4): 508-513.

Corcoran, R. B. and Scott, M. P. (2006). "Oxysterols stimulate Sonic hedgehog signal transduction and proliferation of medulloblastoma cells." Proc Natl Acad Sci U S A **103**(22): 8408-8413.

Costa, E. M. and Feldman, D. (1987). "Measurement of 1,25-dihydroxyvitamin D3 receptor turnover by dense amino acid labeling: changes during receptor up-regulation by vitamin D metabolites." Endocrinology **120**(3): 1173-1178.

Cunniff, C., Kratz, L. E., Moser, A., Natowicz, M. R. and Kelley, R. I. (1997). "Clinical and biochemical spectrum of patients with RSH/Smith-Lemli-Opitz syndrome and abnormal cholesterol metabolism." Am J Med Genet **68**(3): 263-269.

Dai, P., Akimaru, H., Tanaka, Y., Maekawa, T., Nakafuku, M. and Ishii, S. (1999). "Sonic Hedgehog-induced activation of the Gli1 promoter is mediated by GLI3." J Biol Chem **274**(12): 8143-8152.

Deeb, K. K., Trump, D. L. and Johnson, C. S. (2007). "Vitamin D signalling pathways in cancer: potential for anticancer therapeutics." Nat Rev Cancer **7**(9): 684-700.

DeLuca, H. F. (2004). "Overview of general physiologic features and functions of vitamin D." Am J Clin Nutr **80**(6 Suppl): 1689S-1696S.

Denef, N., Neubuser, D., Perez, L. and Cohen, S. M. (2000). "Hedgehog induces opposite changes in turnover and subcellular localization of patched and smoothened." Cell **102**(4): 521-531.

Dietrich, W. F., Lander, E. S., Smith, J. S., Moser, A. R., Gould, K. A., Luongo, C., Borenstein, N. and Dove, W. (1993). "Genetic identification of Mom-1, a major modifier locus affecting Min-induced intestinal neoplasia in the mouse." Cell **75**(4): 631-639.

Dockendorff, C., Nagiec, M. M., Weiwer, M., Buhrlage, S., Ting, A., Nag, P. P., Germain, A., Kim, H. J., Youngsaye, W., Scherer, C., Bennion, M., Xue, L., Stanton, B. Z., Lewis, T. A., Macpherson, L., Palmer, M., Foley, M. A., Perez, J. R. and Schreiber, S. L. (2012). "Macrocyclic Hedgehog Pathway Inhibitors: Optimization of Cellular Activity and Mode of Action Studies." ACS Med Chem Lett **3**(10): 808-813.

Doring, M., Eikemeier, M., Cabanillas Stanchi, K. M., Hartmann, U., Ebinger, M., Schwarze, C. P., Schulz, A., Handgretinger, R. and Muller, I. (2015). "Antifungal prophylaxis with posaconazole vs. fluconazole or itraconazole in pediatric patients with neutropenia." Eur J Clin Microbiol Infect Dis.

Dwyer, J. R., Sever, N., Carlson, M., Nelson, S. F., Beachy, P. A. and Parhami, F. (2007). "Oxysterols are novel activators of the hedgehog signaling pathway in pluripotent mesenchymal cells." J Biol Chem **282**(12): 8959-8968.

Echelard, Y., Epstein, D. J., St-Jacques, B., Shen, L., Mohler, J., McMahon, J. A. and McMahon, A. P. (1993). "Sonic hedgehog, a member of a family of putative signaling molecules, is implicated in the regulation of CNS polarity." Cell **75**(7): 1417-1430.

Ecke, I., Rosenberger, A., Obenauer, S., Dullin, C., Aberger, F., Kimmina, S., Schweyer, S. and Hahn, H. (2008). "Cyclopamine treatment of full-blown Hh/Ptch-associated RMS partially inhibits Hh/Ptch signaling, but not tumor growth." Mol Carcinog **47**(5): 361-372.

Epstein, E. H. (2008). "Basal cell carcinomas: attack of the hedgehog." Nat Rev Cancer **8**(10): 743-754.

FitzPatrick, D. R., Keeling, J. W., Evans, M. J., Kan, A. E., Bell, J. E., Porteous, M. E., Mills, K., Winter, R. M. and Clayton, P. T. (1998). "Clinical phenotype of desmosterolosis." Am J Med Genet **75**(2): 145-152.

Fritsch, A. (2014). Analysen zu Interaktionen zwischen dem Vitamin-D-Rezeptor Signalweg und der Hedgehog-Signalkaskade, Georg-August Universität Göttingen.

Garland, C. F. and Garland, F. C. (1980). "Do sunlight and vitamin D reduce the likelihood of colon cancer?" Int J Epidemiol **9**(3): 227-231.

Goodrich, L. V., Milenkovic, L., Higgins, K. M. and Scott, M. P. (1997). "Altered neural cell fates and medulloblastoma in mouse patched mutants." Science **277**(5329): 1109-1113.

Gorlin, R. J. and Goltz, R. W. (1960). "Multiple nevoid basal-cell epithelioma, jaw cysts and bifid rib. A syndrome." N Engl J Med **262**: 908-912.

Gupta, S., Takebe, N. and Lorusso, P. (2010). "Targeting the Hedgehog pathway in cancer." Ther Adv Med Oncol **2**(4): 237-250.

Hahn, H., Nitzki, F., Schorban, T., Hemmerlein, B., Threadgill, D. and Rosemann, M. (2004). "Genetic mapping of a Ptch1-associated rhabdomyosarcoma susceptibility locus on mouse chromosome 2." Genomics **84**(5): 853-858.

Hahn, H., Wicking, C., Zaphiropoulous, P. G., Gailani, M. R., Shanley, S., Chidambaram, A., Vorechovsky, I., Holmberg, E., Unden, A. B., Gillies, S., Negus, K., Smyth, I., Pressman, C., Leffell, D. J., Gerrard, B., Goldstein, A. M., Dean, M., Toftgard, R., Chenevix-Trench, G., Wainwright, B. and Bale, A. E. (1996). "Mutations of the human homolog of Drosophila patched in the nevoid basal cell carcinoma syndrome." Cell **85**(6): 841-851.

Hallikas, O., Palin, K., Sinjushina, N., Rautiainen, R., Partanen, J., Ukkonen, E. and Taipale, J. (2006). "Genome-wide prediction of mammalian enhancers based on analysis of transcription-factor binding affinity." Cell **124**(1): 47-59.

Hansdottir, S., Monick, M. M., Hinde, S. L., Lovan, N., Look, D. C. and Hunninghake, G. W. (2008). "Respiratory epithelial cells convert inactive vitamin D to its active form: potential effects on host defense." J Immunol **181**(10): 7090-7099.

Haussler, M. R., Whitfield, G. K., Haussler, C. A., Hsieh, J. C., Thompson, P. D., Selznick, S. H., Dominguez, C. E. and Jurutka, P. W. (1998). "The nuclear vitamin D receptor: biological and molecular regulatory properties revealed." J Bone Miner Res **13**(3): 325-349.

Heiskanen, T., Backman, J. T., Neuvonen, M., Kontinen, V. K., Neuvonen, P. J. and Kalso, E. (2008). "Itraconazole, a potent inhibitor of P-glycoprotein, moderately increases plasma concentrations of oral morphine." Acta Anaesthesiol Scand **52**(10): 1319-1326.

Hollis, B. W. (2010). "Assessment and interpretation of circulating 25-hydroxyvitamin D and 1,25-dihydroxyvitamin D in the clinical environment." Endocrinol Metab Clin North Am **39**(2): 271-286, table of contents.

Hooper, J. E. and Scott, M. P. (2005). "Communicating with Hedgehogs." Nat Rev Mol Cell Biol **6**(4): 306-317.

Hu, M. C., Mo, R., Bhella, S., Wilson, C. W., Chuang, P. T., Hui, C. C. and Rosenblum, N. D. (2006). "GLI3-dependent transcriptional repression of Gli1, Gli2 and kidney patterning genes disrupts renal morphogenesis." Development **133**(3): 569-578.

Hui, C. C. and Angers, S. (2011). "Gli proteins in development and disease." Annu Rev Cell Dev Biol **27**: 513-537.

Hunter, K. W., Broman, K. W., Voyer, T. L., Lukes, L., Cozma, D., Debies, M. T., Rouse, J. and Welch, D. R. (2001). "Predisposition to efficient mammary tumor metastatic progression is linked to the breast cancer metastasis suppressor gene Brms1." Cancer Res **61**(24): 8866-8872.

Ikram, M. S., Neill, G. W., Regl, G., Eichberger, T., Frischauf, A. M., Aberger, F., Quinn, A. and Philpott, M. (2004). "GLI2 is expressed in normal human epidermis and BCC and induces GLI1 expression by binding to its promoter." J Invest Dermatol **122**(6): 1503-1509.

Jacobs, E. T., Van Pelt, C., Forster, R. E., Zaidi, W., Hibler, E. A., Galligan, M. A., Haussler, M. R. and Jurutka, P. W. (2013). "CYP24A1 and CYP27B1 polymorphisms modulate vitamin D metabolism in colon cancer cells." Cancer Res **73**(8): 2563-2573.

Jehan, F. and DeLuca, H. F. (2000). "The mouse vitamin D receptor is mainly expressed through an Sp1-driven promoter in vivo." Arch Biochem Biophys **377**(2): 273-283.

Jetten, A. M. (1990). "Multi-stage program of differentiation in human epidermal keratinocytes: regulation by retinoids." J Invest Dermatol **95**(5 Suppl): 44S-46S.

Johnson, R. L., Rothman, A. L., Xie, J., Goodrich, L. V., Bare, J. W., Bonifas, J. M., Quinn, A. G., Myers, R. M., Cox, D. R., Epstein, E. H., Jr. and Scott, M. P. (1996). "Human homolog of patched, a candidate gene for the basal cell nevus syndrome." Science **272**(5268): 1668-1671.

Kaseda, R., Hosojima, M., Sato, H. and Saito, A. (2011). "Role of megalin and cubilin in the metabolism of vitamin D(3)." Ther Apher Dial **15 Suppl 1**: 14-17.

Kenney, A. M., Cole, M. D. and Rowitch, D. H. (2003). "Nmyc upregulation by sonic hedgehog signaling promotes proliferation in developing cerebellar granule neuron precursors." Development **130**(1): 15-28.

Kenney, A. M. and Rowitch, D. H. (2000). "Sonic hedgehog promotes G(1) cyclin expression and sustained cell cycle progression in mammalian neuronal precursors." Mol Cell Biol **20**(23): 9055-9067.

Khaliullina, H., Bilgin, M., Sampaio, J. L., Shevchenko, A. and Eaton, S. (2015). "Endocannabinoids are conserved inhibitors of the Hedgehog pathway." Proc Natl Acad Sci U S A.

Khaliullina, H., Panakova, D., Eugster, C., Riedel, F., Carvalho, M. and Eaton, S. (2009). "Patched regulates Smoothened trafficking using lipoprotein-derived lipids." Development **136**(24): 4111-4121.

Kim, D. J., Kim, J., Spaunhurst, K., Montoya, J., Khodosh, R., Chandra, K., Fu, T., Gilliam, A., Molgo, M., Beachy, P. A. and Tang, J. Y. (2014). "Open-label, exploratory phase II trial of oral itraconazole for the treatment of basal cell carcinoma." J Clin Oncol **32**(8): 745-751.

Kim, J., Aftab, B. T., Tang, J. Y., Kim, D., Lee, A. H., Rezaee, M., Kim, J., Chen, B., King, E. M., Borodovsky, A., Riggins, G. J., Epstein, E. H., Jr., Beachy, P. A. and Rudin, C. M. (2013). "Itraconazole and arsenic trioxide inhibit Hedgehog pathway activation and tumor growth associated with acquired resistance to smoothened antagonists." Cancer Cell **23**(1): 23-34.

Kim, J., Tang, J. Y., Gong, R., Kim, J., Lee, J. J., Clemons, K. V., Chong, C. R., Chang, K. S., Fereshteh, M., Gardner, D., Reya, T., Liu, J. O., Epstein, E. H., Stevens, D. A. and Beachy, P. A. (2010). "Itraconazole, a commonly used antifungal that inhibits Hedgehog pathway activity and cancer growth." Cancer Cell **17**(4): 388-399.

Kircik, L. (2009). "Efficacy and safety of topical calcitriol 3 microg/g ointment, a new topical therapy for chronic plaque psoriasis." J Drugs Dermatol **8**(8 Suppl): s9-16.

Kota, B. P., Allen, J. D. and Roufogalis, B. D. (2011). "The effect of vitamin D3 and ketoconazole combination on VDR-mediated P-gp expression and function in human colon adenocarcinoma cells: implications in drug disposition and resistance." Basic Clin Pharmacol Toxicol **109**(2): 97-102.

Kronemann, N., Nockher, W. A., Busse, R. and Schini-Kerth, V. B. (1999). "Growth-inhibitory effect of cyclic GMP- and cyclic AMP-dependent vasodilators on rat

vascular smooth muscle cells: effect on cell cycle and cyclin expression." Br J Pharmacol **126**(1): 349-357.

Kundu, R., Chain, B. M., Coussens, A. K., Khoo, B. and Noursadeghi, M. (2014). "Regulation of CYP27B1 and CYP24A1 hydroxylases limits cell-autonomous activation of vitamin D in dendritic cells." Eur J Immunol **44**(6): 1781-1790.

Kuwabara, P. E. and Labouesse, M. (2002). "The sterol-sensing domain: multiple families, a unique role?" Trends Genet **18**(4): 193-201.

Lam, C. W., Xie, J., To, K. F., Ng, H. K., Lee, K. C., Yuen, N. W., Lim, P. L., Chan, L. Y., Tong, S. F. and McCormick, F. (1999). "A frequent activated smoothened mutation in sporadic basal cell carcinomas." Oncogene **18**(3): 833-836.

Lee, E. Y., Ji, H., Ouyang, Z., Zhou, B., Ma, W., Vokes, S. A., McMahon, A. P., Wong, W. H. and Scott, M. P. (2010). "Hedgehog pathway-regulated gene networks in cerebellum development and tumorigenesis." Proc Natl Acad Sci U S A **107**(21): 9736-9741.

Lee, J., Platt, K. A., Censullo, P. and Ruiz i Altaba, A. (1997). "Gli1 is a target of Sonic hedgehog that induces ventral neural tube development." Development **124**(13): 2537-2552.

Lehmann, B. (1997). "HaCaT cell line as a model system for vitamin D3 metabolism in human skin." J Invest Dermatol **108**(1): 78-82.

Lipinski, R. J., Bijlsma, M. F., Gipp, J. J., Podhaizer, D. J. and Bushman, W. (2008). "Establishment and characterization of immortalized Gli-null mouse embryonic fibroblast cell lines." BMC Cell Biol **9**: 49.

Litman, T., Zeuthen, T., Skovsgaard, T. and Stein, W. D. (1997). "Competitive, non-competitive and cooperative interactions between substrates of P-glycoprotein as measured by its ATPase activity." Biochim Biophys Acta **1361**(2): 169-176.

Loftus, S. K., Morris, J. A., Carstea, E. D., Gu, J. Z., Cummings, C., Brown, A., Ellison, J., Ohno, K., Rosenfeld, M. A., Tagle, D. A., Pentchev, P. G. and Pavan, W. J. (1997). "Murine model of Niemann-Pick C disease: mutation in a cholesterol homeostasis gene." Science **277**(5323): 232-235.

Lomas, A., Leonardi-Bee, J. and Bath-Hextall, F. (2012). "A systematic review of worldwide incidence of nonmelanoma skin cancer." Br J Dermatol **166**(5): 1069-1080.

Lu, X., Liu, S. and Kornberg, T. B. (2006). "The C-terminal tail of the Hedgehog receptor Patched regulates both localization and turnover." Genes Dev **20**(18): 2539-2551.

Ly, L. H., Zhao, X. Y., Holloway, L. and Feldman, D. (1999). "Liarozole acts synergistically with 1alpha,25-dihydroxyvitamin D3 to inhibit growth of DU 145 human prostate cancer cells by blocking 24-hydroxylase activity." Endocrinology **140**(5): 2071-2076.

Ma, Y., Erkner, A., Gong, R., Yao, S., Taipale, J., Basler, K. and Beachy, P. A. (2002). "Hedgehog-mediated patterning of the mammalian embryo requires transporter-like function of dispatched." Cell **111**(1): 63-75.

MacCallum, D. M. and Odds, F. C. (2002). "Efficacy of parenteral itraconazole against disseminated Candida albicans infection in two mouse strains." J Antimicrob Chemother **50**(2): 225-229.

MacDonald, P. N., Dowd, D. R., Nakajima, S., Galligan, M. A., Reeder, M. C., Haussler, C. A., Ozato, K. and Haussler, M. R. (1993). "Retinoid X receptors stimulate and 9-cis retinoic acid inhibits 1,25-dihydroxyvitamin D3-activated expression of the rat osteocalcin gene." Mol Cell Biol **13**(9): 5907-5917.

Machold, R., Hayashi, S., Rutlin, M., Muzumdar, M. D., Nery, S., Corbin, J. G., Gritli-Linde, A., Dellovade, T., Porter, J. A., Rubin, L. L., Dudek, H., McMahon, A. P. and Fishell, G. (2003). "Sonic hedgehog is required for progenitor cell maintenance in telencephalic stem cell niches." Neuron **39**(6): 937-950.

Majewski, S., Skopinska, M., Bollag, W. and Jablonska, S. (1994). "Combination of isotretinoin and calcitriol for precancerous and cancerous skin lesions." Lancet **344**(8935): 1510-1511.

Manenti, G., Gariboldi, M., Fiorino, A., Zanesi, N., Pierotti, M. A. and Dragani, T. A. (1997). "Genetic mapping of lung cancer modifier loci specifically affecting tumor initiation and progression." Cancer Res **57**(19): 4164-4166.

Marigo, V. and Tabin, C. J. (1996). "Regulation of patched by sonic hedgehog in the developing neural tube." Proc Natl Acad Sci U S A **93**(18): 9346-9351.

McCabe, J. M. and Leahy, D. J. (2015). "Smoothened Goes Molecular: New Pieces in the Hedgehog Signaling Puzzle." J Biol Chem **290**(6): 3500-3507.

McCabe, R. E., Remington, J. S. and Araujo, F. G. (1987). "Ketoconazole promotes parasitological cure of mice infected with Trypanosoma cruzi." Trans R Soc Trop Med Hyg **81**(4): 613-615.

Michoel, T. and Nachtergaele, B. (2012). "Alignment and integration of complex networks by hypergraph-based spectral clustering." Phys Rev E Stat Nonlin Soft Matter Phys **86**(5 Pt 2): 056111.

Mill, P., Mo, R., Fu, H., Grachtchouk, M., Kim, P. C., Dlugosz, A. A. and Hui, C. C. (2003). "Sonic hedgehog-dependent activation of Gli2 is essential for embryonic hair follicle development." Genes Dev **17**(2): 282-294.

Mitschele, T., Diesel, B., Friedrich, M., Meineke, V., Maas, R. M., Gartner, B. C., Kamradt, J., Meese, E., Tilgen, W. and Reichrath, J. (2004). "Analysis of the vitamin D system in basal cell carcinomas (BCCs)." Lab Invest **84**(6): 693-702.

Miyama, T., Takanaga, H., Matsuo, H., Yamano, K., Yamamoto, K., Iga, T., Naito, M., Tsuruo, T., Ishizuka, H., Kawahara, Y. and Sawada, Y. (1998). "P-glycoprotein-mediated transport of itraconazole across the blood-brain barrier." Antimicrob Agents Chemother **42**(7): 1738-1744.

Morita, S., Kojima, T. and Kitamura, T. (2000). "Plat-E: an efficient and stable system for transient packaging of retroviruses." Gene Ther **7**(12): 1063-1066.

Muindi, J. R., Yu, W. D., Ma, Y., Engler, K. L., Kong, R. X., Trump, D. L. and Johnson, C. S. (2010). "CYP24A1 inhibition enhances the antitumor activity of calcitriol." Endocrinology **151**(9): 4301-4312.

Munker, R., Kobayashi, T., Elstner, E., Norman, A. W., Uskokovic, M., Zhang, W., Andreeff, M. and Koeffler, H. P. (1996). "A new series of vitamin D analogs is highly active for clonal inhibition, differentiation, and induction of WAF1 in myeloid leukemia." Blood **88**(6): 2201-2209.

Myers, B. R., Sever, N., Chong, Y. C., Kim, J., Belani, J. D., Rychnovsky, S., Bazan, J. F. and Beachy, P. A. (2013). "Hedgehog pathway modulation by multiple lipid binding sites on the smoothened effector of signal response." Dev Cell **26**(4): 346-357.

Nachtergaele, S., Mydock, L. K., Krishnan, K., Rammohan, J., Schlesinger, P. H., Covey, D. F. and Rohatgi, R. (2012). "Oxysterols are allosteric activators of the oncoprotein Smoothened." Nat Chem Biol **8**(2): 211-220.

Nachtergaele, S., Whalen, D. M., Mydock, L. K., Zhao, Z., Malinauskas, T., Krishnan, K., Ingham, P. W., Covey, D. F., Siebold, C. and Rohatgi, R. (2013). "Structure and function of the Smoothened extracellular domain in vertebrate Hedgehog signaling." Elife **2**: e01340.

Nedelcu, D., Liu, J., Xu, Y., Jao, C. and Salic, A. (2013). "Oxysterol binding to the extracellular domain of Smoothened in Hedgehog signaling." Nat Chem Biol **9**(9): 557-564.

Ng, J. M. and Curran, T. (2011). "The Hedgehog's tale: developing strategies for targeting cancer." Nat Rev Cancer **11**(7): 493-501.

Nilsson, M., Unden, A. B., Krause, D., Malmqwist, U., Raza, K., Zaphiropoulos, P. G. and Toftgard, R. (2000). "Induction of basal cell carcinomas and trichoepitheliomas in mice overexpressing GLI-1." Proc Natl Acad Sci U S A **97**(7): 3438-3443.

Nitzki, F. (2008). Patched associated tumors: Modifier genes and pathogenesis Dissertation.

Nitzki, F., Zibat, A., Konig, S., Wijgerde, M., Rosenberger, A., Brembeck, F. H., Carstens, P. O., Frommhold, A., Uhmann, A., Klingler, S., Reifenberger, J., Pukrop, T., Aberger, F., Schulz-Schaeffer, W. and Hahn, H. (2010). "Tumor stroma-derived Wnt5a induces differentiation of basal cell carcinoma of Ptch-mutant mice via CaMKII." Cancer Res **70**(7): 2739-2748.

Nusslein-Volhard, C. and Wieschaus, E. (1980). "Mutations affecting segment number and polarity in Drosophila." Nature **287**(5785): 795-801.

Ohyama, Y., Ozono, K., Uchida, M., Shinki, T., Kato, S., Suda, T., Yamamoto, O., Noshiro, M. and Kato, Y. (1994). "Identification of a vitamin D-responsive element in the 5'-flanking region of the rat 25-hydroxyvitamin D3 24-hydroxylase gene." J Biol Chem **269**(14): 10545-10550.

Opitz, J. M., Penchaszadeh, V. B., Holt, M. C. and Spano, L. M. (1987). "Smith-Lemli-Opitz (RSH) syndrome bibliography." Am J Med Genet **28**(3): 745-750.

Oro, A. E., Higgins, K. M., Hu, Z., Bonifas, J. M., Epstein, E. H., Jr. and Scott, M. P. (1997). "Basal cell carcinomas in mice overexpressing sonic hedgehog." Science **276**(5313): 817-821.

Ortega, M. C., Cases, O., Merchan, P., Kozyraki, R., Clemente, D. and de Castro, F. (2012). "Megalin mediates the influence of sonic hedgehog on oligodendrocyte precursor cell migration and proliferation during development." Glia **60**(6): 851-866.

Oya, N., Zolzer, F., Werner, F. and Streffer, C. (2003). "Effects of serum starvation on radiosensitivity, proliferation and apoptosis in four human tumor cell lines with different p53 status." Strahlenther Onkol **179**(2): 99-106.

Peyrot, S. M., Nachtergaele, S., Luchetti, G., Mydock-McGrane, L. K., Fujiwara, H., Scherrer, D., Jallouk, A., Schlesinger, P. H., Ory, D. S., Covey, D. F. and Rohatgi, R. (2014). "Tracking the subcellular fate of 20(s)-hydroxycholesterol with click chemistry reveals a transport pathway to the Golgi." J Biol Chem **289**(16): 11095-11110.

Polizio, A. H., Chinchilla, P., Chen, X., Manning, D. R. and Riobo, N. A. (2011). "Sonic Hedgehog activates the GTPases Rac1 and RhoA in a Gli-independent manner through coupling of smoothened to Gi proteins." Sci Signal **4**(200): pt7.

Porter, F. D. (2006). "Cholesterol precursors and facial clefting." J Clin Invest **116**(9): 2322-2325.

Porter, F. D. and Herman, G. E. (2011). "Malformation syndromes caused by disorders of cholesterol synthesis." J Lipid Res **52**(1): 6-34.

Prudencio, J., Akutsu, N., Benlimame, N., Wang, T., Bastien, Y., Lin, R., Black, M. J., Alaoui-Jamali, M. A. and White, J. H. (2001). "Action of low calcemic 1alpha,25-dihydroxyvitamin D3 analogue EB1089 in head and neck squamous cell carcinoma." J Natl Cancer Inst **93**(10): 745-753.

Quandt, K., Frech, K., Karas, H., Wingender, E. and Werner, T. (1995). "MatInd and MatInspector: new fast and versatile tools for detection of consensus matches in nucleotide sequence data." Nucleic Acids Res **23**(23): 4878-4884.

Raza, S. M., Fuller, G. N., Rhee, C. H., Huang, S., Hess, K., Zhang, W. and Sawaya, R. (2004). "Identification of necrosis-associated genes in glioblastoma by cDNA microarray analysis." Clin Cancer Res **10**(1 Pt 1): 212-221.

Regl, G., Kasper, M., Schnidar, H., Eichberger, T., Neill, G. W., Ikram, M. S., Quinn, A. G., Philpott, M. P., Frischauf, A. M. and Aberger, F. (2004). "The zinc-finger

transcription factor GLI2 antagonizes contact inhibition and differentiation of human epidermal cells." Oncogene **23**(6): 1263-1274.

Regl, G., Neill, G. W., Eichberger, T., Kasper, M., Ikram, M. S., Koller, J., Hintner, H., Quinn, A. G., Frischauf, A. M. and Aberger, F. (2002). "Human GLI2 and GLI1 are part of a positive feedback mechanism in Basal Cell Carcinoma." Oncogene **21**(36): 5529-5539.

Roberg-Larsen, H., Strand, M. F., Krauss, S. and Wilson, S. R. (2014). "Metabolites in vertebrate Hedgehog signaling." Biochem Biophys Res Commun **446**(3): 669-674.

Rodriguez-Cuesta, J., Hernando, F. L., Mendoza, L., Gallot, N., de Cerio, A. A., Martinez-de-Tejada, G. and Vidal-Vanaclocha, F. (2010). "Candida albicans enhances experimental hepatic melanoma metastasis." Clin Exp Metastasis **27**(1): 35-42.

Roewert-Huber, J., Lange-Asschenfeldt, B., Stockfleth, E. and Kerl, H. (2007). "Epidemiology and aetiology of basal cell carcinoma." Br J Dermatol **157 Suppl 2**: 47-51.

Rohatgi, R. and Scott, M. P. (2007). "Patching the gaps in Hedgehog signalling." Nat Cell Biol **9**(9): 1005-1009.

Ruiz i Altaba, A., Mas, C. and Stecca, B. (2007). "The Gli code: an information nexus regulating cell fate, stemness and cancer." Trends Cell Biol **17**(9): 438-447.

Salzler, H. R., Griffiths, R., Ruiz, P., Chi, L., Frey, C., Marchuk, D. A., Rockman, H. A. and Le, T. H. (2007). "Hypertension and albuminuria in chronic kidney disease mapped to a mouse chromosome 11 locus." Kidney Int **72**(10): 1226-1232.

Sandilands, A., Sutherland, C., Irvine, A. D. and McLean, W. H. (2009). "Filaggrin in the frontline: role in skin barrier function and disease." J Cell Sci **122**(Pt 9): 1285-1294.

Sato, A., Hiramoto, A., Uchikubo, Y., Miyazaki, E., Satake, A., Naito, T., Hiraoka, O., Miyake, T., Kim, H. S. and Wataya, Y. (2008). "Gene expression profiles of necrosis and apoptosis induced by 5-fluoro-2'-deoxyuridine." Genomics **92**(1): 9-17.

Schindelin, J., Arganda-Carreras, I., Frise, E., Kaynig, V., Longair, M., Pietzsch, T., Preibisch, S., Rueden, C., Saalfeld, S., Schmid, B., Tinevez, J. Y., White, D. J., Hartenstein, V., Eliceiri, K., Tomancak, P. and Cardona, A. (2012). "Fiji: an open-source platform for biological-image analysis." Nat Methods **9**(7): 676-682.

Scholz, C. J., Jacob, C. P., Buttenschon, H. N., Kittel-Schneider, S., Boreatti-Hummer, A., Zimmer, M., Walter, U., Lesch, K. P., Mors, O., Kneitz, S., Deckert, J. and Reif, A. (2010). "Functional variants of TSPAN8 are associated with bipolar disorder and schizophrenia." Am J Med Genet B Neuropsychiatr Genet **153B**(4): 967-972.

Sekulic, A., Migden, M. R., Oro, A. E., Dirix, L., Lewis, K. D., Hainsworth, J. D., Solomon, J. A., Yoo, S., Arron, S. T., Friedlander, P. A., Marmur, E., Rudin, C. M., Chang, A. L., Low, J. A., Mackey, H. M., Yauch, R. L., Graham, R. A., Reddy, J. C. and Hauschild, A. (2012). "Efficacy and safety of vismodegib in advanced basal-cell carcinoma." N Engl J Med **366**(23): 2171-2179.

Shabahang, M., Buffan, A. E., Nolla, J. M., Schumaker, L. M., Brenner, R. V., Buras, R. R., Nauta, R. J. and Evans, S. R. (1996). "The effect of 1, 25-dihydroxyvitamin D3 on the growth of soft-tissue sarcoma cells as mediated by the vitamin D receptor." Ann Surg Oncol **3**(2): 144-149.

Shin, K., Lee, J., Guo, N., Kim, J., Lim, A., Qu, L., Mysorekar, I. U. and Beachy, P. A. (2011). "Hedgehog/Wnt feedback supports regenerative proliferation of epithelial stem cells in bladder." Nature **472**(7341): 110-114.

So, P. L., Langston, A. W., Daniallinia, N., Hebert, J. L., Fujimoto, M. A., Khaimskiy, Y., Aszterbaum, M. and Epstein, E. H., Jr. (2006). "Long-term establishment, characterization and manipulation of cell lines from mouse basal cell carcinoma tumors." Exp Dermatol **15**(9): 742-750.

Soriano, P. (1999). "Generalized lacZ expression with the ROSA26 Cre reporter strain." Nat Genet **21**(1): 70-71.

Strutt, H., Thomas, C., Nakano, Y., Stark, D., Neave, B., Taylor, A. M. and Ingham, P. W. (2001). "Mutations in the sterol-sensing domain of Patched suggest a role for vesicular trafficking in Smoothened regulation." Curr Biol **11**(8): 608-613.

Taipale, J., Chen, J. K., Cooper, M. K., Wang, B., Mann, R. K., Milenkovic, L., Scott, M. P. and Beachy, P. A. (2000). "Effects of oncogenic mutations in Smoothened and Patched can be reversed by cyclopamine." Nature **406**(6799): 1005-1009.

Taipale, J., Cooper, M. K., Maiti, T. and Beachy, P. A. (2002). "Patched acts catalytically to suppress the activity of Smoothened." Nature **418**(6900): 892-897.

Takeyama, K., Kitanaka, S., Sato, T., Kobori, M., Yanagisawa, J. and Kato, S. (1997). "25-Hydroxyvitamin D3 1alpha-hydroxylase and vitamin D synthesis." Science **277**(5333): 1827-1830.

Tanaka, H., Abe, E., Miyaura, C., Kuribayashi, T., Konno, K., Nishii, Y. and Suda, T. (1982). "1 alpha,25-Dihydroxycholecalciferol and a human myeloid leukaemia cell line (HL-60)." Biochem J **204**(3): 713-719.

Tang, J. Y., Xiao, T. Z., Oda, Y., Chang, K. S., Shpall, E., Wu, A., So, P. L., Hebert, J., Bikle, D. and Epstein, E. H., Jr. (2011). "Vitamin D3 inhibits hedgehog signaling and proliferation in murine Basal cell carcinomas." Cancer Prev Res (Phila) **4**(5): 744-751.

Teichert, A. E., Elalieh, H., Elias, P. M., Welsh, J. and Bikle, D. D. (2011). "Overexpression of hedgehog signaling is associated with epidermal tumor formation in vitamin D receptor-null mice." J Invest Dermatol **131**(11): 2289-2297.

Teperino, R., Aberger, F., Esterbauer, H., Riobo, N. and Pospisilik, J. A. (2014). "Canonical and non-canonical Hedgehog signalling and the control of metabolism." Semin Cell Dev Biol **33**: 81-92.

Tint, G. S., Irons, M., Elias, E. R., Batta, A. K., Frieden, R., Chen, T. S. and Salen, G. (1994). "Defective cholesterol biosynthesis associated with the Smith-Lemli-Opitz syndrome." N Engl J Med **330**(2): 107-113.

Toledo, M. J., Bahia, M. T., Carneiro, C. M., Martins-Filho, O. A., Tibayrenc, M., Barnabe, C., Tafuri, W. L. and de Lana, M. (2003). "Chemotherapy with benznidazole and itraconazole for mice infected with different Trypanosoma cruzi clonal genotypes." Antimicrob Agents Chemother **47**(1): 223-230.

Tomayko, M. M. and Reynolds, C. P. (1989). "Determination of subcutaneous tumor size in athymic (nude) mice." Cancer Chemother Pharmacol **24**(3): 148-154.

Trump, D. L., Deeb, K. K. and Johnson, C. S. (2010). "Vitamin D: considerations in the continued development as an agent for cancer prevention and therapy." Cancer J **16**(1): 1-9.

Uhmann, A., Dittmann, K., Nitzki, F., Dressel, R., Koleva, M., Frommhold, A., Zibat, A., Binder, C., Adham, I., Nitsche, M., Heller, T., Armstrong, V., Schulz-Schaeffer, W., Wienands, J. and Hahn, H. (2007). "The Hedgehog receptor Patched controls lymphoid lineage commitment." Blood **110**(6): 1814-1823.

Uhmann, A., Niemann, H., Lammering, B., Henkel, C., Hess, I., Nitzki, F., Fritsch, A., Prufer, N., Rosenberger, A., Dullin, C., Schraepler, A., Reifenberger, J., Schweyer, S., Pietsch, T., Strutz, F., Schulz-Schaeffer, W. and Hahn, H. (2011a). "Antitumoral effects of calcitriol in basal cell carcinomas involve inhibition of hedgehog signaling and induction of vitamin D receptor signaling and differentiation." Mol Cancer Ther **10**(11): 2179-2188.

Uhmann, A., Niemann, H., Lammering, B., Henkel, C., Hess, I., Rosenberger, A., Dullin, C., Schraepler, A., Schulz-Schaeffer, W. and Hahn, H. (2012). "Calcitriol inhibits hedgehog signaling and induces vitamin d receptor signaling and differentiation in the patched mouse model of embryonal rhabdomyosarcoma." Sarcoma **2012**: 357040.

Uhmann, A., van den Brandt, J., Dittmann, K., Hess, I., Dressel, R., Binder, C., Luhder, F., Christiansen, H., Fassnacht, M., Bhandoola, A., Wienands, J., Reichardt, H. M. and Hahn, H. (2011b). "T cell development critically depends on prethymic stromal patched expression." J Immunol **186**(6): 3383-3391.

van den Brink, G. R. (2007). "Hedgehog signaling in development and homeostasis of the gastrointestinal tract." Physiol Rev **87**(4): 1343-1375.

Vanden Bossche, H., Ausma, J., Bohets, H., Vermuyten, K., Willemsens, G., Marichal, P., Meerpoel, L., Odds, F. and Borgers, M. (2004). "The novel azole R126638 is a selective inhibitor of ergosterol synthesis in Candida albicans, Trichophyton spp., and Microsporum canis." Antimicrob Agents Chemother **48**(9): 3272-3278.

Vantieghem, K., De Haes, P., Bouillon, R. and Segaert, S. (2006). "Dermal fibroblasts pretreated with a sterol Delta7-reductase inhibitor produce 25-hydroxyvitamin D3 upon UVB irradiation." J Photochem Photobiol B **85**(1): 72-78.

Varjosalo, M. and Taipale, J. (2008). "Hedgehog: functions and mechanisms." Genes Dev **22**(18): 2454-2472.

Walling, H. W., Fosko, S. W., Geraminejad, P. A., Whitaker, D. C. and Arpey, C. J. (2004). "Aggressive basal cell carcinoma: presentation, pathogenesis, and management." Cancer Metastasis Rev **23**(3-4): 389-402.

Wang, C., Ruther, U. and Wang, B. (2007a). "The Shh-independent activator function of the full-length Gli3 protein and its role in vertebrate limb digit patterning." Dev Biol **305**(2): 460-469.

Wang, C., Wu, H., Evron, T., Vardy, E., Han, G. W., Huang, X. P., Hufeisen, S. J., Mangano, T. J., Urban, D. J., Katritch, V., Cherezov, V., Caron, M. G., Roth, B. L. and Stevens, R. C. (2014). "Structural basis for Smoothened receptor modulation and chemoresistance to anticancer drugs." Nat Commun **5**: 4355.

Wang, C., Wu, H., Katritch, V., Han, G. W., Huang, X. P., Liu, W., Siu, F. Y., Roth, B. L., Cherezov, V. and Stevens, R. C. (2013). "Structure of the human smoothened receptor bound to an antitumour agent." Nature **497**(7449): 338-343.

Wang, Y., McMahon, A. P. and Allen, B. L. (2007b). "Shifting paradigms in Hedgehog signaling." Curr Opin Cell Biol **19**(2): 159-165.

Wassif, C. A., Maslen, C., Kachilele-Linjewile, S., Lin, D., Linck, L. M., Connor, W. E., Steiner, R. D. and Porter, F. D. (1998). "Mutations in the human sterol delta7-reductase gene at 11q12-13 cause Smith-Lemli-Opitz syndrome." Am J Hum Genet **63**(1): 55-62.

Waterham, H. R., Koster, J., Romeijn, G. J., Hennekam, R. C., Vreken, P., Andersson, H. C., FitzPatrick, D. R., Kelley, R. I. and Wanders, R. J. (2001). "Mutations in the 3beta-hydroxysterol Delta24-reductase gene cause desmosterolosis, an autosomal recessive disorder of cholesterol biosynthesis." Am J Hum Genet **69**(4): 685-694.

WHO. (2015, Febuary 2015). "Fact sheet No. 297 - Cancer." 2015, from http://www.who.int/mediacentre/factsheets/fs297/en/.

Wiese, R. J., Uhland-Smith, A., Ross, T. K., Prahl, J. M. and DeLuca, H. F. (1992). "Up-regulation of the vitamin D receptor in response to 1,25-dihydroxyvitamin D3 results from ligand-induced stabilization." J Biol Chem **267**(28): 20082-20086.

Wilkinson, S. E., Furic, L., Buchanan, G., Larsson, O., Pedersen, J., Frydenberg, M., Risbridger, G. P. and Taylor, R. A. (2013). "Hedgehog signaling is active in human prostate cancer stroma and regulates proliferation and differentiation of adjacent epithelium." Prostate **73**(16): 1810-1823.

Wilson, C. W., Chen, M. H. and Chuang, P. T. (2009). "Smoothened adopts multiple active and inactive conformations capable of trafficking to the primary cilium." PLoS One **4**(4): e5182.

Winklmayr, M., Schmid, C., Laner-Plamberger, S., Kaser, A., Aberger, F., Eichberger, T. and Frischauf, A. M. (2010). "Non-consensus GLI binding sites in Hedgehog target gene regulation." BMC Mol Biol **11**: 2.

Xie, J., Murone, M., Luoh, S. M., Ryan, A., Gu, Q., Zhang, C., Bonifas, J. M., Lam, C. W., Hynes, M., Goddard, A., Rosenthal, A., Epstein, E. H., Jr. and de Sauvage, F. J. (1998). "Activating Smoothened mutations in sporadic basal-cell carcinoma." Nature **391**(6662): 90-92.

Xu, Y., Iwanaga, K., Zhou, C., Cheesman, M. J., Farin, F. and Thummel, K. E. (2006). "Selective induction of intestinal CYP3A23 by 1alpha,25-dihydroxyvitamin D3 in rats." Biochem Pharmacol **72**(3): 385-392.

Yang, L., Yang, J., Venkateswarlu, S., Ko, T. and Brattain, M. G. (2001). "Autocrine TGFbeta signaling mediates vitamin D3 analog-induced growth inhibition in breast cells." J Cell Physiol **188**(3): 383-393.

Yavari, A., Nagaraj, R., Owusu-Ansah, E., Folick, A., Ngo, K., Hillman, T., Call, G., Rohatgi, R., Scott, M. P. and Banerjee, U. (2010). "Role of lipid metabolism in smoothened derepression in hedgehog signaling." Dev Cell **19**(1): 54-65.

Zehnder, D., Bland, R., Williams, M. C., McNinch, R. W., Howie, A. J., Stewart, P. M. and Hewison, M. (2001). "Extrarenal expression of 25-hydroxyvitamin d(3)-1 alpha-hydroxylase." J Clin Endocrinol Metab **86**(2): 888-894.

Zhou, S. F. (2008). "Structure, function and regulation of P-glycoprotein and its clinical relevance in drug disposition." Xenobiotica **38**(7-8): 802-832.

Zibat, A., Uhmann, A., Nitzki, F., Wijgerde, M., Frommhold, A., Heller, T., Armstrong, V., Wojnowski, L., Quintanilla-Martinez, L., Reifenberger, J., Schulz-Schaeffer, W. and Hahn, H. (2009). "Time-point and dosage of gene inactivation determine the tumor spectrum in conditional Ptch knockouts." Carcinogenesis **30**(6): 918-926.

Zinser, G. M., Suckow, M. and Welsh, J. (2005). "Vitamin D receptor (VDR) ablation alters carcinogen-induced tumorigenesis in mammary gland, epidermis and lymphoid tissues." J Steroid Biochem Mol Biol **97**(1-2): 153-164.

Zinser, G. M., Sundberg, J. P. and Welsh, J. (2002). "Vitamin D(3) receptor ablation sensitizes skin to chemically induced tumorigenesis." Carcinogenesis **23**(12): 2103-2109.

9. Abbreviations

#	number
%	percent
‘	minute
‘’	second
°	degree
µ	micro
µ	micro
1st	first
1α,24,25(OH)3D3	1alpha,24,25-trihydroxy vitD_3
24,25$(OH)_2D_3$	24,25-dihydroxy vitD_3
25$(OH)D_3$	25-hydroxy vitD_3
7-DHC	7-dehydrocholesterol
7TM	seven-transmembraneous domain
∞	unlimited
A	Ampere
Ab	antibody
Ad libitum	lat. at liberty
AD	activation domain
AG	stock company (german: Aktiengesellschaft)
ANOVA	analysis of variance
AU	arbitrary unit
A_{xxx}	absorbance at xxx nm
BCC	basal cell carcinoma
BCNS	basal cell nevus syndrome
BD	binding domain
BD-CP	BODIPY-cyclopamine
BODIPY	boron-dipyrromethene
bp	base pair
BrdU	5-bromo-2’-deoxyuridine
BSA	bovine serum albumin

C	Celsius
c	centi
c	concentration
CA	California
Ca^{2+}	calcium
$CaCl_2$	calcium chloride
cal	calcitriol
CDF	cumulative distribution function
CDK	cyclin-dependent kinase
CDKN1A	cyclin-dependent kinase inhibitor 1A
cDNA	complementary DNA
CHIP	chromatin immunoprecipitation
CI	combination index
Ci	cubitus interruptus
CM	conditioned medium
CMV	cytomegalovirus
Co	company
CoM	control medium
CP	cyclopamine
CRC	concentration-response curve
CRD	cysteine rich domain
Ct	threshold cycle
CTD	C-terminal domain
Cyp24a1	cytochrome P450 24a1
Cyp27a1	cytpchrome P450 27a1
Cyp27b1	cytochrome P450 27b1
D	aspartic acid (amino acid)
DAPI	4′,6-diamidin-2-phenylindol
DBP	vitamin D binding protein
ddH_2O	double-distilled water
DHCR24	3β-Hydroxysterol-δ24-reductase

DHCR7	7-dehydrocholesterolreductase
Dhh	Dessert hedgehog
Disp	Dispatched
DMEM	Dulbecco's modified eagle medium
DMSO	dimethylsulfoxid
DNA	deoxyribonucleic acid
dNTP	deoxynucleotide
DTT	dithiothreitol
E. coli	*Escherichia coli*
e.g.	*exempli gratia* (lat. for example)
EC_{50}	half-maximal effective concentration
ED_{50}	half-maximal effective dose
EDTA	ethylenediaminetetraacetic acid
EGFP	enhanced GFP
EMSA	electrophoretic mobility shift assay
et al.	*et alii* (lat. and others)
EtOH	ethanol
Fa	fractional inhibition
FCS	fetal calf serum
FDA	Federal Drug Agency
Fig	figure
FITC	fluorescin isothiocyanate
Fu	Fused
g	gramm
GAPDH	glyceraldehyde 3-phosphate dehydrogenase
gDNA	genomic DNA
GFP	green fluorescent protein
Gli	Glioma-associated oncogene family member
Gli^{act}	Gli activator form
GliBS	Gli binding site
Gli^{rep}	Gli repressor form

GmbH & Co KG	limited partnership with a limited liability company as general partner (german: Gesellschaft mit beschränkter Haftung Compagnie und Kommanditgesellschaft)
GmbH	limited liability company (german: Gesellschaft mit beschränkter Haftung)
GPCR	G-protein coupled receptor
h	hour
HCl	hydrochloric acid
HE	haematoxylen/eosin
Hh	Hedgehog
HPLC	high-pressure liquid chromatography
Hprt	hypoxanthine phosphoribosyltransferase 1
HRP	horse-raddish peroxidase
HSC70	heat-shock protein 70
i.e.	*id est* (lat. that is)
i.m.	intramuscular
i.p.	intraperitonealy
IC_{50}	half-maximal inhibitory concentration
IHC	immunohistochemistry
Ihh	Indian hedgehog
Inc.	incorporated
ITZ	itraconazole
Ivl	Involucrin
K1	Keratin 1
K10	Keratin 10
KAAD-CP	3-Keto-N-(aminoethyl-N'-aminocaproyldihydrocinnamoyl)-cyclopamine
kb	kilobase
KCl	potassium chloride
KH_2PO_4	monopotassium phosphate
KTZ	ketoconazole
L	leucine (amino acid)
l	liter
LAR II	Luciferase Assay Reagent II

LB	lysogeny broth
LC	liquid chromatography
Leu	leucine (amino acid)
log	logarithm
LOH	loss-of -heterozygosity
Lor	Loricrin
Ltd.	limited
m	meter
m	milli
M	molar
m	murine
M2H	mammalian-two-hybrid
MB	medulloblastoma
MD	Maryland
Mdr	multidrug resistance protein
MEF	mouse embryonic fibroblast
MetOH	methanol
min	minute
MRM	multiple reaction monitoring
MS	mass spectrometry
MSCV	murine stem cell virus
n	nano
n.s.	not significant
Na_2HPO_4	disodium hydrogen phosphate
NaCl	sodium chloride
NAD(P)H	nicotinamide adenine dinucleotide phosphate
NMSC	non-melanoma skin cancer
NPC1	Niemann-Pick C1 disease protein
OD	optical density
O/N	overnight
p	pico

p	plasmid
PBS	phosphate buffered saline
PCR	polymerase chain reaction
P-gp	P-glycoprotein
pH	lat. *potentia hydrogenii*
PI	propidium iodide
PLB	passive lysis buffer
POD	peroxidase
PS	penicillin/streptomycin
PSMF	phenylmethanesulfonylfluoride
Ptch	Patched1
Ptch2	Patched2
qRT-PCR	quantitative real-time PCR
Ras	Rat sarcoma
RMS	rhabdomyosarcoma
RNA	ribonucleic acid
RND	resistance-nodulation-division
ROI	region of interest
rpm	rounds-per-minute
rRNA	ribosomal RNA
RT	room temperature
RXRα	retinoid X receptor alpha
SAG	Smo agonist
SANT1	Smo antagonist 1
SC5D	3β-Hydroxysteroid-δ5-desaturase
SCC	squamous cell carcinoma
SDS	sodium dodecyl sulfate
sec	second
SEM	standard error of the mean
Shh	Sonic hedgehog
SLOS	Smith-Lemli-Opitz syndrome

Smo	Smoothened
SOC	super optimal broth with catabolite repression
SPE	solid phase extraction
SPF	specified pathogen-free
SSD	sterol-sensing domain
Tab	table
TBP	TATA-binding protein
TBS	TRIS-buffered saline
Tet	tetracycline
TF	transcription factor
TGF-β	Transforming growth factor beta
Tgm1	Transglutaminase 1
TK	thymidine kinase
TRIS	tris(hydroxymethyl)aminomethane
Trp	tryptophan (amino acid)
U	unit
USA	United States of America
UV	ultraviolet
V	Volt
v	volume
Vdr	vitamin D_3 receptor
VDRE	vitamin D response element
vismo	vismodegib
$vitD_3$	vitamin D_3
vs	versus
W	tryptophan (amino acid)
W	Watt
w	weight
WHO	World Health Organization
wk	week
Wnt	wingless-type MMTV integration site family

wt	wildtype
x g	gravitational force
x	times
Y	tyrosine (amino acid)
α	alpha
β	beta
Δ	delta

10. Acknowledgements

The ongoing experiments and the writing of this thesis would not have been possible without the aid and continuous support of the people around me who, everyone in their own way, contributed to the preparation and completion of this study.

First of all I would like express my endless gratitude to my supervisor Dr. Anja Uhmann. Thank you for your neverending amount of patience and support and the countless discussions (scientific and elsewise). Anja, keep that course. I also would like to express my deepest gratitude to my doctoral advisor Prof. Dr. Heidi Hahn for your support and for your helpful input into my project. Thank you two for giving me the opportunity to work on this exciting project.

Many thanks also to the members of my thesis committee Prof. Dr. Matthias Dobbelstein and Prof. Dr. Michael Schön for your valuable input and encouraging words during my thesis committee meetings.

Also I like to thank my collaborators at the Helmholtz-centre in Munich Prof. Dr. Jerzy Adamski, Dr. Gabrielle Möller and especially Susanne Weber for the opportunity to gain insights into mass spectrometry and for the many helpful and supporting email and phone conversations.

Special thanks go to Dr. Kai Dittmann for everything related with flow cytometry, for always having an open ear and that you always take a moment for others.

Special thanks also to the animal care takers, especially Ms. Susann Peter and Ms. Jennifer Flemming for the excellent animal care.

Many, many thanks go also to the people I was lucky to work with, many of them became more than colleagues. I learned a lot from and with you, about life, about science, how to approach problems from different perspectives and how to develop techniques to deal with those problems. Thank you, Dr. Frauke Nitzki, Dr. Penelope Pelczar, Dr. Simone König, Dr. Diana Rettberg, Marco Becker, Anke Frommhold and Ina Heß. Thanks as well, Nicole Cuvelier, Rosalie Ridcewski, Julia Dräger, Joana Pycek and Tobias Goldak and to everyone from and with GGNB that I am glad to have met.

Many special thanks go to my family and my friends for their endless support during my studies and my PhD-thesis, especially my parents Heike and Peter and my brother Gerrit. I would not be where I am without you.

<u>- Danke für Alles! -</u>

Most importantly, I would like to express special thanks to my wife and best friend Helga. Thank you for keeping up with me and supporting me in all my weird ways. Without you, I would not have been possible the way I am now. Don’t ever change!

11.Appendix

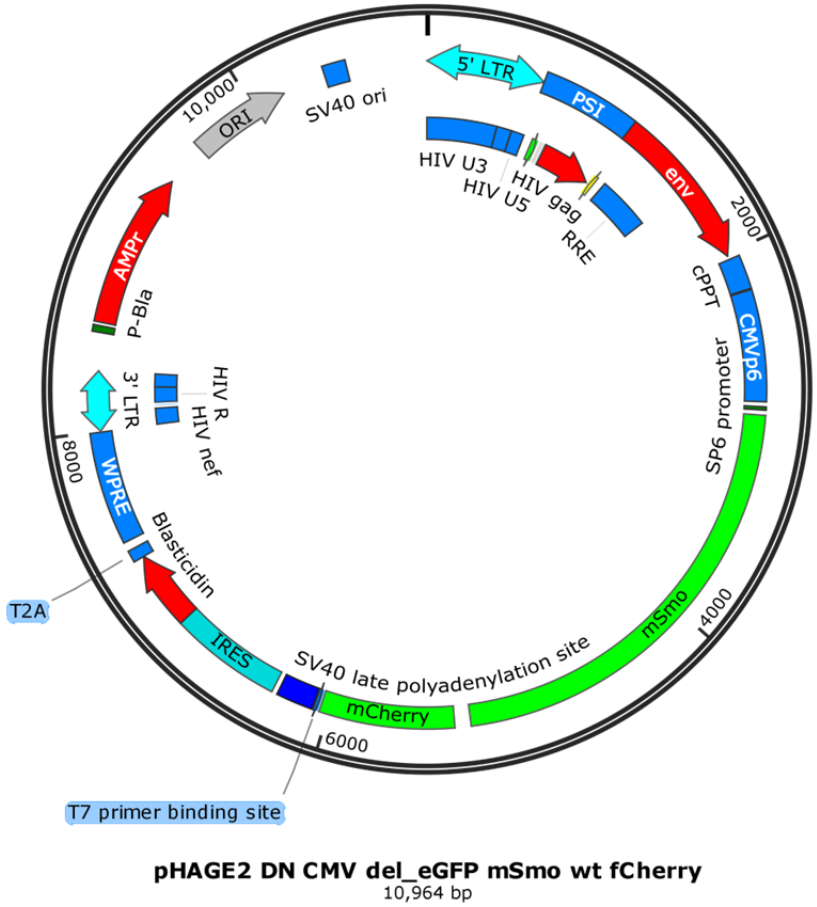

Appendix 01: Plasmid map of pHAGE mSmo cherry plasmid. The plasmid was used to subclone the mSmo mCherry (depicted in green) fusion gene into the pMSCVpuro vector (Clontech, see chapter 4.9, table 12). The map was created using SnapGene Viewer, the sequence was kindly provided by Nedelcu *et al.* (Nedelcu *et al.* 2013).

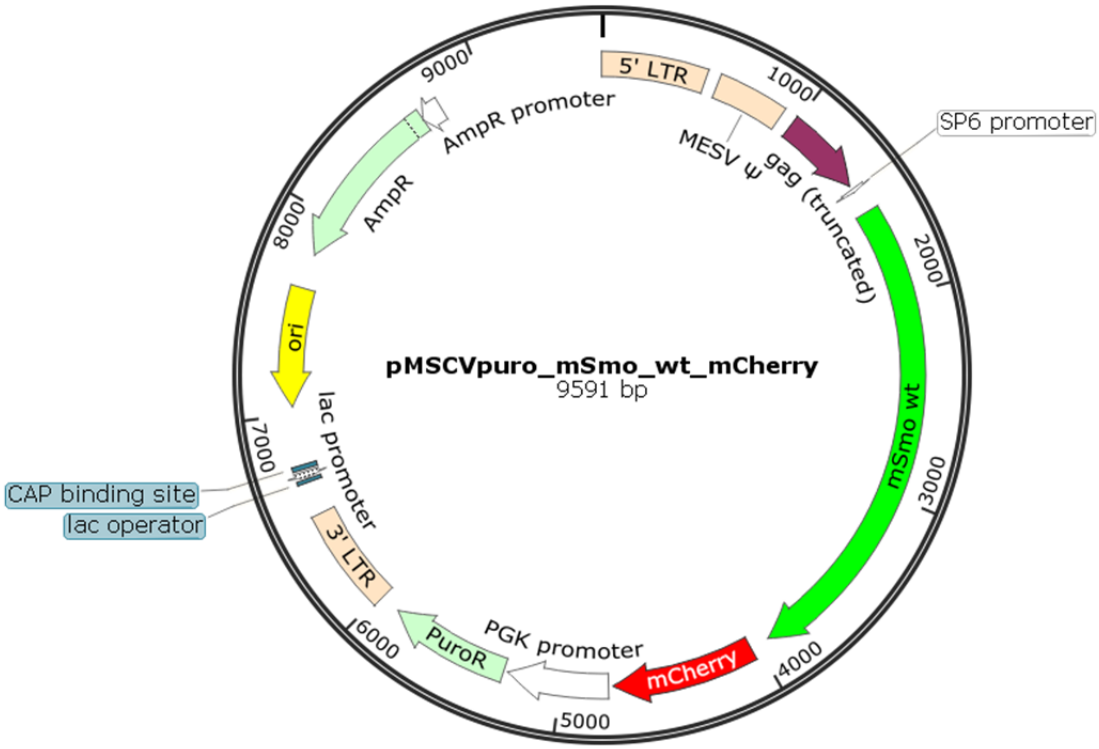

Appendix 02: Plasmid map of pMSCV mSmo^{wt} cherry plasmid. The plasmid was used to generate stably Smo^{wt} overexpressing Shh light II and *Smo*$^{-/-}$ cell lines. The map was created using SnapGene Viewer.

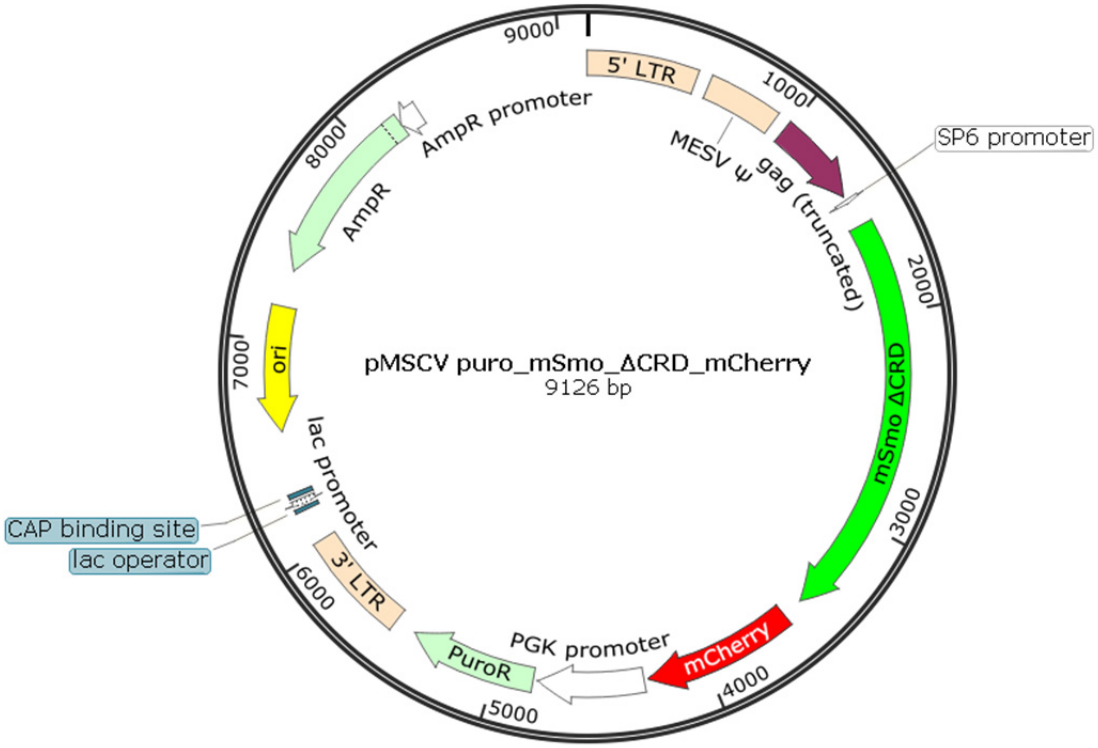

Appendix 03: Plasmid map of pMSCV mSmo$^{\Delta CRD}$ cherry plasmid; The plasmid was used to generate stably Smo$^{\Delta CRD}$ overexpressing Shh light II and *Smo*$^{-/-}$ cell lines. The map was created using SnapGene Viewer.

12.Curriculum vitae

10/2011 – hitherto	**Research assistant (PhD candidate), Georg-August-Univerisity of Göttingen** University Medical Center Göttingen; Institute of Human Genetics, Tumor Genetics group Within the graduate school GGNB (Göttingen Graduate School for Neurosciences, Biophysics and Molecular Biosciences) and the doctoral program Molecular biology of cells that is part of GAUSS (Georg-August University School of Science) Thesis-title: Interaction of Hedgehog and Vitamin D receptor signaling pathways in *Patched*-associated cancers
10/2009 – 09/2011	**M.Sc., Biology, Justus-Liebig-University of Gießen; Fachbereich 08 Biologie und Chemie (final grade: 13/15 points)** Master-Thesis: Analysis of the epigenetic regulation of the ribosomal genes during carcinogenesis
01/2011 – 06/2011	Semester abroad at the Biomedical Faculty of Lund University, Sweden
10/2006 –09/2009	**B.Sc., Biology, Justus-Liebig-University of Gießen Fachbereich 08 Biologie und Chemie (final grade: 2.3)** Bachelor-Thesis: Epigenetic regulation of the genes RASSF10 and ZBTB4 in prostate cancer
07/2008 – 08/2008	Iguana Research and Breeding Station, Utila, Honduras
08/2002 – 06/2005	**Abitur, Goethe-Schule-Wetzlar (final grade: 3.2)** Intensive courses: Biology and Chemistry

Publications

Albert, B. and Hahn, H. (2014). "Interaction of hedgehog and vitamin D signaling pathways in basal cell carcinomas." Adv Exp Med Biol **810**: 329-341.